

Preparation and Characterization of Novel Activated Carbons for Adsorption and Adsorption Assisted Biodegradation of Organic and Inorganic Water Pollutants

*Dissertation submitted in partial fulfillment
for the requirements of the degree of*

*Doctor of Philosophy
in
Chemical Engineering*

by

Arvind Kumar
(Roll Number: 511CH111)

under the supervision of

Dr. Hara Mohan Jena



April, 2017

Department of Chemical Engineering
National Institute of Technology Rourkela



April 07, 2017

Certificate of Examination

Roll Number: 511CH111

Name: Arvind Kumar

Title of Dissertation: *Preparation and Characterization of Novel Activated Carbons for Adsorption and Adsorption Assisted Biodegradation of Organic and Inorganic Water Pollutants*

We the below signed, after checking the dissertation mentioned above and the official record book (s) of the student, hereby state our approval of the dissertation submitted in partial fulfillment of the requirements of the degree of *Doctor of Philosophy in Chemical Engineering at National Institute of Technology Rourkela*. We are satisfied with the volume, quality, correctness, and originality of the work.

.....
Prof. H.M Jena

Supervisor

.....
Prof. (Mrs.) A. Sahoo

Member, DSC

.....
Prof. (Mrs.) S. Mishra

Member, DSC

.....
Prof. D. Sarkar

Member, DSC

.....
Prof. K. Mohanty

External Examiner

.....
Prof. R.K. Singh
Chairperson, DSC

.....
Prof. R.K. Singh

**Head of the
Department**



DEPARTMENT OF CHEMICAL ENGINEERING
NATIONAL INSTITUTE OF TECHNOLOGY

Dr. Hara Mohan Jena
Assistant Professor

April 07, 2017

Supervisor's Certificate

This is to certify that the work presented in this dissertation entitled "*Preparation and Characterization of Novel Activated Carbons for Adsorption and Adsorption Assisted Biodegradation of Organic and Inorganic Water Pollutants*", submitted by Arvind Kumar, Roll Number 511CH111, is a record of original research carried out by him under my supervision and guidance in partial fulfillment of the requirements of the degree of *Doctor of Philosophy in Chemical Engineering*. Neither this dissertation nor any part of it has been submitted for any degree or diploma to any institute or university in India or abroad.

Dr. Hara Mohan Jena

Department of Chemical Engineering

National Institute of Technology, Rourkela

Email: hmjena@nitrkl.ac.in; hara.jena@gmail.com

DEDICATED
TO
ASHUTOSH & ANANYA
&
MY FAMILY

Declaration of Originality

I, Arvind Kumar (Roll Number 511CH111) hereby declare that this dissertation entitled **“Preparation and Characterization of Novel Activated Carbons for Adsorption and Adsorption Assisted Biodegradation of Organic and Inorganic Water Pollutants”** represents my original work carried out as a doctoral student of NIT Rourkela and, to the best of my knowledge, it contains no material previously published or written by another person, nor any material presented for the award of any other degree or diploma of NIT Rourkela or any other institution. Any contribution made to this research by others with whom I have worked at NIT Rourkela or elsewhere, is explicitly acknowledged in the dissertation. Works of other authors cited in this dissertation have been duly acknowledged under the section “Reference”. I have also submitted my original research records to the scrutiny committee for the evaluation of my dissertation.

I am fully aware that in case of any non-compliance detected in future, the Senate of NIT Rourkela may withdraw the degree awarded to me based on the present Dissertation.

April 07, 2017
NIT Rourkela

Arvind Kumar

Acknowledgment

At this moment of accomplishment, first I pay deep gratitude to my guide, Dr. Hara Mohan Jena, for his guidance, support, and encouragement during the course of my doctoral program at the National Institute of Technology, Rourkela. I am especially indebted to him for teaching me both research and writing skills, which have been proven beneficial for my current research and future career. Without his endless efforts, knowledge, patience, and answers to my numerous questions, this research would have never been possible. He has influenced the experimental methods and results presented in this thesis in one way or the other. It has been a great honour and pleasure for me to carry out my research under his supervision.

I am very much indebted to Prof. R.K. Singh, Head of the Department, Chemical Engineering, National Institute of Technology, Rourkela and members of Doctoral Scrutiny Committee (DSC) Prof.(Mrs.) A. Sahoo (Department of Chemical Engineering), Prof.(Mrs.) S. Mishra (Department of Chemical Engineering) and Prof. D. Sarkar (Department of Chemistry), and all the faculty members of Chemical Engineering Department for giving encouragement during my thesis work.

I acknowledge all my seniors like Dr. Nihar Ranjan Biswal, Dr. Gourav Kumar, Dr. Akhilesh Khapre, Dr. Rajib Ghosh Choudhary. I express my special thanks to Mr. Bajun Hansdha, Mr. Sambhurisha Mishra, Mr. Sangram Patil, Mr. Satya Sundar Mohanty, and staff of Chemical Engineering Department for their support during my research work. I must acknowledge the academic resources provided by NIT, Rourkela to carry out this work.

Finally, I thank my wife Mrs. Sona Mishra and my entire family member for their unlimited support and strength. Without their dedication and dependability, I could not have pursued my Ph.D. degree at the National Institute of Technology Rourkela.

April 07, 2017
NIT Rourkela

Arvind Kumar
Roll Number: 511CH111

Abstract

The primary sources of water contamination are industrialization, urbanization, and agricultural activities, which are harmful to the environment and the living beings. The wastewater treatment is very necessary for saving the water to emancipate the living organisms. Among various treatment technologies, adsorption and biodegradation are the most efficient methods for removing various pollutants from wastewater. The integration of adsorption and biodegradation processes for the treatment of organic compounds leads to the enhancement of the degradation rate and adsorption capacity. Among various adsorbents used, the activated carbon is one of the most efficient adsorbents due to high surface area and developed pore structures, and a actual support media for microbial growth.

In this study, the Fox nutshell has been used as a novel precursor material for the preparation of activated carbons. These are the residue with no commercial value. The Fox nutshell contains low ash (5%) content and high volatile matter (70.1%) that is favorable for activated carbon preparation. Therefore, the Fox nutshell has been a worthwhile material for the preparation of the activated carbon. The activated carbons were prepared by chemical activation method using zinc chloride, orthophosphoric acid, and potassium carbonate. The effect of various process parameters such as heating rate, activation time, carbonization temperature and impregnation ratio on porous characteristics of the prepared activated carbons has been investigated. The proximate and ultimate analyses of the prepared activated carbons was carried out by using standard methods and CHNS analyzer, respectively. The prepared activated carbons were characterized by using N₂ adsorption-desorption isotherm at 77 K. The surface functional groups present on the prepared ACs surface were determined by the Fourier Transform Infrared Spectroscopy (FTIR) analysis. The Field Emission Scanning Electron Microscope (FESEM) analysis revealed the surface texture of the ACs while Transmission Electron Microscopy (TEM) analysis is used to visualize the presence of micropores network.

The prepared activated carbon with a ZnCl₂ activator (ACZC-600-2.0) which has the highest BET surface area of 2869 m²/g and pore volume of 1.96 cm³/g is obtained at the following conditions: 600 °C carbonization temperature, 2 impregnation ratio and one hr activation time. The prepared activated carbon with an H₃PO₄ activating agent (ACPA-700-1.5) has the BET surface area of 2636 m²/g and pore volume of 1.53 cm³/g is obtained at 700 °C carbonization temperature, 1.5 impregnation ratio and one hr activation time. The

another prepared activated carbon with a K_2CO_3 activator (ACKC-800-0.5) has the BET surface area of $1236 \text{ m}^2/\text{g}$ and pore volume of $0.98 \text{ cm}^3/\text{g}$ which has the highest surface area and pore volume is obtained at $800 \text{ }^\circ\text{C}$ carbonization temperature, 0.5 impregnation ratio and activation time of one hr.

Batch adsorption experiments of phenol, methylene blue (MB) and Cr(VI) onto prepared activated carbons were carried out at various initial concentration. Adsorption kinetics of phenol, MB and Cr(VI) were studied by using different kinetic models, i.e., the pseudo-first-order model, the pseudo-second-order model, and the intraparticle diffusion model. The experimental adsorption isotherms of these adsorbates on the prepared activated carbons were analyzed using the Langmuir, Freundlich, and Temkin isotherm models. adsorption capacity (q_e) of 500 mg/L of initial phenol concentration onto ACZC-600-2.0 and ACPA-700-1.5 are 75.37 and 83.21 mg/g, respectively. The equilibrium adsorption capacity (q_e) of MB onto ACZC-600-2.0 and ACPA-700-1.5 are 968.74 and 766.53 mg/g, respectively for 500 mg/L of initial concentration. Adsorption capacity (q_e) of 10 mg/L of initial Cr(VI) concentration onto ACZC-600-2.0 and ACPA-700-1.5 are 43.45 and 56.31 mg/g, respectively. The potential applications of the prepared activated carbons for removal of adsorbates have been studied in fixed bed column. The effects of the bed height and flow rate of phenol, MB and Cr(VI) adsorption onto prepared activated carbons were also studied.

The bacterial strain of *Pseudomonas putida* (MTCC 1194) has been taken for the phenol biodegradation in both suspended and immobilized phase. The bacterial strain has been acclimatized up to 1000 mg/L of phenol concentration. Biological granular activated carbon (BGAC) shows more efficiency than the free cells for phenol removal due to both adsorption and biodegradation process. The BGAC has been used in fluidized bed bioreactor for treatment of synthetic phenol wastewater. In fluidized bed bioreactor, effects of inlet flow rate of the wastewater, different phenol concentration solutions, and the ratio of bed (settled) volume to bioreactor volume (V_b/V_R) on the removal of phenol were studied.

Keywords: Wastewater; Fox nutshell; Activated carbons; Phenol; Methylene blue; Cr(VI); Adsorption; Adsorbent regeneration; Column study; Biodegradation; Adsorption assisted biodegradation; Fluidized bed bioreactor.

Contents

| | |
|---|---------------|
| Title Page | i |
| Certificate of Examination | ii |
| Supervisor's Certificate | iii |
| Dedication | iv |
| Declaration of Originality | v |
| Acknowledgement | vi |
| Abstract | vii |
| Contents | ix |
| List of figures | xviii |
| List of tables | xxiv |
| List of symbols | xxvii |
| Abbreviations | xxviii |
| | |
| Chapter 1 Introduction and Literature Review | 1 |
| 1.1. Background | 1 |
| 1.2. Water pollution and pollutants | 2 |
| 1.2.1. Phenolic compounds | 4 |
| 1.2.2. Dyes | 5 |
| 1.2.3. Heavy metals | 7 |
| 1.3. Wastewater treatment technologies | 8 |
| 1.4. Adsorption | 8 |
| 1.5. Activated carbon | 10 |
| 1.5.1. Structure of activated carbon | 11 |
| 1.5.2. Classifications of activated carbon | 12 |
| 1.5.2.1. Powdered activated carbon (PAC) | 12 |
| 1.5.2.2. Granular activated carbon (GAC) | 12 |
| 1.5.2.3. Extruded activated carbon (EAC) | 12 |

| | |
|--|----|
| 1.5.2.4. Impregnated coated carbon | 12 |
| 1.5.2.4. Polymer coated carbon | 13 |
| 1.5.3. Properties of activated carbon | 13 |
| 1.5.3.1. Surface area | 13 |
| 1.5.3.2. Porosity | 15 |
| 1.5.3.3. Surface functional groups | 15 |
| 1.6. Preparation of activated carbon | 17 |
| 1.6.1. Precursors | 17 |
| 1.6.2. Physical activation | 18 |
| 1.6.3. Chemical activation | 20 |
| 1.6.3.1. Activation with $ZnCl_2$ | 21 |
| 1.6.3.2. Activation with H_3PO_4 | 23 |
| 1.6.3.3. Activation with K_2CO_3 | 24 |
| 1.6.4. Adsorption of common pollutants onto activated carbon | 26 |
| 1.6.5. Regeneration of activated carbon | 28 |
| 1.7. Adsorption studies in column | 28 |
| 1.8. Biological treatment | 29 |
| 1.8.1. Biodegradation | 29 |
| 1.8.2. Biodegradation by using immobilized cell | 32 |
| 1.8.3. Adsorption assisted biodegradation | 34 |
| 1.9. Treatment in biofilm reactor | 35 |
| 1.9.1. Bioreactors | 35 |
| 1.9.2. Fluidized bed bioreactor | 36 |
| 1.9.3. Hydrodynamic studies of three-phase fluidized beds with low density particles | 39 |
| 1.10. Scope and objective of the present study | 40 |

| | |
|---|-----------|
| 1.11. Organization of the thesis | 42 |
| Chapter 2 Materials and Methods | 43 |
| 2.1. Activated carbon preparation | 43 |
| 2.1.1. Precursor | 43 |
| 2.1.2. Chemicals used | 44 |
| 2.1.3. Apparatus | 44 |
| 2.1.4. Preparation procedure | 45 |
| 2.1.5. Yield of activated carbon | 46 |
| 2.2. Characterization of Fox nutshell and prepared activated carbon | 46 |
| 2.2.1. Thermogravimetric analysis | 46 |
| 2.2.2. Proximate analysis | 46 |
| 2.2.3. Ultimate analysis | 47 |
| 2.2.4. Determination of bulk density | 48 |
| 2.2.5. Iodine number | 48 |
| 2.2.6. Specific surface area and porosity characterization | 49 |
| 2.2.7. Determination of surface chemistry | 49 |
| 2.2.8. Boehm titration | 49 |
| 2.2.9. pH and point of zero charges (PZC) measurements | 50 |
| 2.2.10. X-Ray Diffraction Spectroscopy | 50 |
| 2.2.11. Surface morphology study | 50 |
| 2.3. Adsorption studies | 50 |
| 2.3.1. Batch adsorption studies | 50 |
| 2.3.1.1. Adsorbates and analytical methods | 50 |
| 2.3.1.2. Batch experiments | 51 |
| 2.3.1.3. Studies on effect of parameters on batch adsorption | 51 |

| | |
|--|----|
| 2.3.1.3.1. Agitation speed | 51 |
| 2.3.1.3.2. pH | 52 |
| 2.3.1.3.3. Temperature | 52 |
| 2.3.1.3.4. Adsorbent dosage | 52 |
| 2.3.1.4. Adsorption characteristic study | 52 |
| 2.3.1.4.1. Adsorption kinetic models | 52 |
| 2.3.1.4.2. Intraparticle diffusion model | 53 |
| 2.3.1.4.3. Adsorption isotherm models | 53 |
| 2.3.1.4.3.1. Langmuir isotherm | 53 |
| 2.3.1.4.3.2. Freundlich isotherm | 54 |
| 2.3.1.4.3.3. Temkin adsorption isotherm | 54 |
| 2.3.2. Regeneration and reuse of adsorbents | 55 |
| 2.3.3. Fixed-bed column adsorption studies | 55 |
| 2.4. Biological treatment of phenol | 57 |
| 2.4.1. Batch biodegradation studies of phenol | 57 |
| 2.4.1.1. Bacterial culture and acclimatization | 57 |
| 2.4.1.2. Sampling and analysis of phenol and biomass | 58 |
| 2.4.1.3. Suspended cell system | 58 |
| 2.4.1.3.1. Effect of physiological parameters | 58 |
| 2.4.1.3.1.1. Inoculum size | 58 |
| 2.4.1.3.1.2. pH | 58 |
| 2.4.1.3.1.3. Temperature | 58 |
| 2.4.1.3.1.4. Initial concentration | 59 |
| 2.4.1.3.2. Biodegradation of phenol | 59 |
| 2.4.1.4. Immobilized cell system | 59 |

| | |
|---|----|
| 2.4.1.4.1. Immobilization of <i>Pseudomonas putida</i> (MTCC 1194) onto ACPA-700-1.5 | 59 |
| 2.4.1.4.2. Morphology study of developed biofilm | 59 |
| 2.4.1.4.3. Biodegradation of phenol | 60 |
| 2.5. Biodegradation studies of phenol in fluidized bed bioreactor (FBBR) | 60 |
| 2.5.1. Experimental setup | 60 |
| 2.5.2. Experimental procedure | 62 |
| Chapter 3 Preparation and Characterization of Activated Carbons | 64 |
| 3.1. Fox nutshell Processing | 64 |
| 3.2. Thermal characterization of Fox nutshell | 65 |
| 3.3. Preparation of activated carbons | 66 |
| 3.3.1. Effect of various processing parameters | 66 |
| 3.3.1.1. Effect of heating rate | 66 |
| 3.3.1.2. Effect of holding time | 67 |
| 3.3.1.3. Effect of carbonization temperature | 68 |
| 3.3.1.4. Effect of impregnation ratio | 69 |
| 3.4. Yields of prepared activated carbons | 70 |
| 3.5. Characterization of prepared activated carbons | 73 |
| 3.5.1. Ultimate analysis | 73 |
| 3.5.2. N ₂ adsorption-desorption isotherms | 76 |
| 3.5.3. Surface area and pore volume | 79 |
| 3.5.3.1. Effect of carbonization temperature | 79 |
| 3.5.3.2. Effect of impregnation ratio | 82 |
| 3.5.4. Surface characteristics comparison with literature data | 87 |
| 3.5.5. Pore size distribution | 89 |

| | |
|--|------------|
| 3.5.6. Fourier Transform Infrared Spectroscopy | 92 |
| 3.5.7. Surface chemistry determination (Boehm titration) | 95 |
| 3.5.8. X - Ray Diffraction (XRD) analysis | 95 |
| 3.5.9. Surface morphology study | 97 |
| 3.5.10. Energy Dispersive X-ray (EDX) spectroscopy | 99 |
| 3.5.11. Transmission Electron Microscopy (TEM) | 100 |
| Chapter-4 Adsorption Studies of Common Water Pollutants | 103 |
| 4.1. Adsorption of Phenol | 104 |
| 4.1.1. Batch adsorption studies | 104 |
| 4.1.1.1. Effect of experimental factors | 104 |
| 4.1.1.1.1. Agitation speed | 104 |
| 4.1.1.1.2. pH | 105 |
| 4.1.1.1.3. Temperature | 106 |
| 4.1.1.1.4. Adsorbent dosage | 107 |
| 4.1.1.1.5. Contact time and initial phenol concentrations | 107 |
| 4.1.1.2. Adsorption Characteristics | 109 |
| 4.1.1.2.1. Adsorption kinetics | 109 |
| 4.1.1.2.2. Intraparticle diffusion | 111 |
| 4.1.1.2.3. Adsorption isotherms | 112 |
| 4.1.1.2.4. Adsorption mechanism | 114 |
| 4.1.1.2.5. Adsorption thermodynamics | 115 |
| 4.1.2. Regeneration and reuse of activated carbons | 116 |
| 4.1.3. Column adsorption study | 117 |
| 4.1.3.1. Effect of bed height | 117 |
| 4.1.3.2. Effect of solution flows rate | 118 |

| | |
|---|-----|
| 4.2. Adsorption of Methylene Blue (MB) | 120 |
| 4.2.1. Batch adsorption studies | 120 |
| 4.2.1.1. Effect of experimental factors | 120 |
| 4.2.1.1.1. Agitation speed | 120 |
| 4.2.1.1.2. pH | 120 |
| 4.2.1.1.3. Temperature | 122 |
| 4.2.1.1.4. Adsorbent dosage | 123 |
| 4.2.1.1.5. Contact time and initial MB concentration | 124 |
| 4.2.1.2. Adsorption Characteristics | 127 |
| 4.2.1.2.1. Adsorption kinetics | 127 |
| 4.2.1.2.2. Intraparticle diffusion model | 129 |
| 4.2.1.2.3. Adsorption isotherms | 130 |
| 4.2.1.2.4. Adsorption mechanism | 133 |
| 4.2.1.2.5. Adsorption thermodynamics | 133 |
| 4.2.2. Regeneration and reuse of activated carbons | 135 |
| 4.2.3. Column adsorption study | 136 |
| 4.2.3.1. Effect of bed height | 136 |
| 4.2.3.2. Effect of solution flows rate | 137 |
| 4.3. Adsorption of Hexavalent Chromium [Cr(VI)] | 139 |
| 4.3.1. Batch adsorption studies | 139 |
| 4.3.1.1. Effect of process parameters | 139 |
| 4.3.1.1.1. Agitation speed | 139 |
| 4.3.1.1.2. pH | 140 |
| 4.3.1.1.3. Temperature | 141 |
| 4.3.1.1.4. Adsorbent dosage | 142 |
| 4.3.1.1.5. Contact time and initial Cr(VI) concentrations | 142 |

| | |
|---|-----|
| 4.3.1.2. Adsorption Characteristics | 145 |
| 4.3.1.2.1. Adsorption kinetics | 145 |
| 4.3.1.2.2. Intraparticle diffusion | 146 |
| 4.3.1.2.3. Adsorption isotherms | 147 |
| 4.3.1.2.4. Adsorption thermodynamics | 149 |
| 4.3.2. Regeneration and reuse of activated carbons | 150 |
| 4.3.3. Column adsorption study | 151 |
| 4.3.3.1. Effect of bed height | 151 |
| 4.3.3.2. Effect of solution flows rate | 153 |
| 4.4. Remarks on the adsorption study | 154 |
| Chapter 5 Adsorption Assisted Biodegradation of Phenol | 156 |
| 5.1. Batch biodegradation by suspended cells | 158 |
| 5.1.1. Effect of physiological parameters | 158 |
| 5.1.1.1. Inoculum size | 158 |
| 5.1.1.2. pH | 159 |
| 5.1.1.3. Incubation temperature | 159 |
| 5.1.1.4. Initial phenol concentration | 160 |
| 5.1.2. Biodegradation of phenol | 161 |
| 5.2. Batch Adsorption assisted biodegradation of phenol | 162 |
| 5.2.1. Phenol adsorption onto ACPA-700-1.5 | 163 |
| 5.2.2. Morphological characterization of biofilm | 163 |
| 5.2.3. Effect of process parameters on adsorption assisted biodegradation of phenol | 164 |
| 5.2.3.1. pH | 164 |
| 5.2.3.2. Temperature | 165 |

| | |
|--|-----|
| 5.2.4. Adsorption assisted biodegradation of phenol | 166 |
| 5.2.5. Adsorption assisted biodegradation kinetics | 167 |
| 5.2.6. Adsorption assisted biodegradation equilibrium isotherm | 168 |
| 5.3. Repeated use of BACPA-700-1.5 | 169 |
| 5.4. Remarks | 170 |
| Chapter-6 Treatment of Phenol in Fluidized Bed Bioreactor | 171 |
| 6.1. Hydrodynamic Studies | 172 |
| 6.1.1. Bed pressure drop and minimum fluidization velocity | 172 |
| 6.1.2. Expanded bed height | 176 |
| 6.1.3. Air holdup | 177 |
| 6.2. Adsorption assisted biodegradation of phenol in fluidized bed biofilm reactor | 179 |
| 6.2.1. Effect of superficial air velocity | 180 |
| 6.2.2. Effect of superficial liquid velocity | 181 |
| 6.2.3. Effect of V_b/V_r ratio | 181 |
| 6.2.4. Effect of initial phenol concentrations | 182 |
| 6.3. Cyclic degradation of phenol in FBBR | 183 |
| Chapter-7 Conclusions and Future Scope | 185 |
| 7.1. Conclusions | 185 |
| 7.2. Future scope of the work | 188 |
| References | 189 |
| Curriculum vitae | |

List of Figures

| Figure No. | Caption | Page No. |
|-------------------|---|-----------------|
| Fig. 1.1. | Comparison of the three-dimensional (a) crystal lattice of graphite and (b) the less ordered structure typical of AC. | 10 |
| Fig. 1.2. | Schematic representation of the structure of activated carbon. | 10 |
| Fig. 1.3. | The structure of hexagonal graphite. | 10 |
| Fig. 1.4. | The classification of pores. | 15 |
| Fig. 1.5. | Surface functional groups of the activated carbon. | 16 |
| Fig. 1.6. | The schema of the process of activated carbon preparation. | 17 |
| Fig. 1.7. | Biofilm reactor configurations (a) USB; (b) BFB; (c) EGSB; (d) BAS; (e) IC | 36 |
| Fig. 2.1. | Fox nut flowering, seedpods, seed, edible part and shell. | 43 |
| Fig. 2.2 | Schematic of the activation furnace. | 45 |
| Fig. 2.3. | Photographic and schematic representation of fixed bed adsorption setup. | 56 |
| Fig. 2.4. | Schematic and photographic view of the experimental set-up. | 61 |
| Fig. 3.1. | TGA and DTA curves of Fox nutshell. | 65 |
| Fig. 3.2. | Effect of carbonization temperature and ZnCl ₂ impregnation ratio on the yield of activated carbon. | 72 |
| Fig. 3.3. | Effect of carbonization temperature and H ₃ PO ₄ impregnation ratio on the yield of activated carbons. | 73 |
| Fig. 3.4. | Effect of carbonization temperatures and K ₂ CO ₃ impregnation ratios on the yield of activated carbons. | 73 |
| Fig. 3.5. | Nitrogen adsorption–desorption isotherms of activated carbons prepared at different carbonization temperature [(a) ZnCl ₂ impregnation ratio = 2.0 and (b) H ₃ PO ₄ impregnation ratio = 1.5]. | 77 |
| Fig. 3.6. | Nitrogen adsorption–desorption isotherms of activated carbons prepared at different; (a) ZnCl ₂ impregnation ratio (carbonization temperature = 600 °C) and (b) H ₃ PO ₄ impregnation ratios (carbonization temperature = 700 °C). | 77 |
| Fig. 3.7. | N ₂ adsorption–desorption isotherms of prepared activated carbon at 800 °C carbonization temperature and K ₂ CO ₃ impregnation ratio of 0.5. | 78 |
| Fig. 3.8. | Effect of carbonization temperature on (a) surface areas and (b) pore volume of activated carbons prepared with ZnCl ₂ impregnation ratio of 2.0. | 79 |
| Fig. 3.9. | Effect of carbonization temperature on (a) surface areas and (b) pore volume of activated carbons prepared with H ₃ PO ₄ impregnation ratio of 1.5. | 81 |

| | | |
|------------|--|-----|
| Fig. 3.10. | Effect of carbonization temperature on (a) surface area and (b) pore volume of activated carbons prepared with K_2CO_3 impregnation at ratio of 0.5. | 82 |
| Fig. 3.11. | Effect of $ZnCl_2$ impregnation ratio on (a) surface areas and (b) pore volume of activated carbons prepared at 600 °C carbonization temperature. | 83 |
| Fig. 3.12. | Effect of H_3PO_4 impregnation ratio on (a) surface area and (b) pore volume of activated carbons prepared at 700 °C carbonization temperature. | 85 |
| Fig. 3.13. | Effect of K_2CO_3 impregnation ratio on (a) surface area and (b) pore volume of activated carbons prepared at 800 °C carbonization temperature. | 86 |
| Fig. 3.14. | Pore size distribution of activated carbons prepared at (a) different carbonization temperatures ($ZnCl_2$ impregnation ratio = 2.0) and (b) different $ZnCl_2$ impregnation ratios (carbonization temperature = 600 °C). | 90 |
| Fig. 3.15. | Pore size distribution of activated carbons prepared at (a) different carbonization temperatures (H_3PO_4 impregnation ratio = 1.5) and (b) different H_3PO_4 impregnation ratios (carbonization temperature = 700 °C). | 91 |
| Fig. 3.16. | Pore size distribution of activated carbon prepared at carbonization temperature of 800 °C and impregnation ratio of 0.5. | 91 |
| Fig. 3.17. | FTIR spectra of the Fox nutshell. | 92 |
| Fig. 3.18. | FTIR spectra of prepared activated carbon ACZC-600-2.0. | 94 |
| Fig. 3.19. | FTIR spectra of prepared activated carbon ACPA-700-1.5. | 94 |
| Fig. 3.20. | FTIR spectra of prepared activated carbon ACPC-800-0.5. | 95 |
| Fig. 3.21. | XRD pattern of the Fox nutshell and prepared activated carbon ACZC-600-2.0. | 96 |
| Fig. 3.22. | XRD pattern of the prepared activated carbon ACPA-700-1.5. | 96 |
| Fig. 3.23. | XRD pattern of the prepared activated carbon ACPC-800-0.5. | 96 |
| Fig. 3.24. | FESEM images of (a) Fox nutshell and (b) NaOH treated FNS. | 98 |
| Fig. 3.25. | FESEM images of the prepared activated carbon ACZC-600-2.0. | 98 |
| Fig. 3.26. | FESEM images of the prepared activated carbon ACPA-700-1.5. | 99 |
| Fig. 3.27. | FESEM images of the prepared activated carbon ACPC-800-0.5. | 99 |
| Fig. 3.28. | EDX analysis of Fox nutshell. | 100 |
| Fig. 3.29. | EDX analysis of (a) ACZC-600-2.0 and (b) ACPA-700-1.5. | 100 |
| Fig. 3.30. | HRTEM image of ACZC-600-2.0 activated carbon. | 101 |
| Fig. 3.31. | HRTEM image of ACPA-700-1.5 activated carbon. | 101 |
| Fig. 3.32. | HRTEM image of ACPC-800-0.5 activated carbon. | 102 |

| | | |
|------------|---|-----|
| Fig. 4.1. | Effect of agitation speed on % removal of phenol ($C_0 = 100$ mg/L, $m_s = 0.05$ g/100mL, temperature = 30 °C, and contact time = 3 hr). | 105 |
| Fig. 4.2. | Effect of pH on % removal of phenol ($C_0 = 100$ mg/L, $m_s = 0.05$ g/100mL, temperature = 30 °C, and contact time = 3 hr). | 106 |
| Fig. 4.3. | Effect of temperatures on % removal of phenol ($C_0 = 100$ mg/L, $m_s = 0.05$ g/100mL, pH = 7, and contact time = 3 hr). | 106 |
| Fig. 4.4. | Effect of adsorbent dosage on % removal of phenol ($C_0 = 100$ mg/L, pH = 7, temperature 30 °C, and contact time = 3 hr). | 107 |
| Fig. 4.5. | Effects of contact time on the adsorption capacity of ACZC-600-2.0 at different initial concentrations ($m_s = 0.50$ g, pH = 7, temperature = 30 °C, and contact time = 3 hr). | 108 |
| Fig. 4.6. | Effects of contact time on the adsorption capacity of ACPA-700-1.5 at different initial concentrations ($m_s = 0.55$ g, pH = 7, temperature = 30 °C, and contact time = 3 hr). | 109 |
| Fig. 4.7. | Pseudo-first-order kinetics for the phenol adsorption onto ACZC-600-2.0 and ACPA-700-1.5 at 30 °C. | 110 |
| Fig. 4.8. | Pseudo-second-order kinetics for the phenol adsorption onto ACZC-600-2.0 and ACPA-700-1.5 at 30 °C. | 110 |
| Fig. 4.9. | Intraparticle diffusion plots for phenol adsorption onto ACZC-600-2.0 and ACPA-700-1.5 at 30 °C. | 112 |
| Fig. 4.10. | Langmuir isotherms for the adsorption of phenol onto ACs at 30 °C. | 113 |
| Fig. 4.11. | Freundlich isotherms for the adsorption of phenol onto ACs at 30 °C. | 113 |
| Fig. 4.12. | Temkin isotherms for the adsorption of phenol onto ACs at 30 °C. | 114 |
| Fig. 4.13. | Plots of $\ln K_C$ versus $1/T$ for 100 mg/L initial phenol concentration onto ACZC-600-2.0 and ACPA-700-1.5. | 116 |
| Fig. 4.14. | Readsorption of phenol after desorption. | 116 |
| Fig. 4.15. | Breakthrough curves for phenol adsorption onto ACZC-600-2.0 and ACPA-700-1.5 at different bed heights ($C_0 = 100$ mg/L, flow rate = 5 mL/min, and pH = 7). | 118 |
| Fig. 4.16. | Breakthrough curves for phenol adsorption onto ACZC-600-2.0 and ACPA-700-1.5 at different flow rates ($C_0 = 100$ mg/L, bed height = 4 cm, and pH = 7). | 119 |
| Fig. 4.17. | Effect of agitation speed on % removal of MB ($C_0 = 100$ mg/L, $m_s = 0.03$ g/100mL, temperature = 30 °C, and contact time = 3 hr). | 121 |
| Fig. 4.18. | Effect of pH on % removal of MB ($C_0 = 100$ mg/L, $m_s = 0.03$ g/100mL, temperature = 30 °C, and contact time = 3 hr). | 121 |

| | | |
|------------|--|-----|
| Fig. 4.19. | Effect of temperature on % removal of MB ($C_0 = 100$ mg/L, $m_s = 0.03$ g/100mL, pH = 11, contact time = 3 hr). | 122 |
| Fig. 4.20. | Effect of adsorbent dosage on % removal of MB ($C_0 = 100$ mg/L, pH = 11, contact time = 3 hr, and temperature 30 °C). | 123 |
| Fig. 4.21. | Effects of contact time on the adsorption capacity of ACZC-600-2.0 at different MB initial concentrations ($C_0 = 100$ mg/L, $m_s = 0.04$ g/100mL, pH = 11, temperature = 30 °C, and contact time = 3 hr). | 124 |
| Fig. 4.22. | Effects of contact time on the adsorption capacity of ACPA-700-1.5 at different MB initial concentrations ($C_0 = 100$ mg/L, $m_s = 0.045$ g/100mL, pH = 11, temperature = 45 °C, and contact time = 3 hr). | 125 |
| Fig. 4.23. | Pseudo-first order kinetics for the MB adsorption onto ACZC-600-2.0 (at 30 °C) and ACPA-700-1.5 (45 °C). | 127 |
| Fig. 4.24. | Pseudo-second order kinetic plots for the MB adsorption onto ACZC-600-2.0 (at 30 °C) and ACPA-700-1.5 (at 45 °C). | 128 |
| Fig. 4.25. | Intraparticle diffusion plots for the MB adsorption onto ACZC-600-2.0 (at 30 °C) and ACPA-700-1.5 (at 45 °C). | 129 |
| Fig. 4.26. | Adsorption isotherms of MB onto ACZC-600-2.0 (at 30 °C) and ACPA-700-1.5 (at 45 °C). | 130 |
| Fig. 4.27. | Langmuir isotherms for the adsorption of MB onto ACZC-600-2.0 (at 30 °C) and ACPA-700-1.5 (at 45 °C). | 131 |
| Fig. 4.28. | Freundlich isotherms of the adsorption of MB onto ACZC-600-2.0 (at 30 °C) and ACPA-700-1.5 (at 45 °C). | 132 |
| Fig. 4.29. | Temkin isotherms for the adsorption of MB onto ACZC-600-2.0 (at 30 °C) and ACPA-700-1.5 (at 45 °C). | 133 |
| Fig. 4.30. | Plots of $\ln K_C$ versus $1/T$ for 100 mg/L initial MB concentration onto ACZC-600-2.0 and ACPA-700-1.5. | 135 |
| Fig. 4.31. | Readsorption of MB after desorption. | 136 |
| Fig. 4.32. | Breakthrough curves for MB adsorption onto ACZC-600-2.0 and ACPA-700-1.5 at different bed heights ($C_0 = 100$ mg/L, flow rate = 5 mL/min, and pH = 11). | 137 |
| Fig. 4.33. | Breakthrough curves for MB adsorption onto ACZC-600-2.0 and ACPA-700-1.5 at different flow rates ($C_0 = 100$ mg/L, bed height = 4 cm, and pH = 11). | 138 |
| Fig. 4.34. | Effect of agitation speed on % removal of Cr(VI) ($C_0 = 10$ mg/L, $m_s = 0.03$ g/100mL, temperature = 30 °C, and contact time = 3 hr). | 139 |
| Fig. 4.35. | Effect of pH on the % removal of Cr(VI) ($C_0 = 10$ mg/L, $m_s = 0.03$ g/100mL, temperature = 30 °C, and contact time = 3 hr). | 141 |

| | | |
|------------|---|-----|
| Fig. 4.36. | Effect of temperatures on % removal of Cr(VI) ($C_0 = 10$ mg/L, $m_s = 0.03$ g/100 mL, pH = 2, and contact time = 3 hr). | 141 |
| Fig. 4.37. | Effect of adsorbent dosage on % removal of Cr(VI) ($C_0 = 10$ mg/L, pH = 2, temperature = 30 °C, and contact time = 3 hr). | 142 |
| Fig. 4.38. | Effects of contact time on the adsorption capacity of ACZC-600-2.0 at different initial concentrations ($m_s = 0.05$ g, pH = 2, temperature = 45 °C, and contact time = 3 hr). | 143 |
| Fig. 4.39. | Effects of contact time on the adsorption capacity of ACPA-700-1.5 at different initial concentrations ($m_s = 0.04$ g, pH = 2, temperature = 45 °C, and contact time = 3 hr). | 144 |
| Fig. 4.40. | Pseudo-first-order kinetics for Cr(VI) adsorption onto ACs at 45°C. | 146 |
| Fig. 4.41. | Pseudo-second-order kinetics for Cr(VI) adsorption onto ACs at 45°C. | 146 |
| Fig. 4.42. | Intraparticle diffusion plots for Cr(VI) adsorption onto ACs at 45°C. | 147 |
| Fig. 4.43. | Langmuir isotherms for the adsorption of Cr(VI) onto ACs at 45 °C. | 148 |
| Fig. 4.44. | Freundlich isotherms for the adsorption of Cr(VI) onto ACs at 45 °C. | 149 |
| Fig. 4.45. | Temkin isotherms for the adsorption of Cr(VI) onto ACs at 45 °C. | 149 |
| Fig. 4.46. | Plots of $\ln K_C$ versus $1/T$ for 100 mg/L initial Cr(VI) concentration onto ACZC-600-2.0 and ACPA-700-1.5. | 150 |
| Fig. 4.47. | Readsorption of Cr(VI) after desorption. | 151 |
| Fig. 4.48. | Breakthrough curves for Cr(VI) adsorption onto ACZC-600-2.0 and ACPA-700-1.5 at different bed heights ($C_0 = 10$ mg/L, flow rate = 5 mL/min, and pH = 2). | 153 |
| Fig. 4.49. | Breakthrough curves for Cr(VI) adsorption onto ACZC-600-2.0 and ACPA-700-1.5 at different flow rates ($C_0 = 10$ mg/L, bed height = 4 cm, and pH = 2). | 153 |
| Fig. 5.1. | Effect of inoculum size on % removal of phenol ($C_0 = 1000$ mg/L, and temperature = 30 °C). | 158 |
| Fig. 5.2. | Effect of pH on % removal of phenol ($C_0 = 1000$ mg/L, and temperature = 30 °C). | 159 |
| Fig. 5.3. | Effect of temperature on % removal of phenol ($C_0 = 1000$ mg/L, and pH = 7). | 160 |
| Fig. 5.4. | Effect of initial concentration of phenol on % removal (pH = 7, and temperature = 30 °C). | 161 |
| Fig. 5.5. | Residual of phenol concentration with time (pH = 7, and temperature = 30 °C). | 161 |
| Fig. 5.6. | Biodegradation curve and OD ₆₀₀ of suspended <i>P. putida</i> (MTCC 1194) ($C_0 = 1000$ mg/L, pH = 7, and temperature = 30 °C). | 162 |
| Fig. 5.7. | Residual phenol concentrations in solution ($m_s = 0.55$ g/100mL, pH= 7, and temperature= 30 °C). | 163 |

| | | |
|------------|---|-----|
| Fig. 5.8. | FESEM images of (a) ACPA-700-1.5 AC, and (b) biofilm supported on ACPA-700-1.5 at 30 °C. | 164 |
| Fig. 5.9. | Effect of pH on % removal of phenol ($C_0 = 1000$ mg/L, $m_s = 0.55$ g, and temperature = 30 °C). | 165 |
| Fig. 5.10. | Effect of temperature on % removal of phenol ($C_0 = 1000$ mg/L, $m_s = 0.55$ g, and pH = 7). | 166 |
| Fig. 5.11. | Adsorption–biodegradation process of BACPA-700-1.5 ($m_s = 0.55$ g/100mL, pH = 7, and temperature = 30 °C). | 166 |
| Fig. 5.12. | Intraparticle diffusion kinetic plots for phenol removal by BACPA-700-1.5 at 30 °C. | 168 |
| Fig. 5.13. | Repeated use of BACPA-700-1.5 ($C_0 = 2300$ mg/L, pH = 7 and temperature = 30 °C). | 170 |
| Fig. 6.1. | Variation of bed pressure drop with superficial water velocity for different bed mass. | 173 |
| Fig. 6.2. | Comparison of bed pressure drop variation. | 174 |
| Fig. 6.3. | Variation of bed pressure drop with superficial air velocity at different constant water velocities. | 175 |
| Fig. 6.4. | Variation of bed pressure drop with superficial water velocity at different constant air velocities. | 176 |
| Fig. 6.5. | Variation of bed expansion ratio with superficial water velocity at constant air velocities. | 177 |
| Fig. 6.6. | Variation of fractional air holdup with superficial water velocity at different values of fixed superficial air velocities. | 178 |
| Fig. 6.7. | Effect of superficial air velocity on phenol biodegradation. | 180 |
| Fig. 6.8. | Degradation of phenol with time at different superficial liquid velocities. | 181 |
| Fig. 6.9. | Degradation of phenol with time for various V_b/V_r ratios by BPAC-700-1.5. | 182 |
| Fig. 6.10. | Degradation of phenol of different initial concentration by BACPA-700-1.5. | 183 |
| Fig. 6.11. | Cyclic degradation of phenol in FBBR. | 184 |

List of tables

| Table No. | Topic | Page No. |
|------------------|--|-----------------|
| Table 1.1 | Common water pollutants and their effects | 3 |
| Table 1.2 | Physicochemical properties of Phenol | 4 |
| Table 1.3 | Classification of dye based on their industrial applications | 6 |
| Table 1.4 | Physicochemical properties of MB | 7 |
| Table 1.5 | Advantages and disadvantages of some adsorbents used for the pollutants removal | 9 |
| Table 1.6 | IUPAC classification of pore sizes | 15 |
| Table 1.7 | Different precursors used for AC production with ZnCl ₂ activating agent | 22 |
| Table 1.8 | Different precursors with H ₃ PO ₄ activating agent used for AC production | 24 |
| Table 1.9 | Different precursors with K ₂ CO ₃ activating agent used for AC production | 25 |
| Table 1.10 | Phenol, methylene blue and Cr(VI) adsorption on various adsorbents | 26 |
| Table 1.11 | Biodegradation of phenolic compounds by free microbial cells | 30 |
| Table 1.12 | Biodegradation of phenol by immobilized cells | 33 |
| Table 1.13 | Removal of adsorbates onto biological activated carbons | 34 |
| Table 1.14 | Literature review of phenol and other organic compounds treatment in bioreactors | 38 |
| Table 2.1 | Scientific classification of Fox nut | 44 |
| Table 2.2 | Experimental values of the parameters used in chemical activation process | 46 |
| Table 2.3 | Experimental conditions of the fixed bed adsorption studies | 55 |
| Table 3.1 | Proximate and ultimate analyzes of raw material | 64 |
| Table 3.2 | (a) Effect of heating rate on iodine number | 67 |
| | (b) Effect of activation time on iodine number | 67 |
| | (c) Effect of carbonization temperature on iodine number | 68 |
| | (d) Effect of impregnation ratio on iodine number | 70 |
| Table 3.3 | Ultimate analysis of prepared activated carbons with ZnCl ₂ activation | 74 |

| | | |
|------------|--|-----|
| Table 3.4 | Ultimate analysis of prepared activated carbons with H ₃ PO ₄ activation | 75 |
| Table 3.5 | Ultimate analysis of prepared activated carbons with K ₂ CO ₃ activation | 76 |
| Table 3.6 | BET surface area, total pore volume, micropore volume of prepared activated carbons with carbonization temperatures | 80 |
| Table 3.7 | BET surface area, total pore volume, micropore volume of prepared activated carbons with different chemical impregnation | 84 |
| Table 3.8 | Preparation conditions and porous characteristics of ACs | 86 |
| Table 3.9 | Comparison of surface area of prepared ACs with literature ones | 87 |
| Table 3.10 | FTIR spectrum band detected in the Fox nutshell and prepared activated carbons | 93 |
| Table 3.11 | Quantities of the acidic and basic surface functional groups in prepared ACs | 95 |
| Table 4.1 | Constant parameters and correlation coefficients calculated for pseudo-first and pseudo-second-order kinetic models | 109 |
| Table 4.2 | Intraparticle diffusion constants for phenol adsorption | 111 |
| Table 4.3 | Isotherm constants for adsorption of phenol | 113 |
| Table 4.4 | Thermodynamic parameters of phenol adsorption onto ACZC-600-2.0 and ACPA-700-1.5 | 115 |
| Table 4.5 | Column parameters obtained at different bed heights and flow rates | 117 |
| Table 4.6 | Comparison of MB adsorption on various adsorbents | 126 |
| Table 4.7 | Constant parameters and correlation coefficients calculated for pseudo-first and pseudo-second-order kinetic models | 128 |
| Table 4.8 | Intraparticle diffusion constants for MB adsorption | 129 |
| Table 4.9 | Isotherms constants for adsorption of MB | 131 |
| Table 4.10 | Thermodynamic parameters of MB adsorption onto ACZC-600-2.0 and ACPA-700-1.5 | 134 |
| Table 4.11 | Column parameters obtained at different bed heights and flow rates | 137 |
| Table 4.12 | Comparison of Cr(VI) adsorption on various adsorbents | 144 |
| Table 4.13 | Constant parameters and correlation coefficients calculated for pseudo-first and pseudo-second-order kinetic models | 145 |
| Table 4.14 | Intraparticle diffusion constants for Cr(VI) adsorption | 147 |
| Table 4.15 | Isotherms constants for adsorption of Cr(VI) | 148 |

| | | |
|------------|--|-----|
| Table 4.16 | Thermodynamic parameters of Cr(VI) adsorption onto ACZC-600-2.0 and ACPA-700-1.5 | 150 |
| Table 4.17 | Column parameters obtained at different bed heights and flow rates | 152 |
| Table 5.1 | Phenol levels reported in industrial wastewaters | 156 |
| Table 5.2 | Kinetics parameters of phenol adsorption assisted biodegradation on BACPA-700-1.5 | 167 |
| Table 5.3 | Isotherm model parameters for phenol adsorption assisted biodegradation on BACPA-700-1.5 | 169 |

List of Symbols

| | |
|--------------------|---|
| A: | Temkin isotherm constant (L/g) |
| B: | Heat of adsorption (J/mol) |
| B ₁ : | Weight of crucible (g) |
| b: | Temkin isotherm constant |
| C ₁ : | Weight of crucible plus original sample (g) |
| C _{ad} : | Adsorbed solute concentration (mg/L) |
| C _e : | Equilibrium concentration of adsorbate in solution (mg/L) |
| C ₀ : | Initial concentration of adsorbate in solution (mg/L) |
| C _t : | Concentration of adsorbate in solution at time t (mg/L) |
| D ₁ : | Weight of crucible plus ashed sample (g) |
| D _p : | Pore diameter |
| ΔG ^o : | Gibbs free energy |
| ΔH ^o : | Change in enthalpy |
| k ₁ : | Rate constant of the pseudo-first-order (min ⁻¹) |
| k ₂ : | Rate constant of pseudo-second-order (g/min/mg) |
| K _C : | Apparent equilibrium constant (In this case, the equilibrium constant of Langmuir model, k _L) |
| k _F : | Freundlich constant [(mg/g) (L/mg) ^{1/n}] |
| k _i : | Intraparticle diffusion rate constant (mg g ⁻¹ min ^{-1/2}) |
| k _L : | Langmuir constant (L/mg) |
| q _{bed} : | Bed capacity (mg/g) |
| q _{cal} : | Calculated adsorption capacity predicted by the model (mg/g) |
| q _e : | Equilibrium adsorption capacity (mg/g) |
| q _{exp} : | Experimental adsorption capacity (mg/g) |
| q _t : | Adsorption capacity (mg/g) at different contact time t (min) |
| q _{tot} : | Total adsorbed quantity of adsorbate in column (mg) |
| q _m : | Maximum adsorption capacity of the solid phase loading |
| m _s : | Dry weight of the adsorbent (g) |
| m _{tot} : | Quantity of adsorbate sent to the column (mg) |
| N: | Number of experimental data points |
| 1/n: | Dimensionless heterogeneity factor |
| R: | Universal gas constant (8.314 J/mol/K) |
| R _L : | Dimensionless separation factor |
| S _{BET} : | BET surface area |
| S _m : | Mesopore surface area |
| S _μ : | Micropore surface area |
| T: | Temperature (K) |
| ΔS ^o : | Change in entropy |
| U _g : | Superficial gas velocity (m/s) |
| U _L : | Superficial liquid velocity (m/s) |
| U _{Lmf} : | Minimum liquid fluidization velocity (m/s) |

| | |
|-------------|------------------------|
| V: | Volume of solution (L) |
| V_{μ} : | Micropore volume |
| V_m : | Mesopore volume |
| V_T : | Total Pore volume |

Abbreviations

| | |
|--------------------|---|
| AC: | Activated Carbon |
| ACF: | Activated Carbon Fibers |
| ACPA-700-1.5: | Activated Carbon prepared by Phosphoric Acid activation |
| ACPC-800-0.5: | Activated Carbon prepared by Potassium carbonate activation |
| ACZC-600-2.0: | Activated Carbon prepared by Zinc Chloride activation |
| BET: | Brunauer Emmett Teller |
| BGAC: | Biological Granular Activated Carbon |
| BAC: | Biological Activated Carbon |
| DR: | Dubinín Radushkevich |
| DTA: | Differential Thermal Analysis |
| EDX: | Energy Dispersive X-ray Spectroscopy |
| FBBR: | Fluidized Bed Bioreactor |
| FESEM: | Field Emission Scanning Electron Microscope |
| FNAC: | Fox nutshell activated carbon |
| FTIR: | Fourier Transform Infrared spectroscopy |
| GAC: | Granular Activated Carbon |
| HK: | Horvath and Kawazoe |
| LB: | Luria Bertani |
| MB: | Methylene Blue |
| MSM: | Minimal Salts Medium |
| PAC: | Powdered Activated Carbon |
| <i>P. putida</i> : | <i>Pseudomonas putida</i> |
| PID: | Proportional Integral Derivative |
| PSD: | Pore Size Distribution |
| PZC: | Point of Zero Charge |
| SSE: | Normalized standard deviation |
| TEM: | Transmission Electron Microscope |
| TGA: | Thermogravimetric Analysis |
| XRD: | X-Ray Diffraction |

Chapter 1

Introduction and Literature Review

1.1. Background

Water is a limited natural resource and essential for the existence of life. About 70% of the earth's surface is covered with water. Around two-thirds of that is folded in frozen glaciers and unavailable for our use. Most of the water on the earth is salt water and is unsuitable for drinking and other human needs. The actual water available for human consumption is less than 1% of the earth's water. The quality of water decides the life of the animal and plant. Water utilization is increasing day by day due to the ever-increasing population and rapid industrialization. This leads to the generation of huge amount of waste in various forms and its release into the environment that pollutes the ecosystem. Most of the waste generated is discharged into various water bodies, thus contaminating them. This, in turn, leads to the scarcity of the drinking water.

Approximately 10 to 20% of the total freshwater usage is used by the industrial and domestic sectors (Water, 2014). These sectors produce a substantial amount of wastewater that is being disposed of untreated into the water bodies. They not only pollute the water bodies but also the nearby aquifers as well as the ground water. Industrial wastewater contains a wide range of hazardous contaminants that were released into the water bodies along with them. These pollutants are harmful to both aqueous ecosystems as well as human health. The pollutants present in the wastewaters can be broadly categorized into two types: inorganic and organic contaminants. Inorganic wastewaters are generated from industries such as coal and steel industries along with non-metallic industries and mineral processing industries. Contaminants, such as dyes, lubricants, detergents, solvents, pesticides, preservatives, etc. are known as organic contaminants (Dias et al., 2007). In addition to having adverse health implications, wastewater contamination also has natural and ecological effects.

Nevertheless, to ensure a sustainable quality of life, the environmental impact of these activities must be minimized. While conservation and better utilization of resources have the greatest influence on the sustainability of the planet; reduced generation, improved

treatment technology and utilization of wastes are the best techniques for the maintenance of the environmental quality. Different types of pollutants will be treated differently. Therefore, it is very important to employ appropriate strategies for wastewater treatment. The most widely used methods for removing organic and inorganic pollutants from wastewater systems include physicochemical, chemical, and biological methods such as flocculation, coagulation, precipitation, adsorption, membrane filtration, electrochemical techniques, ozonation, and biodegradation (Aksu, 2005; Yang et al., 2015). Among these treatment methods, adsorption and biodegradation are the most efficient methods for removing pollutants from wastewater due to its more promising and economical. Adsorption is considered as the best wastewater treatment method due to its universal nature, most cost-effective and ease of operation (Ali et al., 2012; Crini, 2005; Yang et al., 2015).

1.2. Water pollution and pollutants

Any undesirable change in the physical, chemical, or biological characteristics of water is called water pollution that can harmfully affect the health, survival, or activities of human or other living organisms (Agarwal, 2005). The major sources of water pollution can be classified as municipal, industrial and agriculture. Municipal water pollution consists of wastewater from domestic and commercial establishments. The industrial wastewater characteristics depend on the type of industry and manufacturing process. Agriculture wastewater contain pollutants come from farm building (dwellings and animal stables) and crops land (Brink, 1975).

The most common water pollutants are nutrients, organic matter, heavy metals, microbial contaminants, toxic organic compounds (oil, pesticides, some plastics, and other industrial chemicals), salts, acids, sediments and suspended solids, and high temperature (Revenge and Mock, 2000). These pollutants affect the environment as well as living organisms (animals as well as a plant). The quantity of the pollutants present in the wastewater varies with sources. Table 1.1 presents some common water pollutants, their primary sources, and effects.

Table 1.1: Common water pollutants and their effects (Revenge and Mock, 2000)

| Pollutant | Primary source | Effects |
|--|---|---|
| Toxic organic compounds (oil, pesticides, plastics, industrial chemicals) | A wide variety of sources such as industrial sites to automobiles, and runoff from agricultural lands. | Toxic effects like mild immune suppression, acute poisoning, as well as reproductive failure. |
| Excess nutrients (nitrates, phosphorous) | Runoff from agricultural lands and urban areas. | Overstimulates growth of algae (eutrophication), which decomposes. High nitrates level in drinking water lead to illness in humans. |
| Heavy metals | Industries and mining sites. | Persists in freshwater environments such as river sediments and wetlands for long periods. Accumulates in the fish and shellfish. Harmful to both aquatic organisms as well as human. |
| Microbial contaminants (e.g., cryptosporidium, cholera, and other bacteria, amoebae, etc.) | Domestic sewage, cattle, natural sources. | Contaminated water spreads infectious diseases. |
| Dissolved salts (salinization) | Leached from alkaline soils by over irrigation, or drawn into coastal aquifers from over-drafting of groundwater. | Leads to salt build-up in soils, which kills crops or cuts yields. Increases freshwater as undrinkable. |
| Acid precipitation or acidic runoff | Deposition of sulfate particles, mostly from coal combustion. Acid runoff from mine tailings and sites. | Acidified lakes and streams, which harms or kills aquatic organisms and leaches heavy metals such as aluminium from soils into water bodies. |
| Silt and suspended particles | Soil erosion and construction activities in watersheds. | Reduces water quality for drinking and recreation and degrades aquatic habitats by smothering them with silt, disrupting spawning, and interfering with feeding. |

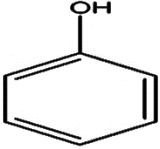
In the present study, some pollutants that are commonly present in wastewater released from various industries like paper, textiles, leather, plastics, petroleum refining, etc. were investigated in details. The discharge of these pollutants containing wastewater in the environment is worrisome for both toxicological and aesthetic reasons.

1.2.1. Phenolic compounds

Phenolic compounds are discharged into the wastewater streams of various industries such as coal conversion, wood preservation, metal casting and pulp and paper manufacturing. Most of these compounds are toxic and have been classified as hazardous pollutants (Caza et al., 1999). Phenols are considered as priority pollutants since they are harmful to organisms even at low concentrations (Ahmaruzzaman, 2008). The major sources of phenol in the aquatic environment are wastewaters from paint, pesticide, coal conversion, polymeric resin, and petroleum and petrochemicals industries. Phenols in water have adverse effects since as little as 0.005 mg/L of phenol will cause unpleasant taste and odor of drinking due to the formation of chlorophenols (Lanouette, 1977). As per Indian standard, phenol contents in the drinking water should not exceed 0.002 mg/L (Ahmaruzzaman, 2008). Phenol is one of the first compounds inscribed into The List of Priority Pollutant by the US Environmental Protection Agency (US EPA). According to its regulations, wastewater should contain less than 1 mg/L of phenol (Banat et al., 2000).

The physicochemical properties of phenol are tabulated in Table 1.2. Phenol (Hydroxybenzene) is a colorless crystalline substance of characteristic odor and soluble in water and organic solvents. Phenol is synthesized on an industrial scale by extraction from coal tar as it is formed by a transformation of high quantities of cumene present in plants. It is also obtained by a reaction between chlorobenzene and sodium hydroxide, benzene and propylene, and oxidation of toluene.

Table 1.2: Physicochemical properties of Phenol

| Molecular Structure | Molecular formula | pK _a | MW (g/mol) | Charge | Dimensions X,Y,Z (nm) |
|---|---------------------------------|-----------------|------------|--------|-------------------------|
|  | C ₆ H ₆ O | 9.89 | 94.11 | -1 | 0.675 0.706 0.296 |

Phenol is commonly used in different branches of the industry including chemical production of alkyl phenols, cresols, xylenols, phenolic resins, aniline and other compounds. It is also used in pesticides, explosives, dyes and textiles production (Michałowicz and Duda, 2007). The largest single use of phenol is as an intermediate in the production of phenolic resins. However, it is also used in the production of caprolactam (which is employed in the manufacture of nylon 6 and other synthetic fibers) and bisphenol

A (which is utilized in the production of epoxy and other resins) (Ahmaruzzaman, 2008). Phenol is mainly accumulated in brain, kidney, liver and muscle. Phenol irritates skin and causes its necrosis; it damages kidney, liver, muscle and eyes. Damage to the skin is caused by its coagulation related to reaction to phenol with amino acids of keratin of epidermis and collagen in the inner skin (Michałowicz and Duda, 2007). Phenol acute poisoning is characterized by dryness of throat and mouth, dark colored urine and high irritation of mucous membranes. The investigations showed that chronic exposure of workers to phenol vapors causes loss of body weight, weakness, headache, muscles pain and icterus (Michałowicz and Duda, 2007).

1.2.2. Dyes

Dyes are used in large quantities in many industries including textile, leather, cosmetics, paper, printing, plastic, pharmaceuticals, food, etc. to color their products (Garg et al., 2004b). Henry Perkin discovered the World's first commercially successful synthetic dye as Mauvein (CI 50245) in 1856 (Venkataraman, 2012). The dye can be defined as a colored substance capable of application in aqueous or non-aqueous solution or aqueous dispersion to a substrate and that substrate acquires a colored appearance. About 40,000 different dyes and pigments are listed which consist of over 7000 different chemical structures (Chakrabarti et al., 1988). It was estimated about 10,000 of various commercial dyes and pigments exist and over 7×10^5 tons of dyes are produced annually worldwide (Demirbas, 2009). About 10-15% of worldwide produced dyes are lost with wastewater during synthesis and processing (Gupta et al., 2006; Sahoo et al., 2005; Saquib and Muneer, 2002). There are several ways for classification of commercial dyes in terms of structure, color and application methods (Yagub et al., 2014). However, due to the complexities of the color nomenclature from the chemical structure system, the classification based on application (Yagub et al., 2014) are shown in Table 1.3.

In past, synthetic dyes were known as basic dyes. By definition, basic dyes are cationic dyes with cationic properties originating from positively charged nitrogen or sulfur atoms. The charge is delocalized throughout the chromophoric system, although it is probably more localized on the nitrogen atoms. In fact, basic dyes are so named due to their affinity for basic textile materials with net negative charge (Juang and Swei, 1996). Most basic dyes are beautiful, shiny, crystalline compounds, and their most outstanding property is brilliance. The tinctorial value of basic dye is very high; less than 1 ppm of the dye produces

a striking coloration (Holme and Griffiths, 1984; McKay et al., 1981). Basic dyes have been classified as toxic colorants (Anliker et al., 1988).

Table 1.3: Classification of dye based on their industrial applications (Yagub et al., 2014)

| Class | Substrate | Method of application | Chemical types |
|----------|--|--|---|
| Acid | Wool, nylon, silk, inks, leather and paper | Generally from neutral to acidic bath | Anthraquinone, xanthene, azo (including nitroso, premetallized), nitro, and triphenylmethane |
| Basic | Inks, paper, polyacrylonitrile, treated nylon, and polyester | Applied from acidic dye baths | Hemicyanine, azo, cyanine, diazahemicyanine, azine diphenylmethane, xanthene, triarylmethane, acridine, anthraquinone and oxazine |
| Direct | Nylon, rayon, paper, leather and cotton. | Applied from neutral or a little alkaline bath containing additional electrolyte | Phthalocyanine, azo, oxazine, and stilbenes |
| Disperse | Polyamide, acrylic polyester, acetate, and plastics | Fine aqueous dispersions often applied by high temperature/pressure; dye may be padded on cloth and thermo fixed | Benzodifuranone, azo, anthraquinone, nitro, and styryl |
| Reactive | Wool, cotton, silk, and nylon | Responsive site on dye reacts with functional group on fiber to bind dye covalently under the influence of heat and pH | Anthraquinone, formazan, phthalocyanine, azo, oxazine and basic |
| Sulphur | Rayon and cotton | Aromatic substrate vatted with sodium sulfide and reoxidised to insoluble sulphur-containing products on fiber | Indeterminate structures |
| Vat | Wool and cotton | Water-insoluble dyes solubilised by dropping in sodium hydrogen sulfite then exhausted on reoxidised and fiber | Indigoids and anthraquinone |

Basic dyes are widely used in acrylic, wool, nylon and silk dyeing. These dyes include different chemical structures based on substituted aromatic groups. These groups of basic dyes are toxic in nature and can cause harmful effects such as allergic dermatitis, skin irritation, mutations and cancer (Salleh et al., 2011). Methylene blue (MB) can be employed as a thiazine (cationic or basic) dye; the most commonly used dye for colouring among all other dyes of its category (Berrios et al., 2012). The molecular structure and physical

properties of the MB are exhibited in Table 1.4. It is a dark-green powder or a crystalline solid cationic dye. MB is an oxidation/reduction indicator with blue/gray color, respectively and use in medical applications such as stain tissues, the determination of manganese and as an antidote for cyanide poisoning in the body (Ghaedi et al., 2014; Reddy et al., 2016). The complex structure of MB dye makes it very stable and difficult to degrade leading to many environmental problems such as preventing sunlight penetration into water, reducing photosynthetic activity and causing the bad appearance of water surfaces (Özer et al., 2007). MB may cause cyanosis, increases heart rate, vomiting, shock, Heinz body formation, jaundice, quadriplegia and tissue necrosis in humans (Program, 1990).

Table 1.4: Physicochemical properties of MB

| Molecular Structure | Molecular formula | pK _a | MW (g/mol) | Charge | Dimensions X,Y,Z (nm) |
|---------------------|--|-----------------|------------|--------|-------------------------|
| | C ₁₆ H ₁₈ N ₃ SCl | 3.8 | 319.85 | +1 | 1.641 0.744 0.617 |

1.2.3. Heavy metals

Heavy metals are considered to be one of the most hazardous contaminants in wastewater. Primary sources of wastes containing heavy metals are the industrial activities (e.g. mining, painting, car manufacturing, metal plating, and tanneries) and agricultural activities (when fertilizers and fungicidal sprays are intensively used) (Dias et al., 2007). Cadmium, chromium, copper, lead, mercury, and nickel are most toxic metals according to the WHO, 2004 and WHO, 2006 (Dias et al., 2007). Among these heavy metals, chromium is very toxic to the living being.

Chromium is an essential nutrient for plant and animal metabolism (glucose metabolism, amino, and nucleic acid synthesis). When accumulated at high levels, chromium can generate serious problems (nausea, skin ulcerations, lung cancer), and concentration reaches 0.1 mg/g body weight, it can ultimately become lethal (Richard and Bourg, 1991). Chromium pollutant is introduced into natural waters by a variety of industrial wastewaters including those from textile, steel fabrication, agricultural runoff, paint manufacturing, leather tanning, electroplating, and metal finishing industries (Schneider et al., 2007; Selvi et al., 2001; Sharma and Forster, 1995). Chromium is also used in explosives, ceramics and photography (Selvi et al., 2001). Chromium occurs as both trivalent [Cr(III)] and hexavalent

[Cr(VI)] states in the aquatic environment. Hexavalent chromium is primarily present in the form of chromate (CrO_4^-) and dichromate (Cr_2O_7^-). Cr(VI) possesses significantly higher levels of toxicity than the other valence states (Selvi et al., 2001; Sharma and Forster, 1995). The tolerance limit for Cr(VI) for discharge into inland surface waters is 0.1 mg/L and in potable water is 0.05 mg/L (Kobya, 2004).

Above mentioned pollutants are very common in wastewater and its toxicity may cause various problems to the living being and adverse impact on the environment. Therefore, specific methods and technologies are required to remove these pollutants present in various kinds of industrial wastewater streams as well as to protect the environment and life.

1.3. Wastewater treatment technologies

Various methods of wastewater treatment have been widely studied, and generally it can be divided into the physico-chemical and biological treatment method. The physico-chemical treatment methods include the use of coagulants, oxidising agents, photocatalysis, ultrafiltration, electrochemical and adsorption techniques. Among these various physico-chemical treatment methods, adsorption onto activated carbon has proven to be one of the most effective and reliable physico-chemical treatments (Berrios et al., 2012). Biological treatment methods involve living organisms using pollutants as a carbon for energy source, and completely changing their chemical and physical characteristics. Removal of pollutants from the environment by biological methods has significant advantages over other methods because of the adaptability of various microorganisms in degrading different compounds.

The activated carbon adsorption and biological degradation are two methods that play an important role in the treatment of industrial wastewater. The adsorption and biodegradation processes successfully supplement each other in the various schemes of wastewater treatment. The activated carbon adsorption can possibly allow the removal of toxic contaminants from the wastewater and thus ensure a stable biological post-treatment of the wastewater (Ong et al., 2007).

1.4. Adsorption

Adsorption technology is widely used for different purposes, such as air purification, wastewater or drinking water purification, recovery of useful materials, storage of materials, refining of sugar, removal of harmful substances and many others. Adsorption is defined as the removal of materials from either gaseous or liquid solutions onto adsorbents. There are

two types of adsorption: physical and chemical adsorption. Physical adsorption is achieved by Van der Waals forces, dipole interactions, and hydrogen bonding. There is no activation energy required for physical adsorption due to no electron exchange between adsorbent and adsorbate, and the time needed to reach equilibrium is very short. Physical adsorption is a non-specific and a reversible process. Chemical adsorption results from the chemical bonds as ionic and covalent between adsorbent and adsorbate molecule. Therefore it is specific as well as irreversible (Mohamed, 2011).

As advances are made in adsorption technology, researchers continuously seek “effective” adsorbents, in terms of good adsorption capacity, good selectivity and cost effectiveness. Table 1.5 listed some commonly used adsorbents.

Table 1.5: Advantages and disadvantages of some adsorbents used for the pollutants removal (Crini, 2005)

| Adsorbent | Advantages | Disadvantages |
|-------------------------|---|---|
| Activated carbon | The most effective adsorbent contains very high surface area with pores arrangement, high capacity and high rate of adsorption, great capacity to adsorb a broad range of pollutants with a high-quality treated effluent | Expensive, high reactivation costs, reactivation results in a loss of the carbon |
| Ion-exchange resin | Full range of pore structure and physicochemical characteristics ion, good surface area, active sorbent, excellent selectivity toward aromatic solutes, regeneration: no adsorbent loss | Expensive, derived from petroleum-based raw materials, sensitive to particle, performance is dependent on the type of resin used, not sufficient for all dyes, ph-dependence, weak contact with aqueous pollution, requires modification for enhanced the water wettability |
| Chitosan-based material | Low-cost natural polymer, environmentally friendly, extremely cost-effective, outstanding metal and dye binding capacities, high efficiency and selectivity in detoxifying both very dilute or concentrated solutions excellent diffusion properties, easy regeneration if required | Nonporous sorbent, the sorption capacity depends on the origin of the polysaccharide and the degree of <i>n</i> -acetylation, variability in the bead characteristics, ph-dependence, calls for chemical modification to improve its performance, low affinity for basic dyes |
| Starch-based material | Abundant natural biopolymer and widely available, renewable resource, economically attractive and feasible, easy to prepare with relatively inexpensive reagents, high swelling capacity in water, good pollutants removal, applicable to a | Little surface area, calls for chemical derivatization to improve its sorption capacities, variability in the bead characteristics, its use in sorption columns is limited since the features of the particles introduce |

| | | |
|--|--|---|
| | wide variety of process, easy regeneration if required | hydrodynamic limitations and column fouling |
|--|--|---|

1.5. Activated carbon

Activated carbon in the broadest sense are heat treated, highly porous internal surface area carbon-based materials. Activated carbon (AC) as defined by International Union of Pure and Applied Chemistry (IUPAC) is: “a porous carbon material, a char which has been subjected to reaction with gases, sometimes with the addition of chemicals, e.g. $ZnCl_2$, before, during or after carbonization to increase its adsorptive properties” (Fitzer et al., 1995). “Activated carbon is porosity (space) enclosed by carbon atoms” (Marsh, 2006).

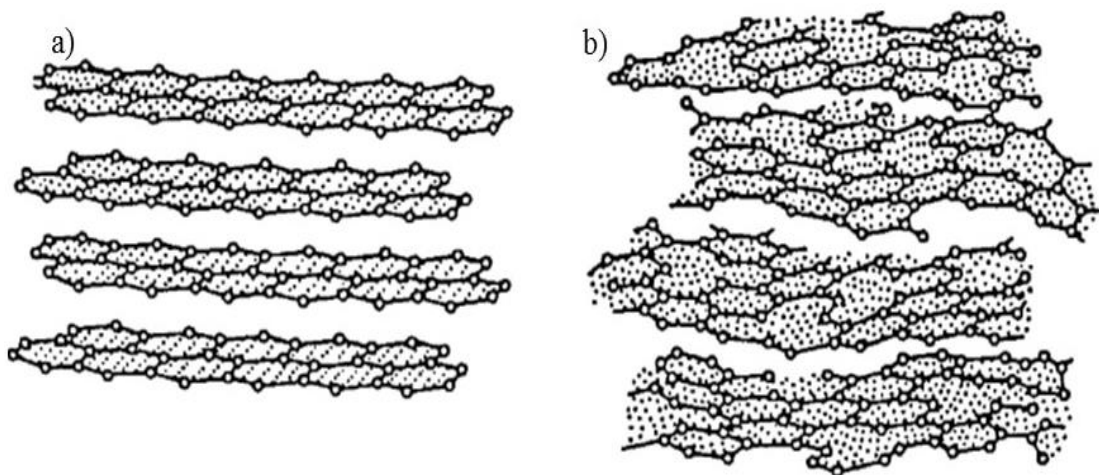


Fig. 1.1. Comparison of the three-dimensional (a) crystal lattice of graphite and (b) the less ordered structure typical of AC (Bansal and Goyal, 2005).

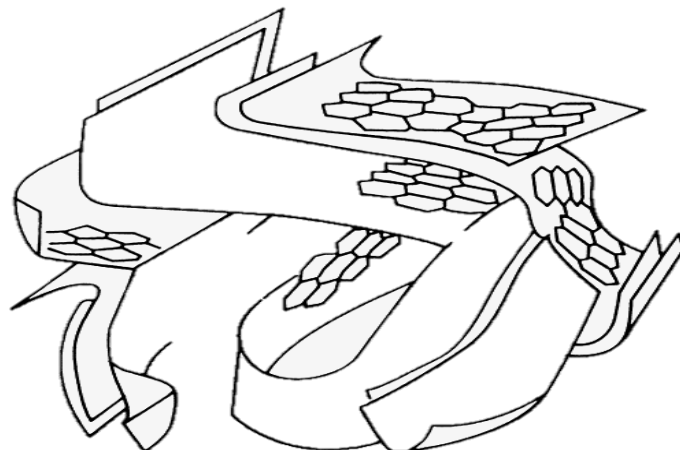


Fig. 1.2. Schematic representation of the structure of activated carbon (Rodriguez-Reinoso and Molina-Sabio, 1998).

Activation processes (physical or chemical) affects the surface area and complex pore structure of the activated carbon. The role of AC as an adsorbent material to remove contaminants from liquids and gases is well established (Bansal and Goyal, 2005). AC is partial amorphous in nature having a poorly ordered microcrystalline structure as shown in

Fig. 1.1. These are constituted by imperfect sections of graphitic lamellae of small size, which are crumpled and have many structural defects, bonded together to create a three-dimensional network, the spaces between them constituting the carbon porosity, as shown in Fig. 1.2. The variations in size, shape, deformation and cross-linking among the lamellae not only cause differences in porosity but also in physical properties such as bulk density, hardness, etc. (Rodríguez-Reinoso and Molina-Sabio, 1998).

1.5.1. Structure of activated carbon

Both the porous structure and chemical nature of the activated carbon surface are significantly related to its crystalline structure. The formation of the crystalline structure of activated carbon begins early in the carbonization process. Thus, sets of condensed aromatic rings of various numbers that are the nascent centers of graphite-like micro-crystallites are formed. Although their structure resembles that of a crystal of graphite, there exist deviations from that structure. It is composed of stacks of graphene layers cross-linked in a random manner. Most of the sheets are wrinkled which helps to create porosity. The wrinkles are possibly due to the presence of five and seven-membered rings. The deviations from the ordering characteristics of graphite can be described by the term 'turbostratic structure' (Biscoe and Warren, 1942).

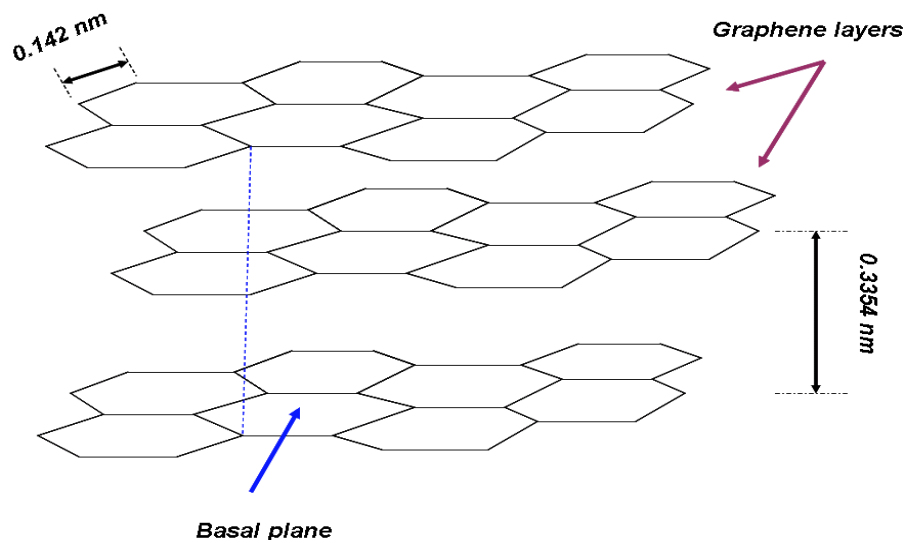


Fig. 1.3. The structure of hexagonal graphite (Marsh and Reinoso, 2006).

The disordering of the crystal lattice may be caused by its defects (e. g. vacant lattice sites) and the presence of built-in heteroatoms. This result from the nature of the starting material, the method, and conditions used to prepare AC. The significant difference between the structure of graphite and active carbon lies in the quantity and mutual orientation of the crystallites. The order range of the crystal structure, that is very high in the case of graphite

but is very limited for ACs. The structure of the graphite crystal was first established by Bernal in 1924 as a result of X-ray studies (Bernal, 1924). It consisted of layers of carbon atoms and arranged in a honeycomb lattice with separation of 0.142 nm while the separation of the planes (d-spacing) is 0.3354 nm (Fig. 1.3.).

1.5.2. Classifications of activated carbon

Activated carbons are complex products that are difficult to classify by their behavior, surface characteristics and preparation methods. However, broad classification are made for general purpose based on their physical characteristics.

1.5.2.1. Powdered activated carbon (PAC)

PAC is made in a particular form of powders or fine granules less than 1.0 mm in size with an average diameter between 0.15 and 0.25 mm. Thus, they present a large surface to volume ratio with a small diffusion distance. PAC is made up of crushed carbon particles, 95-100% of which will pass through a designated mesh sieve. The ASTM classifies particle sizes corresponding to an 80-mesh sieve (0.177 mm) and smaller as PAC. PAC is not commonly used in a dedicated vessel, owing to the high head loss that would occur. PAC is added directly to other process units, such as raw water intakes, rapid mix basins, clarifiers and gravity filters (Bansal et al., 1988).

1.5.2.2. Granular activated carbon (GAC)

The GAC is relatively larger particle size compared to PAC and consequently presents a smaller external surface. Diffusion of the adsorbate is a significant factor. These carbons are therefore preferred for all adsorption of gases and vapors as their rate of diffusion are faster. Granulated carbons are used for water treatment, deodorization, and separation of components of the flow system.

1.5.2.3. Extruded activated carbon (EAC)

It consists of extruded and cylindrical shaped activated carbon with diameters from 0.8 to 45 mm. These are mainly used for gas phase applications because of their low pressure drop, high mechanical strength, and low dust content.

1.5.2.4. Impregnated coated carbon

The porous carbons containing several types of inorganic impregnants such as iodine, silver, and cation (such as Al, Mn, Zn, Fe, Li, and Ca) have also been prepared for particular

application in air pollution control, especially in museums and galleries. Due to antimicrobial/antiseptic properties, silver loaded activated carbon is used as an adsorbent for purifications of domestic water. Drinking water can be obtained from natural water by treating with a mixture of activated carbon and flocculating agent $\text{Al}(\text{OH})_3$. Impregnated carbons are also used for the adsorption of H_2S and mercaptans. Adsorption rates for H_2S as high as 50% by weight have been reported in earlier studies (Bansal et al., 1988).

1.5.2.5. Polymer coated carbon

The carbon can be coated with a biocompatible polymer to give a smooth and permeable coat without blocking the pores. The resulting carbon is useful for hemoperfusion. Hemoperfusion is a treatment technique in which large volumes of the patient's blood are passed over an adsorbent substance to remove toxic substances from blood (Bansal et al., 1988).

1.5.3. Properties of activated carbon

1.5.3.1. Surface area

The Brunauer-Emmett-Teller (BET) analysis method is the most common method used to characterize internal surface area (Brunauer et al., 1938). They extended the Langmuir mechanism to multilayer adsorption. The Langmuir model is more applicable to some forms of chemisorption (Rouquerol et al., 2013). The BET model is used for describing physical adsorption and is based on the following assumptions (Lynch, 2003; Rouquerol et al., 2013):

- i) Each site is similar in nature and can accept one adsorbed molecule, and the surface is homogeneous.
- ii) The adsorbate molecule is small enough to cover the surface completely.
- iii) No interaction between the adsorbed molecules
- iv) For the second and higher layers, the adsorption energy is equal to that of the condensation and is constant for all layers.

The BET equation can be shown as follows:

$$\frac{p}{V_a(p^\circ - p)} = \frac{1}{V_m C} + \frac{C - 1}{V_m C} \left\{ \frac{p}{p^\circ} \right\} \quad (1.1)$$

where, V_m = monolayer capacity, p° = gas saturation pressure, p = gas pressure, C = constant which is related exponentially to the heat of the first-layer adsorption [$\exp(q_1 - q_L)/(R \cdot T_a)$], and V_a = amount of gas adsorbed on the surface at pressure p . According to this equation, a plot of $p/[V_a(p^\circ - p)]$ vs. p/p° should yield a straight line with an intercept of $1/V_m C$ and

slope of $(C-1)/V_m C$. Therefore, the values of V_m and C can be calculated using this line. Practically, the linearity of this plot is always restricted to a part of the isotherm (Gregg, 1982). For many materials, the range of linearity is for the relative pressure of 0.05-0.3, but for activated carbons, it is limited to relative pressures less than 0.1.

The pore filling by adsorbate includes a two-step process for defined range of relative pressure; monolayer formation followed by a condensation process. Micropores can be divided into two groups: a) Ultramicropores (pore diameter less than 7 Å) and b) Supermicropores (pore diameter in the range of 7-20 Å). This mechanism can be used for adsorption on supermicropores at high relative pressures (Gregg, 1982). However, in narrow micropores (ultramicropores), the pore fills in a single step over a narrow range of relative pressure. The smallest pores commence filling at very low relative pressure, e.g. 10^{-8} , which is associated with enhanced adsorbent-adsorbate interactions (Rouquerol et al., 2013). The micropores are occupied by adsorbates before the formation of monolayer coverage on the surface. The BET equation is the most commonly used isotherm equation for microporous materials and can be utilized for comparing the surface area of activated carbons.

In the last 50 years, many researchers tried to develop new methods for study the porous structure of micropores and their pore size distribution. Dubinin's theory of pore filling in micropores was used in the development of some equations such as Dubinin-Radushkevich (DR) and Dubinin-Astakhov (DA) (Dubinin and Astakhov, 1971) to calculate pore size distribution in micropores. There is some other methods for calculation of pore size distribution based on t-curve methods such as MP method (Mikhail et al., 1968) and Horvath-Kawazoe (HK) method (Horváth and Kawazoe, 1983).

Horvath and Kawazoe (HK) method is a semi-empirical, analytical method to calculate pore size distribution using nitrogen adsorption isotherm for microporous materials. The basis of this approach is a statistical analysis of a fluid with slit pores which applies to active carbons (Lowell et al., 2012). Everett and Powl (Everett and Powl, 1976) calculated the potential energy profiles of noble gas atoms adsorbed in a slit between two graphitized carbon layer planes. Horvath and Kawazoe related this power to free energy change of adsorption, resulting in a relation between filling pressure and the effective pore width. The basic idea of HK method is that the relative pressure required for the filling of micropores with a given size and shape is a function of adsorbent-adsorbate interaction energy (Rouquerol et al., 2013). This method is not applicable for mesopore size analysis (Lowell et al., 2012). The

accuracy of this approach is under discussion because of; a) the assumption that the fluid confined in the pore is similar to bulk fluid, b) the density of fluid is assumed not to be a function of its distance to the pore wall, and c) discontinuous mechanism believed for pore filling (Lowell et al., 2012).

The limitations of macroscopic thermodynamic approaches, e.g. the DR method, and semi-empirical methods such as Horvath-Kawazoe (HK) method for explaining the micropore filling resulted in using molecular-based theories based on the molecular modeling of adsorption phenomena. Seaton et al. (Seaton and Walton, 1989) were the first to propose a density functional (DFT) model for calculating the pore size distribution from adsorption isotherms, and it has been soon acknowledged that DFT provides a more reasoned and versatile approach to calculating the pore structure parameters compared to the conventional methods.

1.5.3.2. Porosity

The range of pore sizes which is defined according to the IUPAC is summarized in Table 1.6 (Sing, 1985). The porous structure of activated carbon is formed by three types of pores as shown in Fig. 1.4.

Table 1.6: IUPAC classification of pore sizes

| Pores | Pore width (W;nm) |
|-----------------|------------------------|
| Ultramicropores | $W < 0.7\text{nm}$ |
| Supermicropores | $0.7 < W < 2\text{nm}$ |
| Micropores | $W < 0.2$ |
| Mesopores | 2-50 |
| Macropores | $W > 50$ |

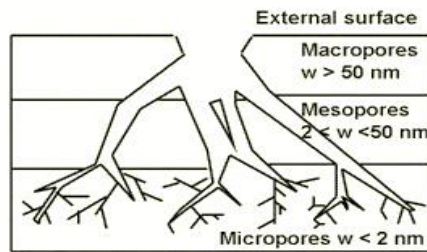


Fig. 1.4. The classification of pores.

1.5.3.3. Surface functional groups

The adsorption capacity of an AC is determined not only by the textural properties but also by the chemical nature of its surface (Bansal et al., 1988). The surface of ACs is

heterogeneous; it consists of faces of graphite sheets and edges of such layers. The edge sites are much more reactive than the atoms in the interior of the graphite sheets; chemisorbed different heteroatom, mainly containing nitrogen, hydrogen, halogen and particularly oxygen, are predominantly located on the edges (El-Sayed and Bandosz, 2004).

Oxygen in the surface oxides is bound in the form of various functional groups. The surface chemical functional groups mainly derive from activation process, precursor, heat treatment, and post chemical treatment. The surface functional groups can be classified into two broad groups; acidic groups consisting mainly carboxylic, lactones and phenols, and basic groups such as pyrone, chromene, ethers and carbonyls (Boehm, 1994; Shen et al., 2008) (Fig.1.5).

In the case of adsorption from the liquid phase, the type of surface functional groups influences the process to a large extent changing the character of interactions between the adsorbate molecules and carbon surface (Derylo-Marczewska et al., 2008; Moreno-Castilla, 2004). Thus, the acidic or basic complexes formed on adsorbent surface determine the charge, the hydrophobicity, and the electronic density of the graphite layers, explaining the adsorbent activity differences towards various substances.

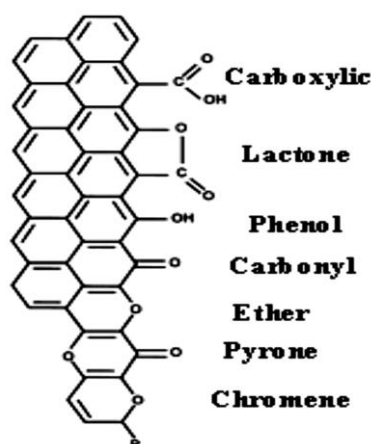


Fig. 1.5. Surface functional groups of the activated carbon.

An increase of adsorption is observed with the decrease of concentration of acidic surface groups (Moreno-Castilla, 2004; Radovic et al., 2001). The increase of acidic surface functional groups reinforces the hydrophilic nature of carbonic and thus decreases its affinity to non-polar organic compounds and conversely increases the adsorption capacity for polar molecules (Huang et al., 2008; Kim and Park, 2006; Le Leuch and Bandosz, 2007). On the other hand, basic functional groups lead mainly to hydrophobic carbons and display a strong affinity for organic molecules which have a limited solubility in water, like phenols (Stoekli and Hugi-Cleary, 2001).

Moreover, the surface charge of carbon depends on the solution pH and its point of zero charges (PZC); the pH value at which the surfaces charge is zero. For typical amphoteric carbons, the carbon surface is positively charged at $\text{pH} < \text{PZC}$ and negatively charged at $\text{pH} > \text{PZC}$. A negative charge will result from the dissociation of surface oxygen complexes of acid character such as carboxylic and phenolic groups. The positive surface charge may be due to surface oxygen complexes of basic characters like pyrones or chromenes, or due to the existence of electron-rich regions within the graphene layers acting as Lewis basic centers, which accept protons from the aqueous solution (Moreno-Castilla, 2004).

1.6. Preparation of activated carbon

Carbonization and activation are the two crucial stages in the activated carbon preparation. The essential reaction-taking place during carbonization of precursor material is the elimination of non-carbon elements (O and H are stripped off from the carbon precursor). The residual carbon atoms group into sheets of condensed aromatic system, which are often relatively irregular and disordered, leaving free interstices that, may be filled or blocked by tar deposition. Interstices or voids are formed in the char due to the misalignment of sheets of condensed aromatic systems about each other. The porosity of the char is not completely accessible. Preparation of activated carbon and development of pore structure in the char can be performed by physical or chemical activation method (Kumar and Jena, 2015; Sudaryanto et al., 2006) (Fig. 1.6).

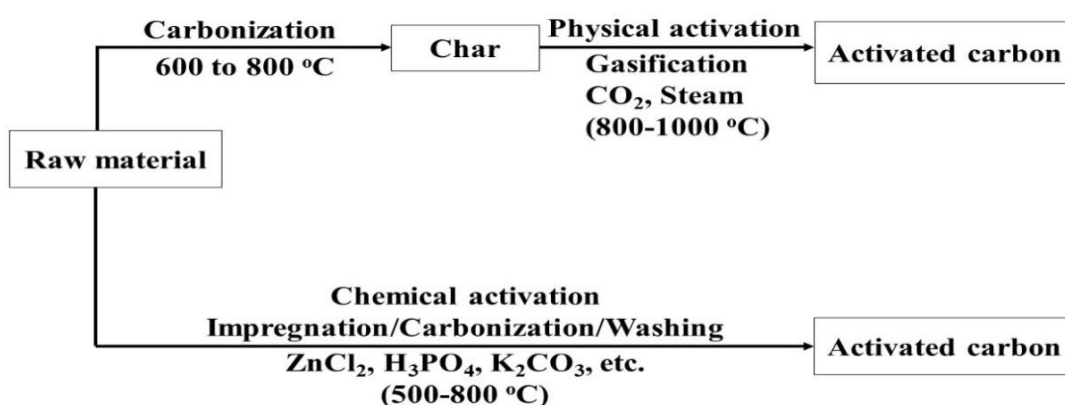


Fig.1.6. The schema of the process of activated carbon preparation.

1.6.1. Precursors

Activated carbons (ACs) can be prepared from a wide variety of cheap materials with a high carbon content and low inorganic content. The most frequently used precursors for the activated carbon preparation on a commercial scale are peat, coal, lignite, wood and coconut shell (Bansal et al., 1988). Agricultural by-products have proved to be promising raw

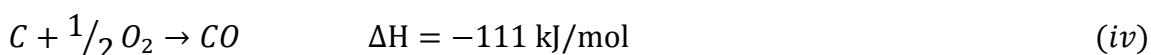
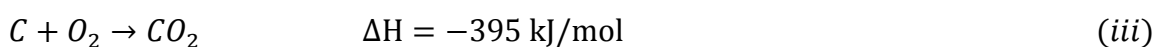
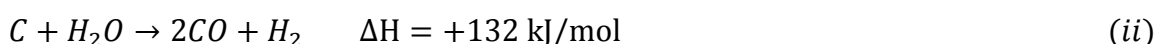
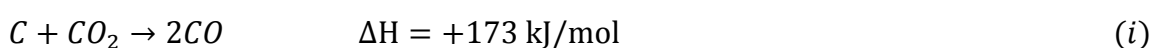
materials for the production of ACs because of their availability at a low price. They can be used for the production of ACs with a high adsorption capacity, considerable mechanical strength, and low ash content (Ioannidou, 2007); therefore, conversion of agricultural wastes into ACs is a promising alternative to solve environmental problems and also to reduce the costs of AC preparation. Literature survey indicates that many low-cost ACs have been developed from various agricultural wastes such as Vine shoot (*Vitis vinifera*) (Corcho-Corral et al., 2006), Cassava peel (Sudaryanto et al., 2006), Olive Pit (Martinez et al., 2006), Olive cake (Baçaoui et al., 2001), Date pit (Bouchenafa-Saib et al., 2005; Girgis and El-Hendawy, 2002; Haimour and Emeish, 2006), Walnut Shell (Kim et al., 2001; Martinez et al., 2006; Zabihi et al., 2010), Coffee bean husk (Baquero et al., 2003), Corn cob (Chang et al., 2000; Tsai et al., 1997; Tsai et al., 2000), Pistachio nut shells (Yang and Lua, 2003), Cherrystone (Lussier et al., 1994), Pistachio nut shells (Lua and Yang, 2005), Paulownia wood (Yorgun et al., 2009), Plum kernels (Tseng, 2007), Jatropha hull (Duan et al., 2011), Rice straw (Gao et al., 2011), Cotton stalks (Deng et al., 2009), Bagasse (Tsai et al., 2001a), Bamboo (Liu et al., 2010a), Oil-palm stones (Lua and Guo, 2001), Oil-palm stones (Lua and Guo, 2001), Seaweed (Rathinam et al., 2011), *Tectona grandis* sawdust (Mohanty et al., 2005), Vetiver roots (Altenor et al., 2009), Soybean straw (Miao et al., 2013), Pomegranate seeds (Uçar et al., 2009), Waste potato residue (Zhang et al., 2015), Sunflower oil cake (Karagöz et al., 2008), Cattle manure compost (Qian et al., 2007) and Herb residues (Yang and Qiu, 2011).

1.6.2. Physical activation

Physical activation is usually carried out via a two-step process. In the first step (carbonization), the carbonaceous precursor is pyrolyzed at a relatively low temperature in the absence of air. The resultant char is a cheap surface area material with almost no activity for pollutant sequestration (Bansal et al., 1988; Cuhadar, 2005). In this process, the carbonization temperature has the most significant effect, followed by heating rate, nitrogen flow rate, and finally, residence time (Ioannidou and Zabaniotou, 2007). Typically, higher carbonization temperatures (600–700 °C) result in reduced yield of char while increasing the liquid and gases release rate (Ioannidou and Zabaniotou, 2007). A Higher temperature will also increase ash and fixed carbon content and lower amount of volatile matter (Ioannidou and Zabaniotou, 2007; Lua et al., 2006). Thus, high temperatures result in better quality char but also decrease yield. This is due to the primary decomposition of biomass at higher temperatures and also secondary decomposition of char residue (Ioannidou and

Zabaniotou, 2007). Thus, as the temperature of primary degradation increased or the residence times of primary vapors inside the cracked particle is shorter, the char yields decrease (Pütün et al., 2005).

The second step involves the activation of the obtained char under an oxidizing atmosphere (steam or CO₂) in order to increase substantially its surface area so that the developed porosity enhances the pollutant removal from the environment. Some literature has integrated these two processes and has developed a single stage activation method. During activation, the temperature is set between 800 and 1000 °C to improve the porosity and surface area of lignocellulosic carbon (Crini, 2006; Gupta, 2009). For physical activation, steam is more efficient than CO₂, because activated carbon with a relatively higher surface area can be produced. The smaller molecule size of water is responsible for facilitating diffusion within the char's porous structure (Cagnon et al., 2009; Mak et al., 2009). Steam activation is reported to be two or three times faster than CO₂ at the same degree of conversion (Nowicki et al., 2010; Plaza et al., 2010). In the single step physical activation process, the pyrolysis is carried out under a stream of an oxidizing gas such as steam, carbon dioxide, air or a mixture (see Reactions (i)–(iv)) (Gergova and Eser, 1996; Plaza et al., 2014; Plaza et al., 2010). Due to the exothermic nature of the reaction between carbon and oxygen (air) and the difficulty of the response temperature control, steam and CO₂ are the most preferred options. Despite the advantages of a single to two-step activation process, the latter method results in the development of a higher porosity in the activated carbon (Alaya et al., 2000):



Rodríguez-Reinoso and Molina-Sabio produced four series of activated carbons from lignocellulosic materials (almond shells and olive and peach stones) by either physical activation-gasification (uncatalysed and iron catalyzed) in CO₂ or in a water-nitrogen mixture of chars or direct chemical activation with ZnCl₂ of the precursor. Activation with CO₂ opens and widens the microporosity of the char with even a shift to meso and macroporosity. The iron catalyzed CO₂ gasification and gasification with water-nitrogen mixture produce carbons with a well-developed macroporosity, although the latter has the

advantage of maintaining a well-developed micro and mesoporosity. Direct chemical activation of the precursor with ZnCl_2 provides, in only one step, a larger yield of activated carbon having microporosity as well developed as in the CO_2 gasification of the char, with the advantage of producing a much greater mesopore volume (Rodriguez-Reinoso and Molina-Sabio, 1992).

Zhang et al. (2004) were prepared activated carbon from some agricultural and forest residues, including oak wood waste, corn hulls, and corn stover. Microporous activated carbons were prepared by physical activation with CO_2 as the activating agent. The produced activated carbons had the BET surface areas ranging from 400 to 1000 m^2/g , and ratios of micropore volume to total pore volume ranging from 0.38 to 0.66. Higher the activation temperature better will be the surface areas and micropore volumes of the resultant activated carbons. The activated carbons were prepared from bagasse at a low temperature (160 °C) using chemical carbonization treatment and gasification with carbon dioxide at 900 °C. The BET surface area and median pore size of the prepared activated carbons were 614–1433 m^2/g and from 0.45 to 1.2 nm, respectively (Valix et al., 2004).

1.6.3. Chemical activation

Chemical activation is a single step process (carbonization and activation) in which the carbonaceous precursor is soaked in a dehydrating agent, such as potassium hydroxide, phosphoric acid, potassium carbonate and zinc chloride, and then activated at relatively high temperatures under an inert atmosphere. The chemical activation technique offers some advantages over the physical activation method, namely, low activation temperature, shorter heat treatment, and higher carbon yield, although it suffers from the high cost of the activating agent and the need for an extra washing step (Kaludjerović et al., 2014). It is noteworthy that applying an oxidizing environment instead of an inert atmosphere has also been reported to have a significant effect both on the porosity of the resultant activated carbons and the surface functional groups (de Yuso et al., 2014). The application of an air/steam will increase the oxygen content on the surface of the activated carbon (Puziy et al., 2007) and also will enhance the surface area and the mesopore volume due to the pore structure widening during the activation process although it may slightly decrease the yield (Hu et al., 2001; Laine and Calafat, 1989). The activating reagents for activated carbons preparation by chemical activation method are mainly alkali (KOH, K_2CO_3 , and NaOH) (Cazetta et al., 2011; Hayashi et al., 2000; Liu et al., 2013), alkali earth metal salts (FeCl_3 , and ZnCl_2) (Azevedo et al., 2007; Lua and Yang, 2005; Mohanty et al., 2005; Oliveira et

al., 2009; Ozdemir et al., 2014; Uçar et al., 2009; Yorgun et al., 2009; Zhang et al., 2015) and some acids (H₃PO₄ and H₂SO₄) (Kumar and Jena, 2016a; Karagöz et al., 2008; Liu et al., 2010a; Olivares-Marín et al., 2007; Prahas et al., 2008; Sych et al., 2012; Yorgun and Yıldız, 2015).

In the chemical activation method, the activating reagents act as dehydrating agents that inhibits the formation of tar as well as volatile substances during the process, which helps to enhance the yield of porous carbon and to decrease the activation temperature and activation time compared with the physical activation method (Lua and Yang, 2005; Pezoti et al., 2014; Yang and Qiu, 2010; Yorgun et al., 2009). Some disadvantages of the chemical activation process are corrosiveness of the process and the washing step (Lillo-Ródenas et al., 2003).

1.6.3.1. Activation with ZnCl₂

The ZnCl₂ is a dehydrating agent that may alter the pyrolysis behavior of carbon precursor materials. After mixing with carbonaceous materials, ZnCl₂ can be intercalated in the carbon matrix. Hu and Vansant, (1995) proposed the mechanism, the impregnated ZnCl₂ dehydrates the carbon material after pyrolysis, which results in charring and carbon skeleton aromatization and the pore structure creation. When the temperatures are higher than its melting point, 283 °C, liquid ZnCl₂ is formed, which is very mobile. Furthermore, temperatures higher than its boiling point, 732 °C, result in a close interaction between the zinc compounds and the carbon atoms. At 283–732 °C, a decomposition could take place:



However, temperatures higher than 732 °C are favorable for the ZnCl₂ evaporation. As a result, atomic layers of carbon may be widened, and pores are formed in the carbon matrix. During the pyrolysis, ZnCl₂ eliminates hydrogen and oxygen atoms of carbon materials as water, rather than as oxygenated organic compounds (Hu and Vansant, 1995). To get high specific surface area, ZnCl₂ is used as activating reagent among the various chemical activating agents (Azevedo et al., 2007; Hu and Vansant, 1995; Ozdemir et al., 2014; Yorgun et al., 2009). Many researchers prepared activated carbons with a high surface area from agriculture wastes by chemical activation with ZnCl₂ are shown in Table 1.7.

Table 1.7: Different precursors used for AC production with ZnCl₂ activating agent

| Raw material | Atmosphere | AT (°C) | IR | Activation time (h) | S _{BET} (m ² /g) | References |
|--|-----------------|---------|------|---------------------|--------------------------------------|--------------------------------|
| Peach stone | N ₂ | 500 | 0.96 | - | 2000 | (Caturla et al., 1991) |
| Elutrilithe (waste from coal) | - | 950 | 0.6 | 4 | 1465 | (Hu and Vansant, 1995) |
| Waste corn cob | N ₂ | 550 | 1.75 | - | 1400 | (Tsai et al., 1997) |
| Bituminous coal | - | 500 | 1.0 | 1 | 1644 | (Ahmadpour and Do, 1997) |
| Paper mill sludge | N ₂ | 800 | 3.5 | 2 | 1000 | (Khalili et al., 2000) |
| Coconut shells | N ₂ | 800 | 2 | - | 2400 | (Hu et al., 2001) |
| Pistachio nut shell | N ₂ | 400 | 0.75 | 1 | 1635.37 | (Lua and Yang, 2005) |
| | Vacuum | 400 | 0.75 | 1 | 1647.16 | |
| | Vacuum | 500 | 1.5 | 2 | 2527 | |
| Tectona grandis sawdust | N ₂ | 500 | 2 | 1 | 585 | (Mohanty et al., 2005) |
| Cattle-manure compost | N ₂ | 400 | 1.5 | 0.5 | 2170 | (Qian et al., 2007) |
| Bagasse | N ₂ | 600 | 1 | 0.5 | 750 | (Kalderis et al., 2008) |
| Rice husk | N ₂ | 600 | 0.75 | 0.5 | 674 | (Kalderis et al., 2008) |
| Olive stone | N ₂ | 650 | 0.2 | 2 | 790.25 | (Kula et al., 2008) |
| Paulownia (<i>P. tomentose</i>) | N ₂ | 400 | 4 | 1 | 2736 | (Yorgun et al., 2009) |
| Chinese fir sawdust | Vacuum | 500 | 1 | 1 | 1079 | (Juan and Ke-Qiang, 2009) |
| Pomegranate seeds | N ₂ | 600 | 2 | 1 | 978.8 | (Uçar et al., 2009) |
| Walnut shells | Vacuum | 450 | 2 | 1 | 1800 | (Yang and Qiu, 2010) |
| Sugar beet bagasse | N ₂ | 700 | 3 | 1.5 | 1826 | (Demiral and Gündüzoğlu, 2010) |
| Herb residues | Vacuum | 450 | 2.5 | | 1952 | (Yang and Qiu, 2011) |
| Safflower seed press cake | N ₂ | 900 | 4 | 1 | 801.5 | (Angin et al., 2013) |
| Grape stalk | CO ₂ | 700 | 2 | 2 | 1411 | (Ozdemir et al., 2014) |
| Sour cherry (<i>Prunus cerasus</i> L.) stones | N ₂ | 700 | 3 | 2 | 1704 | (Angin, 2014) |
| Pumpkin seed shell | - | 500 | 3 | - | 1564 | (Demiral et al., 2015) |
| Potato residue | N ₂ | 600 | 1 | 1 | 1357 | (Zhang et al., 2015) |

1.6.3.2. Activation with H₃PO₄

Among the various dehydrating agents used for chemical activation, phosphoric acid is preferred recently due to environmental and economic concerns (Yorgun and Yıldız, 2015). When compared to zinc chloride, phosphoric acid is the most preferred because of the environmental disadvantages like the corrosion and low chemical recovery. Moreover, the carbons obtained by using ZnCl₂ as an activating agent cannot be used in pharmaceutical and food industries as they may contaminate the product (Prahas et al., 2008). Phosphoric acid allows the developing both micropores and mesopores of the resulting activated carbon (Yorgun and Yıldız, 2015).

At high concentration, the phosphoric acid may exist in different forms. As the reaction/activation temperature increases, elimination of water molecules resulting in the H₃PO₄ transformation into polyphosphoric acids of a general formula of H_{n+2}P_nO_{3n+1}. It enhances the acids interactions with lignocellulosic material and phosphorylation of cellulose (Jagtoyen and Derbyshire, 1998; Jibril et al., 2008; Olivares-Marín et al., 2006). Polyphosphoric acids are formed by condensation of two or more H₃PO₄ molecules with the elimination of water as a complex mixture of linear molecules of various chain lengths (Olivares-Marín et al., 2006). This leads to the formation of phosphate esters and increases in cross-linking reactions and pore development. The oligomerized H₃PO₄ that become part of the carbon matrix decomposes and involves in gasification reactions above 350–400 °C (Olivares-Marín et al., 2006). Therefore, acid impregnation increases the density of the sample carbonized at 400 °C. Above 450 °C, the polyphosphoric acids decompose to eliminate H₃PO₄ from cellulose phosphate esters (Jagtoyen and Derbyshire, 1998). This generates more pores and hence a relative decrease in density. Furthermore, the polyphosphoric acids melt between 500 and 600 °C. In such molten form, the reactions with carbon matrix increases at high temperatures. These develop more pores and release P₄, CO₂, H₂O and other volatile materials, based on the following suggested mechanism (Olivares-Marín et al., 2006):



Many researchers prepared activated carbons with a high surface area from agriculture wastes by chemical activation with H₃PO₄ are shown in Table 1.8.

Table 1.8: Different precursors with H₃PO₄ activating agent used for AC production

| Raw material | Atmosphere | AT (°C) | IR | Activation time (h) | S _{BET} (m ² /g) | References |
|---------------------------------------|----------------|---------|------|---------------------|--------------------------------------|-------------------------------|
| Date pits | - | 700 | 60% | 2 | 945 | (Girgis and El-Hendawy, 2002) |
| Chestnut wood | N ₂ | 500 | 0.35 | 3 | 783 | (Gomez-Serrano et al., 2005) |
| Woody biomass birch | N ₂ | 600 | 1.5 | 1 | 1360 | (Budinova et al., 2006) |
| Vine shoots (<i>Vitis vinifera</i>) | N ₂ | 400 | 60% | 2 | 1666 | (Corcho-Corral et al., 2006) |
| Cherry stones | N ₂ | 500 | 3.44 | 2 | 1688 | (Olivares-Marín et al., 2007) |
| Jackfruit peel | N ₂ | 550 | 4.0 | 0.75 | 1260 | (Prahas et al., 2008) |
| Tunisian olive-waste cakes | N ₂ | 450 | 1.75 | 2 | 1062 | (Baccar et al., 2009) |
| Durian shell | - | 500 | 30% | 0.33 | 1404 | (Tham et al., 2011) |
| Olive stones | N ₂ | 500 | 60% | 2 | 1218 | (Yakout and El-Deen, 2011) |
| Corn cob | Ar | 400 | 1 | 1 | 2081 | (Sych et al., 2012) |
| <i>Lemna minor</i> | N ₂ | 500 | 3 | 2 | 531.9 | (Huang et al., 2014) |
| <i>Acacia mangium</i> wood | - | 900 | 40% | 0.75 | 1767 | (Danish et al., 2014) |
| Marigold straw | - | 400 | 2 | 2 | 1344.23 | (Qin et al., 2014) |
| Reedy grass leaves | N ₂ | 500 | 0.88 | 2 | 1474 | (Xu et al., 2014) |

1.6.3.3. Activation with K₂CO₃

Even though, the use of alkali metal hydroxides like KOH and NaOH as activating agents offers the advantage of producing high specific surface area carbon materials. The alkali metal hydroxides are corrosive, hazardous and environmentally unfriendly. Use of alkali metal carbonates such as K₂CO₃ can be a substitute for the use of alkali metal hydroxides.

Okada et al. have evaluated the effect of the nature of activating agent (Li₂CO₃, Na₂CO₃, K₂CO₃, Rb₂CO₃, and Cs₂CO₃) on the process of activation of carbon material produced from newspaper waste. The textural properties (specific surface area values and specific pore volume values) were found to be a function of the size (radii) of the alkali metal cation. Larger the cationic size (Rb and Cs) of the activating agent larger is the specific surface area value and smaller the cationic size of the activating agent smaller is the specific surface area value. Thus, the size of the alkali metal cation is an important parameter determining

the effectiveness of activating agent in the chemical activation process (Okada et al., 2003). Equations are given below describe several reactions becoming spontaneous during K_2CO_3 activation (McKee, 1983).



The atomic K may intercalate and expand the inter layers of adjacent hexagonal network planes consisting of C atoms, enhancing pore formation through hexagonal planes that are not well-developed as in graphite (Okada et al., 2003). The adjacent graphene planes are separated because of the K intercalation. Even after removal of K, either by washing with H_2O or acid, the rearranged or disordered graphene sheets of the carbon crystallite cannot go back to their original position thus leaving pores and voids. This results in an activated carbon material with high porosity and specific surface area value (Viswanathan et al., 2009). Many researchers prepared activated carbons with a large surface area from agriculture wastes by chemical activation with K_2CO_3 in N_2 or CO_2 atmosphere are shown in Table 1.9.

Table 1.9: Different precursors with K_2CO_3 activating agent used for AC production

| Raw material | Atmosphere | AT (°C) | IR | Activation time (h) | S_{BET} (m ² /g) | References |
|----------------------------|------------|---------|------|---------------------|-------------------------------|-------------------------|
| Corn cob | CO_2 | 800 | 0.15 | 1 | 1266 | (Tsai et al., 2001b) |
| Chickpea husk | N_2 | 800 | 1 | 1 | 1778 | (Hayashi et al., 2002a) |
| Pistachio shell | N_2 | 800 | 1 | 1 | 1800 | (Hayashi et al., 2002b) |
| Palm shell | CO_2 | 800 | 2 | 1 | 1170 | (Adinata et al., 2007) |
| Mangosteen shell | - | 900 | 1 | 2 | 1123 | (Chen et al., 2011) |
| Sisal waste | N_2 | 700 | 0.5 | 1 | 1038 | (Mestre et al., 2011) |
| Sunflower seed oil residue | N_2 | - | 0.67 | - | 1411.55 | (Foo and Hameed, 2011) |
| Wood sawdust | N_2 | - | 1.25 | - | 1496.05 | (Foo and Hameed, 2012a) |
| Orange peel | N_2 | - | 1.25 | - | 1104.45 | (Foo and Hameed, 2012b) |
| Waste tea | N_2 | 900 | 1 | 1 | 1722 | (Gurten et al., 2012) |
| Wool fibers | N_2 | 600 | 2 | - | 438 | (Chen et al., 2013) |

1.6.4. Adsorption of common pollutants onto activated carbon

Adsorption by activated carbon (AC) is the most attractive physicochemical treatment method for the removal of dissolved organics as well as heavy metals from wastewater. Activated carbon is used as adsorbent due to high surface area and internal pore arrangement, and presence of high surface functional groups on the surface. Many researchers have shown that AC is an effective adsorbent for some common pollutants removal, especially for phenol, methylene blue dye as well as Cr(VI) metal ion are tabulated in Table 1.10.

Table 1.10: Phenol, methylene blue and Cr(VI) adsorption on various adsorbents

| Adsorbents | Initial conc. of adsorbates (mg/L) | Q _m (mg/g) | Reference |
|---|------------------------------------|-----------------------|---------------------------------|
| Phenol | | | |
| Filtrisorb100 (commercial) | - | 206 | (Hu and Srinivasan, 1999) |
| Rice husk char | 1000 | 142.8 | (Ahmaruzzaman and Sharma, 2005) |
| <i>Tectona grandis</i> | 100 | 2.82 | (Mohanty et al., 2005) |
| Commercial activated carbon | 100 | 49.72 | (Özkaya, 2006) |
| Activated carbon-commercial grade (ACC) | 100 | 30.2187 | (Srivastava et al., 2006) |
| Activated carbon-laboratory grade (ACL) | 100 | 24.6458 | (Srivastava et al., 2006) |
| Sugarcane bagasse fly ash | 100 | 23.832 | (Srivastava et al., 2006) |
| PAC6 (commercial from PICA) | - | 154 | (Figaro et al., 2006) |
| Activated coal | 15 | 1.481 | (Vazquez et al., 2007) |
| Rattan sawdust based activated carbon | 200 | 149.25 | (Hameed and Rahman, 2008) |
| CAC1 (commercial, from Norit) | 100 | 104 | (Fierro et al., 2008) |
| CAC2 (commercial, from Norit) | 100 | 73 | (Fierro et al., 2008) |
| CS850A | 500 | 205.8 | (Din et al., 2009) |
| Vet-H ₂ O | 100 | 145 | (Altenor et al., 2009) |
| VetP0.5 | 100 | 122 | (Altenor et al., 2009) |
| WTAC | 350 | 108.4 | (Gokce and Aktas, 2014) |
| Methylene blue | | | |

| | | | |
|---|------|--------|-----------------------------|
| Rattan sawdust AC | 500 | 294.12 | (Hameed et al., 2007a) |
| Oil palm shell AC | 500 | 243.90 | (Tan et al., 2008a) |
| Vet-H ₂ O | 300 | 375 | (Altenor et al., 2009) |
| Calgon (F-400) AC | 500 | 470 | (Rodríguez et al., 2009) |
| Cotton stalk | 1500 | 315.04 | (Deng et al., 2009) |
| VetP0.5 | 300 | 423 | (Altenor et al., 2009) |
| Commercial AC | 1000 | 370 | (Reffas et al., 2010) |
| Coffee grounds AC | 1000 | 367 | (Reffas et al., 2010) |
| Coconut shell AC | 1000 | 916 | (Cazetta et al., 2011) |
| Cocoa shell AC | 250 | 213 | (Ahmad et al., 2012) |
| NAC60 | 350 | 683.6 | (Gokce and Aktas, 2014) |
| Buriti shells (<i>Mauritia flexuosa</i> L.)AC | 500 | 275 | (Pezoti et al., 2014) |
| Pine Cone AC | 100 | 60.97 | (Özhan et al., 2014) |
| Grape industrial processing waste AC | 900 | 417 | (Saygılı et al., 2015) |
| Tomato processing solid waste AC | 900 | 400 | (Saygılı and Güzel, 2015) |
| Grapefruit AC (GAC) | 220 | 456.28 | (Nowicki et al., 2016) |
| Cr(VI) | | | |
| Coconut shell carbon | - | 20.00 | (Alaerts et al., 1989) |
| Sugarcane bagasse | 500 | 13.40 | (Sharma and Forster, 1994) |
| Leaf mould | 1000 | 43.10 | (Sharma and Forster, 1995) |
| Hazelnut shell | - | 17.70 | (Cimino et al., 2000) |
| Tyres activated carbon | 60 | 58.50 | (Hamadi et al., 2001) |
| Coconut tree saw dust | 20 | 3.6 | (Selvi et al., 2001) |
| F400 (CAC) | 60 | 48.54 | (Hamadi et al., 2001) |
| Beech sawdust | 200 | 16.10 | (Acar and Malkoc, 2004) |
| Coconut shell carbon | 25 | 10.88 | (Babel and Kurniawan, 2004) |
| Treated sawdust of Indian rosewood | 10 | 10.00 | (Garg et al., 2004a) |
| <i>Hevea Brasiliensis</i> (Rubber wood) sawdust | - | 44.05 | (Karthikeyan et al., 2005) |

The table shows the good adsorption capacity of the various adsorbents prepared from different carbonaceous materials with different initial concentrations of the adsorbates.

1.6.5. Regeneration of activated carbon

Reuse of activated carbon reduces the cost of the adsorption process. It is to desorb the retained substances efficiently and again repeated use of the adsorbent (Chiang et al., 1997; Sabio et al., 2004). Spent activated carbon can be regenerated by methods such as chemical regeneration, thermal regeneration, and electrochemical treatment. Among these methods, the thermal regeneration is the most commonly used because of its simplicity, high efficiency and solvent free process (Chiang et al., 1997; Torrents et al., 1997). Thermal regeneration consists of the following processing steps (Suzuki et al., 1978; Van Deventer and Camby, 1988): (1) drying at around 105 °C, (2) pyrolysis under an inert atmosphere and (3) gasification of residual organics by oxidizing gas, such as steam or CO₂. The second step is a complicated process consisting of thermal decomposition, thermal cracking, desorption of decomposition products, and partial cracking followed by polymerisation of the residuals (Sabio et al., 2004; Suzuki et al., 1978) , and the yield of the spent carbon decreases after processing.

1.7. Adsorption studies in column

The batch adsorption experiments are usually done to measure the effectiveness of adsorption for removing adsorbates as well as to determine the maximum adsorption capacity. Batch reactors are comfortable to use in the laboratory scale study but less convenient for industrial applications. The continuous adsorption in the fixed-bed column is frequently applied to industrial applications (Ahmad and Hameed, 2010; Chern and Chien, 2002; Dwivedi et al., 2008). The fixed-bed columns are simple to operate and can be scaled-up from a laboratory process. Fixed-bed adsorption has been applied to remove organic contaminants from many years with encouraging results. The reason is the high adsorption capacities in equilibrium with the influent concentration rather than the effluent concentration can be achieved (Dwivedi et al., 2008). A continuous packed bed does not operate under equilibrium conditions. The effect of flow condition (hydrodynamics) at any cross-section in the column affects the flow behavior. The flow behavior and mass transfer aspects become different beyond a particular length to diameter ratio of the column (Ahmad and Hameed, 2010; Singh et al., 2009b).

In dynamic column adsorption process, solution continuously enters and leaves to the column, so that the complete equilibrium is never established at any stage between the solute and the amount adsorbed. At each time, it meets the fresh concentrations, and hence, the established equilibrium in column mode is termed as dynamic equilibrium (Dwivedi et al., 2008).

In order to design and operate fixed-bed adsorption process successfully, the breakthrough (BT) curves under specified operating conditions must be predictable. The shape of the BT curve is influenced by the special transport process in the column filled with an adsorbent (Ahmad and Hameed, 2010; Vázquez et al., 2006). Adsorption in fixed-bed columns using activated carbon has been widely employed in industrial processes for the removal of contaminants from effluents, since it does not require the addition of chemical compounds in the separation process (Ahmad and Hameed, 2010; Chern and Chien, 2003; Walker and Weatherley, 1997).

1.8. Biological treatment

Biological treatments are effective secondary treatment methods for treatment of highly polluted industrial wastewaters. These are economical and eco-friendly than any other advanced wastewater treatment due to its low operating and maintenance cost. Several types of biological processes are used to treat wastewater, including activated sludge process, constructed wetlands, and various types of filtration. The anaerobic and aerobic systems are commonly used to deal with the wastewater in biological method (Pant and Adholeya, 2007).

1.8.1. Biodegradation

Biodegradation is a process by which microorganism breakdown the toxic chemical compounds found in the environment through metabolic or enzymatic action. A large number of natural and synthetic organic compounds are utilized by the microbes as their energy and nutrient source. A portion of the organic material, serving as a primary electron and energy source, is converted to oxidized end products through oxidation/reduction reactions. The another portion of the organic carbon is converted into the cellular material (Basha et al., 2010). They are biodegraded into less complex metabolites, and through mineralization into inorganic minerals, H_2O , CO_2 (aerobic) or CH_4 (anaerobic). Biodegradation of pollutants depends on various factors such as the environmental conditions, number and type of the microorganisms, nature and chemical structure of the

contaminant. The rate of biodegradation depends on parameters like pH, temperature, oxygen, microbial population, the degree of acclimation, accessibility of nutrients, the chemical structure of the compound, the concentration of pollutants, cellular transport properties, and chemical partitioning in growth medium (Gargouri et al., 2011; Haritash and Kaushik, 2009).

Advantages and limitations of bioremediation techniques

➤ Advantages of bioremediation

- It is cost effective and ecofriendly in nature.
- Toxic chemicals are removed from the environment and not just merely separated.
- Less energy and manual supervision is required as compared to other technologies.

➤ Limitations of bioremediation

- The process of bioremediation is slow and time required is in the days to months.
- For in situ bioremediation site must have soil with high permeability.
- Substantial gaps exist in the understanding of microbial ecology, physiology and genetic expression. A stronger scientific base is required for rational designing of process and implementation.

Phenol is a very common organic pollutant found in the effluents of industries like petrochemical, coke ovens, phenolic resin production and fiber glass manufacturing at very high concentrations. Phenol containing wastewater cannot be discharged in to the environment without prior treatment because of its high toxicity. Biodegradation is very suitable for the treatment of phenol present in wastewater. A number of microorganisms have been reported to degrade phenol at various concentrations as tabulated in Table 1.11.

Table 1.11: Biodegradation of phenolic compounds by free microbial cells

| Microorganism | Pollutants | Source of isolation | Maximum phenol conc. degraded (mg/L) | Time required (hr) | References |
|--|------------|---------------------|--------------------------------------|--------------------|-----------------------|
| <i>Acinetobacter calcoaceticus</i> (NCIB 8250) | Phenol | Culture collection | 280 | 120 | (Paller et al., 1995) |
| <i>Arthrobacter</i> species (MTCC 1553) | Phenol | - | 50-100 | - | (Kar et al., 1997) |

| | | | | | |
|--|------------------------------|--|-------------|-------|------------------------------|
| <i>Alcaligenes fecalis</i> | Phenol | Amazonian forest soil | - | - | (Bastos et al., 2000) |
| <i>Pseudomonas putida</i> DSM 548 | Phenol | - | 1-100 | - | (Monteiro et al., 2000) |
| Mixed culture. | Phenol | Saline environments | 320 | 68 | (Peyton et al., 2002) |
| <i>Pseudomonas putida</i> (MTCC 1194) | Phenol | - | 1000 | 162 | (Kumar et al., 2005) |
| <i>Acinetobacter</i> sp. | Phenol | Aerobic granules | 1000 | - | (Adav et al., 2007) |
| <i>Alcaligenes faecalis</i> | Phenol | Activated sludge from municipal gasworks | 1600 | 76 | (Jiang et al., 2007) |
| <i>Acinetobacter</i> sp. | Phenol | Activated sludge of wastewater treatment plant | 1100 | - | (Ying et al., 2007) |
| <i>pseudomonas putida</i> (ATCC 31800) | Phenol | - | 200 | - | (Annadurai et al., 2008) |
| Mixed culture | Phenol | Sewage treatment plant | 100-800 | 10-70 | (Saravanan et al., 2008b) |
| <i>Paenibacillus</i> sp. and <i>Bacillus cereus</i> (Mixed culture) | Lignin and pentachlorophenol | Paper and pulp mill effluent sludge | 500 | 168 | (Singh et al., 2009a) |
| <i>Pseudomonas</i> sp. | Phenol | Pharmaceutical industry wastewater sludge | 700 | 30 | (Shourian et al., 2009) |
| <i>Bacillus</i> sp. | Phenol | Oil refinery and exploration sites | 1000 | - | (Banerjee and Ghoshal, 2010) |
| <i>Pseudomonas putida</i> Tan-1 and <i>Staphylococcus aureus</i> Tan-2 | Phenol | Soil | 600 and 800 | 35 | (Senthilvelan et al., 2014) |

| | | | | | |
|----------------------------------|---------------------------|------------------|--------------------------|----|----------------------|
| <i>Pseudomonas putida</i> CSY-P1 | p-hydroxybenzoic acid | Soil | 500 | 48 | (Chen et al., 2015) |
| <i>Pseudomonas putida</i> LY1 | Phenol and 4-chlorophenol | River sediment | (20-400) and (15 and 40) | - | (Wang et al., 2015) |
| <i>Acinetobacter</i> sp. BS8Y | Phenol | Activated sludge | 600 | 24 | (Jiang et al., 2013) |

1.8.2. Biodegradation by using immobilized cell

Immobilized cell technology is an advanced technique allowing for compacting and maintaining a large number of cells in biotreatment systems for removing organic pollutants from contaminated wastewater. Immobilization of cells as biocatalysts is almost as common as enzyme immobilization. Immobilization is the restriction of cell mobility within a defined space (Aksu and Bülbül, 1999; Lin et al., 2009). Immobilization of microorganisms on inert supports shows an increasing interest to allow obtaining much more profit from the process. It improves microbial performance, and provides excellent operational stability. The main advantages in the use of immobilized cells in comparison with suspended ones include the retention in the reactor of higher concentrations of microorganisms, protection of cells against toxic substances and eliminates the costly processes of cell recovery and cell recycle (Dursun and Tepe, 2005). Apart from these advantages, the use of immobilized microbial cells also has few disadvantages. One of the major problems of immobilization is diffusion limitation. In such case, the control of micro-environmental conditions is difficult because of the resulting heterogeneity in the system. With viable cells, growth and gas evolution can lead to significant mechanical disruption of the immobilizing matrix (Aksu and Bülbül, 1999; Chung et al., 2003; Dursun and Tepe, 2005; Prieto et al., 2002).

Immobilized microbial cells produce extracellular polymeric substances or exopolysaccharides (EPS) in order to adhere to a solid support, protect themselves from the toxic environment. The EPS composition plays an important role during the operation of a bioreactor (Liu and Fang, 2002; Rangappa et al., 2016). The EPS is comprised of polysaccharides, proteins, humic substances, lipids and other minute substances. It is produced by microbial cells from a complex matrix where microbial cells are embedded within and are called biofilm. It helps in adhesion and cohesion of the biofilm on a solid support and provides structural strength for the biofilm (Andersson et al., 2009; Rangappa et al., 2016). The EPS composition depends on the microbial genetics, environmental

conditions and the substrate nature. These conditions, in turn, are the key factors for biofilm properties like biofilm density, porosity, water content, etc. (Rangappa et al., 2016).

Biodegradation of phenol using pure and mixed cultures of suspended bacteria has been widely studied. However, at a higher initial concentration of phenol, the growth as well as the degradation activity of the free cells gets inhibited due to toxicity. Hence, a number of strategies have been developed to overcome this problem. Immobilization of cells is a very useful technique for protecting the microbial cells against toxic shock from high phenol concentration (Dursun and Tepe, 2005). Various studies where phenol has been treated by immobilized cell technology are tabulated in Table 1.12.

From Table 1.12, it can be concluded that the activated carbon is more beneficial for the microbial growth than other supporting materials such as Ca-alginate beads, polyacrylamide, etc. Biological activated carbon (activated carbon with attached microorganism) can be utilized at very high concentrated phenolic wastewater due to its higher adsorption capacity than other supporting materials. It minimizes the toxic effect of the high phenol concentration by sudden decrease in the concentration. Therefore, the combined process of adsorption and biodegradation can be the future of the treatment techniques for the removal of organic pollutants like phenol from the wastewater.

Table 1.12: Biodegradation of phenol by immobilized cells

| Microorganism | Immobilization material | Pollutants | Conc. mg/L | References |
|--|-------------------------|------------|------------|-------------------------------|
| <i>Pseudomonas putida</i> | Polysulfone fibers | Phenol | 2000, 3500 | (Loh et al., 2000) |
| <i>Pseudomonas putida</i> MTCC 1194 | Ca-alginate | Phenol | 100-1000 | (Bandhyopadhyay et al., 2001) |
| <i>Candida tropicalis</i> | Polyacrylamide (PAA) | Phenol | 1000-5000 | (Chen et al., 2002) |
| <i>Pseudomonas putida</i> CCRC14365 | Ca-alginate | Phenol | 1000 | (Chung et al., 2003) |
| <i>Ralstonia eutropha</i> | Ca-alginate | Phenol | 100 | (Dursun and Tepe, 2005) |
| <i>Acinetobacter</i> sp. XA05 and <i>Sphingomonas</i> sp. FG03 | Polyvinyl alcohol (PVA) | Phenol | 800 | (Liu et al., 2009) |

| | | | | |
|-----------------------------------|----------------------------|--------|-------|------------------------|
| <i>Pseudomonas putida</i> | Polyvinyl alcohol (PVA) | Phenol | 300 | (El-Naas et al., 2009) |
| <i>Bacillus amyloliquefaciens</i> | Alginate–chitosan–alginate | Phenol | 2-20 | (Lu et al., 2012) |
| <i>Pseudomonas putida</i> | Activated carbon fiber | Phenol | 10000 | (Ma et al., 2013) |

1.8.3. Adsorption assisted biodegradation

Activated carbon adsorption has been widely applied in removing organic matters from wastewater as it has a large surface area and a strong affinity for attaching organic substances even at low concentration. Granular activated carbon (GAC) is one of the best adsorbents for removing various organic contaminants (Nishijima et al., 1997). The GAC adsorption systems are therefore considered to be employed in sewage treatment plant producing high quality effluent of which it can be reused for various purposes. However, even though it has high adsorption capacity, GAC can only maintain its adsorption capability for a short period of time until all its available active site gets exhausted with organic pollutants (Aktaş and Çeçen, 2007). It is well known that GAC is also a good support media for microbial growth. Thus, biological GAC (BGAC) with attached biomass can effectively remove organic contaminants both by adsorption and biodegradation (Carvalho et al., 2007; Nishijima et al., 1997). The concept of bioadsorption is more dominant till GAC is in full adsorption capacity and after that biodegradation play a significant role (Aktaş and Çeçen, 2007; Hoang, 2005). The GAC bio-adsorption is usually applied in the bioreactors with either fixed bed or fluidized bed configurations (Aktaş and Çeçen, 2007). Many researchers investigated the removal of various contaminants by the biological activated carbons and a few has been tabulated in Table 1.13.

Table 1.13: Removal of adsorbates onto biological activated carbons

| Microorganism | Immobilization material | Pollutants | Conc. mg/L | Efficiency | References |
|---|-------------------------|------------|------------|------------|-------------------------------|
| Microorganisms | Activated Carbon | Phenol | 1.9-1000 | 92-100% | (Ivancev-Tumbas et al., 1998) |
| <i>Pseudomonas pictorum</i> (NICM-2077) | Activated Carbon | Phenol | 200-600 | - | (Annadurai et al., 2000) |

| | | | | | |
|-------------------------------------|--|--------------------|------------|------------------|----------------------------------|
| Microorganisms | Powdered activated carbon | 2-chlorophenol | 100-800 | - | (Lee and Lim, 2005) |
| <i>Pseudomonas putida</i> | activated carbon | Phenol | 1,000 | - | (Wang and Li, 2007) |
| <i>Pseudomonas putida</i> | Granular activated carbon | Cyanide | 100 | 96.7% | (Dash et al., 2009) |
| <i>Bacillus amyloliquefaciens</i> | Alginate–chitosan–alginate | Phenol | 2-20 | - | (Lu et al., 2012) |
| <i>Micrococcus</i> sp. | Activated carbon | 2-methylisoborneol | 515 | 98.4% | (Yuan et al., 2012) |
| <i>Serratia</i> sp. | Iron Impregnated-Granular Activated Carbon | Phenol and Cyanide | 200 and 20 | 99% | (Agarwal and Balomajumdar, 2013) |
| <i>Pseudomonas putida</i> | Activated carbon fiber | Phenol | 10000 | - | (Ma et al., 2013) |
| <i>Serratia odorifera</i> MTCC 5700 | Activated carbon | Phenol and cyanide | 300 and 30 | 89.88 and 93.06% | (Singh et al., 2016) |

Treatment of the wastewater by the biofilm reactor is more efficient than the suspended cell reactor (Qureshi et al., 2005). Various advantages of the application of biofilm reactor are the retention of higher concentrations of microorganisms in the reactor, protection of cells against toxic shock due to high concentration of contaminants and cell recovery as well as cell recycle.

1.9. Treatment in biofilm reactor

1.9.1. Bioreactors

The main reactor types applicable for the suspension of particulate biofilm in wastewater treatment processes are Biofilm upflow sludge blanket (BUSB), Fluidized bed bioreactor (FBBR), Expanded granular sludge blanket (EGSB), Biofilm airlift suspension (BAS), and Internal circulation (IC) reactors (Fig. 1.7). These reactors are better than the conventional freely suspended cell bioreactors due to the potential advantages of continuous reactor

operation at any desired liquid throughput without risk of cell washout, protection of cells from toxic substrates, higher growth rate resulting in high concentration of cells in the reactor, easy cell-treated water separation, enhanced gas-liquid mass transfer rate, plug flow operation by maintaining the immobilized cells as a stationary phase (Jena et al., 2005).

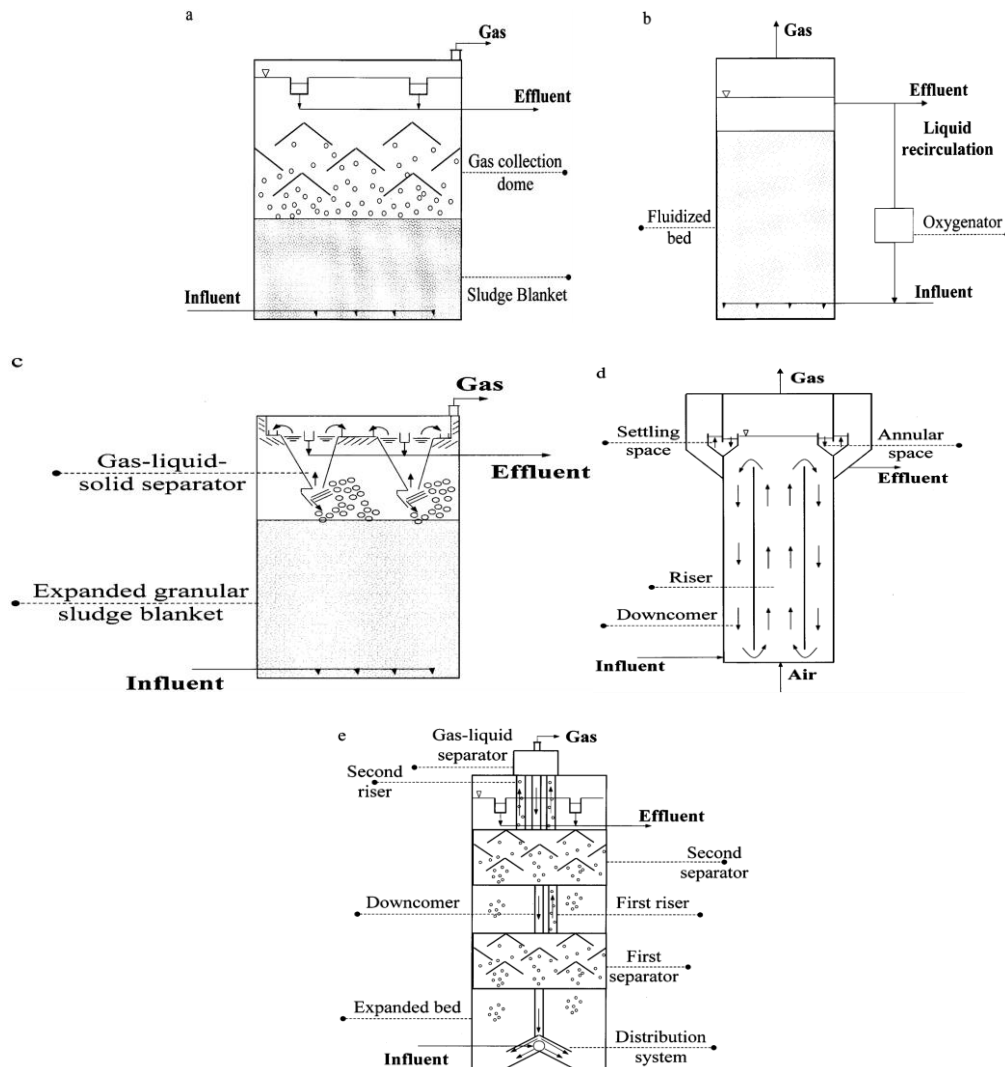


Fig. 1.7. Biofilm reactor configurations (a) USB; (b) BFB; (c) EGSB; (d) BAS; (e) IC (Nicolella et al., 2000).

The fluidized bed bioreactor is shown to perform better than other types of bioreactors (Tang et al., 1987; Vinod and Reddy, 2005). The superior performance of the fluidized bed bioreactor is due to high biomass concentration because of immobilization of cells onto the solid particles.

1.9.2. Fluidized bed bioreactor

During the past few years, the application of the fluidization technique in the field of biotechnology has increased considerably (Rajasimman and Karthikeyan, 2007; Tang and

Fan, 1989). The main application of fluidization principle is in the field of environmental biotechnology. Fluidized bed bioreactor has several advantages over other conventional reactors for the treatment of wastewater. Fluidized bed bioreactor (FBBR) is conventionally operated with up flow systems for either gas-solid, liquid-solid or gas-liquid-solid phases where the density of bioparticles (support particles coated with biofilm) is higher than the density of the medium (Begum and Radha, 2014; Tang and Fan, 1989). The achievement of high biomass concentration in FBBR makes its superior performance over that of the conventional packed bed fixed film bioreactor in a variety of wastewater treatment applications. The fluidized bed bioreactors are superior in performance due to cells immobilization on solid particles reducing the time of treatment, the volume of the reactor is extremely small, lack of clogging of biomass and removal of a pollutant like phenol even at lower concentrations (Jena et al., 2005).

The limitation of the fluidized bed reactor in wastewater treatment is the biofilm thickness as microorganism in a biofilm multiply, biofilm thickness increases. This limits diffusion of oxygen and the organic substrate to the deeper layers of the biofilm. Starvation of the microorganisms at the lower layer of the biofilm causes pieces of the biofilm to detach and leads to ineffective bioreactor operation. In the fluidized bed bioreactor with low-density particles, the control of biofilm thickness is achieved within a narrow range and it was found that this bioreactor is more efficient when used for biological aerobic wastewater treatment (Nikolov and Karamanev, 1987; Rajasimman and Karthikeyan, 2007).

In FBR, the prevailing turbulence may release part of the biomass that covers the solid particles thus maintaining a proper mass transfer rate through the microbial film. However, an excessive detachment and washout of the microbial biofilm adhered to solid particles could diminish the volumetric reaction rate. Biomass detachment could be reduced using porous particles as carriers, such as granular activated carbon (GAC) and a non-turbulent regime in the FBR. The adsorption of microbial cells onto granular activated carbon (GAC) offers a naturally immobilized cell system in which microorganisms are attached to their support by weak (noncovalent), electrostatic interactions (Junter and Jouenne, 2004). Under suitable environmental conditions, the adsorption step may be followed by microbial colonization of the microtubular network of the porous support. The biological activity of the activated carbon is meaningful in removing dissolved pollutants from wastewater. The porous support material may adsorb the organic pollutant and by microbial action, the GAC is bioregenerated. The role of bioregeneration process in renewing the adsorbent surface for

further adsorption of organics during simultaneous adsorption and biodegradation processes has been well recognized (Lee and Lim, 2005). Various researchers studied the removal of phenol, and other organic compounds by the immobilized microbial particles in fluidized bed bioreactor as well as other bioreactors, which has been tabulated in Table 1.14.

Table 1.14: Literature review of phenol and other organic compounds treatment in bioreactors

| Microorganism | Pollutants | Immobilization material | Efficiency in terms of Phenol degradation | Reactor | References |
|---|------------|---|--|------------------------------|-------------------------------|
| <i>Pseudomonas putida</i> | Phenol | Activated carbon | 5×10^{-7} kg phenol per kg active carbon particle | FBBR | (Beyenal and Tanyolaç, 1998) |
| Mixed culture of NCIB 8250 (<i>Acinetobacter</i> sp.), NCIB 10535 (<i>Pseudomonas</i> sp.), and NCIB 1015 (<i>Pseudomonas</i> sp.) | Phenol | Calcined diatomaceous earth, Celite R-632 | Complete degradation of feed concentration of 200 mg/L phenol with dilution rate of 0.15-0.2.5 h ⁻¹ | FBBR | (Livingston and Chase, 1989) |
| <i>Candida tropicalis</i> | Phenol | 4% Agar solution | 3500 mg/L | FBR | (Juárez-Ramírez et al., 2001) |
| <i>Pseudomonas putida</i> | Phenol | Calcium alginate beads | 500 mg/L/d | FBBR | (Gonzalez et al., 2001) |
| <i>Pseudomonas putida</i> Q5 | Phenol | Sand particles | 251- 592 mg/L phenol | FBBR | (Onysko et al., 2002) |
| Activated sludge | Phenol | Polypropylene (KMT) particles | 99% degradation of 990 mg/L | FBBR | (Sokół and Korpál, 2004) |
| Mixed culture | Phenol | - | 100-2500 mg/L | Activated sludge reactor | (Amor et al., 2005) |
| Mixed culture | Phenol | Membrane | 500-3000 mg/L | Immersed membrane bioreactor | (Marrot et al., 2006) |

| | | | | | |
|--|-------------------------------|------------------|--|--------------------|------------------------------|
| <i>Pseudomonas</i> sp. | Phenol | Plastic beads | Complete degradation of 1034 mg/L | FBBR | (Vinod and Reddy, 2006) |
| Mixed culture | Phenol/m-cresol | - | 600 mg/L | Airlift bioreactor | (Saravanan et al., 2008a) |
| <i>Thiobacillus</i> RAI01 | Toxic petroleum spent caustic | Ca-alginate | - | FBBR | (Potumarthi et al., 2008) |
| Undefined microbial culture | Phenol | Plastic beads | 10×10^{-2} to 30×10^{-2} kg/m ³ | FBBR | (Eswari and Rajendran, 2012) |
| Undefined microbial consortium | Trichlorophenol and phenol | Activated carbon | 99.9 % degradation of 30 mg/L | FBBR | (Poggi-Varaldo et al., 2012) |
| <i>Burkholderia multivorans</i> , <i>Polaromonas jejuensis</i> and <i>Roseomonas</i> sp. | Oil sands | GAC | - | FBBR | (Islam et al., 2014) |
| <i>Bacillus cereus</i> (AKG1 MTCC 9817 and AKG2 MTCC 9818) | Petroleum wastewater | Ca-alginate | 2545 mg/L (98.03%) | FBBR | (Banerjee and Ghoshal, 2016) |

1.9.3. Hydrodynamic studies of three-phase fluidized beds with low-density particles

Low-density solid particles found huge application in bioreactor for aerobic wastewater treatment. Hydrodynamics study of three-phase fluidized bed with low density particles are rarely found in literature although a tremendous research work exists for moderate or high density solid particles (Mishra, 2013). Under conditions typically suitable to biochemical application, Nore, et al. (1992) studied hydrodynamics, gas-liquid mass transfer and particle-liquid heat and mass transfer in three-phase fluidized bed with light particles. Polypropylene beads with inclusion of mica in the density range from 1130 to 1700 kg/m³ was reported to be used in the study. The study mainly focused on the effect of liquid and gas velocities on hydrodynamic parameters such as; bed porosity and liquid holdup. An increase in bed porosity for both increase in the gas velocity and the liquid velocity has been reported. Sokół and Halfani (1999) investigated hydrodynamic behaviour of low-density solid [Kaldnes Miljotechnologies AS (KMS)] support in gas-liquid-solid fluidized bed. They reported dependence of minimum fluidization air velocity on the ratio of bed to reactor

volume and mass of cell growth on the particles. They were also established that the air hold depends on air velocity, ratio of bed to reactor volume and mass of biomass-laden particles. Significance of operational parameters on biodegradation of organics in fluidized bed bioreactor with low-density solid particles were studied by Sokół (2001) and Sokół and Korpál (2004).

Three-phase fluidized bed hydrodynamics by statistical, fractal, chaos and Brians and Ellis (2005) characterized wavelet analysis. They determined optimum fluid velocity and ratio of volume of bed to volume of reactor for largest degradation of phenol. Hydrodynamic parameters; the minimum fluidization velocity, the pressure drop, the expansion, the bed porosity, the gas retention and the stirring velocity were studied by Allia et al. (2006) using solid particles covered with a biofilm fluidized by air and contaminated water. Rajasimman and Karthikeyan (2006) have determined the optimum air holdup and expanded bed height for maximum aerobic digestion of starch wastewater in fluidized bed bioreactor with low-density particles. Mishra, 2013 have characterized the minimum fluidization velocity and bed expansion behaviour of low-density particles (polypropylene beads with filler to vary the density) in a three-phase fluidized bed with air and water as the gas and liquid phases respectively. It has been reported that the minimum fluidization velocity and bed expansion are not a function of the bed mass (initial static bed height).

Although some studies on hydrodynamics are found in literature with low density solid particles, but the use of granular activated carbon as the solid phase were not established. In addition, the low-density particles used in the previous studies are of moderately higher size. Smaller low-density particles of size less than 2 mm were not observed.

1.10. Scope and objective of the present study

Literature study reveals that adsorption is one of the most desirable method for the treatment of various organic and inorganic pollutants present in the wastewater. Even though activated carbons are highly versatile adsorbents, the main drawback of the adsorption process associated with them is the cost of the activated carbons. Various attempts have been made to prepare activated carbons from cheap and easily available raw materials or waste materials. Agricultural and industrial wastes are used as an alternative raw material to prepare low cost activated carbons. Agricultural wastes are mostly focused as they have low ash content and high carbon and volatile matter, which is a prerequisite for being the precursor of a competent activated carbon. Fox nutshell is an agricultural waste obtained from Fox nut processing units. The Fox nut (*Euryale ferox*) belongs to water lily family

(Nymphaeaceae) is cultivated in perennial water bodies in tropical as well as subtropical climate. It is commonly known as Makhana, Black Diamond or Gorgon Nut. It is a widely cultivated plant in India. The fox nut shells meets all the prescribed criteria for being a precursor of efficient activated carbon. Its low ash content, high carbon and volatile material along with easy availability makes it a suitable candidate.

As evidenced from the literature, several types of organic and inorganic pollutants has been detected in both industrial as well as municipal wastewaters. They can be categorized mainly into the hydrocarbons (predominantly phenolic compounds), dyes and heavy metals. These are highly toxic in nature and affects both terrestrial as well as aquatic life adversely. Hence remediation of these pollutants employing various treatment techniques has been the focus of research for a quite long time. Available treatment methods can be categorized into physicochemical methods and biological treatment methods. The physicochemical methods are mostly employed for the treatment of the inorganic pollutants, while organic pollutants are treated efficiently using the biological treatment methods. Among the physicochemical methods, adsorption is able to treat wastewater containing high concentration of the pollutants but to completely remediate the pollutants from the wastewater, biological treatment method is being opted. Hence, if both the treatment methods were been combined, then wastewater containing high concentration of contaminants can be remediated completely.

Literature suggests, wastewater treatment using biofilm reactor has a better efficiency than the suspended cell bioreactor. Among the available reactor types, fluidized bioreactors demonstrate a better performance due to employment of cell immobilization technique. Therefore, incorporation of the above treatment methods in the fluidized bed bioreactor will open the gateway for the efficient treatment of highly concentrated wastewater in industrial scale.

In the present study, an attempt has been made to prepare and characterize activated carbon from cheap and easily available agricultural waste, fox nut shell. The prepared activated carbons were to be utilized for the treatment of synthetic wastewater containing various organic and inorganic contaminants in both batch as well as continuous scale. The primary objectives of the present research work are summarized below:

1. Preparation and characterization of activated carbon from Fox nutshell, a potential precursor with high carbon and high volatile matter content, under ideal operating

conditions such as; activation time, heating rate, activation temperature and chemical impregnation ratio.

2. To study the adsorption potential of the prepared activated carbons for the removal of various organic and inorganic water pollutants such as; phenol, methylene blue, and Cr(VI).
3. Fixed column study to characterize the performance of prepared activated carbons for the adsorption of phenol, methylene blue, and Cr(VI), as batch adsorption study is unable to generate sufficient necessary information for designing and operation of continuous treatment system.
4. Evaluation of various process parameters and the efficiency of adsorption assisted biodegradation. Characterization of the process for phenol biodegradation by biological granular activated carbon (BGAC) in batch scale.
5. Hydrodynamic studies of three-phase Fluidized bed reactor by using granular activated carbon (GAC).
6. Characterization of Fluidized bed bioreactor for biodegradation of phenol by biological granular activated carbon (BGAC).

1.11. Organization of the thesis

The main thesis comprises of seven chapters. Chapter-1 deals with the introduction and literature review. Chapter-2 details on the experimental aspects starting from materials and experimental setups to techniques. Chapter-3 presents the preparation and characterization of activated carbons prepared from Fox nutshell through chemical activation route using different chemical activators. Adsorption studies of the various types of the adsorbates like phenol, methylene blue and Cr(VI) in batch, and in fixed bed is discussed in chapter-4. Chapter-5 reports the experimental results obtained by application of developed biological activated carbon for adsorption assisted biodegradation of phenol in batch scale. In Chapter-6, a fluidized bed bioreactor with granular activated carbons is first characterized for hydrodynamic behavior then the performance of the same for biodegradation with immobilization of bacterial strain of *Pseudomonas putida* (MTCC 1194) is evaluated. In Chapter-7, overall conclusions and scope for future work have been presented.

Chapter 2

Materials and Methods

This chapter describes in detail about the materials and methods and laboratory experimental setup used and the experimental procedure adopted in this research work. The details include the raw material selection, the procedure adopted for the preparation of activated carbons, experimental procedure related to the application of prepared activated carbons in adsorption of phenol, methylene blue and Cr(VI) removal from synthetic wastewater. Finally, methods of adsorption assisted biodegradation study and treatment of phenol in fluidized bed bioreactor (FBBR) including its hydrodynamics are also discussed in this chapter.

2.1. Activated carbon preparation

2.1.1. Precursor

In this study, the Fox nutshell (*Euryale ferox*) (see Fig. 2.1) was used as a precursor material for activated carbons preparation due to its relatively small ash and high carbon content. The botanical classification of the Fox nut is shown in Table 2.1. The Fox nutshell was collected from a local Fox nut-processing unit from Madhubani district of Bihar state of East India. Before chemical activation process, the collected Fox nutshell was dried naturally and then at 110 °C for 24 hr.



Fig. 2.1. Fox nut flowering, seedpods, seed, edible part and shell.

Table 2.1: Scientific classification of Fox nut

| | |
|-------------------|------------------------------|
| Kingdom | Plantae |
| (unranked) | Angiosperms |
| Phylum | Tracheophyta |
| Class | Magnoliopsida |
| Order | Nymphaeales |
| Family | Nymphaeaceae |
| Genus | <i>Euryale</i> Salisb. |
| Species | <i>ferox</i> |
| Binomial name | <i>Euryale ferox</i> Salisb. |
| Source: Wikipedia | |

The dried Fox nutshell was crushed and sieved to obtain a particle size of range 1.4-2.0 mm. The sieved Fox nutshell was soaked in 0.5N NaOH solution and left for 12 hr to remove all impurities like mud and ash present in the Fox nutshell during harvesting and processing. After soaking, the Fox nutshell was properly washed with distilled water until the washed solution pH achieved about 7. The cleaned material was dried at 110 °C for 24 hr for further experiments.

2.1.2. Chemicals used

All chemicals used in this work were purchased from Merck, India. The chemicals used in this study includes; zinc chloride, orthophosphoric acid, potassium carbonate, hydrochloric acid, iodine, sodium thiosulfate, potassium iodide, potassium iodate, sodium hydroxide, sodium carbonate, sodium bicarbonate, phenol, methylene blue and potassium dichromate.

2.1.3. Apparatus

The preparation of activated carbon was performed in a horizontal tube furnace. The alumina tube of the horizontal tubular furnace was of 1 m long and 0.66 m internal diameter. The furnace use a Kanthal heating rod for heating and is equipped with a proportional integral derivative (PID) temperature controller. The heating zone of the furnace was in the middle section of the furnace and was of 20 cm long. To maintain inert atmosphere purified nitrogen gas (99.99%) was used, and the flow rate was controlled by using a rotameter. The maximum temperature of operation of the furnace was 1550 °C. A schematic of the furnace is shown in Fig. 2.2.

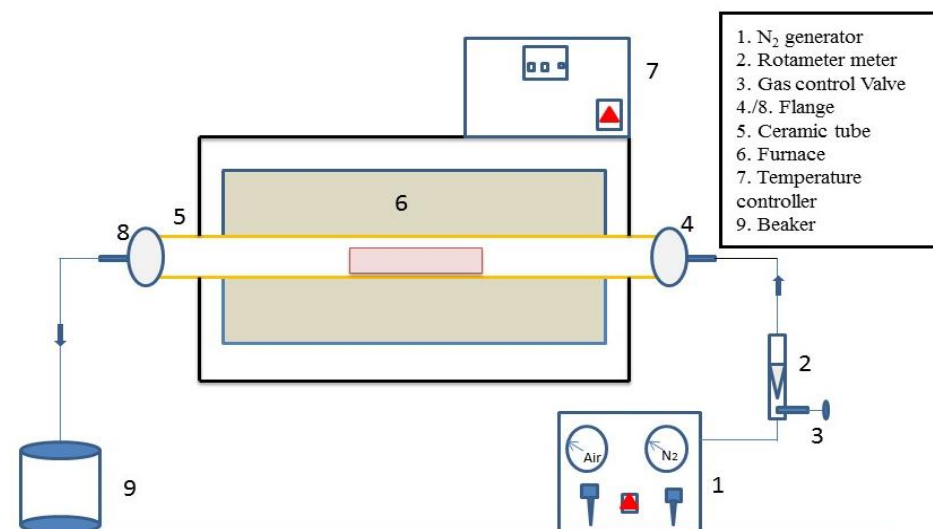


Fig. 2.2. Schematic of the activation furnace.

2.1.4. Preparation procedure

Preparation of activated carbon from Fox nutshell was carried in two steps, which includes base-leaching and activation. The first step is already discussed in the precursor part. In the second step, the base leached Fox nutshell was impregnated with ZnCl_2 , H_3PO_4 and K_2CO_3 solution in different concentrations. The impregnation ratio was considered as the ratio of the weight of activating agents to the weight of the dried Fox nutshell (Yorgun et al., 2009). For ZnCl_2 impregnation, 20 to 50 g of ZnCl_2 was dissolved in 150 mL distilled water, and 20 g of the Fox nutshell was mixed at 80 °C to obtain the impregnation ratios as of 1, 1.5, 2.0 and 2.5. For H_3PO_4 impregnation, the required H_3PO_4 volumes per 20 g dry raw material were 6.5, 12.99, 19.49 and 25.98 mL for the impregnation ratios of 0.5, 1, 1.5 and 2.0, respectively. For impregnation, 20 g of Fox nutshell was dissolved in 150 mL solution of H_3PO_4 with different concentration and stirred at approximately 80 °C. For K_2CO_3 impregnation, 5 to 20 g of K_2CO_3 was dissolved in 150 mL distilled water, and 20 g of the Fox nutshell was mixed at 80 °C to obtain the impregnation ratios as of 0.25, 0.5, 0.75, and 1.0. The mixtures were left for 24 hr at room temperature, during this period the mixture was mixed at a fixed time interval of 6 hr. After that, the impregnated samples were evaporated and dried at 110 °C for 24 hr in a hot oven.

A weighed amount of impregnated Fox nutshell was placed in a ceramic crucible and inserted at the middle of the horizontal electric tubular furnace tube. The sample was heated from room temperature to a final preselected temperature ranging from 500 to 800 °C with the N_2 flow of 150 mL/min. Different process parameters such as heating rate, activation time, carbonization temperatures and impregnation ratios were studied to estimate their

effect on porous activated carbons characteristics. Table 2.2 detailed the values of the parameters used in the chemical activation process for the activated carbon preparation from Fox nutshell.

Table 2.2: Experimental values of the parameters used in chemical activation process

| | |
|--|--|
| Chemical activation (Heating rate, °C/min) | 2, 5, and 8 |
| Activation time (min) | 30, 60, 90 and 120 |
| Ratio of the chemicals to the Fox nutshell | 0.5, 1.0, 1.5, 2.0, and 2.5 (ZnCl ₂) 0.5, 1.0, 1.5, 2.0, and 2.5 (H ₃ PO ₄) 0.25, 0.5, 0.75 and 1 (K ₂ CO ₃) |
| Activation Temperature (°C) | 500, 550, 600, 650, 700 (ZnCl ₂) 500, 550, 600, 650, 700, 750 and 800 (H ₃ PO ₄) 600, 650, 700, 750, 800, 850 and 900 (K ₂ CO ₃) |

2.1.5. Yield of activated carbon

The yield of activated carbon was calculated by dividing the mass of the resultant activated carbon by the initial mass of the raw material used for activation (Yorgun et al., 2009). The activated carbon yield was calculated using Eq. (2.1).

$$\text{Yield (wt\%)} = \frac{\text{Final weight of activated carbon}}{\text{Initial weight of Fox nutshell}} \times 100 \quad (2.1)$$

2.2. Characterization of Fox nutshell and prepared activated carbon

2.2.1. Thermogravimetric analysis

The combustion characteristics of Fox nutshell were studied using a thermal analyzer (Shimadzu, Japan). The sample was heated under N₂ flow rate of 30 mL/min and a heating rate of 5 °C/min from ambient to 800 °C. An approximately 8±0.5 mg of Fox nutshell was used. The mass loss (TGA) and derivative curves (DTG) of the samples were represented as a function of temperature. The TGA–DTG method was applied to calculate the combustion characteristics during the process.

2.2.2. Proximate analysis

The amount of moisture in the sample was determined using the following procedure: 5 g of sample was added to vials, which was weighed beforehand. The vials were placed in an

oven at 105 °C, dried before being transferred into a desiccator for 1 hr, and reweighed to determine the percentage of moisture in the sample.

Ash content determination was done according to the ASTM D2866-94 method. Dry sample (1.0 g) was placed in a porcelain crucible and transferred into a preheated muffle furnace set at a temperature of 650±25 °C. The furnace was left on for one hr, after which the crucible and its content was transferred to desiccators and allowed to cool. The crucible and content were reweighed, and the weight loss was recorded as the ash content of the raw sample. Then the % ash content (dry basis) was calculated from Eq. (2.2).

$$\text{Total ash \%} = [(D_1 - B_1) \div (C_1 - B_1)] \times 100, \quad (2.2)$$

where,

B_1 = Weight of crucible (g)

C_1 = Weight of crucible with original sample (g)

D_1 = Weight of crucible with ashed sample (g)

Volatile organic matter content (wt%) was determined by the ASTM 5832 method. Approximately 1 g of the sample was taken in a crucible with cover (of known weight). The covered crucible was placed in muffle furnace regulated at 950 °C for 7 min. Then the covered crucible was cooled to room temperature in a desiccator and recorded for the weight. The percentage weight loss was regarded as the percentage of volatile matter.

$$\text{Volatile organic content \%} = (D_1 - B_1) \div (C_1 - B_1) \times 100, \quad (2.3)$$

where,

B_1 = Weight of crucible (g)

C_1 = Weight of crucible with original sample (g)

D_1 = Weight of crucible with burnt sample (g)

Fixed carbon is a calculated value and it is the resultant of summation of percentage moisture, ash, and volatile matter subtracted from 100.

$$\text{Fixed carbon\%} = [100 - (\text{moisture\%} + \text{ash\%} + \text{volatile matter\%})], \quad (2.4)$$

2.2.3. Ultimate analysis

The total nitrogen, carbon, and sulfur of the Fox nutshell and the prepared activated carbons were determined using an elemental analyzer (Elementar, Germany). For the CHNS analysis, dried crushed samples were weighed (5-10 mg) and mixed with an oxidizer (vanadium pentoxide, V₂O₅ ensures complete conversion of inorganic sulfur in the sample

to sulfur dioxide) in a tin capsule, which is then combusted in a reactor at a temperature of 1000 °C. The tin capsule with sample melt and the tin promotes a violent reaction (flash combustion) in a temporarily enriched oxygen atmosphere. The combustion products CO₂, SO₂, and NO₂ were carried by a constant flow of carrier gas (helium) that passes through a glass column packed with an oxidation catalyst of tungsten trioxide (WO₃) and a copper reducer, both kept at 1000 °C. At this temperature, the nitrogen oxide was reduced to N₂. The N₂, CO₂, and SO₂ are then transported by the helium too, and separated by a 2 m long packed column and quantified with a thermal conductivity detector (TCD - set at 290 °C). The CHNS elemental contents are reported in weight percent. The oxygen contents were calculated by difference.

2.2.4. Determination of bulk density

The volume and the mass of a fixed amount of the sample were measured to determine the bulk density. Mass measurements were performed with a regular laboratory balance; the volume of the sample was determined by using a graduated cylinder. The average bulk density was calculated as the ratio of mass to volume and was taken as the average of three measurements per sample.

2.2.5. Iodine number

The iodine number (mg/g) of the prepared activated carbons were evaluated using the procedure proposed by the Standard Test Method (ASTM D 4607-94). The AC (1.0 g) was placed in a 250 mL dry Erlenmeyer flask and was treated with 10 mL of 5% HCl. The mixture was boiled for 30 s and then cooled. Afterward, 100 mL of 0.1N iodine solutions was added to the mixture and stirred for 30 s. After a quick filtration, 50 mL of the filtrate solution was titrated with 0.1N sodium thiosulfate until the solution became pale yellow.

The X/M value was calculated by the Equation 2.5.

$$\frac{X}{M} = \left[\frac{A - (DF)(B)(S)}{M} \right] \quad (2.5)$$

where X/M = iodine absorbed per gram
of carbon, mg/g,
A = (N₂) (12693.0),
N₂ = iodine, N
B = (N₁) (126.93),
N₁ = sodium thiosulfate, N

DF (dilution factor) = (I+H)/F,
I = iodine, mL,
H = 5 % hydrochloric acid used, mL,
F = filtrate, mL,
S = sodium thiosulfate, mL, and
M = carbon used, g

Two milliliters of starch indicator solution (1 g/L) were added, and the titration was continued with sodium thiosulfate until the solution became colorless. The concentration of iodine in the solution was thus calculated from the total volume of sodium thiosulfate used.

2.2.6. Specific surface area and porosity characterization

The specific surface area and pore structure characteristic of the prepared activated carbons were determined by nitrogen adsorption at $-196\text{ }^{\circ}\text{C}$ by the surface area analyzer (Quantachrome, USA). The samples were degassed under vacuum at $300\text{ }^{\circ}\text{C}$ for 3 hr before the measurement. The surface area (S_{BET}) of prepared activated carbon was estimated by BET (Brunauer–Emmett–Teller) method. The t-plot method was used to calculate the micropore surface area (S_{μ}). The mesopore surface area (S_{m}) was calculated by subtracting S_{m} from S_{BET} ($S_{\text{m}} = S_{\text{BET}} - S_{\mu}$) (Yorgun et al., 2009). The total pore volume (V_{T}) was estimated to be the liquid volumes of N_2 at relative high pressure ($P/P_0 \sim 0.99$). The micropore volume (V_{μ}) was obtained using the DR method, and mesopore volume (V_{m}) was calculated by subtracting V_{μ} from V_{T} ($V_{\text{m}} = V_{\text{T}} - V_{\mu}$). The pore size distribution of the prepared activated carbon was determined by density functional theory (DFT) method. The mean pore diameter (D_{P}) was calculated from $D_{\text{P}} = 4V_{\text{T}}/S_{\text{BET}}$ (Cazetta et al., 2011).

2.2.7. Determination of surface chemistry

The surface functional groups of the Fox nutshell and prepared activated carbons were identified by Fourier transform infrared spectroscopy (Thermo Scientific Nicolet™ iS10), recorded from wavenumbers of $400\text{--}4000\text{ cm}^{-1}$. The pellet was prepared by mixing a sample (0.1 mg each) with KBr (100 mg) in a mortar pestle and resultant mixtures pressed in the hydraulic pump.

2.2.8. Boehm titration

The Boehm titration method was used for the determination of the acidic as well as basic properties of the carbon surface (Boehm, 2002). The Boehm titration method can be described as: 0.5 g of the prepared activated carbon was placed in a series of flasks containing 50 mL of 0.05M NaOH, NaHCO_3 , Na_2CO_3 , and HCl solutions. The flasks were sealed and shaken for 48 hr at room temperature. Each solution is filtered, and 10 mL of the solution was titrated with 0.05M HCl or NaOH, depending on the original solution used. Some acidic groups on the prepared activated carbon were calculated based on the assumptions that NaOH neutralizes carboxylic, lactonic, and phenolic groups; Na_2CO_3 ,

carboxylic and lactonic groups; NaHCO_3 , only carboxylic group. The basic surface group was calculated from the amount of HCl that reacted with the carbon.

2.2.9. pH and point of zero charges (PZC) measurements

0.05 g of activated carbon was mixed in 50 mL of distilled water at a temperature of 25 °C to determine the pH of the solution containing the activated carbon by using the pH meter (Systronic, Model-361, India). After agitation, the pH of each sample was measured (Ketcha et al., 2012). The PZC was measured as follows: 20 mL of NaCl solution (0.1N) was placed in an Erlenmeyer flask including 0.1 g of AC. The initial pH was adjusted between 2 and 12 by the addition of NaOH or HCl (0.1N). After a contact time of 24 hr under magnetic agitation, the final pH was determined and plotted versus the initial pH (Franz et al., 2000).

2.2.10. X-Ray Diffraction Spectroscopy

Crystallinity and amorphous structure of the raw sample and prepared activated carbon was determined by X-ray diffraction (Rigaku Japan/Ultima-IV) with Cu K (35 kV and 30 mA) radiation at a scan rate of 2°/min and analyzed using standard software provided with the instrument. The diffraction angle (2-theta) was set to 10 to 60° for all studies.

2.2.11. Surface morphology study

The surface morphology of the raw material and prepared activated carbons were carried out by Field emission scanning electron microscopy (Nova NanoSEM 450). Porosity development in the prepared activated carbon was studied by FESEM. Transmission Electron Microscope (TECNAI, FEI Tecnai™) analyzed the micropore arrangement of the prepared activated carbons.

2.3. Adsorption studies

2.3.1. Batch adsorption studies

2.3.1.1. Adsorbates and analytical methods

Phenol ($\text{C}_6\text{H}_5\text{OH}$), methylene blue ($\text{C}_{16}\text{H}_{18}\text{N}_3\text{SCl}_3\cdot 3\text{H}_2\text{O}$) and Cr(VI) adsorbates were used in the adsorption study. Stock solutions of 1000 mg/L of the adsorbates were prepared by dissolving an appropriate quantity of the adsorbates in a liter of distilled water. The working solutions were prepared by diluting the stock solution with distilled water.

Aliquots of the adsorbates were withdrawn from the suspension at pre-set time intervals and were centrifuged by centrifuge (REMI, Model-CM-8 Plus, India). Aliquot of 2 mL was centrifuged at 10,000 rpm for 5 min to remove the adsorbent particles before analytical measurements were made. The concentrations of phenol before and after adsorption were measured by using UV–Visible spectrophotometer (Jasco, Model V-530, Japan) at 268 nm. The concentrations of MB before and after adsorption were measured at 664 nm by using UV–Visible spectrophotometer. The Cr(VI) ions concentrations were measured according to 1,5-diphenylcarbazide spectrophotometry using a visible spectrophotometer at 540 nm.

2.3.1.2. Batch experiments

The batch adsorption experiments were conducted in a set of 250 mL of Erlenmeyer flasks containing 100 mL of phenol and MB (100, 200, 300, 400 and 500 mg/L) solution, and Cr(VI) (10, 15, 20 and 25 mg/L) with predetermined amount of adsorbents. The flasks were agitated in an isothermal orbital shaker (Incon, India) at pre-selected rpm until the equilibrium is reached. The equilibrium adsorption capacity, q_e (mg/g) and percentage removal, R (%) were determined using the following relations:

$$q_e = \frac{(C_0 - C_e)V}{m_s}, \quad (2.6)$$

$$R(\%) = \frac{C_0 - C_e}{C_0} \times 100, \quad (2.7)$$

Kinetic studies were also performed according to the method described in batch equilibrium method stated above. The adsorption capacity q_t (mg/g) at different contact time t (min) was determined using the following equation:

$$q_t = \frac{(C_0 - C_t)V}{m_s}, \quad (2.8)$$

where C_0 , C_e , and C_t are the initial, equilibrium, and at time t (min) of adsorbate concentrations (mg/L) respectively, V the volume of solution (L) and m_s the dry weight of the added adsorbent (g).

2.3.1.3. Studies on effect of parameters on batch adsorption

2.3.1.3.1. Agitation speed

In the batch adsorption study, agitation speed plays a significant role in affecting the external boundary film and the distribution of the solute in the bulk solution (Weng et al., 2009). A range of 90-170 rpm investigated the effect of agitation speed. A series of agitation

speed experiments were performed at 30 °C for 3 hr by using prepared activated carbons. 100 mL solutions of phenol and MB of initial concentrations 100 mg/L and Cr(VI) of initial concentration 10 mg/L for Cr(VI) were used.

2.3.1.3.2. pH

The adsorption of phenol, MB, and Cr(VI) onto the prepared activated carbons was investigated over a pH range of 3–12 and the studies were carried out for 3 hr. The pH was adjusted by adding a few drops of 0.1N NaOH or 0.1N HCl (Systronic, Model-361, India). The initial concentration of phenol and MB was 100 mg/L, and the adsorbent dose was kept at 0.05 g and 0.03 g for phenol and MB, respectively. The initial concentration of Cr(VI) was 10 mg/L, and the adsorbents dose was kept at 0.02 g. The mixture was agitated in an orbital shaker at an optimum agitation speed of 150 rpm at 30 °C. At equilibrium, the samples were filtered and analyzed by using UV–Visible spectrophotometer (Jasco, Model V-530, Japan).

2.3.1.3.3. Temperature

The effect of temperature on phenol, MB, and Cr(VI) adsorption was studied at different temperatures in the range of 25, 30, 35 and 45 °C for 100 mg/L for phenol and MB, and 10 mg/L concentration of Cr(VI).

2.3.1.3.4. Adsorbent dosage

To study the effect of adsorbents dose (g) on phenol, MB, and Cr(VI) uptake, experiments were conducted at an initial solution concentration of 100 mg/L for phenol and MB, and 10 mg/L for Cr(VI) at 30 °C while the amount of adsorbent added was varied.

2.3.1.4. Adsorption Characteristic study

2.3.1.4.1. Adsorption kinetic models

The study of adsorption kinetics is significant as it provides valuable insight into the reaction pathways and into the mechanism of the reaction. In the present study, the most used kinetic models of pseudo-first-order (Budinova et al., 2006) and pseudo second order (Ho and McKay, 1999) were used to fit the experimental data. Linear forms of pseudo-first and pseudo-second-order kinetic equations are given in equations (2.9) and (2.10), respectively.

$$\ln(q_e - q_t) = \ln q_e - k_1 t, \quad (2.9)$$

$$\frac{t}{q_t} = \frac{1}{k_2 q_e^2} + \left(\frac{1}{q_e}\right) t, \quad (2.10)$$

where q_e (mg/g) and q_t (mg/g) are the amounts of adsorbate adsorbed onto the prepared activated carbon at the equilibrium and at any time t (min) respectively, and k_1 (min^{-1}) and k_2 (g/min/mg) are the rate constant of the pseudo-first and pseudo second-order adsorption.

In order to quantitatively compare the applicability of the model in fitting the data, a normalized standard deviation, Δq (%) was calculated from Eq. (2.11).

$$\Delta q (\%) = \sqrt{\frac{\sum[(q_{e,exp} - q_{e,cal})/q_{e,exp}]^2}{(N - 1)}} \times 100, \quad (2.11)$$

where $q_{e,exp}$ and $q_{e,cal}$ refer to the experimental and calculated values and N is the number of data points.

2.3.1.4.2. Intraparticle diffusion model

Since neither the pseudo-first-order nor the pseudo-second-order model can identify the diffusion mechanism. The kinetic results were analyzed by the intraparticle diffusion model (Hameed and Rahman, 2008) to elucidate the diffusion mechanism. The intraparticle diffusion model is given by Eq. (2.12);

$$q_t = k_i t^{0.5} + c, \quad (2.12)$$

where k_i is the intraparticle diffusion rate constant ($\text{mg g}^{-1} \text{min}^{-1/2}$), and c is the intercept.

2.3.1.4.3. Adsorption isotherm models

Adsorption isotherm curve is utilized to obtain information concerning the desorption mechanism strictly connected with the interaction between the adsorbent and adsorbate molecules. The most common isotherm equations used for theoretical interpretations of adsorption isotherms were used in the present study.

2.3.1.4.3.1. Langmuir isotherm

The Langmuir isotherm is valid for monolayer and homogeneous sites within the adsorbent surface with a uniform distribution of energy level. The model assumes uniform adsorption and no transmigration in the plane of the adsorbent surface (Langmuir, 1918). The linear form of the Langmuir equation is represented as follows:

$$\frac{C_e}{q_e} = \frac{1}{k_L q_m} + \frac{C_e}{q_m}, \quad (2.13)$$

where q_m represents the maximum adsorption capacity of the solid phase loading and k_L is the energy constant related to the heat of adsorption.

The separation factor (R_L) is dimensionless quantity and it is an essential characteristic of the Langmuir isotherm (Hall et al., 1966) and is defined as:

$$R_L = \frac{1}{(1 + k_L C_0)}, \quad (2.14)$$

where k_L is the Langmuir constant and C_0 is the highest adsorbate concentration (mg/L). The value of R_L indicates the isotherm to be either unfavourable ($R_L > 1$), linear ($R_L = 1$), favourable ($0 < R_L < 1$) or irreversible ($R_L = 0$).

2.3.1.4.2. Freundlich isotherm

The Freundlich isotherm equation is based on sorption onto a heterogeneous surface and is given as (Freundlich, 1906):

$$q_e = k_F + C_e^{1/n}, \quad (2.15)$$

The linear form of equation (2.15) is

$$\ln q_e = \ln k_F + \frac{1}{n} \ln C_e, \quad (2.16)$$

where $k_F [(mg/g)(L/mg)^{1/n}]$ and n are Freundlich constants related to adsorption capacity and adsorption intensity, respectively. The n is defined as heterogeneity factor and indicates when the adsorption process is linear ($n = 1$), physical ($n > 1$) or chemical ($n < 1$) (Pezoti et al., 2014). The ratio $1/n$ allows the adsorption intensity or the surface heterogeneity, i.e., as closest to zero, more heterogeneous is the surface of the analyzed material (Auta and Hameed, 2011).

2.3.1.4.3. Temkin adsorption isotherm

Temkin and Pyzhev suggested that due to the indirect adsorbate/adsorbent interaction, the heat of adsorption of all the molecules in the layer would decrease linearly with coverage (Aksu, Z., 2005). The linear form of Temkin isotherm can be written as:

$$q_e = B \ln(A) + B \ln C_e, \quad (2.17)$$

where $B=RT/b$ is related to the heat of adsorption (J/mol), b is Temkin isotherm constant and A is Temkin isotherm equilibrium binding constant (L/g). R is the universal gas constant (8.314 J/mol/K), and T (K) is the solution temperature.

2.3.2. Regeneration and reuse adsorbents

Regeneration and recovery of the activated carbon are critical aspects of wastewater treatment processes. Regeneration of adsorbent, as well as recovery of adsorbate material, was achieved by desorbing the adsorbate into 0.14N NaOH. The prepared granular activated carbons of fixed dosage loaded with adsorbate were placed in the desorbing medium (0.14N NaOH solution) and were continuously stirred on a rotatory shaker at 150 rpm for 3 hr at 30 °C. The sample was washed with distilled water until the pH of the water reached near to neutral and dried in a hot oven for 24 hr at 110 °C. Obtained dried activated carbon again reused for adsorbates adsorption. The above procedure was repeated repeatedly for readsorption experiments.

2.3.3. Fixed-bed column adsorption studies

A Perspex glass cylindrical tube of 2.5 cm internal diameter and 20 cm height was used to construct the adsorption column. The photographic and schematic view of the fixed bed adsorption setup is shown in Fig. 2.3. The column was packed with the adequate amount of the prepared activated carbon to obtain the desired bed height. The bed was held in place between two plugs of cotton. The cotton in the lower and upper part of the column was supported by glass beads. The volumetric Flow rate of adsorbate solution was adjusted from 5-15 mL/min in the experiments. The column was kept at room temperature. The adsorbates solutions were fed continuously to the column in an upward flow mode using a peristaltic pump. The change of phenol, MB, and Cr(VI) concentration in the column effluent was determined by following the same method mentioned above (subsection 2.3.1.1). The range of variables investigated and packed bed characteristics is summarized in Table 2.3.

Table 2.3: Experimental conditions of the fixed bed adsorption studies

| | |
|------------------------|---------------------|
| Bed diameter | 2.5 cm |
| Column height | 20 cm |
| Bed height | 2, 3, and 4 cm |
| Flow rate | 5, 10 and 15 mL/min |
| Influent concentration | |
| MB and Phenol | 100 mg/L |
| Cr(VI) | 10 mg/L |
| GAC particle diameter | 1.0 mm |

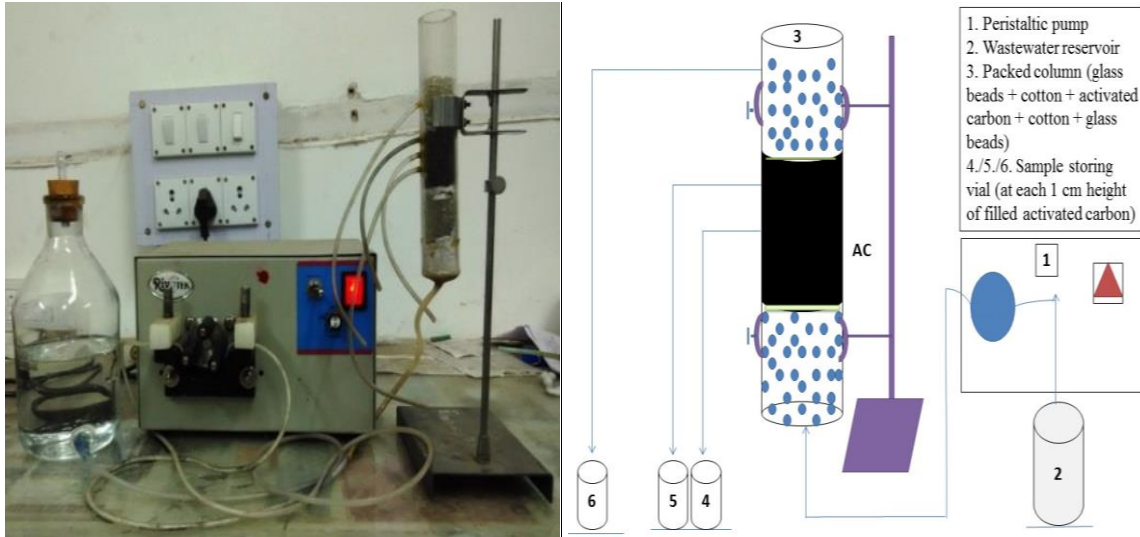


Fig. 2.3. Photographic and schematic representation of fixed bed adsorption setup.

The loading behavior of adsorbates [phenol, MB, and Cr(VI)] in its dynamic adsorption from by prepared activated carbons could be shown in the form of breakthrough (BT) curves. It is usually expressed in terms of normalized concentration, defined as the ratio of outlet adsorbate concentration to the inlet adsorbate concentration (C_t/C_0) or the adsorbed solute concentration (C_{ad}), which is the difference between inlet adsorbate concentration and outlet adsorbate concentration ($C_0 - C_t$), as a function of time (t) for a given bed height.

The breakthrough point was taken as the position at which $C_t/C_0 = 0.05$ and the exhaustion point when $C_t/C_0 = 0.95$ (Salman et al., 2011). The time taken for outlet concentration of adsorbate to reach the breakthrough point is known as breakthrough time. The area under the BT curve which was obtained by integrating the plot, was used to estimate the total adsorbed quantity of adsorbate, q_{tot} (mg) in the column for a given inlet concentration and flow rate was obtained by the equation given by Eq. (2.18) (Aksu and Gönen, 2004; Kumar and Jena, 2016b; Salman et al., 2011).

$$q_{tot} = \frac{Q}{1000} \int_{t=0}^{t=t_{tot}} C_{ad} dt, \quad (2.18)$$

where Q (mL/min) is the volumetric flow rate, C_{ad} (mg/L) is the difference between the initial and final concentrations of adsorbates at the end of the total flow time till exhaustion t_{tot} (min). Equilibrium adsorbates uptake in the column or maximum capacity of the column (bed capacity), q_{bed} (mg/g) was obtained using Eq. (2.19) (Aksu and Gönen, 2004; Salman et al., 2011):

$$q_{bed} = \frac{q_{tot}}{W}, \quad (2.19)$$

The quantity of adsorbate sent to the column (m_{tot}) was calculated using Eq. (2.20) (Girish and Murty, 2015):

$$m_{tot} = \frac{C_0 Q t_{tot}}{1000}, \quad (2.20)$$

The total adsorbate removed (% removal) on the adsorbates feed entering the column was estimated by the Eq. (2.21):

$$\% \text{ removal} = \frac{q_{tot}}{m_{tot}} \times 100, \quad (2.21)$$

2.4. Biological treatment of phenol

2.4.1. Batch biodegradation studies of phenol

2.4.1.1. Bacterial culture and acclimatization

A pure strain of *Pseudomonas putida* (MTCC 1194) in lyophilized form was procured from Microbial Type Culture Collection and Gene Bank, Institute of Microbiology (IMTECH), Chandigarh, India and it has the potential to phenol degrade (Kumar et al., 2005). The phenol was used as the sole carbon and energy source. Before experiments, Luria Bertani (LB) liquid medium (Beef extract, 1.0 g/L; Yeast extract, 2.0 g/L; Peptone, 5.0 g/L; NaCl, 5.0 g/L), minimal salts medium (MSM) solution with the following composition (in mg/L): $(\text{NH}_4)_2\text{SO}_4$ (212), KH_2PO_4 (32), K_2HPO_4 (180), MgSO_4 (49), NaHCO_3 (354), $\text{FeCl}_3 \cdot 6\text{H}_2\text{O}$ (18.8) and CaCl_2 (40) (Oh et al., 2011) and all the apparatus were autoclaved at 121 °C for 15 min, and the glucose and phenol were separately sterilized by membrane filtration (0.22 μm). *P. putida* (MTCC 1194) strain was revived in the LB liquid medium. After that, the *P. putida* (MTCC 1194) was transferred to 100 mL MSM solution containing glucose (a commonly used organic carbon source) of 1000 mg/L and incubated at 30 °C, 120 rpm.

The cultures were acclimatized to phenol by exposing the cultures to a series of shake flasks (250 mL), wherein the content of glucose was decreased, and that of phenol increased over a period of three months. In the beginning, 1000 mg/L initial glucose concentration was used as a carbon source, and after that, the phenol was periodically added in increments of 100 mg/L phenol with glucose decrement as the same manor until the increasing concentration of phenol was reached to 1000 mg/L. After phenol concentration was reached to 1000 mg/L, then the culture incubated for 10 days and the same process was repeated 10 times. The *P. putida* (MTCC 1194) was acclimatized to take phenol as a sole carbon and

energy source. The acclimatized *P. putida* (MTCC 1194) was then used for further experiments by both free cells and immobilized cells.

2.4.1.2. Sampling and analysis of phenol and biomass

2 mL sample was taken out from the shake flask at regular time interval and centrifuged at 10,000 rpm for 5 min to remove the biomass before analytical measurements were made. Supernatant was taken for phenol concentration measurement and pellet for the determination of biomass concentration. The concentration of phenol was measured at 268 nm and biomass concentration was measured at 600 nm by using UV–Visible spectrophotometer (Jasco, Model V-530, Japan).

2.4.1.3. Suspended cell system

2.4.1.3.1. Effect of physiological parameters

Physiological parameters play a significant role in the growth and biodegradation behaviour of the microorganisms. Microorganism grows within a range of physiological parameters, but maximum growth is achieved only at the specific conditions of the physiological parameters. In the present study, the effect of physiological parameters studied include; inoculum size, pH, temperature and initial concentration of phenol.

2.4.1.3.1.1. Inoculum size

Inoculum size plays a major role in phenol biodegradation. The study of inoculum size effect was performed in the range of 1 to 6% (v/v) with 1000 mg/L of initial phenol concentration for 72 hr.

2.4.1.3.1.2. pH

The internal environment of all living cell is believed to be neutral (Annadurai et al., 1999). To determine the optimal pH for the biodegradation of phenol by *P. putida* (MTCC 1194) were carried out at different pH (4–10) with an initial phenol concentration of 1000 mg/L for 72 hr.

2.4.1.3.1.3. Temperature

Temperature exerts a significant regulatory influence on the rate of metabolism and enhances the microbial activity on phenol and other contaminants (Annadurai et al., 1999; Vela and Rainey, 1976). To determine the optimal temperature for the biodegradation of

phenol were carried out at temperature range of 25–40 °C with an initial phenol concentration of 1000 mg/L for 72 hr.

2.4.1.3.1.4. Initial concentration

Substrate concentration is also a significant parameter for the growth of the microorganisms. In this study, phenol acts as a substrate for the *P. putida* (MTCC 1194) to take energy for various metabolic activities. At initial phenol concentrations between 200-1200 mg/L was taken for the study of concentration effect.

2.4.1.3.2. Biodegradation of phenol

All biodegradation experiments were performed in 250 mL Erlenmeyer flask containing 100 mL of MSM containing phenol at a concentration ranging from 100 mg/L to 1200 mg/L at 30 °C incubation temperature in orbital shaker under agitation speed of 120 rpm. The samples were withdrawn at regular time interval and analysed for residual phenol concentration by using UV–Visible spectrophotometer at 268 nm.

2.4.1.4. Immobilized cell system

2.4.1.4.1. Immobilization of *Pseudomonas putida* (MTCC 1194) onto ACPA-700-1.5

The acclimatized *Pseudomonas putida* (MTCC 1194) was incubated at 30 °C in 250 mL Erlenmeyer flask containing 100 mL LB, and after that, the sterilized 0.55 g of prepared activated carbon (ACPA-700-1.5) was added into the culture. The immobilization was carried out for 10 days in the orbital shaker at 120 rpm with constant temperature 30 °C.

2.4.1.4.2. Morphology study of developed biofilm

Morphology of the biofilm formed on the surface of ACPA-700-1.5 activated carbon was investigated by using a Field Emission Scanning Electron Microscope (FESEM). The sample for FESEM was prepared by fixing the sample with 25% aqueous solution of glutaraldehyde for 30 min. After that, the sample was washed twice with distilled water. It was followed by dehydration by washing in a graded ethanol series (25%, 50%, 75% and finally absolute ethanol), at least twice in each concentration (Ahammad et al., 2013). The sample was dried in a desiccator. The dried sample was mounted on sample mounts, sputter-coated with gold and observed using the field emission scanning electron microscope.

2.4.1.4.3. Biodegradation of phenol

All biodegradation experiments were performed in 250 mL Erlenmeyer flask containing 100 mL of MSM containing phenol at a concentration ranging from 1000 mg/L, 1500 and 2300 mg/L at 30 °C incubation temperature in orbital shaker under agitation speed of 120 rpm, samples were withdrawn at regular time interval, and analyzed for residual phenol concentration.

2.5. Biodegradation studies of phenol in fluidized bed bioreactor (FBBR)

2.5.1. Experimental setup

A fluidized bed reactor was designed and fabricated to study the biodegradation characteristics of phenol by immobilized *pseudomonas putida* (MTCC 1194) on ACPA-700-1.5 and the hydrodynamic behavior to evaluate energy consumption and ascertain operation limits. The fluidized bed assembly consists of three sections, viz., the test section, the gas-liquid distributor section, and the gas-liquid disengagement section. Fig. 2.4 shows the schematic and photographic representation of the experimental setup used in the hydrodynamic and biodegradation study.

The test section is the main component of the fluidized bed where fluidization and maximum biodegradation takes place. It is a vertical cylindrical Plexiglas column of 4.9 cm internal diameter, 60 cm height with 8 cm protrudes inside the disengagement section. The fluidizer is a volume of 1.13 liters. During the experiment, there is a chance of particle elutriation because of excess growth of biomass on particles or a particle driven by an upward moving bubble. To prevent entrainment biomass laden particle a 60-mesh screen (BSS) of stainless steel (SS) was fixed to the top of the column.

The gas-liquid distributor is located at the bottom of the test section and is designed in such a manner that uniformly distributed liquid and gas mixture enters the test section. The distributor section made of stainless steel is frusto-conical of 19 cm in height and has a divergence angle of 4.4°. The liquid inlet of 1.27 cm in internal diameter is located centrally at the lower cross-sectional end. The higher cross-sectional end was flanged to the test section, with a 60-mesh screen (BSS) of stainless steel of 10 cm diameter. A cross-type air sparger of 4.3 cm diameter with 8 number of 1 mm holes was fixed below the distributor plate and screwed to the main body of the distributor for the generation of fine bubbles

uniformly distributed along the column cross-section of the fluidizer. It was observed visually that the distributor arrangement used allows a uniform flow of gas and liquid to the test section containing fine gas bubbles. In the gas-liquid distributor section, the gas and the liquid streams were merged and passed through the wired mesh. The mixing section and the grid ensured that the gas and the liquid were well mixed and evenly distributed into the bed.

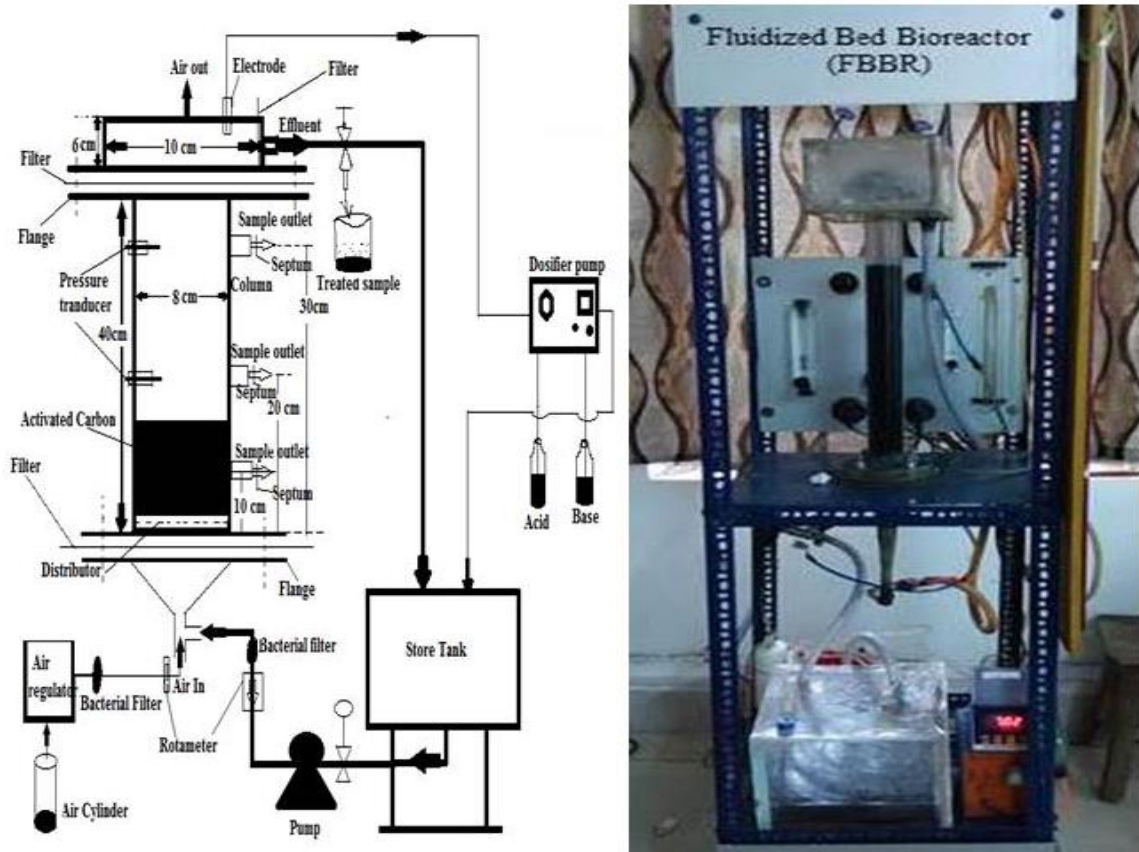


Fig. 2.4. Schematic and photographic view of the experimental set-up.

The gas-liquid disengagement section of volume 3.9 L is at the top of the fluidizing section and is a rectangular box of 18 cm height and 12 cm x 12 cm cross-section assembled to the test section with 8 cm of the test section inside it, which allows gas to escape and liquid to be circulated through the outlet of 1.27 cm internal diameter at the bottom of this section.

The working synthetic phenolic water was stored in a reservoir of a capacity of 12.5 L and dimension, 25 cm x 25 cm x 20 cm. The phenolic water was pumped to the fluidized bed by means of a fractional horsepower (FHP) pump through water Rotameter used to measure the flow rate of water, and circulated with the circulating facility. The centrifugal pump is of make Tullu, single phase, 0.05 kw, 7000 rpm, and discharge capacity of 10 lpm. Water rotameter used for the measurement of flow rate is in the range 0 to 10 lpm,

The air was supplied from an Air compressor through the air sparger. The Air compressor was of 0.037 kw, 1440 rpm with maximum air discharge capacity of 15 lpm at 2 bar pressure. The airflow rate was measured using a rotameter with a needle valve. Air rotameter was of the range 0 to 2 lpm.

For the measurement of pressure drop in the bed, the pressure ports were provided in the column and fitted to the manometers filled with water and carbon tetrachloride as the manometric fluid for the accurate measurement of pressure. To maintain the pH of the water under treatment, a pH control system was installed, consisting of a pH-meter and micro-pumps supplying base or acid; as required. To measure the holdup of the liquid and gas phases in the reactor, quick closing valves were put in the lines of gas and liquid flow. The biomass support was the prepared activated carbon, ACPA-700-1.5 particles of density 1150 kg/m^3 , of average size 1.85 mm and sphericity of 0.70.

2.5.2. Experimental procedure

The three-phase solid, liquid and gas were GAC (ACPA-700-1.5), distilled water and oil free compressed air, respectively. The air-water flow was concurrent and upwards. Accurately weighed the amount of prepared material was fed into the column and adjusted for a specified initial static bed height. Water was pumped to the bed at the desired flow rate using calibrated water rotameter. The air was then introduced into the column through the air sparger at a desired flow rate using calibrated air rotameter.

All experiments were started with the column completely filled with water and material (ACPA-700-1.5) and the initial level of manometer adjusted to have zero level. For the liquid-solid experiment, the liquid flow rate was gradually increased. Approximately five minutes were allowed to make sure that the steady state was reached. Then the readings of the manometers and the expanded heights of the bed were noted. For the gas-liquid-solid experiment, with a little flow of liquid close to zero, the air was slowly introduced and gradually increased to the desired flow rate after which the liquid flow rate was increased, and the readings were noted down, as mentioned above. For the gas holdup measurement, the flow of water and air to the system was simultaneously and suddenly stopped. After escape of the air from the system, the height of the liquid in the column was noted down. The procedure was repeated for different values of initial static bed height and gas velocity. For biodegradation experiments, carrier particles (GAC) were screened by ISS sieves to obtain particles with an average diameter of 1.85 mm. These particles were washed with

distilled water to remove carbon dust on their surface. Calculated amount (for volume of bed to volume of reactor ratios; 0.5, 0.55 and 0.6) of carrier particles and 1.0 L of nutrient broth media were sterilized and after completion of sterilization both were put into the laminar hood for cooling. The cooled sterilized GAC was put into the fluidized bed column. The sterilized nutrient broth media was inoculated with the *Pseudomonas putida* (MTCC 1194) and left for 12 hr in an orbital shaker at 30 °C of temperature with 120 rpm speed. After 12 hr, the inoculated media was added into the reactor column and closed the total opening and holes of the reactor. After adding of the inoculated media, the GAC bed was left for 10 days for the biofilm formation and periodic aeration by allowing the flow of air into the reactor in each hour time interval was done. After 10 days the culture media was drained out, and GAC was washed two times with distilled water for removing all the media present in the reactor.

GAC particles were taken out from the reactor for visualizing the developed biofilm on the supporting particles by Field Emission Electron Microscope (FESEM). Five liters of different concentrations of phenol containing synthetic wastewater was prepared using sterilized distilled water and put into the storage tank. After that, the treatment process was started. Synthetic phenolic wastewater was treated in fluidized bed bioreactor at the variation of different parameters such as superficial gas velocity, superficial liquid velocity, V_b/V_R and phenol concentration.

Chapter 3

Preparation and Characterization of Activated Carbons

The raw material, Fox nutshell was characterized to estimate its suitability for the preparation of activated carbon (AC). Activated carbons were prepared by chemical activation by impregnating the raw material with different activating agents such as $ZnCl_2$, H_3PO_4 , and K_2CO_3 . The optimum conditions as heating rate and holding time for the preparation of AC was fixed by iodine number. Effect of preparation parameters like impregnation ratio and carbonization temperature on porous characteristics of ACs were determined by N_2 gas adsorption-desorption isotherms. Various characterizations such as pore size distribution (PSD), Fourier transform infrared spectroscopy (FTIR), X-ray powder diffraction (XRD), Field emission scanning electron microscope (FESEM), Energy-dispersive X-ray spectroscopy (EDS) and Transmission electron microscopy (TEM) analysis were carried out on prepared ACs.

3.1. Fox nutshell Processing

The Fox nutshell is a novel precursor material used for the activated carbon preparation. Because of little ash (5%) and high volatile matter (70.1%), it can be a potential precursor for the production of activated carbons. Proximate and ultimate analyses of cleaned Fox nutshell and NaOH treated Fox nutshell, and chemical component of Fox nutshell is tabulated in Table 3.1. From the result, it is evident that NaOH treatment decreased the ash content (to 4.62% from 5.0%) while the volatile content was increased from 70.1% to 71.70%. The NaOH-treated Fox nutshell was used as a precursor for conversion to activated carbon. The dried Fox nutshell was crushed and sieved to obtain a particle size of range 1.4-2.0 mm.

Table 3.1: Proximate and ultimate analyzes of raw material

| Analysis | Fox nutshell | NaOH-treated Fox nutshell |
|------------------|--------------|---------------------------|
| Proximate | | |
| Moisture | 4.0 | 3.71 |
| Volatile matter | 70.1 | 71.70 |
| Ash | 5.0 | 4.62 |

| | | |
|-----------------------------|-------|----------------------------------|
| Fixed carbon ^a | 20.9 | 19.97 |
| Ultimate | | |
| Carbon | 42.30 | 44.27 |
| Hydrogen | 4.30 | 4.32 |
| Nitrogen | 0.82 | 0.24 |
| Sulphur | 0.07 | 0.08 |
| Oxygen ^a | 52.51 | 51.09 |
| Chemical Composition | | ^a by the difference |
| Cellulose | 20.3 | All quantities are in wt% |
| Lignin | 33.4 | |
| Hemicellulose ^a | 46.3 | |

3.2. Thermal characterization of Fox nutshell

Thermogravimetric analyses (TGA/ DTA) in an inert atmosphere (N₂) achieved to evaluate the pyrolytic behavior of the Fox nutshell. Biomass combustion can be divided into three stages. During the initial stage, loss of adsorbed water and the organic matter decomposes into the intermediate of smaller molar mass and releases the gaseous volatiles (Liou and Wu, 2009). The intermediates further decompose to form other volatile species, tar, and char during the second stage. The TGA-DTA graphs of the Fox nutshell is shown in Fig. 3.1.

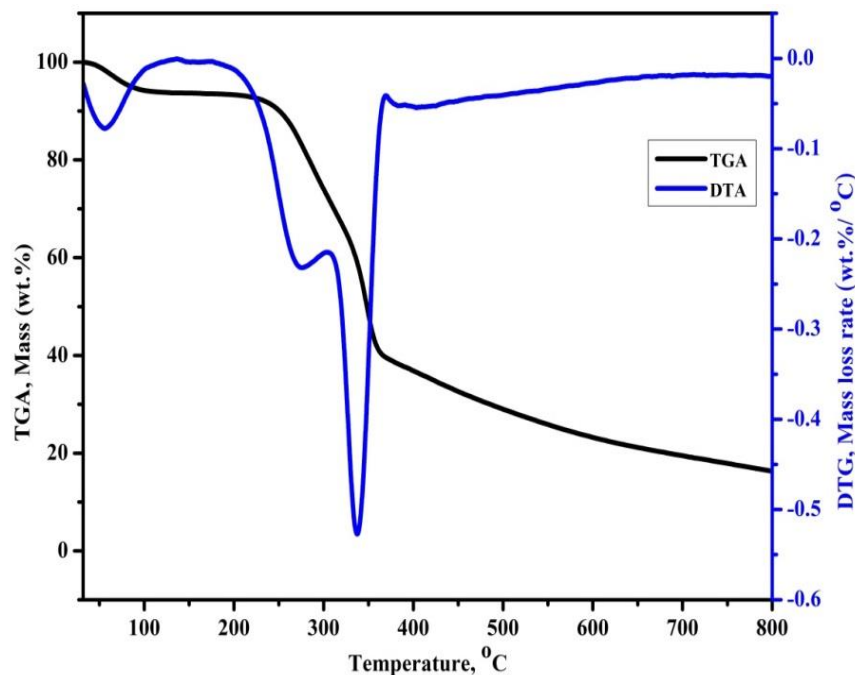


Fig.3.1. TGA and DTA curves of Fox nutshell.

From the figure, it is seen that the thermal decomposition of Fox nutshell occurs in three stages: 1) dehydration stage: room temperature to 230 °C; 2) acute weight loss stage: 260-365 °C; 3) slow weight loss stage: 375-800 °C. In the dehydration period of Fox nutshell, a weight loss of 8% in TGA curve is due to moisture as well as some low molecular weight volatile compounds. The peak at 65 °C in DTA curve is due to the moisture loss of 4.5%. This value is close to the moisture percentage of the Fox nutshell (Table 3.1). Significant weight loss of 51.60% of Fox nutshell occurred in the temperature range of 260-365 °C due to the degradation of Fox nutshell and distillation of tar; finally, no major weight loss is observed above 400 °C (Hayashi et al., 2000; Ozdemir et al., 2014). The two peaks seen in the DTA curve for the Fox nutshell at 285 and 350 °C may be due to the thermal decomposition of hemicellulose and cellulose respectively.

3.3. Preparation of activated carbons

A weighed amount of dried impregnated Fox nutshell was placed in a ceramic crucible and inserted into the furnace tube. The sample was heated from room temperature to a final preselected temperature at a preselected heating rate and activation time with the N₂ flow of 150 mL/min.

3.3.1. Effect of various processing parameters

In the preparation of activated carbons by chemical activation, the porosity development depends on the different process parameters such as heating rate, holding time, carbonization temperature and impregnation ratio. The parameters associated with the preparation of activated carbon were optimized based on the iodine numbers obtained for each carbon prepared.

3.3.1.1. Effect of heating rate

In order to examine the effect of the heating rate on the activated carbon produced, the heating rate was varied from 2 to 8 °C/min. Table 3.2(a) shows the effect of heating rate on iodine number of ACZC (activated carbon prepared with ZnCl₂ activating agent), ACPA (activated carbon prepared with an H₃PO₄ activating agent) and ACPC (activated carbon made with a K₂CO₃ activating agent). The heating rate influences the porous texture of the resulting activated carbon. Maximum values of iodine number obtained at a heating rate of 5 °C/min for all carbons i.e. ACZC, ACPA, and ACPC. Hence, the heating rate 5 °C/min was considered for all further production activated carbons.

Table 3.2: (a) Effect of heating rate on iodine number

| ACs | Heating rate (°C/min) | Holding Time (min) | Carbonization temperature (°C) | Impregnation ratio | Iodine Number (mg/g) |
|------|-----------------------|--------------------|--------------------------------|--------------------|----------------------|
| ACZC | 2 | 60 | 500 | 0.5 | 465.82 |
| | 5 | 60 | 500 | 0.5 | 489.86 |
| | 8 | 60 | 500 | 0.5 | 475.37 |
| ACPA | 2 | 60 | 500 | 0.5 | 409.52 |
| | 5 | 60 | 500 | 0.5 | 412.65 |
| | 8 | 60 | 500 | 0.5 | 410.48 |
| ACPC | 2 | 60 | 500 | 0.5 | 274.54 |
| | 5 | 60 | 500 | 0.5 | 283.28 |
| | 8 | 60 | 500 | 0.5 | 272.08 |

3.3.1.2. Effect of holding time

To study the effect of holding time (activation time), the activation time was varied from 30 min to 120 min at activation temperature of 500 °C and impregnation ratio of 0.5 for ACZC, ACPA, and ACPC. The iodine number of activated carbons thus prepared using these conditions is tabulated in Table 3.2(b). The maximum iodine number of 489.86, 412.65 and 283.28 mg/g observed at 60 min activation time for all the carbons. Activation time of 60 min was considered for further preparation of ACZC, ACPA, and ACPC. 60 min may be the adequate time for reaction with activators and decomposition of the tar substances. Further increase in activation time above 60 min the iodine number for prepared activated carbons is found to decrease. This may be because of increasing the activation time, the pores might get widened to an enormous extent, carbon burnt off is very high and resulting reduction in the surface area available for iodine adsorption.

Table 3.2 (b): Effect of activation time on iodine number

| ACs | Activation Time (min) | Heating rate (°C/min) | Carbonization temperature (°C) | Impregnation ratio | Iodine Number (mg/g) |
|------|-----------------------|-----------------------|--------------------------------|--------------------|----------------------|
| ACZC | 30 | 5 | 500 | 0.5 | 415.83 |
| | 60 | 5 | 500 | 0.5 | 489.86 |
| | 90 | 5 | 500 | 0.5 | 455.52 |
| | 120 | 5 | 500 | 0.5 | 410.34 |
| ACPA | 30 | 5 | 500 | 0.5 | 379.07 |
| | 60 | 5 | 500 | 0.5 | 412.65 |

| | | | | | |
|------|-----|---|-----|-----|--------|
| | 90 | 5 | 500 | 0.5 | 367.68 |
| | 120 | 5 | 500 | 0.5 | 356.42 |
| ACPC | 30 | 5 | 500 | 0.5 | 262.31 |
| | 60 | 5 | 500 | 0.5 | 283.28 |
| | 90 | 5 | 500 | 0.5 | 271.04 |
| | 120 | 5 | 500 | 0.5 | 254.81 |

3.3.1.3. Effect of carbonization temperature

In order to examine the effect of the carbonization temperature on the activated carbon preparations, the activation temperatures were varied from 500 to 900 °C with an interval of 50 °C. Table 3.2(c) shows the effect of carbonization temperature on the prepared activated carbons. The impregnation ratio of 0.5 and an activation time of 60 min was fixed for all activated carbons preparation. The maximum iodine number achieved are 685.19 mg/g at 600 °C for ACZC, 646.44 mg/g at 700 °C for ACPA and 612.70 mg/g at 800 °C for ACPC.

Table 3.2 (c): Effect of carbonization temperature on iodine number

| ACs | Carbonization temperature (°C) | Holding Time (min) | Heating rate (°C/min) | Impregnation ratio | Iodine Number (mg/g) |
|------|--------------------------------|--------------------|-----------------------|--------------------|----------------------|
| ACZC | 500 | 60 | 5 | 0.5 | 489.86 |
| | 550 | 60 | 5 | 0.5 | 559.24 |
| | 600 | 60 | 5 | 0.5 | 685.19 |
| | 650 | 60 | 5 | 0.5 | 618.69 |
| | 700 | 60 | 5 | 0.5 | 570.75 |
| ACPA | 500 | 60 | 5 | 0.5 | 412.65 |
| | 550 | 60 | 5 | 0.5 | 468.27 |
| | 600 | 60 | 5 | 0.5 | 524.66 |
| | 650 | 60 | 5 | 0.5 | 571.38 |
| | 700 | 60 | 5 | 0.5 | 646.44 |
| | 750 | 60 | 5 | 0.5 | 564.61 |
| | 800 | 60 | 5 | 0.5 | 510.24 |
| ACPC | 500 | 60 | 5 | 0.5 | 283.28 |
| | 600 | 60 | 5 | 0.5 | 376.98 |
| | 650 | 60 | 5 | 0.5 | 432.06 |
| | 700 | 60 | 5 | 0.5 | 552.62 |

| | | | | | |
|--|-----|----|---|-----|--------|
| | 750 | 60 | 5 | 0.5 | 579.82 |
| | 800 | 60 | 5 | 0.5 | 612.70 |
| | 850 | 60 | 5 | 0.5 | 604.30 |
| | 900 | 60 | 5 | 0.5 | 572.34 |

At particular carbonization temperature the iodine number of the prepared carbon was maximum (chemical agent specific), but at lower and higher temperatures the iodine number is less. The reason may be at lower activation temperature, the blockage of the entrances to the micropores and mesopores by tar, which results in less adsorption. With the increase in activation temperature, reactions with activating agents increase and there is decomposition of the tar substances, hence higher iodine number. At still higher temperatures, the iodine number is again less may be because of the widening of pores to a considerable extent; the percentage of carbon that is burnt off is very high which may be reducing the surface area available for adsorption. Similar variations are reported in the previous works; for activated carbons derived from various lignocellulosic precursors like cotton stalk (Deng et al., 2009), woody biomass birch (Budinova et al., 2006), macro-algal biomass (Aravindhana et al., 2009), rubber wood sawdust (Srinivasakannan and Bakar, 2004).

3.3.1.4. Effect of impregnation ratio

Impregnation ratio is defined as the ratio of the weight of the activating agent to the weight of the raw material to be activated. In order to examine the effect of the impregnation ratio on the activated carbon produced, the impregnation ratio was increased in steps for different activating agents at different ranges. Table 3.2(d) lists the iodine number of ACZC, ACPA and ACPC prepared at various impregnation ratios. Table 3.2(d) shows an increase in the iodine number till a particular impregnation ratio and a further increase in the impregnation ratio indicated that iodine number decreases. These phenomena are observed for all the activated carbons obtained from various activating agents used. The used amounts of $ZnCl_2/H_3PO_4/K_2CO_3$ in the impregnation ratio strongly influence the porous texture of the resulting activated carbons. The development of new pores and a widening process of micropores with an increase in impregnation ratio are specified.

Table 3.2 (d): Effect of impregnation ratio on iodine number

| ACs | Impregnation ratio | Holding Time (min) | Heating rate (°C/min) | Carbonization temperature (°C) | Iodine Number (mg/g) |
|------|--------------------|--------------------|-----------------------|--------------------------------|----------------------|
| ACZC | 0.5 | 60 | 5 | 600 | 685.19 |

| | | | | | |
|------|------|----|---|-----|---------|
| | 1.0 | 60 | 5 | 600 | 848.79 |
| | 1.5 | 60 | 5 | 600 | 906.62 |
| | 2.0 | 60 | 5 | 600 | 1015.19 |
| | 2.5 | 60 | 5 | 600 | 912.39 |
| ACPA | 0.5 | 60 | 5 | 700 | 646.44 |
| | 1.0 | 60 | 5 | 700 | 857.54 |
| | 1.5 | 60 | 5 | 700 | 963.44 |
| | 2.0 | 60 | 5 | 700 | 886.36 |
| | 2.5 | 60 | 5 | 700 | 819.85 |
| ACPC | 0.25 | 60 | 5 | 800 | 578.46 |
| | 0.5 | 60 | 5 | 800 | 612.70 |
| | 0.75 | 60 | 5 | 800 | 542.26 |
| | 1.0 | 60 | 5 | 800 | 490.61 |

Maximum values of iodine number are obtained at impregnation ratios of 2.0, 1.5 and 0.5 for ACZC, ACPA, and ACPC, respectively. With further increase in the impregnation ratio, the iodine number is decreased. This is because of more amount of activating agent degraded the biomass to a much large extent causing the micropores to combine together to produce large pores that are decreasing the surface area available for iodine adsorption. A similar variation was observed for the activation of the cotton stalk (Deng et al., 2009), vetiver roots (Altenor et al., 2009), and Tunisian olive-waste cakes (Baccar et al., 2009), rubber wood sawdust (Srinivasakannan and Bakar, 2004).

3.4. Yields of prepared activated carbons

Fox nutshell is a composite material formed of natural polymers (cellulose, hemicellulose, and lignin). In activation or carbonization at high temperature, the polymeric structures of the biomass decompose and liberate most of the non-carbon elements, mainly hydrogen, oxygen and nitrogen in the form of liquid (called as tars) and gases, leaving behind a rigid carbon skeleton in the form of aromatic sheets and strips (Prahas et al., 2008). As noted in Table 3.1, the raw material Fox nutshell was used in this study has low ash and high volatile matter contents. The high volatile matter and low ash content of a biomass resource make it a suitable starting material for preparing activated carbon (Yorgun et al., 2009). The yield of activated carbon was calculated by dividing the mass of the resulted activated carbon with the initial mass of the raw material used for activation (Qian et al., 2007; Yorgun et

al., 2009). The final carbonization temperature and impregnation ratio play a significant role on the yield of activated carbon.

The yield of activated carbons without and with ZnCl_2 impregnation at various impregnation ratios and carbonization temperature are shown in Fig. 3.2. The figure indicates higher yields with impregnation than without impregnation in the carbonization temperature range of 500-700 °C. The activation of the Fox nutshell without ZnCl_2 impregnation results in a relatively small yield % of 27.25-21.25%, since a lot of carbons removed as CO , CO_2 , CH_4 , aldehydes and tar coupling with O and H atoms (Miao et al., 2013; Qian et al., 2007). However, ZnCl_2 would selectively stripe H and O away from the Fox nutshell as H_2O and H_2 rather than CO , CO_2 or hydrocarbons (Miao et al., 2013; Qian et al., 2007). From Fig. 3.2, the yield % of carbon decreases above 500 °C of carbonization due to the increase of tar release (Hsu and Teng, 2000). The yield of the activated carbons with low ZnCl_2 /Fox nutshell ratio of 1.0 gets a higher value in the range of 43.64-38.12% at activation temperatures between 500-700 °C. As the impregnation ratio increases from 1.0 to 2.5, more carbon burned, and micropore widens into mesopore by extra ZnCl_2 , resulting in lower yield values (Miao et al., 2013).

Figure 3.3 displays the yield of the prepared activated carbons at different carbonization temperature and H_3PO_4 impregnation ratios. From the figure, it is observed that the activated carbon yields in the entire range of study are between 24.31 to 41.13%. The yield is comparable to those obtained in some other studies (Gomez-Serrano et al., 2005; Prahas et al., 2008; Yorgun and Yıldız, 2015), 33.18%-25.16% from paulownia wood, 42.15-56.25% from jackfruit peel, 37.2-42.3% from chestnut wood, 31.9-48.5% from fruit stones. The yield of activated carbon increases due to the presence of phosphoric acid up to impregnation ratio value of 1, then it decreases with higher impregnation ratio. This may be because of during activation with H_3PO_4 , promotes depolymerization, dehydration, and redistribution of constituent biopolymers, and also favoring the conversion of aliphatic to aromatic compounds (Yakout and El-Deen, 2016).

The yield with a low H_3PO_4 impregnation ratio of 1.0 resulted in higher and in the range of 41.13-37.84% between activation temperatures of 600 to 800 °C. At each carbonization temperature, the yield of activated carbon decreases with increasing impregnation ratio above 1.0. This may be due to the phosphoric acid reacted with the char and volatile matter and diffused quickly out of the surfaces of particles during the activation process. Therefore, with a high impregnation ratio, the gasification of surface carbon atoms became primary,

leading to an increase in the weight loss and a low carbon yield during activation process (Prahas et al., 2008). Similar results of activated carbon yields have been previously reported (Prahas et al., 2008; Yorgun and Yıldız, 2015).

Yield of prepared activated carbons at different carbonization temperature and K_2CO_3 impregnation ratios is shown in Fig. 3.4. It is found that the yield of activated carbon decreases with increase in activation temperature due to the release of volatile products as a result of intensifying dehydration and elimination reaction; it is also indicated that char of the biomass was gasified by K_2CO_3 in an inert atmosphere (Hayashi et al., 2002b; Okada et al., 2003).

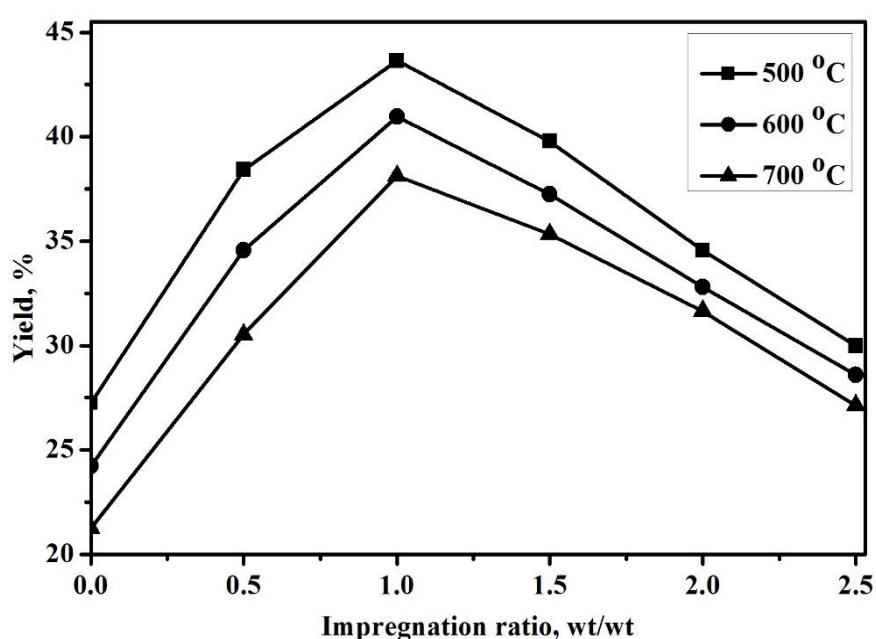


Fig. 3.2. Effect of carbonization temperature and $ZnCl_2$ impregnation ratio on the yield of activated carbon.

During the thermal decomposition of lignocellulosic precursors, the presence of K_2CO_3 in the interior of the precursor restricted the formation of tar as well as other liquids such as acetic acid and methanol by formation of cross-links, and inhibited the shrinkage of the precursor particle by occupying certain substantial volumes (Adinata et al., 2007; Guo and Lua, 2003). The yield of the activated carbons decreases from 30.11–19.02% with increasing carbonization temperature from 600 to 900 °C at 0.5 impregnation ratio. The yield of the prepared activated carbon decreases from 28.14–17.12% with increasing impregnation ratio from 0.25 to 1.0 at 800 °C activation temperature. The yield is strongly affected by the impregnation ratio at all temperatures. Yield is decreased with increased the impregnation ratio due to increased burn-off of Fox nutshell (Adinata et al., 2007).

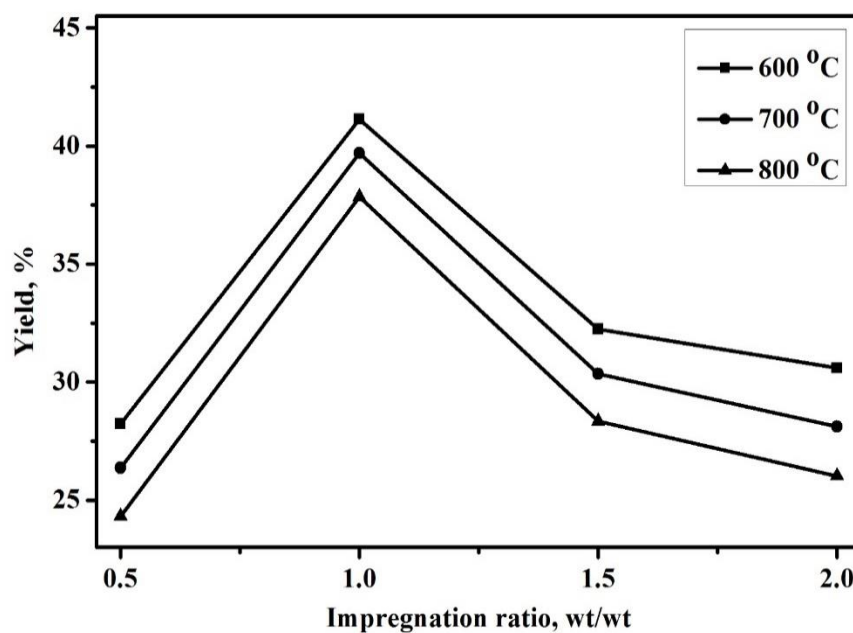


Fig. 3.3. Effect of carbonization temperature and H₃PO₄ impregnation ratio on the yield of activated carbons.

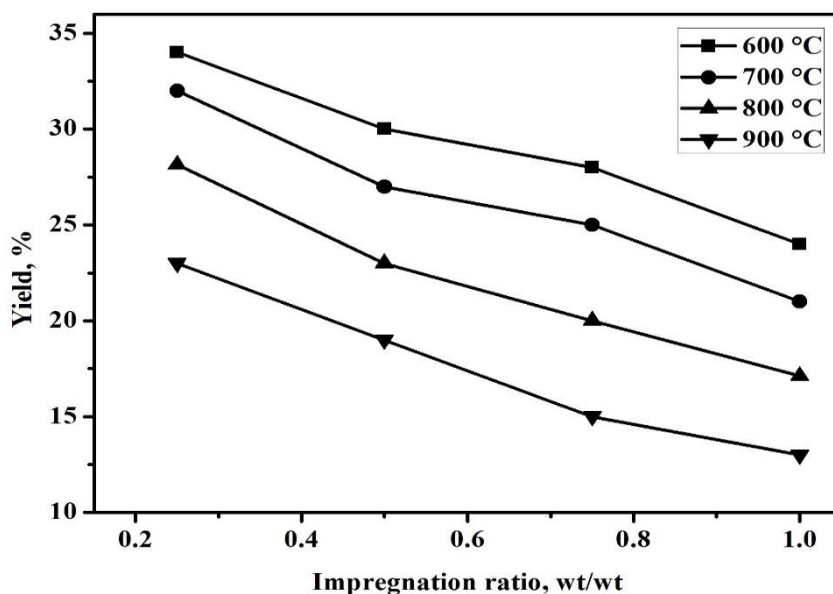


Fig. 3.4. Effect of carbonization temperatures and K₂CO₃ impregnation ratio on the yield of activated carbons.

3.5. Characterization of prepared activated carbons

3.5.1. Ultimate analysis

The results of the elemental analysis of the prepared activated carbons (ACZC) at various carbonization temperatures and ZnCl₂ impregnation ratios are tabulated in Table 3.3. From the table, it is observed that the carbon content of activated carbon increases with carbonization temperature to some extent and then decreases. The C content of the activated carbon increases with the increase in carbonization temperature from 500 to 600 °C due to

an increasing degree of aromaticity (Fierro et al., 2006). The carbon content of the activated carbon also increases with the increase in impregnation ratio. A maximum carbon content of 92.85 wt% obtained at carbonization temperature of 600 °C and impregnation ratio of 2.5.

Table 3.3: Ultimate analysis of activated carbons prepared with ZnCl₂ activation

| Prepared ACs | Ultimate analysis (wt%) | | | | |
|---|-------------------------|------|------|------|----------------------|
| | C | H | N | S | O (by difference) |
| ZnCl₂ impregnation ratio: 2 | | | | | |
| Carbonization temperature (°C) | | | | | |
| 500 | 70.11 | 3.72 | 0.98 | 0.07 | 25.12 |
| 600 | 89.77 | 2.33 | 0.43 | 0.06 | 7.41 |
| 700 | 78.75 | 2.51 | 0.35 | 0.04 | 18.35 |
| Carbonization temperature: 600 °C | | | | | |
| Impregnation ratio | | | | | |
| 1 | 69.15 | 3.82 | 0.87 | 0.06 | 26.10 |
| 1.5 | 74.43 | 2.37 | 0.18 | 0.09 | 22.93 |
| 2 | 89.77 | 2.33 | 0.43 | 0.06 | 7.41 |
| 2.5 | 92.85 | 2.12 | 1.12 | 0.08 | 3.83 |

The hydrogen and oxygen content is decreased with impregnation ratio as well as carbonization temperature increases. The increase in carbon content and a reduction in hydrogen, nitrogen, and oxygen contents with an increase in impregnation ratios may be because of the following reasons. In the pyrolysis and activation process, the Fox nutshell is decomposed. During the decomposition, the volatile compounds containing mainly H, O, and N leave the carbonaceous product that becomes rich in carbon. This could be attributed to the fact that ZnCl₂ would selectively stripe H and O away from the Fox nutshell as H₂O and H₂ rather than CO, CO₂ or hydrocarbons (Miao et al., 2013; Yorgun et al., 2009).

The results of the elemental analysis of the activated carbons (ACPA) at various carbonization temperatures and H₃PO₄ impregnation ratios are tabulated in Table 3.4. From the table it is observed that the activated carbon prepared at 700 °C possess maximum carbon content of 64.25 wt% at 1.5 impregnation ratio, whereas the hydrogen and oxygen content are the least 4.52 wt% and 29.24 wt%, respectively. The activated carbons prepared at lower and higher activation temperatures of 600 and 800 °C, contain relatively less amount of carbon. The reason may be due to an increased degree of aromaticity at 700 °C

(Fierro et al., 2006). The effects of impregnation ratios on the elemental composition of activated carbons studied at 700 °C activation temperature are tabulated in Table 3.4. With increasing impregnation ratio, the carbon content of activated carbons increases from 51.29 to 68.75 wt%, while hydrogen, nitrogen, and oxygen contents decrease till the impregnation ratio of 2.0 in the range of study. Variation of the carbon content of the prepared activated carbons by both activating agents with temperature shows a good agreement with the results reported by Fierro et al. and Angin (Angin, 2014; Fierro et al., 2006).

Table 3.4: Ultimate analysis of activated carbons prepared with H₃PO₄ activation

| Prepared ACs | Ultimate analysis (wt%) | | | | |
|--|-------------------------|------|------|------|----------------------|
| | C | H | N | S | O (by difference) |
| H₃PO₄ impregnation ratio: 1.5 | | | | | |
| Carbonization temperature (°C) | | | | | |
| 600 | 63.89 | 4.74 | 1.68 | 0.16 | 29.53 |
| 700 | 64.85 | 4.52 | 1.24 | 0.15 | 29.24 |
| 800 | 55.60 | 4.68 | 1.45 | 0.13 | 38.14 |
| Carbonization temperature: 700 °C | | | | | |
| Impregnation ratio | | | | | |
| 0.5 | 51.29 | 4.80 | 1.42 | 0.09 | 42.40 |
| 1 | 61.28 | 4.59 | 1.30 | 0.13 | 32.70 |
| 1.5 | 64.85 | 4.52 | 1.24 | 0.15 | 29.84 |
| 2 | 68.75 | 4.29 | 1.16 | 0.15 | 25.65 |

The results of the elemental analysis of the activated carbons (ACPC) at various carbonization temperatures and K₂CO₃ impregnation ratios are tabulated in Table 3.5. An increase in carbon content from 60.6 to 68.2 wt% of activated carbons observed at 0.5 impregnation ratio with an increasing of activation temperature from 600 to 800 °C; with further increase of temperature to 900 °C the carbon content decreases to a value of 67.46 wt%. The hydrogen and oxygen content is found to decrease from 1.9 to 1.6 wt%, and 36.19 to 29.37 wt%, respectively. The effect of impregnation ratio on the elemental composition of activated carbons studied at 800 °C carbonization temperature are also tabulated in Table 3.5. With increasing impregnation ratio, the carbon content of activated carbons increases from 62.5 to 69.85%, and hydrogen, nitrogen, and oxygen contents decrease till the maximum impregnation ratio value of 1.0.

Table 3.5: Ultimate analysis of activated carbons prepared with K₂CO₃ activation

| Prepared ACs | Ultimate analysis (wt%) | | | | |
|--|-------------------------|------|------|------|----------------------|
| | C | H | N | S | O (by difference) |
| K₂CO₃ impregnation ratio: 0.5 | | | | | |
| Carbonization temperature (°C) | | | | | |
| 600 | 60.6 | 1.9 | 1.29 | 0.02 | 36.19 |
| 700 | 64.03 | 1.7 | 0.95 | 0.03 | 33.29 |
| 800 | 68.2 | 1.6 | 0.82 | 0.01 | 29.37 |
| 900 | 67.46 | 1.4 | 0.77 | 0.01 | 30.36 |
| Carbonization temperature: 800 °C | | | | | |
| Impregnation ratio | | | | | |
| 0.25 | 62.5 | 2.2 | 1.84 | 0.04 | 33.42 |
| 0.5 | 68.2 | 1.6 | 0.82 | 0.01 | 29.37 |
| 0.75 | 69.3 | 1.4 | 0.95 | 0.03 | 28.32 |
| 1 | 69.85 | 1.92 | 0.24 | 0.15 | 27.84 |

3.5.2. N₂ adsorption-desorption isotherms

Nitrogen adsorption, because of the relatively small molecular diameter of nitrogen, is frequently used at 77 K to study porosity and surface area and also a standard procedure for the characterization of the porous structures of carbonaceous adsorbents (Ryu et al., 2000). Adsorption processes can be divided into several distinct stages at relative pressures of 10^{-6} – 10^{-4} , 10^{-4} – 10^{-2} , 10^{-2} – 10^{-1} , and 0.9–1.0 which can be attributed to multiple stage pore filling processes (Gregg et al., 1967; Ryu et al., 2000), such as: (i) filling of narrow micropores such as ultramicro pores; (ii) monolayer formation on the surfaces of wider micropores such as supermicropores; (iii) monolayer formation and filling of mesopores by capillary condensation, and (iv) filling of macropores by capillary condensation, which takes place at relative pressures close to unity.

The N₂ adsorption-desorption isotherms of the prepared ACs at different carbonization temperature ranging from 500 to 800 °C and impregnation ratios from 0.25 to 2.5 were carried out to investigate the porous characteristics. The nitrogen adsorption-desorption isotherms for the prepared activated carbons are shown in Figs. 3.5 and 3.6. It is evident from all figures that the shape of N₂ adsorption-desorption isotherm gradually changes with an increase in carbonization temperatures and ZnCl₂ or H₃PO₄/Fox nutshell mass ratio. From Figs. 3.5(a-b) and 3.6(a-b), a rapid rise in the adsorption-desorption isotherms

observed at low relative pressures (< 0.4), which is followed by a nearly horizontal plateau at higher relative pressures.

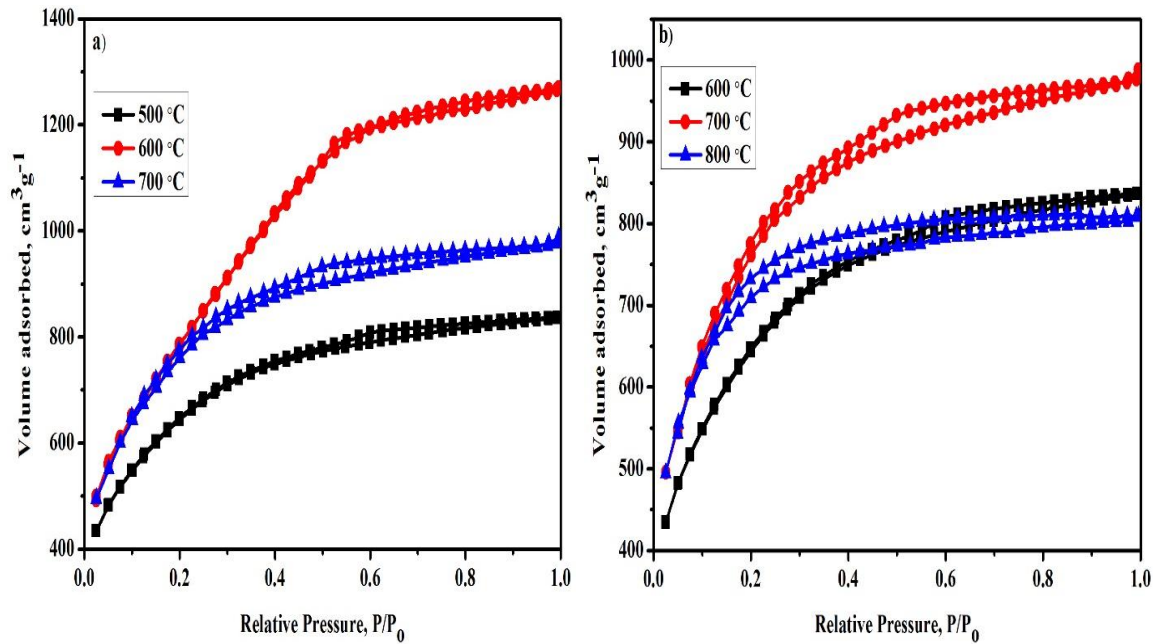


Fig. 3.5. Nitrogen adsorption–desorption isotherms of activated carbons prepared at different carbonization temperature [(a) ZnCl_2 impregnation ratio = 2.0 and (b) H_3PO_4 impregnation ratio = 1.5].

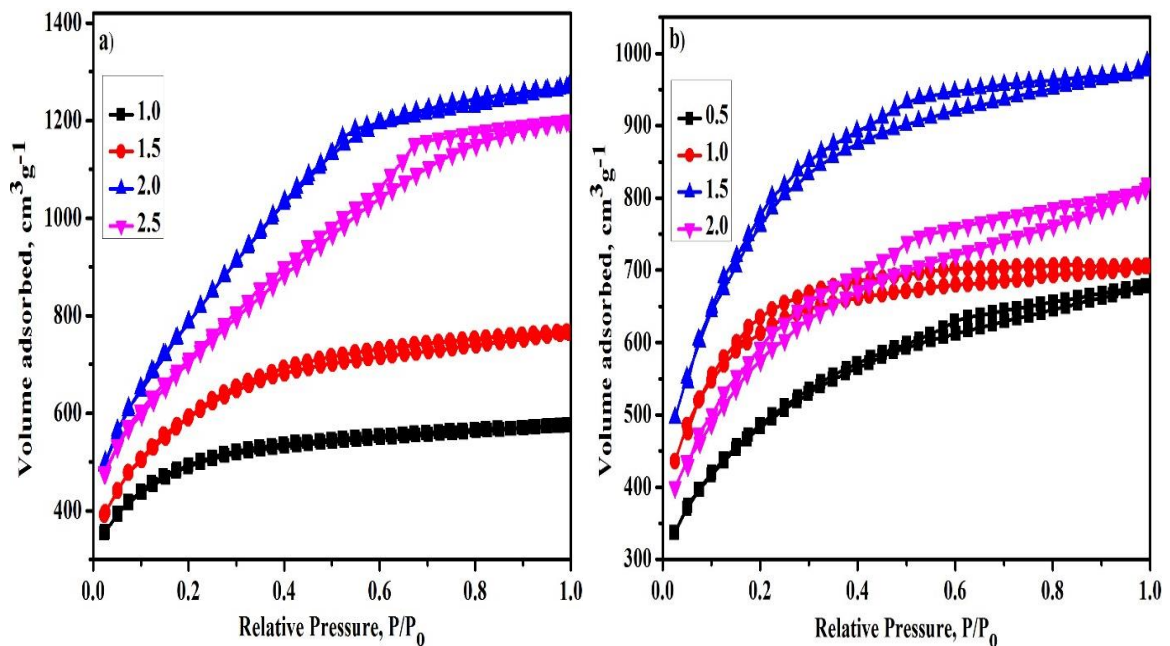


Fig. 3.6. Nitrogen adsorption–desorption isotherms of activated carbons prepared at different; (a) ZnCl_2 impregnation ratio (carbonization temperature = 600 °C) and (b) H_3PO_4 impregnation ratios (carbonization temperature = 700 °C).

These results indicate that all isotherms of all prepared activated carbons belonging to type I isotherm based on the classification of the International Union of Pure and Applied

Chemistry (IUPAC). The type I isotherm represents that micropores are present in the prepared activated carbons (Yorgun et al., 2009; Zhang et al., 2015).

Hysteresis loop (wide knee) in the isotherms indicate the presence of mesoporosity associated with capillary condensation during the adsorption-desorption process (Yorgun et al., 2009; Zhang et al., 2015). According to the IUPAC classification, the prepared activated carbons exhibit a hysteresis loop type 4, that is very frequent (Fierro et al., 2006; Ozdemir et al., 2014). From Figs. 3.5 and 3.6, the knee width increases with increasing of carbonization temperature and impregnation ratio in both types of prepared activated carbons. This confirms that an increase in mesoporosity due to the merging of micropores with an increase in carbonization temperature and impregnation ratio.

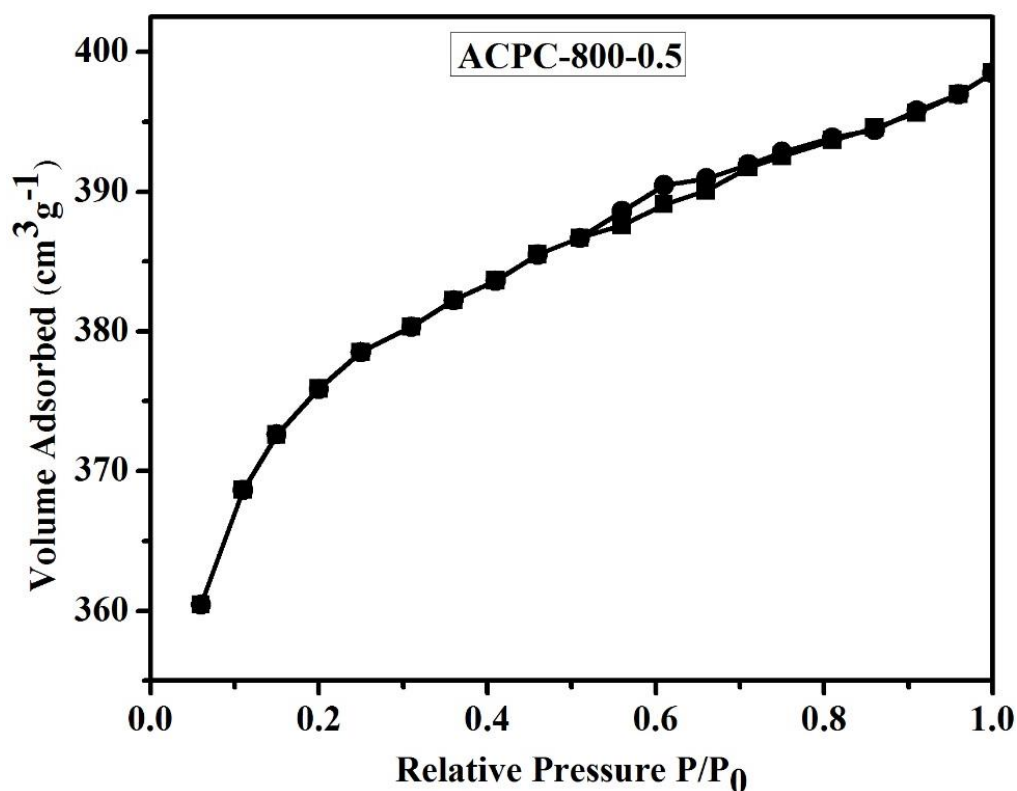


Fig. 3.7. N₂ adsorption–desorption isotherms of activated carbon prepared at 800 °C carbonization temperature and K₂CO₃ impregnation ratio of 0.5.

Iodine numbers of the prepared activated carbons with K₂CO₃ activator is lower than those prepared with ZnCl₂ and H₃PO₄ activators. For K₂CO₃ activated carbons, due to some instrumental issues a 20 point N₂ adsorption-desorption isotherm was generated for the prepared ACPC at 800 °C carbonization temperature and impregnation ratio of 0.5 (Fig. 3.7). The figure shows open knee present in the adsorption isotherm and a hysteresis loop type 4. Thus it is clear that both micropores and mesopores are present the prepared activated carbon.

3.5.3. Surface area and pore volume

3.5.3.1. Effect of carbonization temperature

The final carbonization temperature is an important process parameter in determining the surface area and the pore volume of the activated carbon in the chemical activation process (Yorgun et al., 2009). Using ZnCl_2 as activating reagent as well as various carbonization temperatures from 500 to 700 °C, in the experimental domain all the activated carbons prepared have BET surface areas ranging from 1236 m^2/g to 2869 m^2/g . The effects of carbonization temperature on the surface areas (BET surface area, micropore, and mesopore) and pore volumes (total, micropore, and mesopore) of the prepared activated carbons are shown in Figs. 3.8(a-b) and listed in Table 3.6.

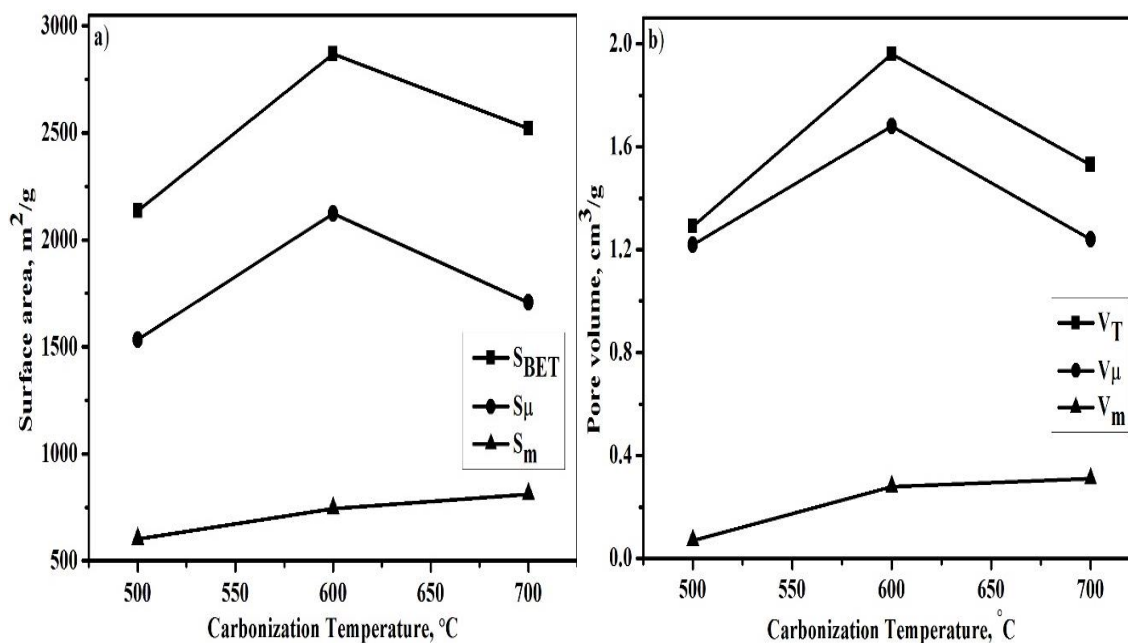


Fig. 3.8. Effect of carbonization temperature on (a) surface area and (b) pore volume of activated carbons prepared with ZnCl_2 impregnation at ratio of 2.0.

The BET surface area and micropore surface area of the activated carbons increase from 500 to 600 °C and decrease with increasing carbonization temperature beyond 600 °C, at impregnation ratio of 2 and 1 hr of holding time. This may be because of reason, above 600 °C, ZnCl_2 does not act as an activation agent, and the surface area and pore volume decrease due to the heat shrinkage, resulting in the narrowing and closing up to some of the pores (Hayashi et al., 2000; Zhang et al., 2015). The total pore volume and micropore volume of the activated carbons increases with increase carbonization temperature from 500 to 600 °C and decreases above 600 °C. From Table 3.6 and Fig. 3.8(b), the mesopore volume of the activated carbons found to increase with increase in carbonization temperature due to the

merging of micropores. For the activated carbon prepared at 600 °C carbonization temperature and impregnation ratio of 2, the S_{BET} , S_{μ} , and S_m are found to be 2869, 2124, and 745 m²/g, respectively [Fig. 3.8(a)]; and V_T , V_{μ} , and V_m are found as 1.96 cm³/g, 1.68 cm³/g, and 0.28 cm³/g, respectively [Fig. 3.8(b)]. Table 3.6 shows that the microporosity decreases from 86.04% to 81.04% with increase in carbonization temperature from 500 to 700 °C due to sintering effect of the volatiles and heat shrinkage of the carbon structure, resulting in the narrowing and closing up to some of the pores (Hayashi et al., 2000; Köseoğlu and Akmil-Başar, 2015; Yang and Qiu, 2010). The above researchers have reported a similar trend.

Table 3.6: BET surface area, total pore volume, micropore volume of prepared activated carbons at different carbonization temperatures

| ACs | S_{BET} (m ² /g) | S_{μ} (m ² /g) | S_m (m ² /g) | V_T (cm ³ /g) | V_{μ} (cm ³ /g) | V_m (cm ³ /g) | V_{μ}/V_T (%) | S_{μ}/S_{BET} (%) | D_p (nm) |
|--|----------------------------------|----------------------------------|------------------------------|-------------------------------|-----------------------------------|-------------------------------|----------------------|--------------------------|---------------|
| ZnCl₂ impregnation ratio: 2 | | | | | | | | | |
| Carbonization temperature (°C) | | | | | | | | | |
| 500 | 2136 | 1533 | 603 | 1.29 | 1.11 | 0.18 | 86.04 | 71.77 | 2.41 |
| 600 | 2869 | 2124 | 745 | 1.96 | 1.68 | 0.28 | 85.71 | 74.03 | 2.73 |
| 700 | 2520 | 1708 | 812 | 1.53 | 1.24 | 0.31 | 81.04 | 67.78 | 2.43 |
| H₃PO₄ impregnation ratio: 1.5 | | | | | | | | | |
| Carbonization temperature (°C) | | | | | | | | | |
| 600 | 2223 | 1733 | 490 | 1.29 | 1.22 | 0.07 | 94.57 | 77.95 | 2.32 |
| 700 | 2636 | 2042 | 594 | 1.53 | 1.32 | 0.21 | 86.27 | 77.46 | 2.32 |
| 800 | 2298 | 1632 | 666 | 1.25 | 1.02 | 0.23 | 81.60 | 71.02 | 3.06 |
| K₂CO₃ impregnation ratio: 0.5 | | | | | | | | | |
| Carbonization temperature (°C) | | | | | | | | | |
| 600 | 582 | 412 | 170 | 0.32 | 0.24 | 0.08 | 75.0 | 25.0 | 2.20 |
| 700 | 856 | 628 | 228 | 0.53 | 0.37 | 0.16 | 69.81 | 30.19 | 2.50 |
| 800 | 1236 | 940 | 296 | 0.98 | 0.68 | 0.30 | 69.39 | 30.61 | 3.17 |
| 900 | 902 | 640 | 262 | 0.73 | 0.42 | 0.31 | 57.54 | 42.46 | 3.24 |
| S_{BET} : BET surface area, S_{μ} : micropore surface area, S_m : mesopore surface area, V_T : total pore volume, V_{μ} : micropore volume, V_m : mesopore volume, $V_{\mu}\%$ = $(V_{\mu}/V_T) \times 100$, $S_{\mu}\%$ = $(S_{\mu}/S_{BET}) \times 100$, D_p : average diameter. | | | | | | | | | |

The surface areas and pore volumes were determined for the prepared activated carbons by using an H₃PO₄ activating agent at different activation temperatures (600–800 °C), and impregnation ratio of 1.5 are listed in Table 3.6 and shown in Figs. 3.9(a-b).

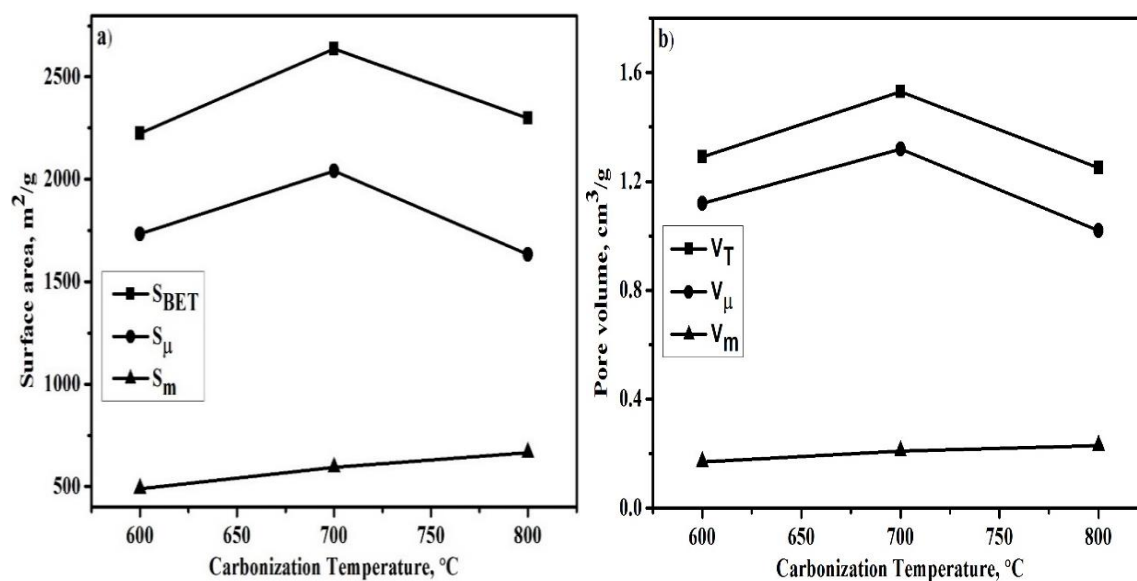


Fig. 3.9. Effect of carbonization temperature on (a) surface area and (b) pore volume of activated carbons prepared with H₃PO₄ impregnation at ratio of 1.5.

Maximum BET surface area and the total pore volumes of the prepared activated carbon at 700 °C of carbonization temperature and 1.5 impregnation ratio are obtained as 2636 m²/g and 1.53 cm³/g respectively. At 800 °C of carbonization temperature, the surface area and total pore volume values 2298 m²/g and 1.25 cm³/g, respectively are obtained. The micropore surface area was obtained by subtracting mesopore surface area from the corresponding BET surface area. The micropore surface area and micropore volume of the prepared activated carbon found to be highest at carbonization temperature of 700 °C. At this temperature and 1.5 impregnation ratio, S_μ, and S_m of prepared activated carbon are found to be 2042, and 594 m²/g, respectively. The micropore volume (V_μ), and mesopore volume (V_m) are found to be 1.32 and 0.21 cm³/g, respectively. The microporosity percentages of the prepared activated carbons at the studied temperatures show a decrease in microporosity with increasing carbonization temperatures (Table 3.6). The microporosity falls from 94.57% to 81.60%, as the temperature raised from 600 to 800 °C. The prepared activated carbon is mainly microporous, but it also contains mesopores that are crucial in facilitating the access of the adsorbate molecules to the interior of the carbon particles (Yorgun and Yıldız, 2015). Other studies also report a similar effect of carbonization temperature on the BET surface area and total pore volume for H₃PO₄ activation of other lignocellulosic precursors (Fierro et al., 2006; Prahas et al., 2008; Yakout and El-Deen, 2016; Yorgun and Yıldız, 2015).

Again, the effect of carbonization temperature on the BET surface area of ACs prepared by K₂CO₃ activation are listed in Table 3.6 and shown in Fig. 3.10. The BET surface area and

total pore volume increases with increase in carbonization temperature from 600 to 800 °C and decreases with increase in temperature to 900 °C. At 800 °C of carbonization temperature and impregnation ratio of 0.5, the BET surface area and total pore volume obtained are 1236 m²/g, and 0.98 cm³/g respectively.

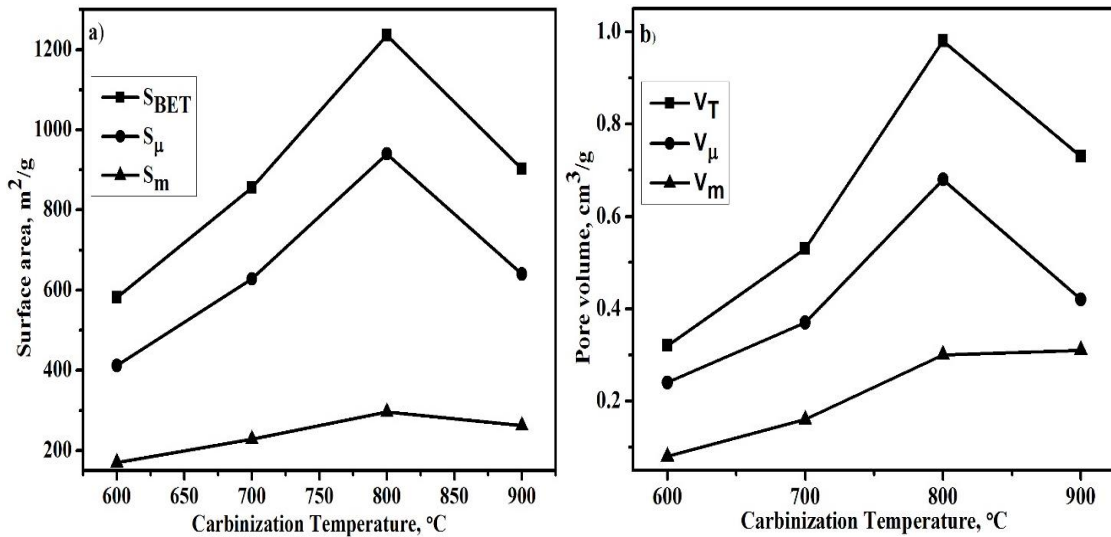


Fig. 3.10. Effect of carbonization temperature on (a) surface area and (b) pore volume of activated carbons prepared with K₂CO₃ impregnation at ratio of 0.5.

The surface area and pore volume increase with temperature may be due to the formation of volatile material that is the result of dehydration and elimination reactions, and cross-linking structure (Gurten et al., 2012). These two changes gradually improve reactions between carbonaceous material and K₂CO₃ that strongly depend on the applied temperature. As reported in the literature, alkali metal atoms are removed from the intercalated system at a higher temperature (Gurten et al., 2012; Hayashi et al., 2002a). Therefore rise in surface area and pore diameter. From Fig. 3.10(b), the total pore volume (micropore volume + mesopore volume) increases with an increase of carbonization temperature up to 800 °C. The micropore volume decreases, but mesopore volume increases above 800 °C. The microporosity drops from 75.0% to 57.54%, as the temperature rise from 600 to 900 °C (Table 3.6).

3.5.3.2. Effect of impregnation ratio

Fox nutshell char prepared at carbonization temperatures of 600, 700 and 800 °C with NaOH soaking and without chemical activation have surface areas of 203, 452 and 186 m²/g, respectively (Table 3.7). The surface area of the Fox nutshell char prepared at 700 °C temperature with 0.5N NaOH soaking is higher (452 m²/g) than the one (326 m²/g) obtained without NaOH soaking. This implies NaOH soaking is an important step during the high

surface area activated carbon preparation. The obtained result agrees with the findings of activated carbon prepared from herb residues (Yang and Qiu, 2011).

The impregnation ratio plays a significant role in getting high surface area activated carbon. The $ZnCl_2$ works as dehydration reagent that lowers the carbonization temperature during chemical activation and restricts the formation of tar as well as promotes charring and aromaticity of carbon (Hayashi et al., 2000; Yorgun et al., 2009; Zhang et al., 2015).

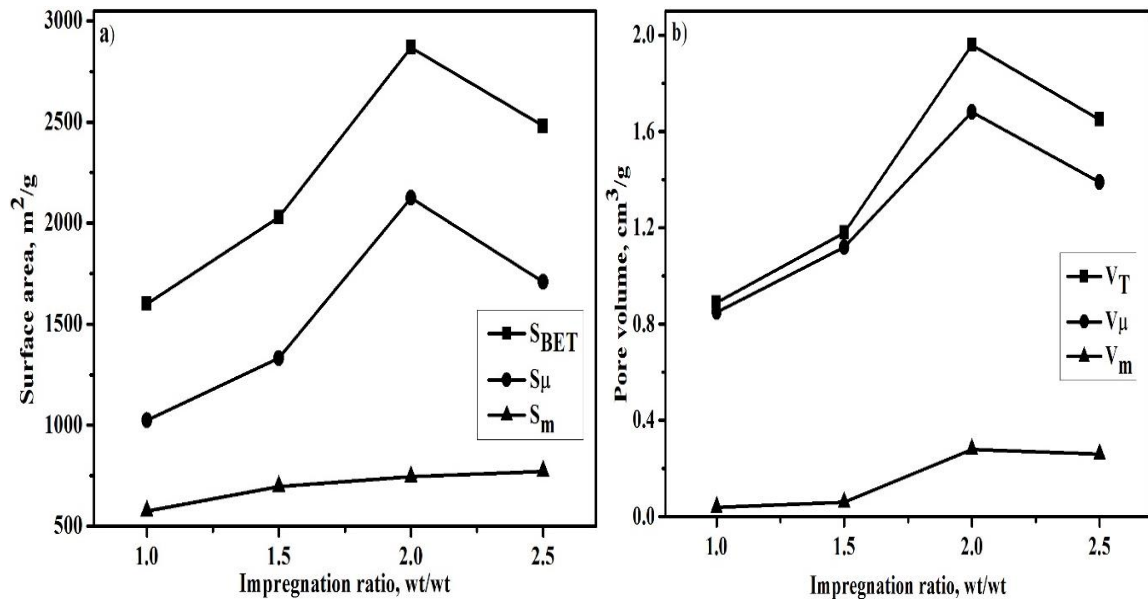


Fig. 3.11. Effect of $ZnCl_2$ impregnation ratio on (a) surface area and (b) pore volume of activated carbons prepared at 600 °C carbonization temperature.

The effect of impregnation ratio on the surface area and pore volume of activated carbons prepared at 600 °C carbonization temperature were studied, and the results are plotted in Fig. 3.11(a-b) and tabulated in Table 3.7. It is observed that the S_{BET} , S_{μ} , and S_m , and V_T , V_{μ} , and V_m of the prepared activated carbon increases rapidly by increasing the impregnation ratio up to 2 and then decreases. Results show that the prepared activated carbon contains a large amount of micropores (Table 3.7). The maximum BET surface area and total pore volume of the activated carbon prepared at 600 °C activation temperature and impregnation ratio of 2 are 2869 m²/g and 1.96 cm³/g, respectively. The micropore percentage of the activated carbon decreases from 95.50 to 84.24% as the impregnation ratio increased from 1 to 2.5. This micropore decrease may be due to the heat shrinking (Hayashi et al., 2000). The maximum percentage of micropore surface area is 74.03% for the prepared activated carbon at 600 °C carbonization temperature and impregnation ratio of 2.

H₃PO₄ activator has two important functions: it promotes the pyrolytic decomposition of the original material and the formation of the cross-linked structure (Yakout and El-Deen, 2016). However, H₃PO₄ allows the development of both micropores and mesopores in the prepared activated carbons.

Table 3.7: BET surface area, total pore volume, micropore volume of activated carbons prepared with different chemical impregnation

| ACs | S _{BET} (m ² /g) | S _μ (m ² /g) | S _m (m ² /g) | V _T (cm ³ /g) | V _μ (cm ³ /g) | V _m (cm ³ /g) | V _μ /V _T (%) | S _μ /S _{BET} (%) | D _p (nm) |
|---|--------------------------------------|------------------------------------|---------------------------------------|--|--|--|---------------------------------------|---|------------------------|
| Without NaOH soaking | | | | | | | | | |
| Carbonization temperature (°C) | | | | | | | | | |
| 700 | 326 | - | - | 0.37 | - | - | - | - | 4.54 |
| With NaOH soaking | | | | | | | | | |
| Carbonization temperature (°C) | | | | | | | | | |
| 600 | 203 | - | - | 0.21 | - | - | - | - | 4.14 |
| 700 | 452 | - | - | 0.43 | - | - | - | - | 3.80 |
| 800 | 186 | - | - | 0.18 | - | - | - | - | 3.87 |
| Carbonization temperature: 600 °C | | | | | | | | | |
| ZnCl₂ Impregnation ratio | | | | | | | | | |
| 1 | 1601 | 1025 | 576 | 0.89 | 0.85 | 0.04 | 95.50 | 64.02 | 2.22 |
| 1.5 | 2028 | 1331 | 697 | 1.18 | 1.12 | 0.06 | 94.91 | 65.63 | 2.32 |
| 2 | 2869 | 2124 | 745 | 1.96 | 1.68 | 0.28 | 85.71 | 74.03 | 2.73 |
| 2.5 | 2480 | 1708 | 772 | 1.65 | 1.39 | 0.26 | 84.24 | 68.87 | 2.66 |
| Carbonization temperature: 700 °C | | | | | | | | | |
| H₃PO₄ Impregnation ratio | | | | | | | | | |
| 0.5 | 1622 | 1193 | 429 | 1.05 | 0.97 | 0.08 | 92.38 | 73.55 | 2.60 |
| 1 | 1989 | 1476 | 627 | 1.09 | 0.95 | 0.14 | 87.15 | 74.21 | 2.19 |
| 1.5 | 2636 | 2042 | 594 | 1.53 | 1.32 | 0.21 | 86.27 | 77.46 | 2.32 |
| 2 | 1943 | 1496 | 447 | 1.27 | 1.00 | 0.27 | 78.74 | 76.99 | 2.61 |
| Carbonization temperature: 800 °C | | | | | | | | | |
| K₂CO₃ Impregnation ratio | | | | | | | | | |
| 0.25 | 464 | 336 | 128 | 0.36 | 0.22 | 0.14 | 61.11 | 72.41 | 3.10 |
| 0.5 | 1236 | 940 | 296 | 0.98 | 0.68 | 0.30 | 69.39 | 76.05 | 3.17 |
| 0.75 | 1022 | 720 | 302 | 0.84 | 0.55 | 0.29 | 65.48 | 74.36 | 3.30 |
| 1 | 867 | 615 | 222 | 0.56 | 0.34 | 0.22 | 60.71 | 70.93 | 2.58 |
| S _{BET} : BET surface area, S _μ : micropore surface area, S _m : mesopore surface area, V _T : total pore volume, V _μ : micropore volume, V _m : mesopore volume, V _μ % = (V _μ /V _T) × 100, S _μ % = (S _μ /S _{BET}) × 100, D _p : average diameter. | | | | | | | | | |

In the present study with H_3PO_4 chemical activation, the effect of different impregnation ratios on the surface area and pore volume of the prepared activated carbons were investigated, and the results are presented in Fig. 3.12(a-b), and Table 3.7. The maximum BET surface area and the total pore volume of $2636 \text{ m}^2/\text{g}$ and $1.53 \text{ cm}^3/\text{g}$ respectively obtained for the activated carbon prepared at activation temperature of $700 \text{ }^\circ\text{C}$ and impregnation ratio of 1.5.

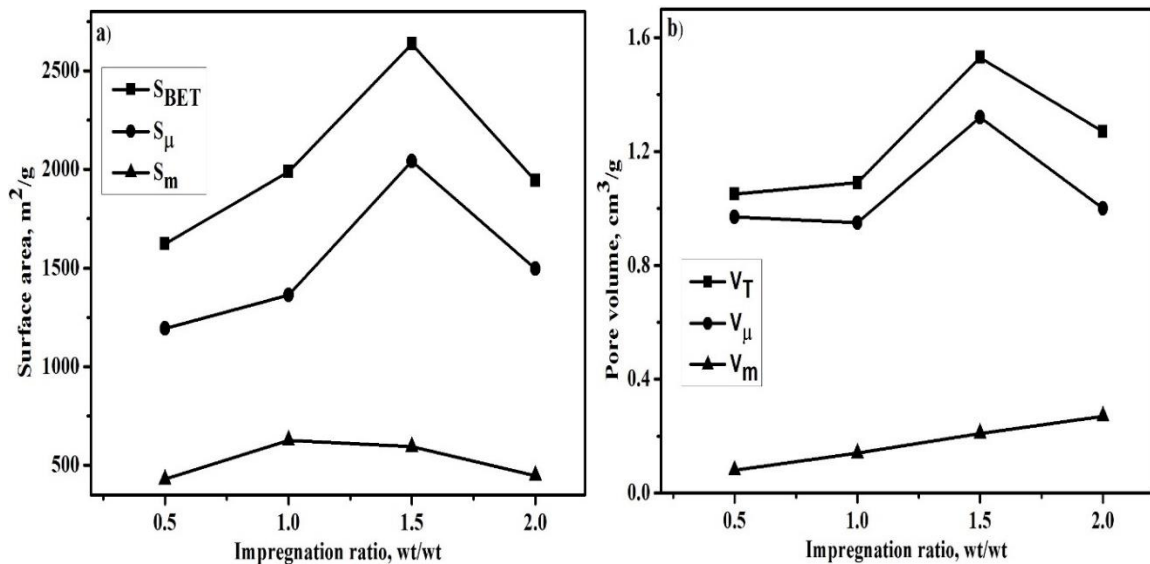


Fig. 3.12. Effect of H_3PO_4 impregnation ratio on (a) surface area and (b) pore volume of activated carbons prepared at $700 \text{ }^\circ\text{C}$ carbonization temperature.

At higher and lower impregnation ratios the BET surface area and total pore volume are less. Thus the impregnation ratio has a significant effect on the S_{BET} , S_μ , and V_μ of the activated carbon. The percentage of micropore volume decreases with the increase in impregnation ratio. As far as the percentage of micropore surface area is concerned, the same trend is obtained as a percentage of micropore volume. Other research works also demonstrate similar variation and the influence of impregnation ratio on the surface area and pore volume of the activated carbon prepared with H_3PO_4 activation using other lignocellulosic materials (Fierro et al., 2006; Prahaz et al., 2008; Yakout and El-Deen, 2016; Yorgun and Yildiz, 2015).

The effect of the initial amount of K_2CO_3 on the final product characteristics was determined using four different impregnation ratios (0.25, 0.5, 1.0, 0.75, and 1.0) at $800 \text{ }^\circ\text{C}$ (Table 3.7 and Fig. 3.13). From Table 3.7 and Fig. 3.13, it is seen that the surface area of activated carbon increase with increasing impregnation ratio from 0.25 to 0.5 and then decrease slightly above ratio of 0.5. However, the mesoporous surface area increases continually. For impregnation ratio of 0.5, the BET surface area is maximum ($1236 \text{ m}^2/\text{g}$).

There is a noticeable decrease in micropore surface area when the ratio is higher than 0.5 due to enlargement of micropores to mesopores (Adinata et al., 2007). The micropore volume of activated carbon prepared at impregnation ratio of 0.5 is maximum (0.98 cm³/g). There is a decrease in micropore volume and the total pore volume (micropore volume and mesopore volume) when the ratio is higher than 0.5. This type of influence of K₂CO₃ impregnation ratio are also reported in literature (Adinata et al., 2007; Chen et al., 2013; Gurten et al., 2012; Hayashi et al., 2002b).

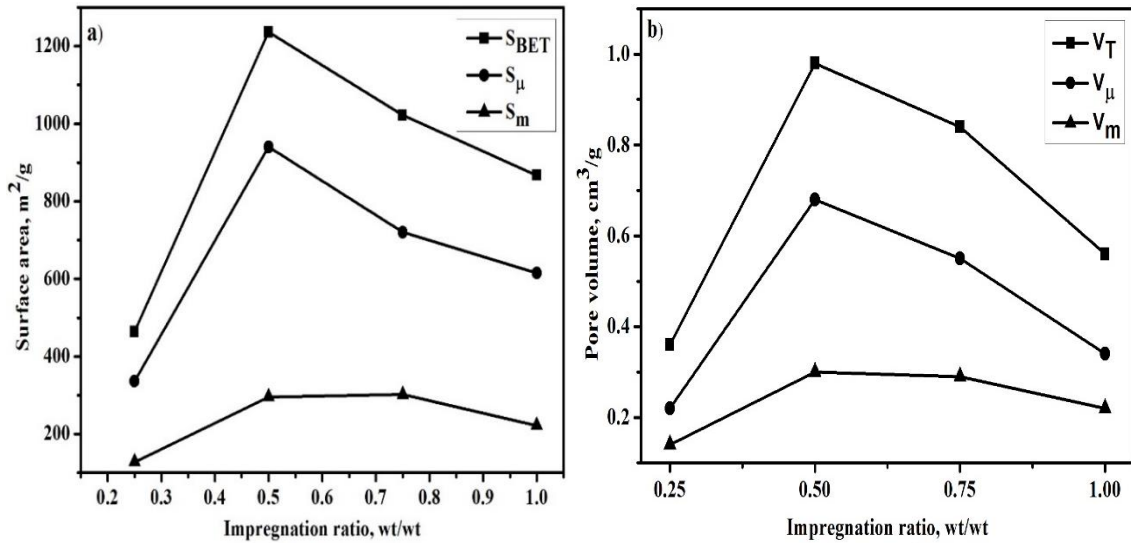


Fig. 3.13. Effect of K₂CO₃ impregnation ratio on (a) surface area and (b) pore volume of activated carbons prepared at 800 °C carbonization temperature.

To summarize, the preparation conditions where high surface area activated carbons are obtained are tabulated in Table 3.8.

Table 3.8: Preparation conditions and porous characteristics of ACs

| Prepared ACs | AT (°C) | IR | AT (min) | S _{BET} (m ² /g) | V _T (cm ³ /g) | V _μ (cm ³ /g) | V _m (cm ³ /g) | V _μ /V _T (%) | D _p (nm) |
|--------------|---------|-----|----------|--------------------------------------|-------------------------------------|-------------------------------------|-------------------------------------|------------------------------------|---------------------|
| ACZC-600-2.0 | 600 | 2.0 | 60 | 2869 | 1.96 | 1.68 | 0.28 | 85.71 | 2.73 |
| ACPA-700-1.5 | 700 | 1.5 | 60 | 2636 | 1.53 | 1.32 | 0.21 | 86.27 | 2.32 |
| ACPC-800-0.5 | 800 | 0.5 | 60 | 1236 | 0.98 | 0.68 | 0.30 | 69.39 | 3.17 |

The prepared activated carbons at the optimized parameters with activating agents as ZnCl₂, H₃PO₄ and K₂CO₃ are named as ACZC-600-2.0, ACPA-700-1.5, and ACPC-800-0.5, respectively. ACZC-600-2.0 has a highest BET surface area (2869 m²/g) over the other two ACPA-700-1.5 (2636 m²/g) and ACPC-800-0.5 (1236 m²/g). The microporosity of ACPA-700-1.5 (86.27%) is higher than the others.

3.5.4. Surface characteristics comparison with literature data

The obtained high surface area activated carbon is comparable to the surface area of commercially available activated carbons are typically ranged from 500 to 2000 m²/g (Uçar et al., 2009; Yorgun et al., 2009). The BET surface area of the activated carbons obtained from three different activators in the present work has been compared with some reported in literature and is tabulated in Table 3.9. Comparison shows that the activated carbon prepared with ZnCl₂ activation in the present work has highest BET surface area of 2869 m²/g. The next higher BET surface area 2636 m²/g of prepared activated carbon with H₃PO₄ activator also more than the ones reported in literature. The activated carbon prepared with K₂CO₃ activation has 1236 m²/g of BET surface area, which is in between the values of previous works. Based on the obtained results, the Fox nutshell appears to be more suitable as a starting material for activated carbon preparation. The prepared activated carbons have high BET surface area and can suitably be used in various applications; one may be in wastewater treatment process.

Table 3.9: Comparison of surface area of prepared ACs with literature ones

| Raw material | Atmosphere | AT (°C) | IR | Activation time (hr) | S _{BET} (m ² /g) | References |
|--|----------------|------------|------------|----------------------|--------------------------------------|--------------------------------|
| ZnCl₂ activation | | | | | | |
| Fox nutshell | N ₂ | 600 | 2.0 | 1 | 2869 | Present study |
| Paulownia (<i>P. tomentose</i>) | N ₂ | 400 | 4 | 1 | 2736 | (Yorgun et al., 2009) |
| Coconut shells | N ₂ | 800 | 2 | - | 2400 | (Hu et al., 2001) |
| Cattle-manure compost | N ₂ | 400 | 1.5 | 0.5 | 2170 | (Qian et al., 2007) |
| Peach stone | N ₂ | 500 | 0.96 | - | 2000 | (Caturla et al., 1991) |
| Herb residues | Vacuum | 450 | 2.5 | | 1952 | (Yang and Qiu, 2011) |
| Sugar beet bagasse | N ₂ | 700 | 3 | 1.5 | 1826 | (Demiral and Gündüzoğlu, 2010) |
| Walnut shells | Vacuum | 450 | 2 | 1 | 1800 | (Yang and Qiu, 2010) |
| Sour cherry (<i>Prunus cerasus</i> L.) stones | N ₂ | 700 | 3 | 2 | 1704 | (Angin, 2014) |
| Bituminous coal | - | 500 | 1.0 | 1 | 1644 | (Ahmadpour and Do, 1997) |

| | | | | | | |
|---|----------------------|------------|------------|----------|-------------|-------------------------------|
| Pumpkin seed shell | - | 500 | 3 | - | 1564 | (Demiral et al., 2015) |
| Elutrilithe (waste from coal) | - | 950 | 0.6 | 4 | 1465 | (Hu and Vansant, 1995) |
| Grape stalk | CO ₂ | 700 | 2 | 2 | 1411 | (Ozdemir et al., 2014) |
| Waste corn cob | N ₂ | 550 | 1.75 | - | 1400 | (Tsai et al., 1997) |
| Pistachio nut shell | N ₂ | 400 | 0.75 | 1 | 1635.37 | (Lua and Yang, 2005) |
| | Vacuum | 400 | 0.75 | 1 | 1647.16 | |
| | Vacuum | 500 | 1.5 | 2 | 2527 | |
| Potato residue | N ₂ | 600 | 1 | 1 | 1357 | (Zhang et al., 2015) |
| Chinese fir sawdust | Vacuum | 500 | 1 | 1 | 1079 | (Juan and Ke-Qiang, 2009) |
| Paper mill sludge | N ₂ | 800 | 3.5 | 2 | 1000 | (Khalili et al., 2000) |
| Pomegranate seeds | N ₂ | 600 | 2 | 1 | 978.8 | (Uçar et al., 2009) |
| Safflower seed press cake | N ₂ | 900 | 4 | 1 | 801.5 | (Angin et al., 2013) |
| Olive stone | N ₂ | 650 | 0.2 | 2 | 790.25 | (Kula et al., 2008) |
| Bagasse | N ₂ | 600 | 1 | 0.5 | 750 | (Kalderis et al., 2008) |
| Rice husk | N ₂ | 600 | 0.75 | 0.5 | 674 | (Kalderis et al., 2008) |
| <i>Tectona grandis</i> sawdust | N ₂ | 500 | 2 | 1 | 585 | (Mohanty et al., 2005) |
| H₃PO₄ activation | | | | | | |
| Fox nutshell | N₂ | 700 | 1.5 | 1 | 2636 | Present study |
| Corn cob | Ar | 400 | 1 | 1 | 2081 | (Sych et al., 2012) |
| <i>Acacia mangium</i> wood | - | 900 | 40% | 0.75 | 1767 | (Danish et al., 2014) |
| Cherry stones | N ₂ | 500 | 3.44 | 2 | 1688 | (Olivares-Marín et al., 2007) |
| Vine shoots (<i>Vitis vinifera</i>) | N ₂ | 400 | 60% | 2 | 1666 | (Corcho-Corral et al., 2006) |
| Reedy grass leaves | N ₂ | 500 | 0.88 | 2 | 1474 | (Xu et al., 2014) |
| Durian shell | - | 500 | 30% | 0.33 | 1404 | (Tham et al., 2011) |
| Woody biomass birch | N ₂ | 600 | 1.5 | 1 | 1360 | (Budinova et al., 2006) |
| Marigold straw | - | 400 | 2 | 2 | 1344.23 | (Qin et al., 2014) |

| | | | | | | |
|---|----------------------|------------|------------|----------|-------------|-------------------------------|
| Jackfruit peel | N ₂ | 550 | 4.0 | 0.75 | 1260 | (Prahas et al., 2008) |
| Olive stones | N ₂ | 500 | 60% | 2 | 1218 | (Yakout and El-Deen, 2016) |
| Tunisian olive-waste cakes | N ₂ | 450 | 1.75 | 2 | 1062 | (Baccar et al., 2009) |
| Date pits | - | 700 | 60% | 2 | 945 | (Girgis and El-Hendawy, 2002) |
| Chestnut wood | N ₂ | 500 | 0.35 | 3 | 783 | (Gomez-Serrano et al., 2005) |
| <i>Lemna minor</i> | N ₂ | 500 | 3 | 2 | 531.9 | (Huang et al., 2014) |
| K₂CO₃ activation | | | | | | |
| Fox nutshell | N₂ | 800 | 0.5 | 1 | 1236 | Present study |
| Pistachio shell | N ₂ | 800 | 1 | 1 | 1800 | (Hayashi et al., 2002b) |
| Chickpea husk | N ₂ | 800 | 1 | 1 | 1778 | (Hayashi et al., 2002a) |
| Waste tea | N ₂ | 900 | 1 | 1 | 1722 | (Gurten et al., 2012) |
| Wood sawdust | N ₂ | - | 1.25 | - | 1496.05 | (Foo and Hameed, 2012a) |
| Sunflower seed oil residue | N ₂ | - | 0.67 | - | 1411.55 | (Foo and Hameed, 2011) |
| Corn cob | CO ₂ | 800 | 0.15 | 1 | 1266 | (Tsai et al., 2001b) |
| Palm shell | CO ₂ | 800 | 2 | 1 | 1170 | (Adinata et al., 2007) |
| Mangosteen shell | - | 900 | 1 | 2 | 1123 | (Chen et al., 2011) |
| Orange peel | N ₂ | - | 1.25 | - | 1104.45 | (Foo and Hameed, 2012b) |
| Sisal waste | N ₂ | 700 | 0.5 | 1 | 1038 | (Mestre et al., 2011) |
| Wool fibers | N ₂ | 600 | 2 | - | 438 | (Chen et al., 2013) |

3.5.5. Pore size distribution

The pore size distributions generally characterize the structural heterogeneity of porous material. It is closely related to both kinetic and equilibrium properties of porous materials applied in industrial application. The pore size distribution of the prepared activated carbons from Fox nutshell at different carbonization temperatures and impregnation ratios are shown in Figs.14(a-b), 3.15(a-b) and 3.16. In the present work, the pore size distribution curves of the prepared activated carbons are obtained by the DFT method using the pore

volumes in the measurement of N₂ desorption isotherms. From these figures, it is evident that the carbonization temperature and impregnation ratio have a significant effect on the pore structure of the activated carbons. At low temperature and impregnation ratio, the pore structure mainly consisted of micropore; however, with the increase of carbonization temperature and impregnation ratio, the creation of micropore structure and widening of micropores to mesopores increases, and also there is increase in the total pore volume of activated carbon. The prepared activated carbons with ZnCl₂, H₃PO₄, and K₂CO₃ impregnation ratios have a narrow pore size distribution with a significant range less than 25 Å.

In the case of ACZC activated carbons prepared at carbonization temperature 500-700 °C and impregnation ratio of 2, present an interesting enough narrow micropore size distribution (centered at 17 Å) and a great adsorption capacity [Fig. 3.14(a)]. Fig. 3.14(b) shows the mesoporosity of the activated carbon is increased with impregnation ratio at 600 °C carbonization temperature.

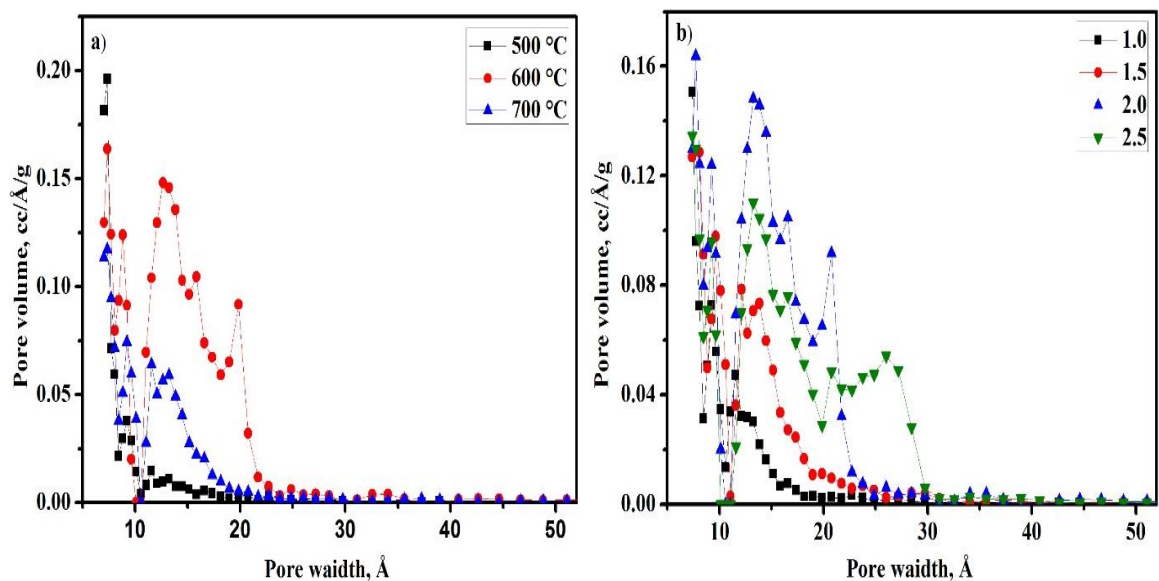


Fig. 3.14. Pore size distribution of activated carbons prepared at (a) different carbonization temperatures (ZnCl₂ impregnation ratio = 2.0) and (b) different ZnCl₂ impregnation ratios (carbonization temperature = 600 °C).

The mesopores increase with increasing ZnCl₂ reagent may be due to the reaction occurred more with biomass and resulted merging of micropores to mesopore and mesopores to macropore. The average pore diameter (D_p) increased from 2.22 to 2.73 nm (Table 3.6). Figure. 3.15(a-b) show the pore size distribution the prepared activated carbons at different carbonization temperatures and different H₃PO₄ ratios. With increase in carbonization temperature the pore size increases. The centered size distribution of the obtained activated

carbon increases with increase in the impregnation ratio at 700 °C carbonization temperature. The activated carbon prepared at 1.5 impregnation ratio and 700 °C carbonization temperature contain mesopores.

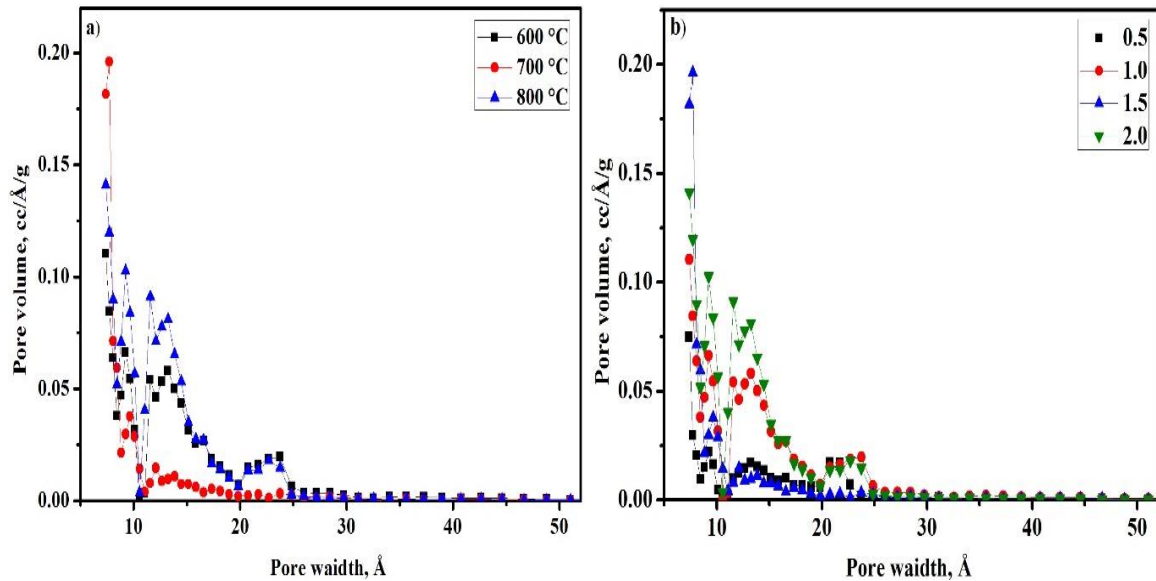


Fig. 3.15. Pore size distribution of activated carbons prepared at (a) different carbonization temperatures (H_3PO_4 impregnation ratio = 1.5) and (b) different H_3PO_4 impregnation ratios (carbonization temperature = 700 °C).

Table 3.6 shows average pore diameter (D_p) increase from 2.19 to 2.61 nm. Fig. 3.16 shows the pore size distribution of the activated carbon prepared at 800 °C of carbonization temperature and 0.5 impregnation ratio. There is micropore size distribution (centered at 15 Å), also it contains mesopores, centered at 22 Å. The average pore diameter (D_p) is 3.17 nm (Table 3.6).

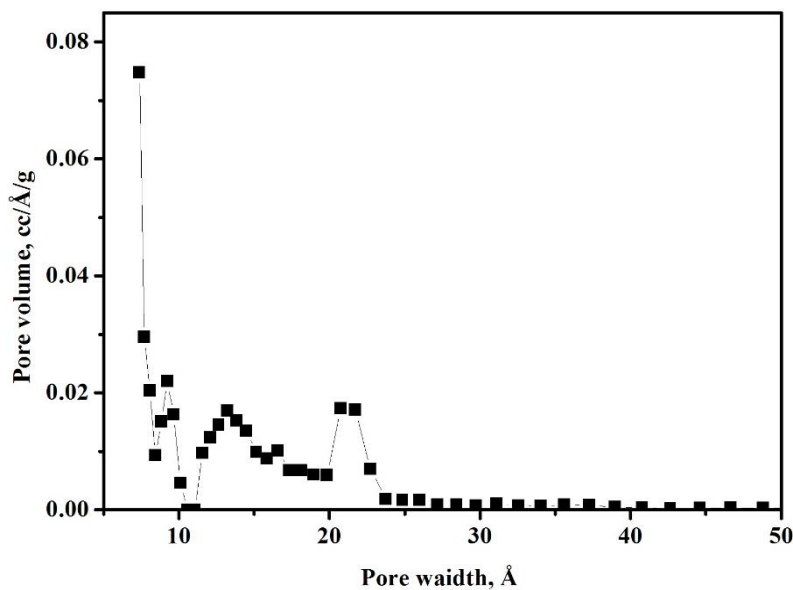


Fig. 3.16. Pore size distribution of activated carbon prepared at carbonization temperature of 800 °C and impregnation ratio of 0.5.

3.5.6. Fourier Transform Infrared Spectroscopy

The carbon matrix does not consist of carbon atoms alone but is also formed by other heteroatoms like hydrogen, oxygen, nitrogen, halogen, sulfur, phosphorus, etc. The surface chemistry of the activated carbon governs by the heteroatoms that are bonded to the edges of the carbon layers (Wibowo et al., 2007). The cell wall of plant cell comprises a super macromolecular compound of hemicellulose, cellulose and lignin fractions and the composition varies with the biomass resource. It is accepted that the pore structure development in the porous material is influenced by many factors including inorganic impurities and internal structure of carbon. The main aim of this study was to examine the surface functional groups present in the precursor material and prepared activated carbons and to identify the groups responsible for the adsorption process. The FTIR spectra were recorded between the wavenumbers 4000-500 cm^{-1} .

Figure 3.17 shows the FTIR spectra of raw Fox nutshell. Table 3.10 indicates the band summary of the wave numbers detected in the Fox nutshell and prepared activated carbons ACZC-600-2.0, ACPA-700-1.5, and ACPC-800-0.5. The broad bands at 3373.84 cm^{-1} correspond to O–H stretching from phenols, alcohol, and water (Alabadi et al., 2015). The band at 2925.77 cm^{-1} and 2845.03 cm^{-1} assigns to the asymmetric C–H representing such as methyl and methylene groups (Yang and Qiu, 2010). The long sharp peak at 1591.12 cm^{-1} may be attributed to the presence of ketones, aldehydes, carboxylic acids, esters, aromatic ring, alkenes groups in hemicellulose compounds and the bond between hemicellulose and lignin. The bands in the region between 1300 and 900 cm^{-1} represents C–O stretching in acids, alcohols, phenols, ethers, and esters (Socrates, 2004).

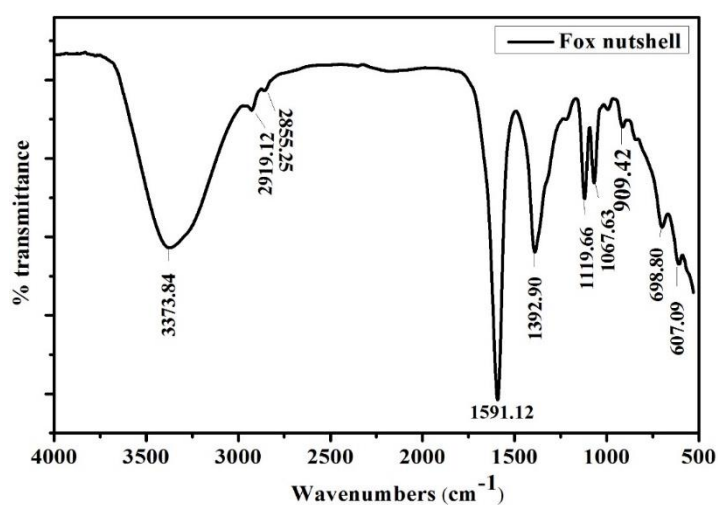


Fig. 3.17. FTIR spectra of the Fox nutshell.

Table 3.10: FTIR spectrum band detected in the Fox nutshell and prepared activated carbons

| Characteristics | Wave numbers range (cm ⁻¹) | FNS | ACZC-600-2.0 | ACPA-700-1.5 | ACPC-800-1.5 | References |
|---------------------------------|--|---------------|------------------------|------------------------|------------------------|----------------------|
| Aliphatic hydrocarbons | | | | | | |
| C-H | 3100-2850 | 2924.99, 2840 | 2926.37, 2838.42 | 2926.37, 2838.42 | 2924.25, 2842.69 | Socrates (2001) |
| C≡C | 2260-2100 | Not detected | Not detected | Not detected | Not detected | Socrates (2001) |
| Aromatic hydrocarbons | | | | | | |
| C-H (out of plane) | <900 | 698.8, 607.09 | 851.12, 699.68, 609.42 | 849.42, 696.50, 609.59 | 850.32, 697.92, 614.37 | Socrates (2001) |
| C-C | 1620-1400 | 1591.12 | 1590.78 | 1590.88 | 1597.75 | Socrates (2001) |
| Oxygen functional groups | | | | | | |
| C-O | 1300-1080 | 1119.66 | 1109.92, 1209.60 | 1111.13, 1212.03 | 1116.49, 1210.18 | Socrates (2001) |
| -OH | 1395 | 1392.90 | 1390.05, | 1392.17 | 1388.13 | Cagnon et al. (2005) |
| O-H | 3600-3200 | 3373.84 | 3278.75 | 3319.52 | 3344.84 | Socrates (2001) |

Figures 3.18 through 3.20 shows the FTIR spectra of ACZC-600-2.0, ACPA-700-1.5, and ACPC-800-0.5, respectively. The FTIR spectra of ACZC-600-2.0 demonstrates a broadband with a maximum peak at 3278.75 cm⁻¹, which corresponds to the characteristic of the stretching vibration of hydrogen bonded hydroxyl groups and adsorbed water. Similar observations are noticed in Figs. 3.19 and 3.20, a broad band of peaks stretching from 3101 cm⁻¹ to 3767 cm⁻¹ with a maximum at 3319.52 cm⁻¹ and 3344.84 cm⁻¹ corresponds to the stretching of hydroxyl groups in ACPA-700-1.5 and ACPC-800-0.5, respectively. The bands observed between 3100-2850 cm⁻¹ assigns to the asymmetric C-H and symmetric C-H bands representing the alkyl groups such as methyl and methylene groups (Socrates, 2004). The strong bands at 1590.78, 1590.88 and 1597.75 cm⁻¹ allocates to C=C aromatic ring stretching vibration (Prahas et al., 2008). The bands at 1390.05, 1392.17 and 1388.13 cm⁻¹ in Figs. 3.18, 3.19 and 3.20 correspond to the vibration of carboxylic O-H group

(Cagnon et al., 2005). The bands in the region between 1300 and 1080 cm^{-1} assign to C–O stretching in acids, alcohols, phenols, ethers, and esters, usually found in oxidized carbons (Socrates, 2004). The band at 1392.90 cm^{-1} (Fig.3.17) of Fox nutshell split into two bands when converted to ACZC-600-2.0 at 1390.05 and 1335.03 cm^{-1} (Fig. 3.18). The bands less than 900 cm^{-1} corresponds to C–H (out of plane) of aromatic hydrocarbons (Socrates, 2004). However, in Fig. 3.19, it is also a characteristic of phosphorous and phosphorous carbonaceous compounds present in the phosphoric acid activated carbon in the band region between 1300 and 900 cm^{-1} . The bands at 1300–900 cm^{-1} tentatively assigned to the following phosphorous species: hydrogen-bonded P=O, O-C stretching vibrations in P-O-C of aromatics and P=OOH (Puziy et al., 2002).

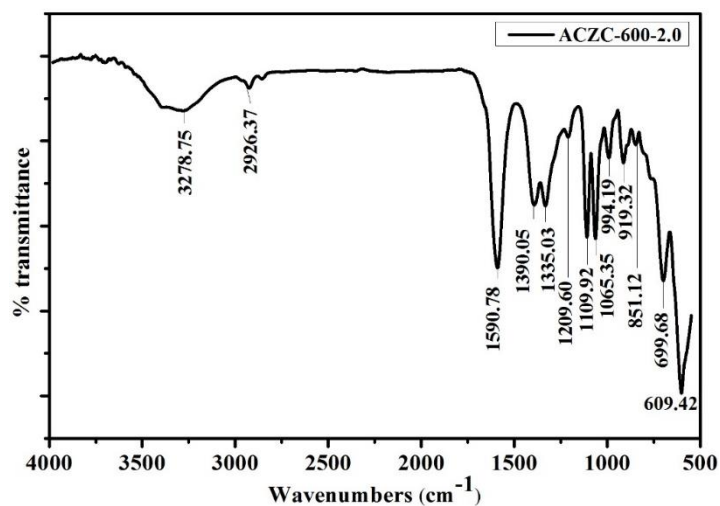


Fig. 3.18. FTIR spectra of prepared activated carbon ACZC-600-2.0.

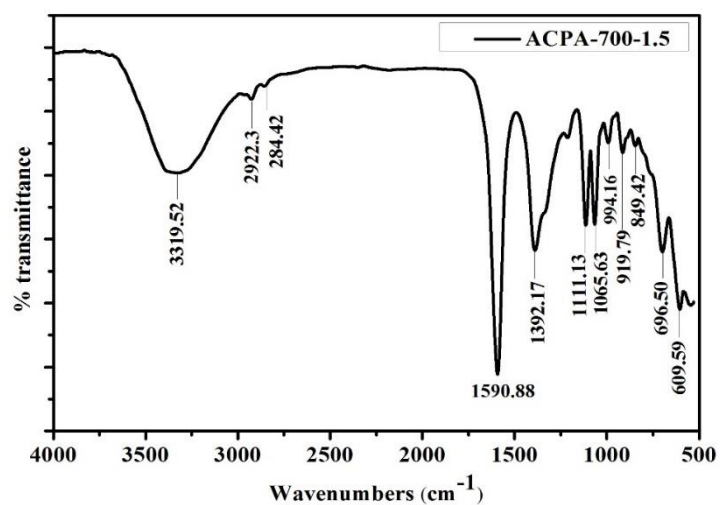


Fig. 3.19. FTIR spectra of prepared activated carbon ACPA-700-1.5.

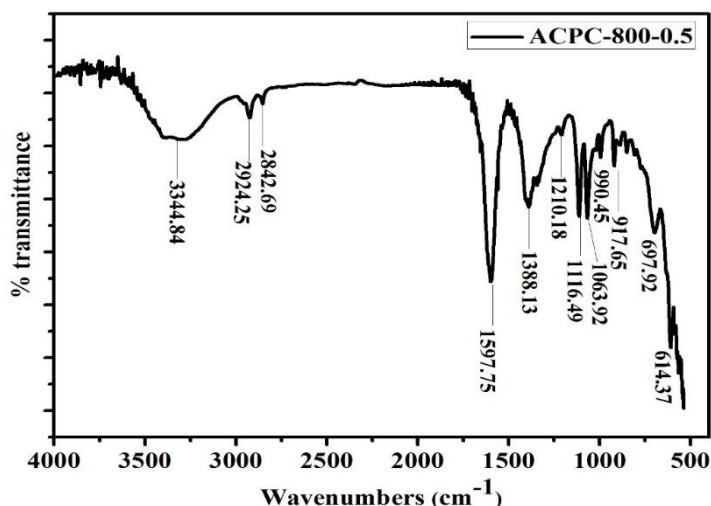


Fig. 3.20. FTIR spectra of prepared activated carbon ACPC-800-0.5.

3.5.7. Surface chemistry determination (Boehm titration)

In Table 3.11, the measured quantities of the acidic and basic surface functional groups are compared. The surface total acidic groups are larger than the total basic groups in all three prepared activated carbons. The phenolic groups are abundant in all the activated carbons and more than the carboxylic group and lactonic groups. In ACZC-600-2.0, lactonic group is more than the carboxylic group, but in the other two carbons, ACPA-700-1.5 and ACPC-800-0.5 the carboxylic group is more than the lactonic group. The basicity of the ACZC-600-2.0 is 0.12 mmol/g, which is larger than the basicity of ACPA-700-1.5 and ACPC-800-0.5 activated carbons. The pH values for the ACZC-600-2.0, ACPA-700-1.5 and ACPC-800-0.5 are found to be 4.3, 2.6 and 4.6, respectively. The PZC values of ACZC-600-2.0, ACPA-700-1.5, and ACPC-800-0.5 are 2.1, 2.7 and 5.4, respectively. The pH value falls in the acidic region and value of PZC < 7 shows dominant of acidic groups over basic groups.

Table 3.11: Quantities of the acidic and basic surface functional groups in prepared ACs

| ACs | Surface functional groups (mmol/g) | | | | | pH | PZC |
|--------------|------------------------------------|----------|----------|---------|----------|-----|-----|
| | Carboxylic | Lactonic | Phenolic | Acidity | Basicity | | |
| ACZC-600-2.0 | 0.019 | 0.045 | 0.058 | 0.122 | 0.120 | 4.3 | 2.1 |
| ACPA-700-1.5 | 0.0444 | 0.012 | 0.0836 | 0.140 | 0.104 | 2.6 | 2.7 |
| ACPC-800-0.5 | 0.0342 | 0.021 | 0.0558 | 0.111 | 0.0896 | 4.6 | 5.4 |

3.5.8. X - Ray Diffraction (XRD) analysis

XRD is the most useful method to visualize the crystalline and amorphous materials. Researchers worked on X-Ray Diffraction analysis of activated carbons, concluded that predominantly amorphous solid having large internal surface area and pore volume. Activated carbon shows the very disordered microcrystalline structure in which graphitic

microcrystals are randomly oriented (Khalil et al., 2013). XRD patterns of Fox nutshell (FNS) and obtained activated carbons are shown in Figs. 3.21, 3.22 and 3.23.

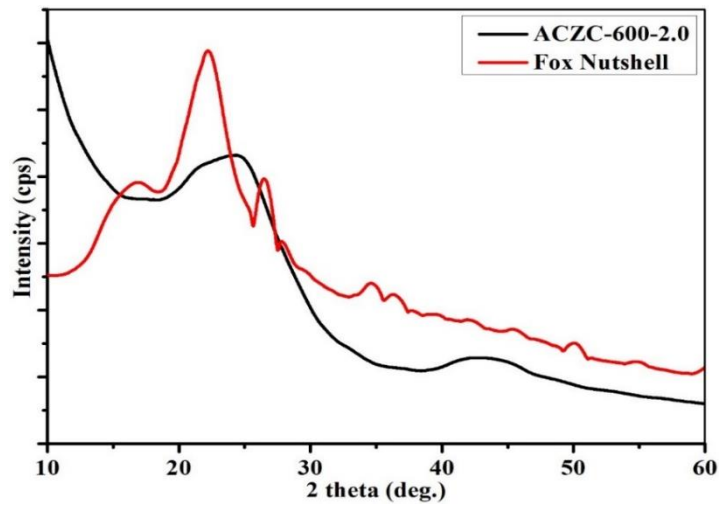


Fig. 3.21. XRD pattern of the Fox nutshell and prepared activated carbon ACZC-600-2.0.

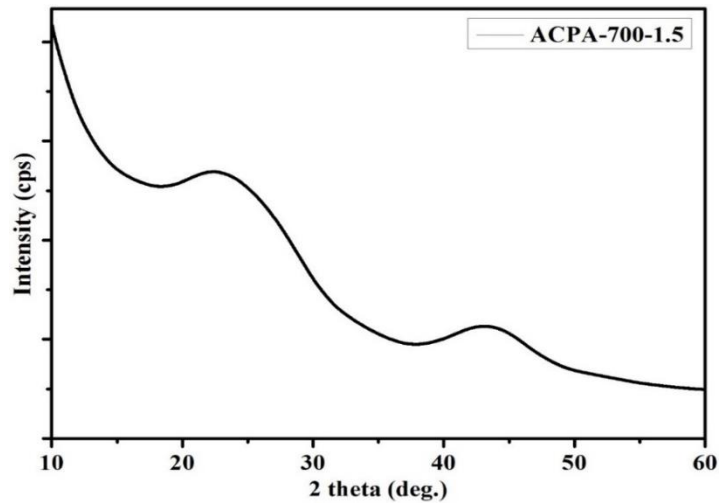


Fig. 3.22. XRD pattern of the prepared activated carbon ACPA-700-1.5.

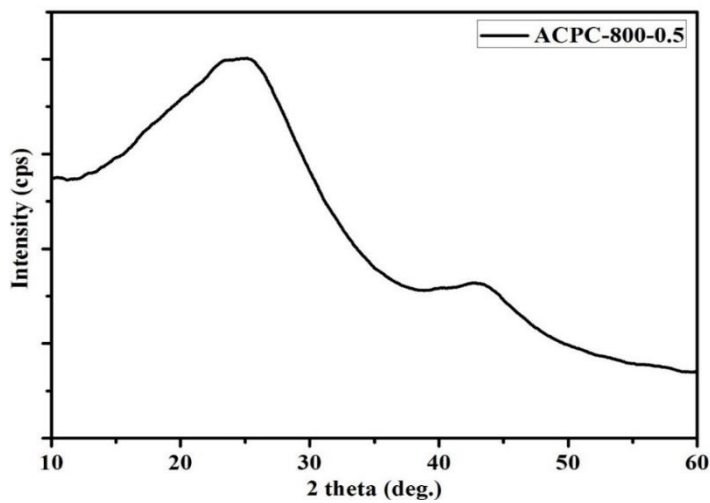


Fig. 3.23. XRD pattern of the prepared activated carbon ACPC-800-0.5.

The XRD patterns of FNS exhibit sharp peaks at $2\theta = 22.5$ (002) denotes the crystalline portion of cellulose and at about $2\theta = 18.7$ (101) indicates the amorphous part (i.e., cellulose, hemicellulose, and lignin).

The XRD patterns have been exhibited broad peaks and absence of a sharp peak in the prepared activated carbons that reveals the predominantly amorphous structure of activated carbon; broad peak is an advantageous property for well-defined adsorbents. Two broad peaks are common to activated carbon, namely (002) and (100) peaks. Occurrence of a sharp peak (Fig. 3.21) in ACZC-600-2.0 at around $2\theta = 26^\circ$ and very small one at $2\theta = 43^\circ$ indicate the formation of (002) and (100) planes corresponding to a predominantly microcrystalline graphitic structure (Penki et al., 2014). In Fig. 3.22 for ACPA-700-1.5, two main diffraction peaks at $2\theta = 23.16$ and 43.59 represent the (002) and (100) planes of the graphite structure. In Fig. 3.23, two main diffraction peaks at $2\theta = 24.79$ and 43.32 also represent the (002) and (100) planes that confirm graphite structure.

3.5.9. Surface morphology study

Surface morphology of the precursor and prepared activated carbons was characterized by using Field Emission Scanning Electron Microscopy (FESEM). The FESEM micrographs of the prepared activated carbons reveal the presence of abundant pores generated during carbonization using activating agents. In the chemical activation process, the new pores are formed due to the reaction between carbon and the activating agent.

The FESEM micrographs of the raw Fox nutshell and NaOH treated Fox nutshell is shown in Figs. 3.24(a-b). In Fig. 3.24(a), the SEM micrographs of raw Fox nutshell shows that there are no pores present on the surface of the raw material and surface is smooth. From Fig. 3.24(b), it is found that the surface is not uniform and is degraded by NaOH.

Figures 3.25-3.27 show the FESEM of the prepared activated carbons ACZC-600-2.0, ACPA-700-1.5, and ACPC-800-0.5, respectively. There are significant differences between the surface morphology of the Fox nutshell and the prepared activated carbons. There are quite large number of pores seen in the prepared activated carbons. From these Figs. 3.25, through 3.27, it can be concluded that the prepared activated carbons have large surface area due to their highly porous structure. Large pores are developed due to evolution of more volatile compounds. It seems that the pores on the surfaces of the prepared activated carbons resulted from the evaporation of the activating agent during carbonization, leaving space previously occupied by the activating agent.

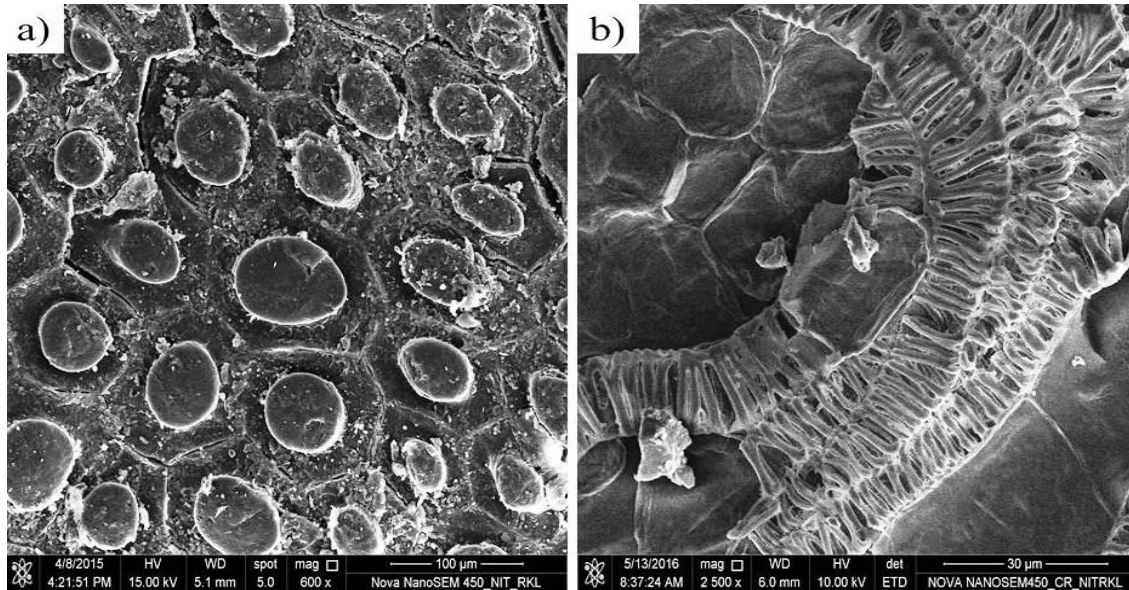


Fig. 3.24. FESEM images of (a) Fox nutshell and (b) NaOH treated FNS.

Mixed pores are developed on the surface of activated carbon, ACZC-600-2.0. Honeycomb shape like structure is formed on the surface of the prepared activated carbon [Fig. 3.25(a)] but pores are of different shapes and sizes [Fig. 3.25(b)]. From Fig. 3.26, the cavities on the surfaces of carbon ACPA-700-1.5 resulted from the evaporation of the phosphoric acid during carbonization and leaving the space previously occupied by the activating agent. In Fig. 3.27, a heterogeneous type pores are seen on the ACPC-800-0.5 surface; it looks like a sponge and pores are of different size and shape.

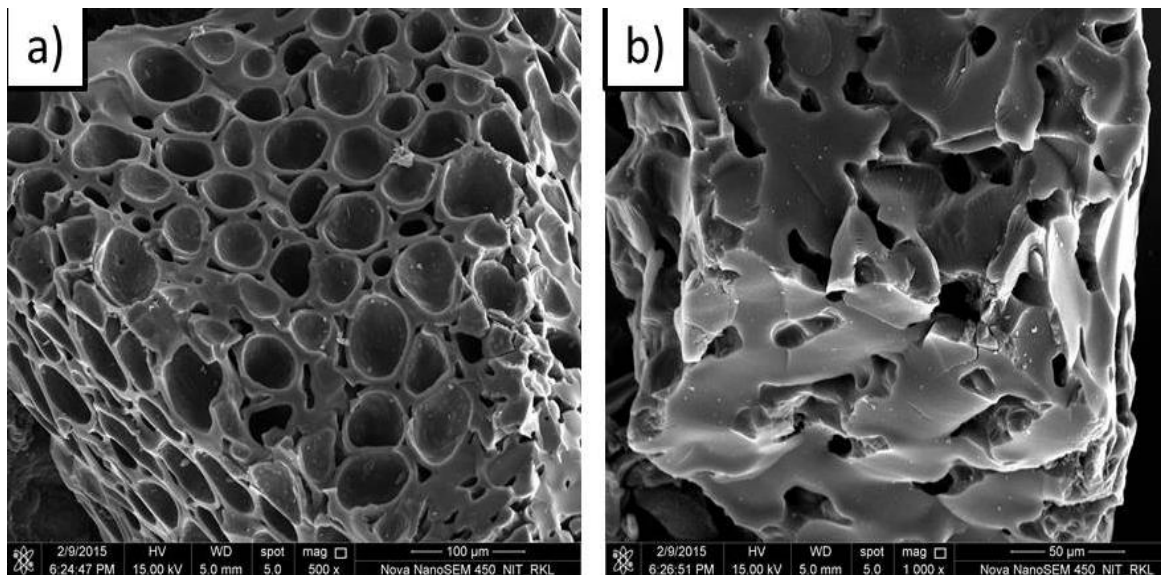


Fig. 3.25. FESEM images of the prepared activated carbon ACZC-600-2.0.

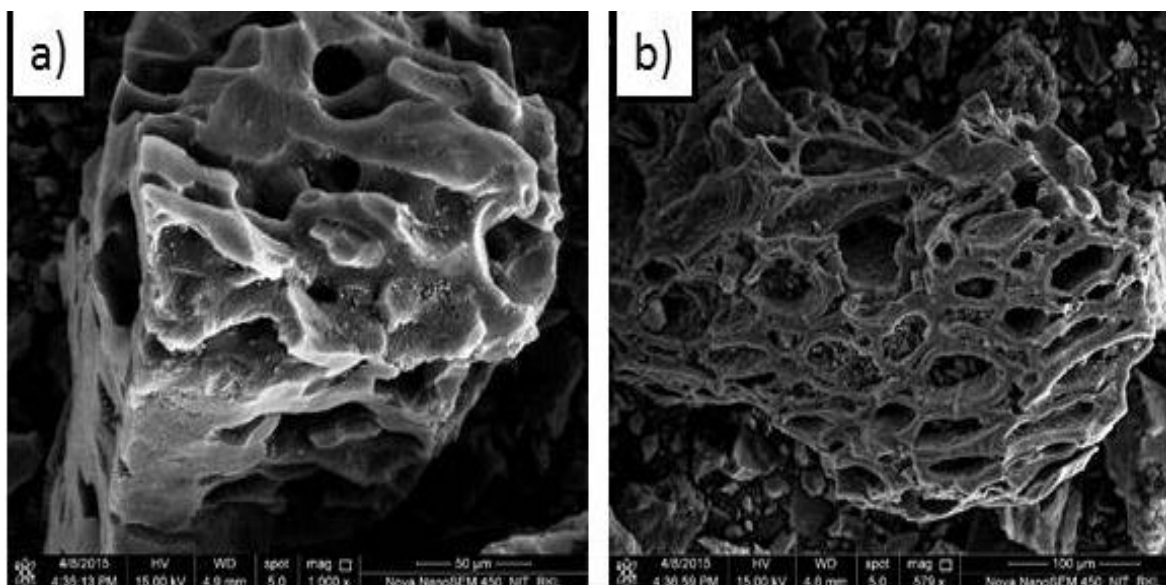


Fig. 3.26. FESEM images of the prepared activated carbon ACPA-700-1.5.

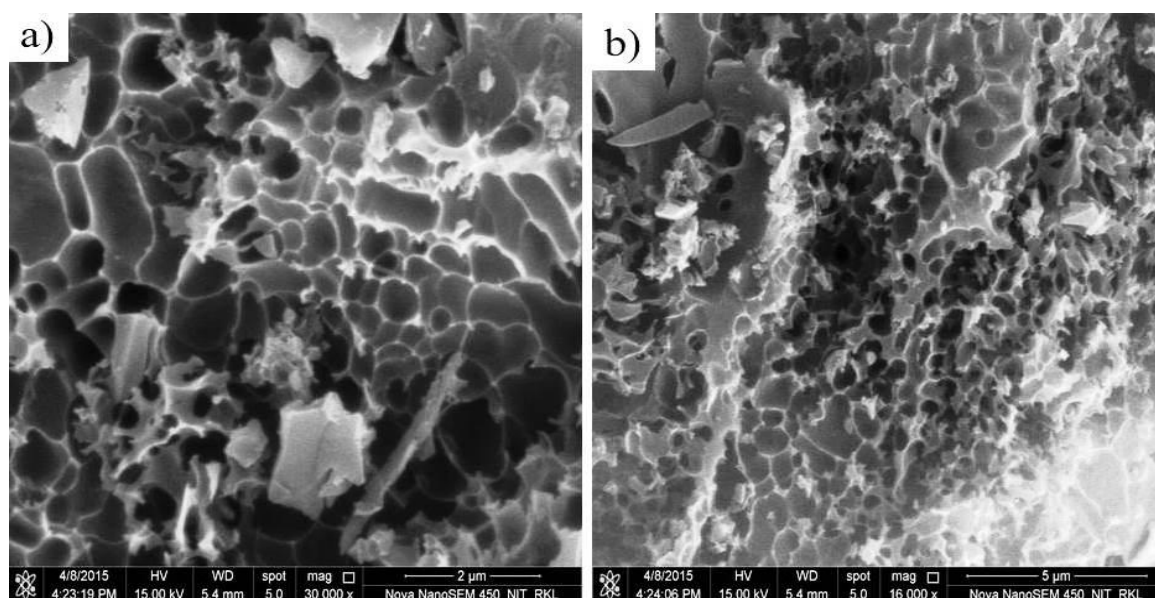


Fig. 3.27. FESEM images of the prepared activated carbon ACPC-800-0.5.

3.5.10. Energy Dispersive X-ray (EDX) spectroscopy

Figs. 3.28 and 3.29(a-b) show the EDX analysis of selected areas of the Fox nutshell and prepared activated carbons respectively for the elemental composition. The EDX elemental analysis highlights the presence of carbon and oxygen ions in the raw sample and prepared activated carbons. Nitrogen is also present in prepared activated carbons in comparison to the raw sample but in less amount compared with carbon and oxygen.

The intensity of the carbon signals is much higher in prepared activated carbons than the raw material. It can be seen that the oxygen elemental concentration reduces during the activation process. In Fig. 3.28, EDX of Fox nutshell many elements like Si, Fe, Al, K, Ca, Mg, and Na are seen, but these elements are almost eliminated in the prepared activated

carbons (Fig. 3.29). The carbon wt% in prepared activated carbons ACZC-600-2.0 and ACPA-700-1.5 are 89.15 and 86.58% and oxygen wt% are 8.98 and 11.56%, respectively. The oxygen wt% is larger in ACPA-700-1.5 than ACZC-600-2.0 means that the oxygen-containing functional groups are present in higher amount in ACPA-700-1.5.

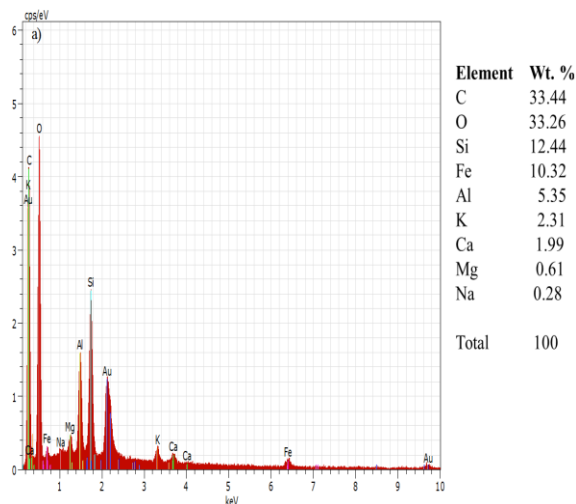


Fig. 3.28. EDX analysis of Fox nutshell.

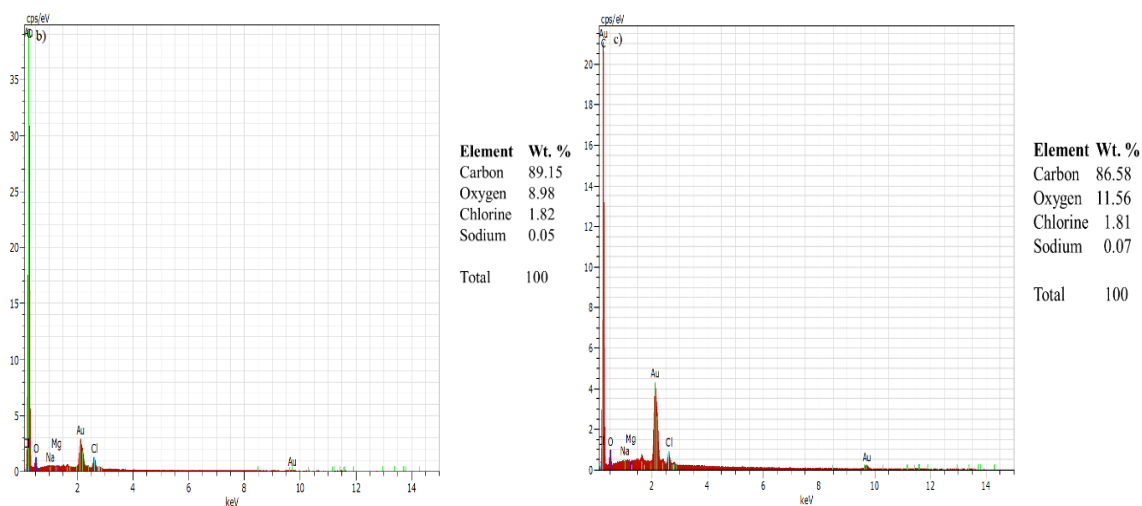


Fig. 3.29. EDX analysis of (a) ACZC-600-2.0 and (b) ACPA-700-1.5.

3.5.11. Transmission Electron Microscopy (TEM)

The microporous network of the prepared ACs was characterized by Transmission Electron Microscope (TEM). The TEM images of prepared activated carbons ACZC-600-2.0, ACPA-700-1.5 and ACPC-800-0.5, are shown in Figs. 3.30, 3.31 and 3.32, respectively. From figures, equal distribution of micropores visualizes in the produced activated carbons, which confirms the prepared ACs have highly microporous in nature means contains the high surface area and micropore volume. Fig. 3.30 presents high-resolution transmission electron microscopy image of ACZC-600-2.0 shows that the formed pores are of different size and shape with average pore diameter of 0.64 nm. The surface of ACZC-600-2.0 looks

like sponge means highly porous. Fig. 3.31 shows that the ACPA-700-1.5 surface is microporous and the pores are of different size and shape. The surface arrangement looks like lamellae and the average pore diameter of micropores is 0.35 nm smaller than the micropore of ACZC-600-2.0, means that ACPA-700-1.5 is more microporous in nature. Fig. 3.32 represents the micropore arrangement on the surface of the activated carbon ACPC-800-0.5. In this carbon, the stacking of the lamellae of average pore diameter of 0.27 nm clearly seen than other prepared activated carbons.

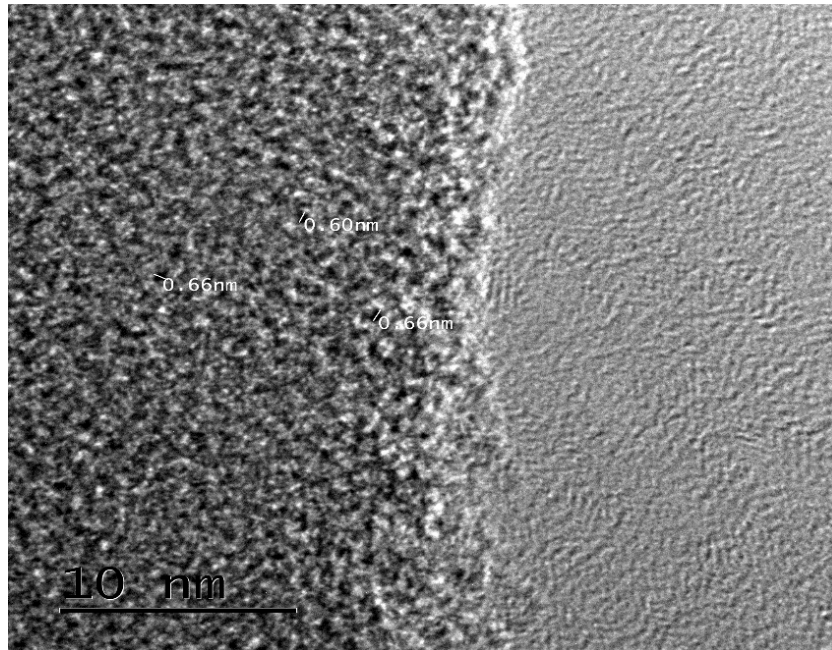


Fig. 3.30. HRTEM image of ACZC-600-2.0 activated carbon.

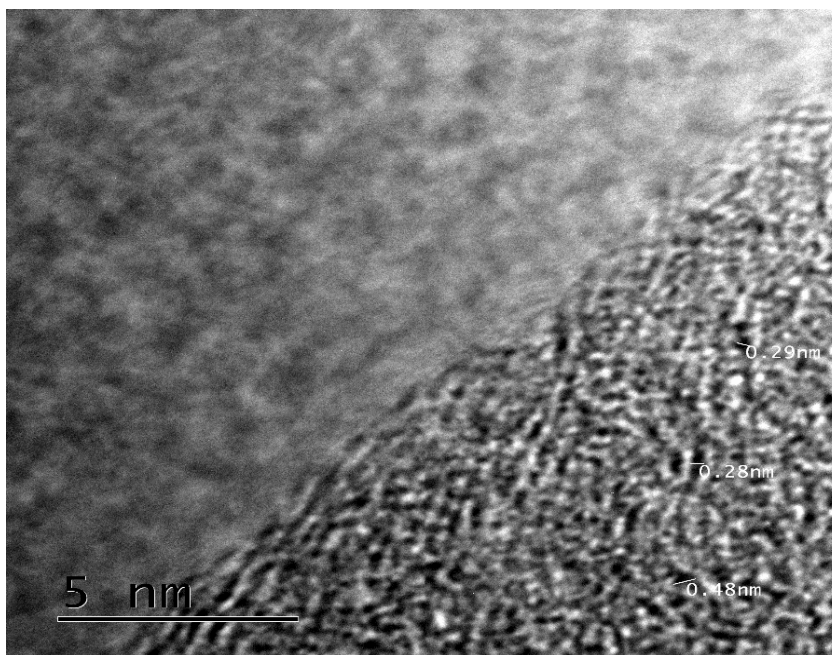


Fig. 3.31. HRTEM image of ACPA-700-1.5 activated carbon.

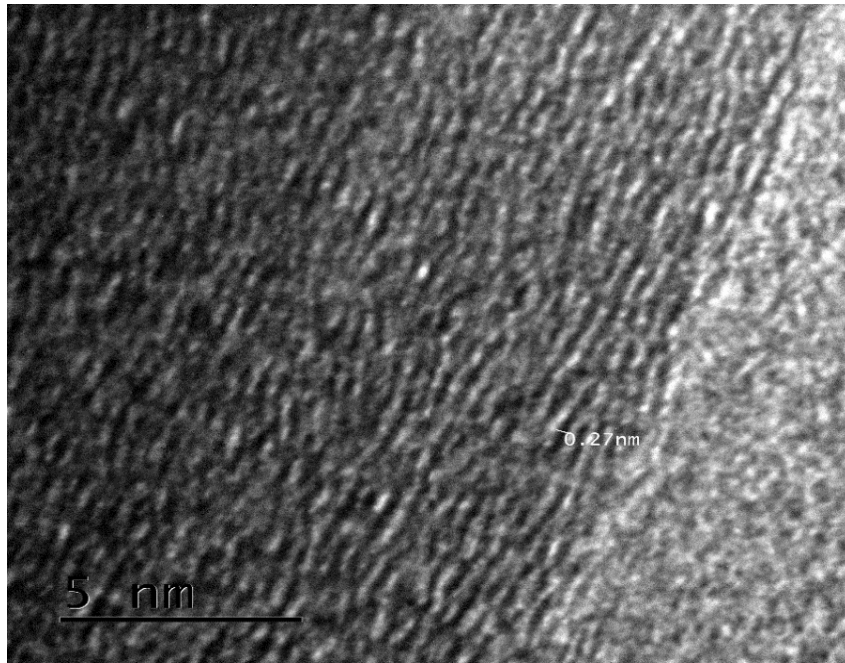


Fig. 3.32. HRTEM image of ACPC-800-0.5 activated carbon.

Chapter-4

Adsorption Studies of Common Water Pollutants

Effluents from various industries such as textile, leather, paper, plastics, municipal sewage and agriculture wastewater are the primary sources of pollution that affect the environment and significantly the living beings. The industrial effluents contain many organic and inorganic pollutants.

There is mainly three class of organic and inorganic pollutants such as; phenols, dyes, and heavy metals. As discussed in chapter-1, the water pollutants phenol, MB and Cr(VI) are highly persistent in the environment because of their broad use in various processing industries. Also, they found in municipal sewage, agriculture runoff, and water from mining activities. Hence for the safe and efficient disposal of wastewater containing pollutants, they should be treated properly. Among all other physico-chemical methods, adsorption using activated carbon as the adsorbent is an attractive and cost-effective method for treatment of water contaminated with phenol, MB, and Cr(VI).

In the present work, adsorption studies were carried out for these common water pollutants separately, and the parameters associated with the adsorption phenomena were characterized. Initially, the batch adsorption experimentation was performed in shake flask. Further column studies were conducted on these pollutants to observe the continuous adsorption characteristics. In the present work, in all the adsorption studies, two (ACZC-600-2.0, ACPA-700-1.5) out of the three activated carbons prepared under optimum preparation conditions with three different chemical activators having very high surface area were used as adsorbents. Lastly, regeneration studies of spent activated carbons by desorption was carried out, and further adsorption studies were carried out to see the effectiveness of the activated carbons for repeated use. The desorption–adsorption was carried out for few cycles. This chapter is divided into three sections; 1) Studies on adsorption of phenol, 2) Studies on adsorption of MB, and 3) Studies on adsorption of Cr(VI).

4.1. Adsorption of Phenol

Adsorption studies on phenol were carried out in both batch (using shake flask) and continuous (using fixed bed column) mode. In the batch adsorption experiments the effect of various experimental parameters on adsorption capacity of ACZC600-2.0 and ACPA-700-1.5 were investigated. The adsorption was characterized by kinetic, intraparticle diffusion, isotherm, and thermodynamic studies. Then the regeneration and re-adsorption studies were carried out. Finally, the continuous adsorption using a fixed bed column was carried out, where the effect of bed height and adsorbate flow rate on break through and exhaustion were characterized. The results of the experimental investigation are represented in the form of graphs; significant values are listed in tables and discussed in the following sections.

4.1.1. Batch adsorption studies

The batch adsorption experiments were carried out at different initial phenol concentrations (100, 200, 300, 400 and 500 mg/L) using a solution volume of 100 mL. Phenol batch adsorption were carried up to 3 hr in an orbital shaker. At preselected time intervals for analysis of adsorbate concentration, the sample was withdrawn from the mixture and centrifuged.

4.1.1.1. Effect of experimental factors

The experimental parameters varied in the study include; agitation speed, pH, temperature, adsorbent dose, and contact time.

4.1.1.1.1. Agitation speed

A series of experiment with varying agitation speed in the range of 90–170 rpm were performed by using 0.05 g of both ACZC600-2.0 and ACPA-700-1.5 for 100 mL phenol solution of the concentration 100 mg/L at 30 °C. Figure 4.1 shows the effect of agitation speed on % removal of phenol by adsorption onto ACZC600-2.0 and ACPA-700-1.5. The removal efficiency of phenol is found to increase with increase in agitation speed and maximum removal by ACZC600-2.0 and ACPA-700-1.5 are achieved at 150 rpm, which remained the same at higher speed also. Thus, the agitation speed was fixed to 150 rpm for phenol adsorption by both the adsorbents in further experiments. These results indicate that an efficient transport of phenol ions towards the adsorbent surfaces occurred, due to less resistance to diffusion at higher agitation speed. Some studies have been reported similar

behaviour between adsorbents and adsorbates at higher agitation speed (Abussaud et al., 2016; Auta and Hameed, 2014; Deng et al., 2009; Yang et al., 2015).

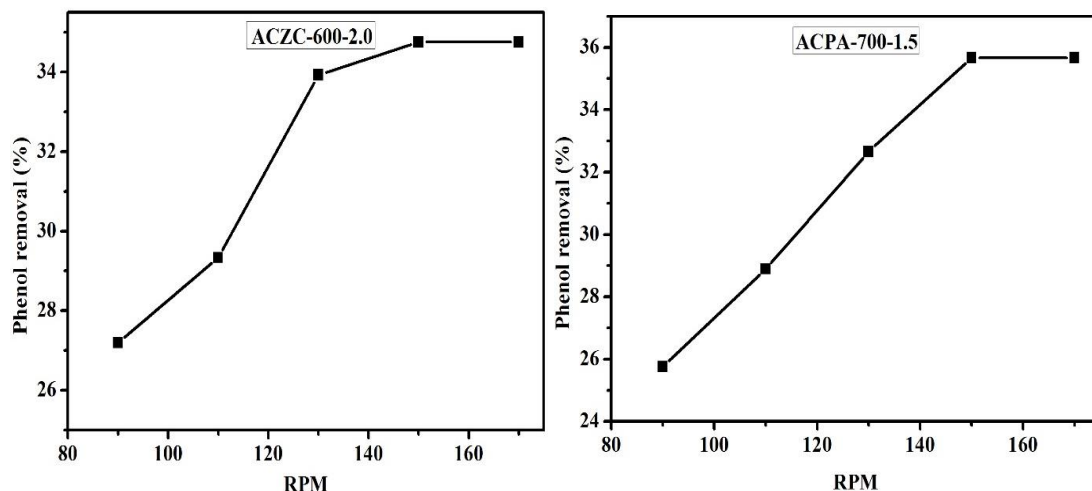


Fig. 4.1. Effect of agitation speed on % removal of phenol ($C_0 = 100$ mg/L, $m_s = 0.05$ g/100mL, temperature = 30 °C, and contact time = 3 hr).

4.1.1.1.2. pH

The most important factor affecting the capacity of adsorbent in wastewater treatment is solution pH. The efficiency of adsorption is dependent on the solution pH since variation in pH leads to the change in the degree of ionization of the adsorptive molecule and the surface properties of adsorbent (Nandi et al., 2009). To study the effect of pH the same was varied from 2 to 9 at 100 mg/L of initial phenol concentration. Fig. 4.2 shows the influence of pH on phenol adsorption by ACZC-600-2.0 and ACPA-700-1.5. The phenol adsorption is maximum and unaffected by the pH of the phenol solution in the range of 2–7. The adsorption of phenol decreases from pH 8.0 for both the adsorbents ACZC-600-2.0 and ACPA-700-1.5. Phenol is a weak acid with $pK_a \approx 9.89$ and is dissociated at $pH > pK_a$. Therefore, the adsorption decrease at higher pH values above 7 due to ionization of adsorbate molecules (Hameed and Rahman, 2008). Similar results were reported in previous works (Rodrigues et al., 2013; Beker et al., 2010; Hameed and Rahman, 2008).

Since the PZC of activated carbons, ACZC-600-2.0 and ACPA-700-1.5 were found to be 2.1 and 2.7, respectively. The surface of carbon is positively charged when $pH < PZC$. As the initial pH increased, phenol molecules started to dissociate into phenol anions, the adsorption amount of phenol decreased. When $pH > pK_a$ of phenol ($pH 9.89$), the carbon surface was negatively charged when the initial pH was higher than PZC. Because of the electrostatic repulsion between phenol anions and AC surface as well as between phenolate–phenolate anions in solution, the adsorption capacity decreased to a minimum

value (Beker et al., 2010; Hameed and Rahman, 2008; Rodrigues et al., 2013; Yang et al., 2014). In all cases there is a reduction in the adsorption at a higher pH which is possibly due to the increased solubility of phenols and the abundance of OH^- ions thereby increasing hindrance to diffusion of phenolate anions.

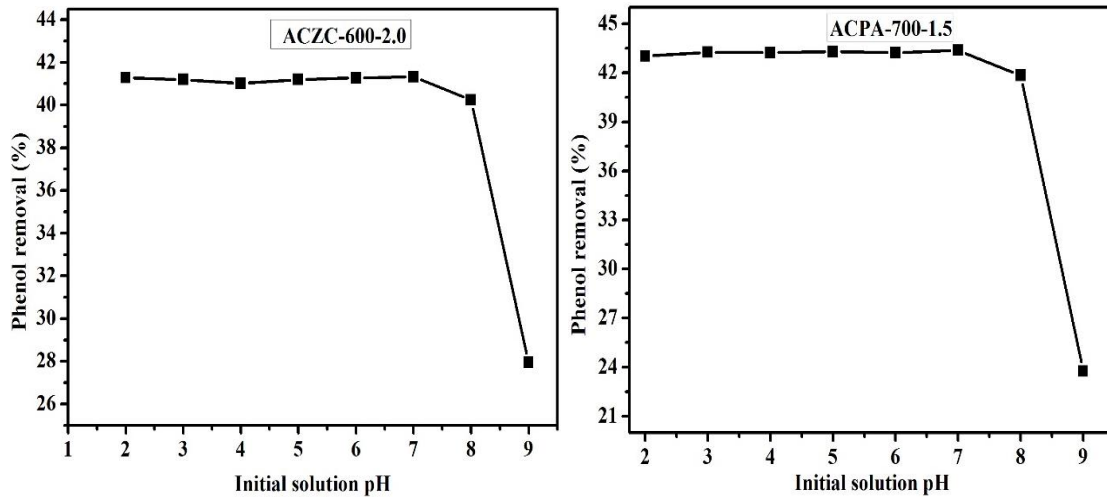


Fig. 4.2. Effect of pH on % removal of phenol ($C_0 = 100 \text{ mg/L}$, $m_s = 0.05 \text{ g/100mL}$, temperature = 30°C , and contact time = 3 hr).

4.1.1.1.3. Temperature

Adsorption is a mass transfer phenomenon, which is affected by temperature. To study the endothermic or exothermic nature of adsorption process, removal of phenol at different temperatures ($25 - 45^\circ\text{C}$) for 100 ml of 100 mg/L phenol with an adsorbent dosage of 0.05 g of ACZC-600-2.0 and ACPA-700-1.5 each over stirring time of 3 hr were investigated.

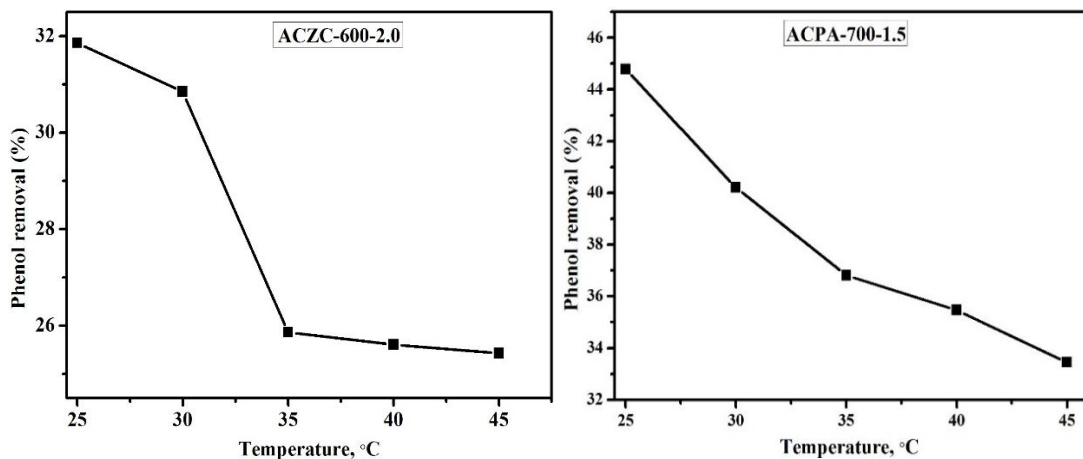


Fig. 4.3. Effect of temperatures on % removal of phenol ($C_0 = 100 \text{ mg/L}$, $m_s = 0.05 \text{ g/100mL}$, pH = 7, and contact time = 3 hr).

A decrease in the percentage removal of phenol with a rise in temperature implies that the process is exothermic in nature (Fig. 4.3). The reduction in adsorption with the increase in temperature may be due to the weakening of adsorptive forces between the active sites of the adsorbent and adsorbate species and also between the adjacent molecules of the

adsorbed phase (Panday et al., 1986; Senturk et al., 2009). The exothermic nature of adsorption of phenol also reported in literature. (Liu et al., 2010b).

4.1.1.1.4. Adsorbent dosage

The amount of adsorbent was varied at an initial substrate concentration of 100 mg/L at 30 °C and pH 7 for ACZC-600-2.0 and ACPA-700-1.5. Fig. 4.4 shows the effect of adsorbent dosage on the % removal of phenol by ACZC-600-2.0 and ACPA-700-1.5. It is found that the removal of phenol increases with the increase in adsorbent dosage up to 0.4 g significantly, and then increased slowly till 0.5 g dose and beyond that remains unchanged for ACZC-600-2.0. Thus, to get the better removal of phenol and to reduce the adsorbent consumption, 0.5 g was chosen as an optimal mass ACZC-600-2.0 considered for the further experiments.

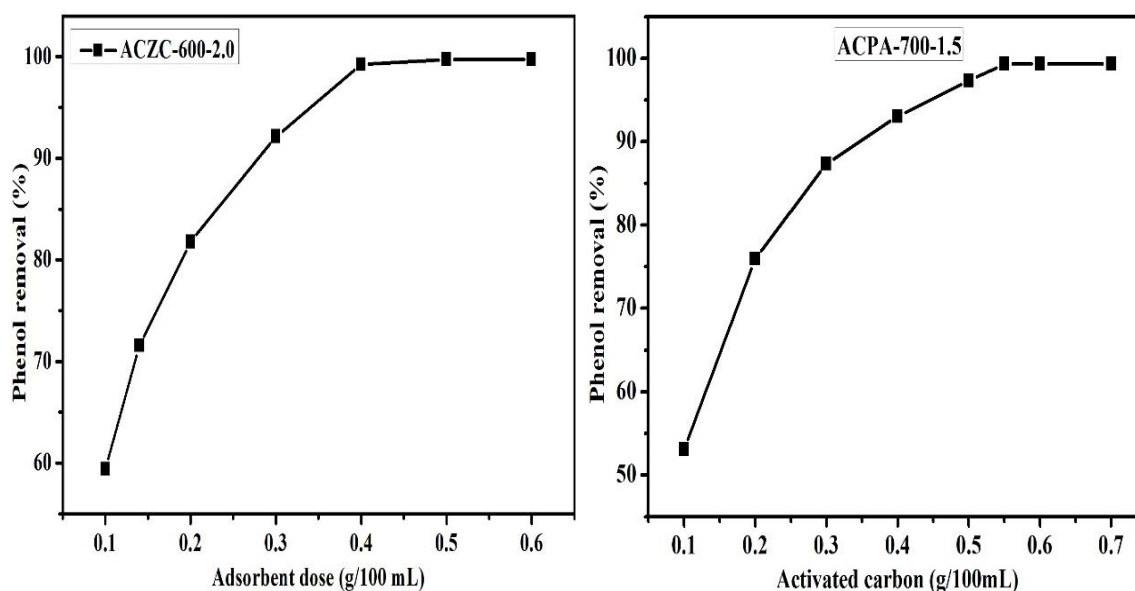


Fig. 4.4. Effect of adsorbent dosage on % removal of phenol ($C_0 = 100$ mg/L, pH = 7, temperature 30 °C, and contact time = 3 hr).

At equilibrium time, the % removal of phenol increased from 59.42 to 99.74% for variation of dose from 0.1 to 0.5 g. For ACPA-700-1.5, the % removal of phenol increases with the increase in adsorbent dosage up to 0.55 g significantly and after that remains unchanged. Thus, 0.55 g was chosen as an optimal mass ACPA-700-1.5 for the further experiments. At equilibrium time, the % removal of phenol increased from 53.11 to 99.32% for dose variation from 0.1 to 0.55 g.

4.1.1.1.5. Contact time and initial phenol concentrations

Figs. 4.5 and 4.6 show the effects of contact time on the adsorption of phenol onto ACZC-600-2.0 and ACPA-700-1.5 at different initial concentrations (100, 200, 300, 400 and 500

mg/L). Adsorption studies were carried out for 3 hr. It can be easily observed that the adsorption capacity of phenol on ACZC-600-2.0 and ACPA-700-1.5 increases steadily during the initial stage and then slowly. The growing trend stops when a state of equilibrium is reached. A larger amount of phenol is removed by ACZC-600-2.0 and ACPA-700-1.5 adsorbents in the first 10 min of contact time, and the equilibrium was established in almost 30 min and 20 min respectively for all absorbent concentrations studied [Fig 4.5(b) and 4.6(b)]. This may be because of availability of a large number of vacant sites with active functional groups on ACZC-600-2.0 and ACPA-700-1.5 at an early stage of adsorption for the phenol molecules. For ACZC-600-2.0, the equilibrium adsorption increases from 19.84 to 75.37 mg/g [Fig. 4.5(a)] with an increase in the initial phenol concentrations from 100 to 500 mg/L while % removal of phenol decreased from 99.19 to 75.37% [Fig. 4.5(b)].

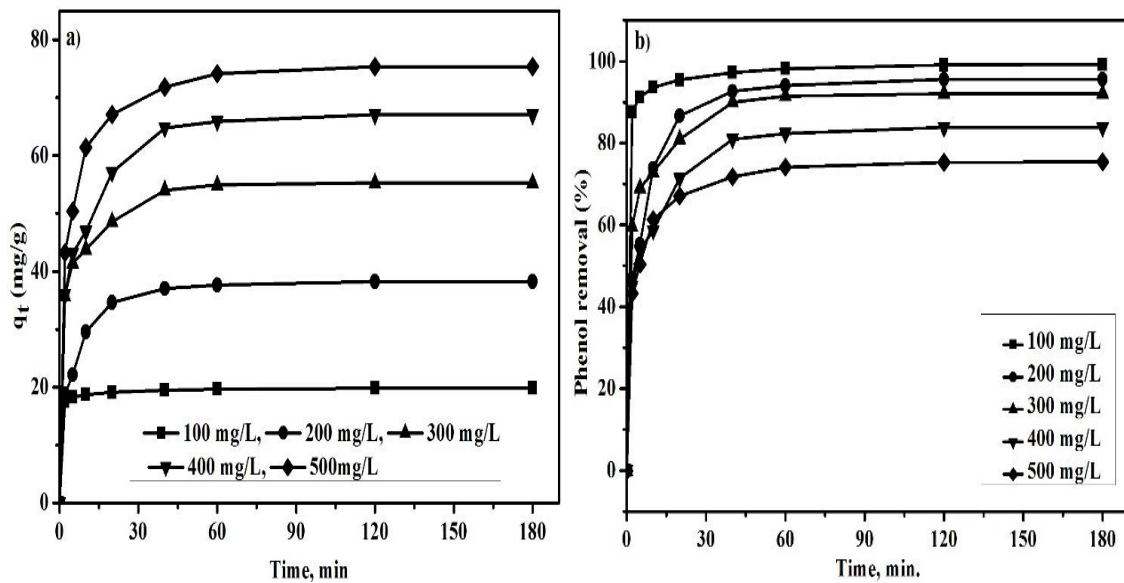


Fig. 4.5. Effects of contact time on the adsorption capacity of ACZC-600-2.0 at different initial concentrations ($m_s = 0.50$ g, pH = 7, temperature = 30 °C, and contact time = 3 hr).

For ACPA-700-1.5, the equilibrium adsorption enhanced from 17.95 to 83.21 mg/g [Fig. 4.6(a)] when phenol initial concentration increases from 100 to 500 mg/L and % removal of phenol as it decreases from 99.75 to 91.53% [Fig. 4.6(b)]. The higher mass transfer is because of increase in the driving force, i.e., the initial concentration of phenol.

From Figs. 4.5 (a) and 4.6 (a), it is observed that the phenol adsorption capacity of ACPA-700-1.5 (83.21 mg/g) is more than that of ACZC-600-2.0 (75.37 mg/g) may be due to high microporosity and presence of specific functional groups.

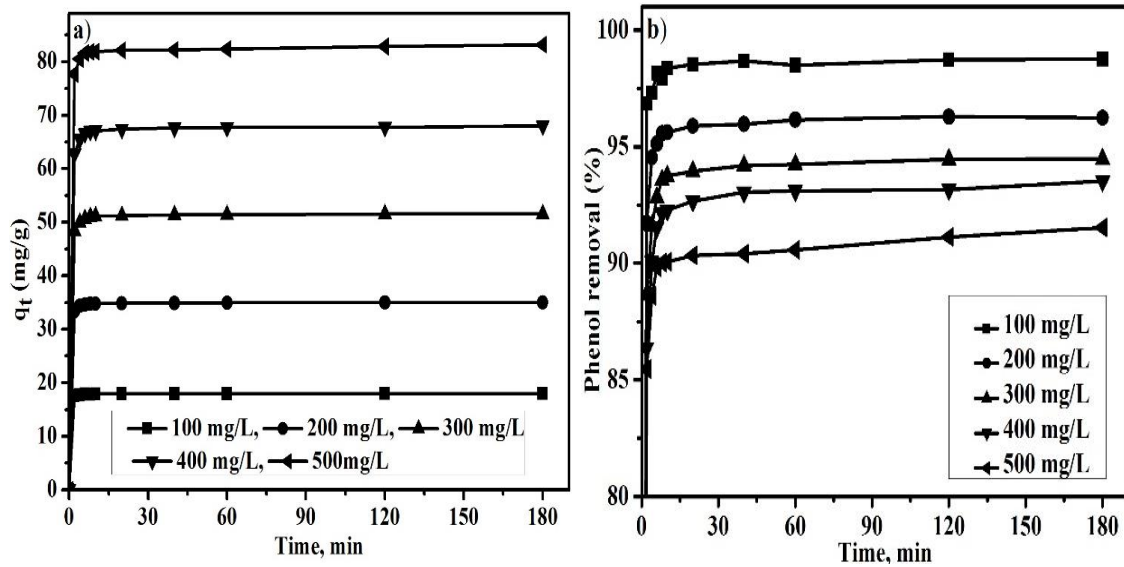


Fig. 4.6. Effects of contact time on the adsorption capacity of ACPA-700-1.5 at different initial concentrations ($m_s = 0.55$ g, pH = 7, temperature = 30 °C, and contact time = 3 hr).

4.1.1.2. Adsorption Characteristics

4.1.1.2.1. Adsorption kinetics

The study of adsorption kinetics describes the solute uptake rate, and evidently, this rate controls the residence time of adsorbate at the solid–solution interface. To evaluate the goodness of fit and suitability of the model, the linear correlation coefficient (R^2) and normalized standard deviation Δq (%) were used in the kinetic model study. A higher value of R^2 and lower value of Δq denoted better model fitting. The adsorption kinetics of pseudo-first-order for phenol adsorption onto ACZC-600-2.0 and ACPA-700-1.5 are shown in Fig. 4.7. The adsorption kinetics of pseudo-second-order for phenol adsorption onto ACZC-600-2.0 and ACPA-700-1.5 are shown in Fig. 4.8. The derived kinetic parameters of pseudo-first and pseudo second-order are listed in Table 4.1.

Table 4.1: Constant parameters and correlation coefficients calculated for pseudo-first and pseudo-second-order kinetic models

| Parameters | ACZC-600-2.0 (30 °C) | | | | | ACPA-700-1.5 (30 °C) | | | | |
|-----------------------------|----------------------|-------|--------|--------|--------|----------------------|--------|--------|--------|--------|
| | Phenol, C_0 (mg/L) | | | | | Phenol, C_0 (mg/L) | | | | |
| | 100 | 200 | 300 | 400 | 500 | 100 | 200 | 300 | 400 | 500 |
| $q_{e,exp}$ (mg/g) | 19.84 | 38.25 | 55.25 | 67.06 | 75.37 | 17.95 | 34.99 | 51.53 | 68.02 | 83.21 |
| Pseudo-first-order | | | | | | | | | | |
| $q_{e,cal}$ (mg/g) | 2.07 | 16.42 | 17.55 | 32.37 | 33.63 | 0.442 | 1.80 | 1.32 | 6.58 | 7.02 |
| h_0 (mg/g/min) | 4.10 | 11.60 | 17.52 | 23.40 | 29.80 | 8.11 | 26.76 | 14.43 | 35.00 | 35.90 |
| k_1 (min^{-1}) | 0.041 | 0.058 | 0.0584 | 0.0585 | 0.0596 | 0.0811 | 0.1338 | 0.0481 | 0.0875 | 0.0718 |
| R^2 | 0.9904 | 0.995 | 0.994 | 0.998 | 0.996 | 0.797 | 0.889 | 0.940 | 0.694 | 0.694 |

| | | | | | | | | | | |
|----------------------------|-------|--------|--------|--------|--------|--------|--------|--------|--------|--------|
| Δq (%) | 20.11 | 9.23 | 9.18 | 6.31 | 6.38 | 32.51 | 31.62 | 32.48 | 30.12 | 30.52 |
| Pseudo-second-order | | | | | | | | | | |
| $q_{e,cal}$ (mg/g) | 19.82 | 38.21 | 55.23 | 67.01 | 75.33 | 17.96 | 35.01 | 50.15 | 68.03 | 84.17 |
| k_2 [g/(mg min)] | 0.081 | 0.0101 | 0.0094 | 0.0051 | 0.0057 | 0.939 | 0.349 | 0.171 | 0.084 | 0.024 |
| h_0 (mg/g/min) | 31.82 | 14.75 | 29.29 | 22.90 | 34.37 | 302.88 | 427.77 | 430.07 | 388.76 | 170.03 |
| R^2 | 0.999 | 0.999 | 0.999 | 0.999 | 0.999 | 1 | 1 | 1 | 1 | 1 |
| Δq (%) | 0.023 | 0.017 | 0.005 | 0.009 | 0.006 | 0.0186 | 0.019 | 0.893 | 0.0049 | 0.384 |

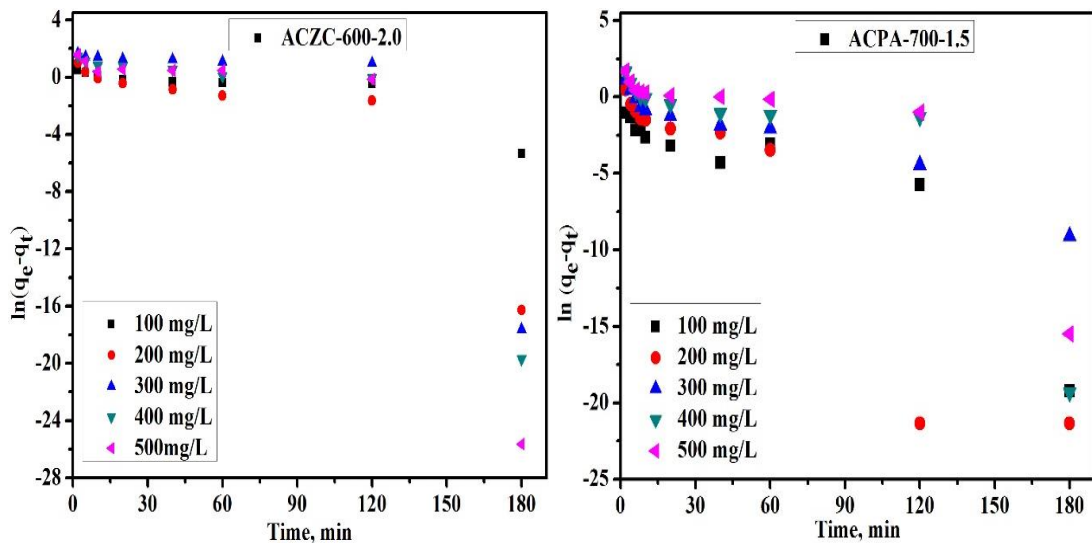


Fig. 4.7. Pseudo-first-order kinetics for the phenol adsorption onto ACZC-600-2.0 and ACPA-700-1.5 at 30 °C.

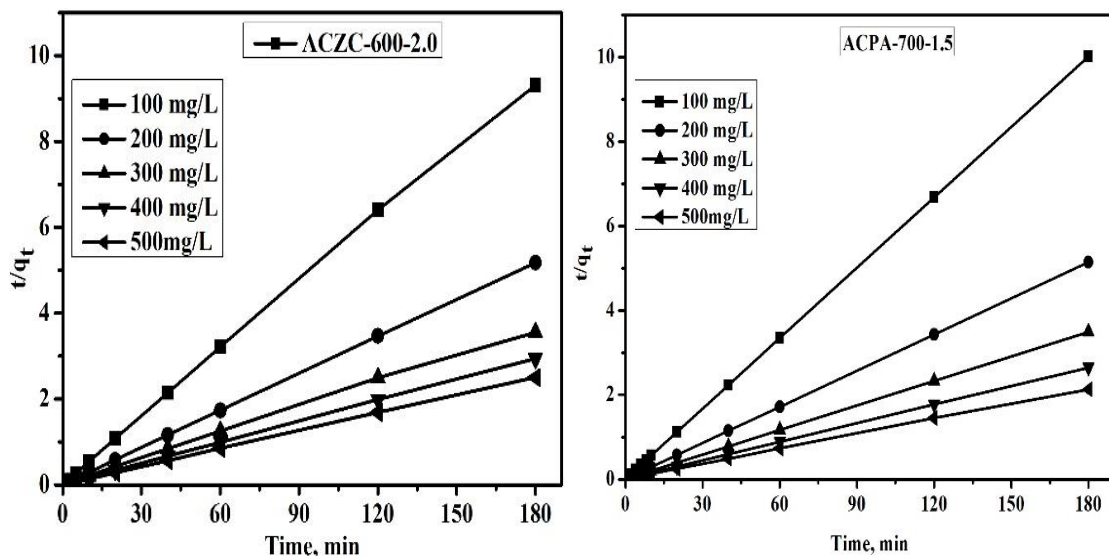


Fig. 4.8. Pseudo-second-order kinetics for the phenol adsorption onto ACZC-600-2.0 and ACPA-700-1.5 at 30 °C.

As observed, the experimental kinetic data are better fitted by the pseudo-second-order model ($R^2 = 0.999$ for ACZC-600-2.0 and 1 for ACPA-700-1.5). Moreover, all the

calculated normalized standard deviation Δq (%) of pseudo-first and pseudo-second-order are shown in Table 4.1. The resulted Δq (%) values are relatively lower for the pseudo-second-order model than the pseudo-first-order model for both adsorbents ACZC-600-2.0 and ACPA-700-1.5. Also, the calculated q_e value derived from the second-order equation is quite similar to those obtained experimentally, which indicates that the second-order model suitably explains the observed kinetics of phenol adsorption onto ACZC-600-2.0 and ACPA-700-1.5.

4.1.1.2.2. Intraparticle diffusion

Since neither the pseudo-first-order nor the pseudo-second-order model can identify the diffusion mechanism, the kinetic results were analyzed by the intraparticle diffusion model to elucidate the diffusion mechanism (Hameed and Rahman, 2008). The constants (k_i) for phenol adsorption were calculated from Fig. 4.9 and tabulated in Table 4.2. If the value of c is zero, then the rate of adsorption is controlled by intraparticle diffusion for the entire adsorption period, but in the present study, c is not zero. However, the plot of q_t against $t^{0.5}$ of both ACZC-600-2.0 and ACPA-700-1.5 adsorbents usually show more than one linear pattern. As seen from Fig. 4.9, the plots are not linear over the time range, that confirms more than one process affects the phenol adsorption (Hameed and Rahman, 2008). These plots have a dual nature, i.e., an initial curved portion and a final linear portion. This is explained by the fact that the initial curved portion represents boundary layer diffusion effects while the final linear portions are a result of intraparticle diffusion effects (Ugurlu et al., 2005).

Table 4.2: Intraparticle diffusion constants for phenol adsorption

| Parameters | ACZC-600-2.0 (at 30 °C) | | | | | ACPA-700-1.5 (at 30 °C) | | | | |
|-----------------------------------|-------------------------|-------|-------|-------|-------|-------------------------|--------|--------|--------|--------|
| | Phenol, C_0 (mg/L) | | | | | Phenol, C_0 (mg/L) | | | | |
| | 100 | 200 | 300 | 400 | 500 | 100 | 200 | 300 | 400 | 500 |
| k_i (mg/g min ^{-1/2}) | 0.17 | 1.48 | 1.52 | 2.51 | 2.41 | 0.021 | 0.075 | 0.154 | 0.248 | 0.262 |
| R^2 | 0.766 | 0.667 | 0.747 | 0.755 | 0.710 | 0.4695 | 0.3006 | 0.3465 | 0.3465 | 0.4067 |
| c | 17.98 | 22.85 | 39.13 | 40.37 | 49.86 | 17.73 | 34.25 | 49.98 | 65.40 | 80.20 |

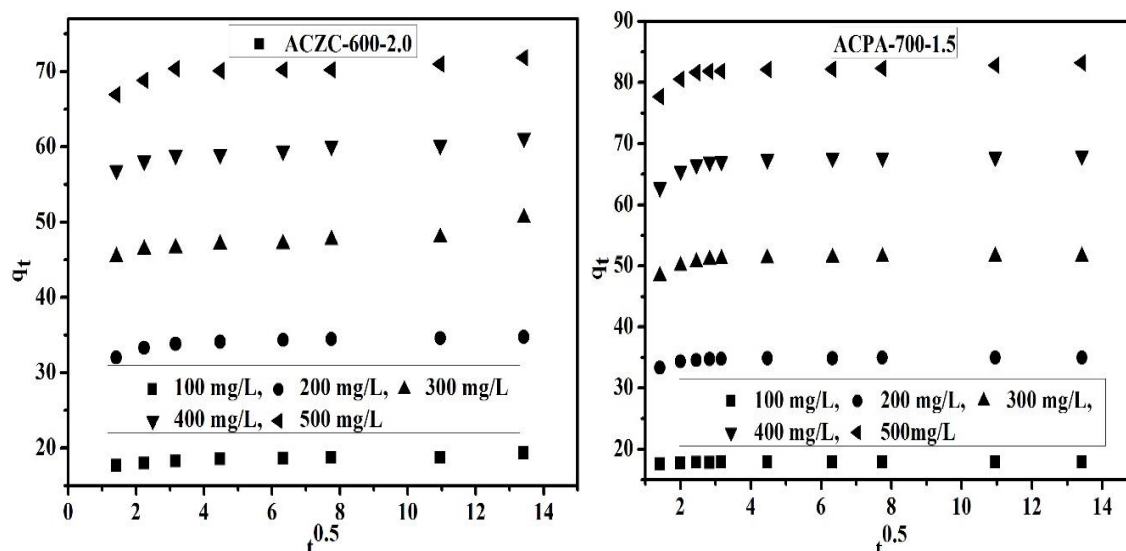


Fig. 4.9. Intraparticle diffusion plots for phenol adsorption onto ACZC-600-2.0 and ACPA-700-1.5 at 30 °C.

4.1.1.2.3. Adsorption isotherms

At equilibrium state, the adsorption isotherm is very useful to describe how the adsorbed molecules distribute between the liquid phase and the solid phase. The Freundlich, Langmuir, and Temkin isotherm models were used for the study of adsorption isotherms of ACZC-600-2.0 and ACPA-700-1.5 adsorbents. Fig. 4.10 shows Langmuir isotherms, a linear relationship of C_e/q_e vs. C_e using experimental data obtained for phenol adsorption of ACZC-600-2.0 and ACPA-700-1.5. The intercept and the slope of the plot results in the q_m and k_L values of ACZC-600-2.0 and ACPA-700-1.5 and are tabulated in Table 4.3. The value of R_L is found to be 0.0153 for ACZC-600-2.0 and 0.023 for ACPA-700-1.5, it confirms that the Langmuir isotherm is favorable for phenol adsorption on the adsorbents under the conditions used in the present study.

The values of Freundlich constants, k_F and $1/n$, were obtained from the linear plot of $\ln q_e$ vs. $\ln C_e$ (Fig. 4.11) and the correlation coefficient ($R^2 > 0.98$ for ACZC-600-2.0 and ACPA-700-1.5). The Freundlich constant $1/n$ was smaller than unity indicated that the adsorption process was favorable under studied conditions. From the results, the adsorption pattern of phenol onto ACs was well fitted with both Langmuir and Freundlich isotherm model. This may be due to both homogeneous and heterogeneous distribution of active sites on the surface of the prepared activated carbons; a possibility of mono and heterolayer phenol formation on the adsorbent surface. Fig. 4.12 shows the linear graph of Temkin isotherms of the adsorbents. The constant A and b values of ACZC-600-2.0 and ACPA-700-1.5 adsorbents along with the correlation coefficient are listed in Table 4.3. Similar results are reported phenol adsorption (Ahmaruzzaman and Sharma, 2005; Din et al., 2009;

Özkaya, 2006). Thus, from Table 4.3, the comparison of tested models for the description of equilibrium adsorption isotherms on the ACZC-600-2.0 follows: Langmuir > Temkin > Freundlich and for ACPA-700-1.5 as Freundlich > Langmuir > Temkin.

Table 4.3: Isotherm constants for adsorption of phenol

| ACs | Langmuir | | | | Freundlich | | | Temkin | | |
|--------------|-----------------|-----------------|-------|--------|---------------------------------------|-------|-------|--------|------------|-------|
| | q_m (mg/g) | k_L (L/mg) | R^2 | R_L | k_F [mg/g(L/mg) ^{1/n}] | 1/n | R^2 | b | A (L/g) | R^2 |
| ACZC-600-2.0 | 78.74 | 0.129 | 0.996 | 0.0153 | 20.42 | 0.286 | 0.987 | 212.24 | 4.26 | 0.988 |
| ACPA-700-1.5 | 101.83 | 0.086 | 0.914 | 0.023 | 15.58 | 0.44 | 0.988 | 136.58 | 1.53 | 0.876 |

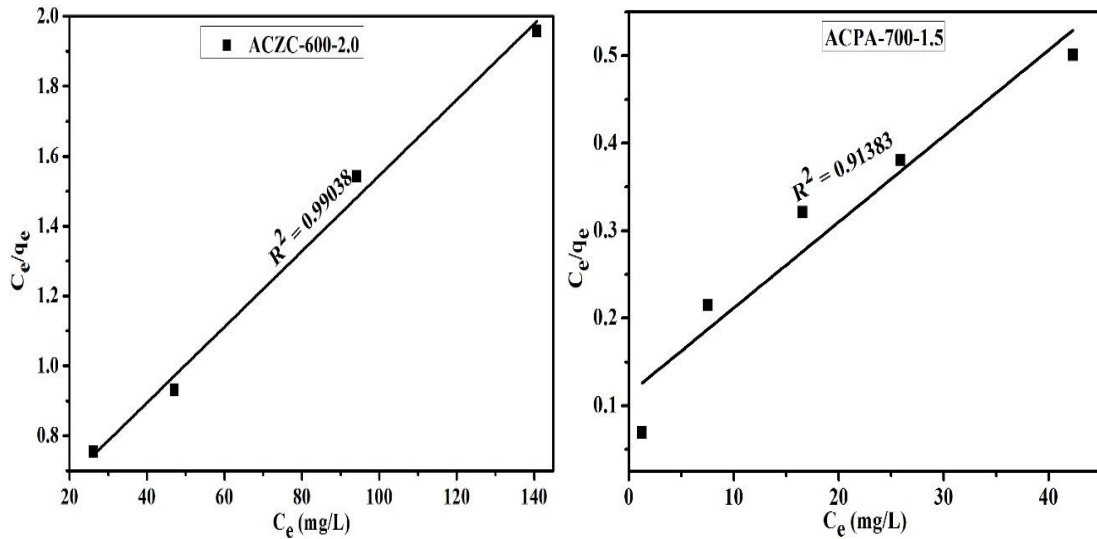


Fig. 4.10. Langmuir isotherms for the adsorption of phenol onto ACs at 30 °C.

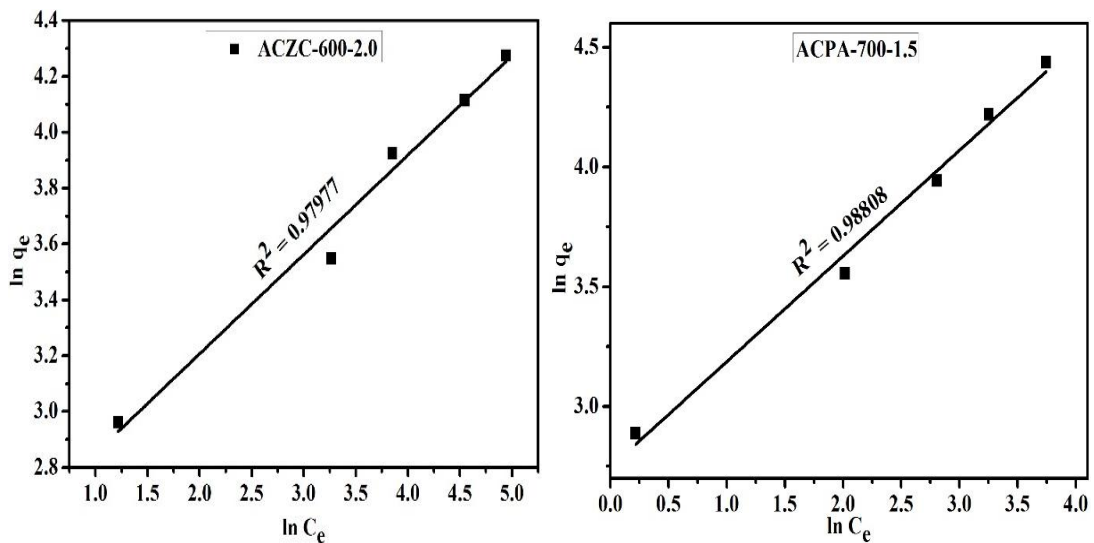


Fig. 4.11. Freundlich isotherms for the adsorption of phenol onto ACs at 30 °C.

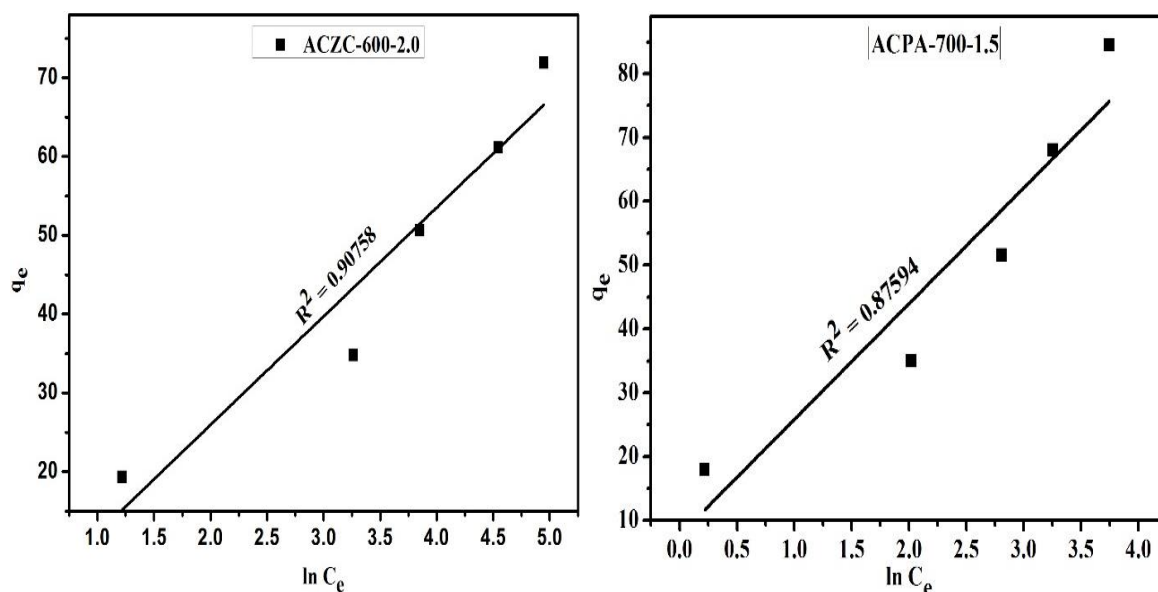


Fig. 4.12. Temkin isotherms for the adsorption of phenol onto ACs at 30 °C.

4.1.1.2.4. Adsorption mechanism

Three adsorption mechanisms are widely accepted and investigated in the phenol adsorption studies: the electron donor–acceptor interaction, the dispersive interaction of π – π electron coupling and competing for adsorption of solvent molecules (Terzyk, 2003). It has been reported that two different ways of electron donor–acceptor interaction occurred during phenol adsorption. One involves the interaction of the aromatic ring of phenol (electron acceptor) with carbonyl groups (electron donor) of AC (Mattson et al., 1969). Another one involves the interaction between aromatic ring (electron acceptor) of phenol and basic sites of AC (electron donor) (Terzyk, 2003). The strength of donor–acceptor interaction during phenol adsorption depends mainly on the dipole moment of the oxygen groups on basal plane. Carbonyl groups on the activated carbon surface are known as strong donors because of their high dipole moments (Gokce and Aktas, 2014). The solvent also affects phenol adsorption onto activated carbon. It occurs when some of the most active sites adsorbing phenols are blocked by water adsorption (Terzyk, 2003). In other words, some pores may be inaccessible to phenol–water aggregates (Hameed and Rahman, 2008). Carboxyl and hydroxyl groups inhibit the adsorption of phenol and increase the affinity of carbon towards the water, and therefore, solvent molecules can block some pores (Dąbrowski et al., 2005). The influence of electrostatic interactions, which strongly depend on pH of the solution, has already been discussed in the pH study.

4.1.1.2.5. Adsorption thermodynamics

Thermodynamic parameters provide an insight of phenol adsorption mechanism and adsorption behaviour of an isolated system. The basic concept assumes that energy cannot be gained or lost, where entropy change is the driving force. The effect of temperature on the phenol adsorption process was investigated with the thermodynamic parameters like a change in Gibbs free energy (ΔG°), change in enthalpy (ΔH°) and change in entropy (ΔS°). The values of ΔH° and ΔS° are determined from the slope and intercept of the van't Hoff plot of $\ln K_C$ vs. $1/T$ (Fig. 4.13). The estimated thermodynamic parameter values were tabulated in Table 4.4. The negative values of ΔG° indicate that adsorption process is spontaneous and thermodynamically favourable. For ACZC-600-2.0 and ACPA-700-1.5, the negative Gibbs free energy (ΔG°) of the experimental value shows a typical physical process (Table 4.4). The negative value of the enthalpy change ($\Delta H^\circ = -16.92$ and -18.33 kJ/mol of ACZC-600-2.0 and ACPA-700-1.5, respectively) indicates that the phenol adsorption process onto ACs is exothermic in nature.

Table 4.4: Thermodynamic parameters of phenol adsorption onto ACZC-600-2.0 and ACPA-700-1.5

| Adsorbents | T(K) | ΔG° (kJ/mol) | ΔH° (kJ/mol) | ΔS° (J/molK) |
|--------------|------|---------------------------|---------------------------|---------------------------|
| ACZC-600-2.0 | 298 | -0.23 | -16.92 | -57.35 |
| | 303 | -0.29 | | |
| | 308 | -0.92 | | |
| | 313 | -0.97 | | |
| | 318 | -0.11 | | |
| ACPA-700-1.5 | 298 | -1.2 | -18.33 | -57.83 |
| | 303 | -0.75 | | |
| | 308 | -0.39 | | |
| | 313 | -0.24 | | |
| | 318 | -0.013 | | |

The decrease in adsorption with the rise of temperature may be due to the weakening of adsorptive forces between the active sites of the adsorbent and adsorbate species and also between the adjacent molecules of the adsorbed phase (Panday et al., 1986; Senturk et al., 2009). The negative values of ΔS° indicate a decrease in the degree of freedom (or disorder) of the adsorbed species which means adsorption decreases with increase in temperature. The exothermic nature of adsorption of phenol onto activated carbon fibers is already

reported (Liu et al., 2010b). Negative ΔH° , ΔS° , and ΔG° values for adsorption of phenol on organomodified Tirebolu bentonite is previously reported (Senturk et al., 2009).

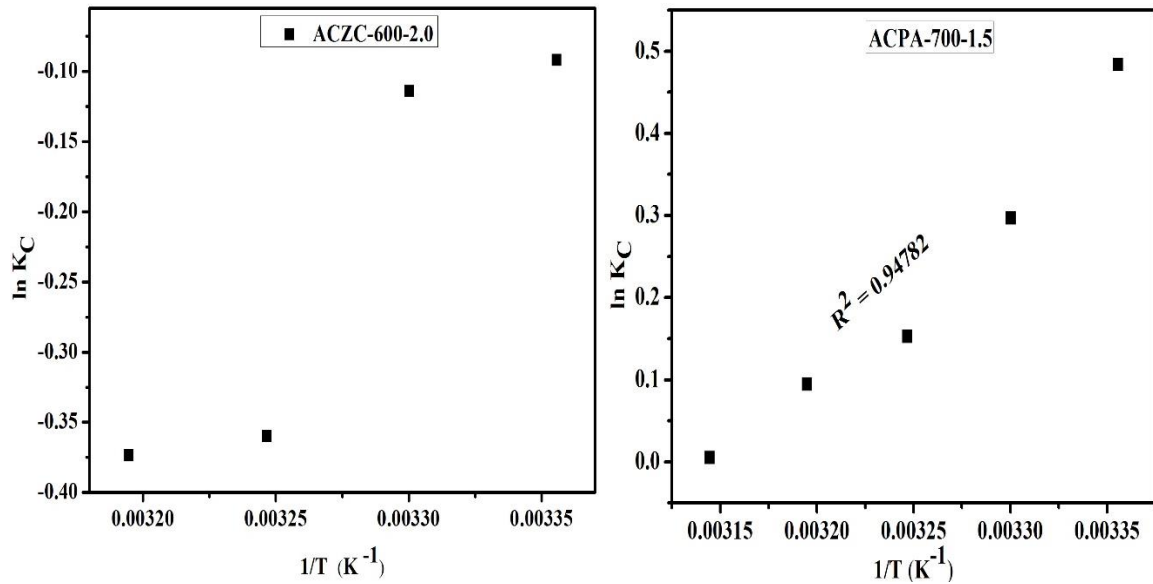


Fig. 4.13. Plots of $\ln K_C$ versus $1/T$ for 100 mg/L initial phenol concentration onto ACZC-600-2.0 and ACPA-700-1.5.

4.1.2. Regeneration and reuse of activated carbons

As per the method mentioned in chapter 2, the regeneration of activated carbons was done and the obtained ACs after desorption of phenol was washed with distilled water several times until neutral pH. The regenerated activated carbons of both types were further used for adsorption of phenol.

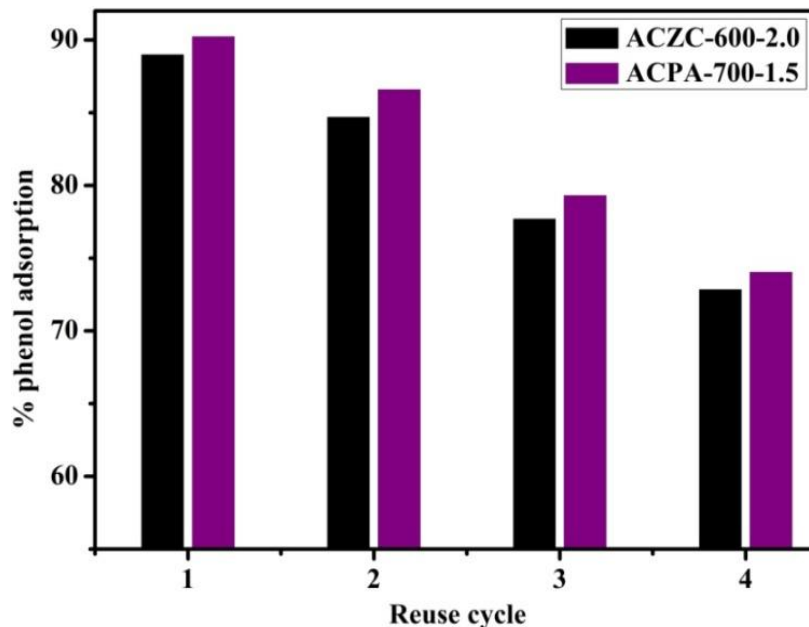


Fig. 4.14. Readsorption of phenol after desorption.

For ACZC-600-2.0 and ACPA-700-1.5, the initial amount was taken as 0.50 and 0.55 g for 100 mL of phenol solution of 100 mg/L concentration. Experiments were carried out up to fourth regeneration cycle. The % removal of phenol using regenerated ACs is represented in Fig. 4.14. It is observed that in the first reused, the % removal of phenol reduced by 11.2 and 9.76% for ACZC-600-2.0 and ACPA-700-1.5, respectively and same reduced by 27.15 and 25.96% after the 4th regeneration.

4.1.3. Column adsorption study

The operating parameters such as volumetric flow rate (Q), and length of the bed (L) have a significant influence on breakthrough and saturation times, and on the dynamics of the column. In the present study, the effect of these parameters on the breakthrough curves of phenol adsorption onto ACZC-600-2.0 and ACPA-700-1.5 adsorbents were investigated. The area under the BT curve which is obtained by integrating the plot was used to estimate the total adsorbed quantity of adsorbate, q_{tot} (mg) in the column for a given inlet concentration and flow rate (Aksu and Gönen, 2004; Salman et al., 2011).

4.1.3.1. Effect of bed height

To perform this investigation, the breakthrough curves at different bed depths (2 to 4 cm) at the influent phenol concentration ($C_0 = 100$ mg/L) and flow rate (5 mL/min) for ACZC-600-2.0 and ACPA-700-1.5, were plotted. The results obtained are shown in Fig. 4.15. It can be seen that with the increase in the column bed height, a much higher removal efficiency of phenol is observed for the used both adsorbents. When the bed height increased, phenol had more time to be in contact with the adsorbents, and this resulted in higher removal efficiency of phenol. Higher uptake of phenol at the highest bed height is due to an increase in the surface area of the adsorbent, which provides more binding sites for the sorption (Tan et al., 2008a). From Table 4.5, it can be observed that the breakthrough time, exhaustion time and percent removal increased as the bed height is increased (Ahmad and Hameed, 2010; Vijayaraghavan et al., 2004).

Table 4.5: Column parameters obtained at different bed heights and flow rates

| ACs | Bed height (cm) | Flow rate (mL/min) | Breakthrough time (min) | Exhaustion time (min) | Bed capacity, q_{eq} (mg/g) | % Removal |
|--------------|-----------------|--------------------|-------------------------|-----------------------|-------------------------------|-----------|
| ACZC-600-2.0 | 2 | 5 | 80 | 960 | 53.78 | 26.89 |
| | 3 | 5 | 130 | 1340 | 56.49 | 35.30 |

| | | | | | | |
|--------------|---|----|-----|------|-------|-------|
| | 4 | 5 | 180 | 1740 | 61.76 | 37.05 |
| | 4 | 10 | 80 | 1320 | 70.56 | 27.19 |
| | 4 | 15 | 30 | 850 | 55.85 | 20.68 |
| ACPA-700-1.5 | 2 | 5 | 20 | 740 | 46.59 | 29.12 |
| | 3 | 5 | 130 | 1080 | 60.14 | 41.0 |
| | 4 | 5 | 240 | 1320 | 60.94 | 54.64 |
| | 4 | 10 | 120 | 1140 | 69.24 | 31.47 |
| | 4 | 15 | 40 | 660 | 65.21 | 25.57 |

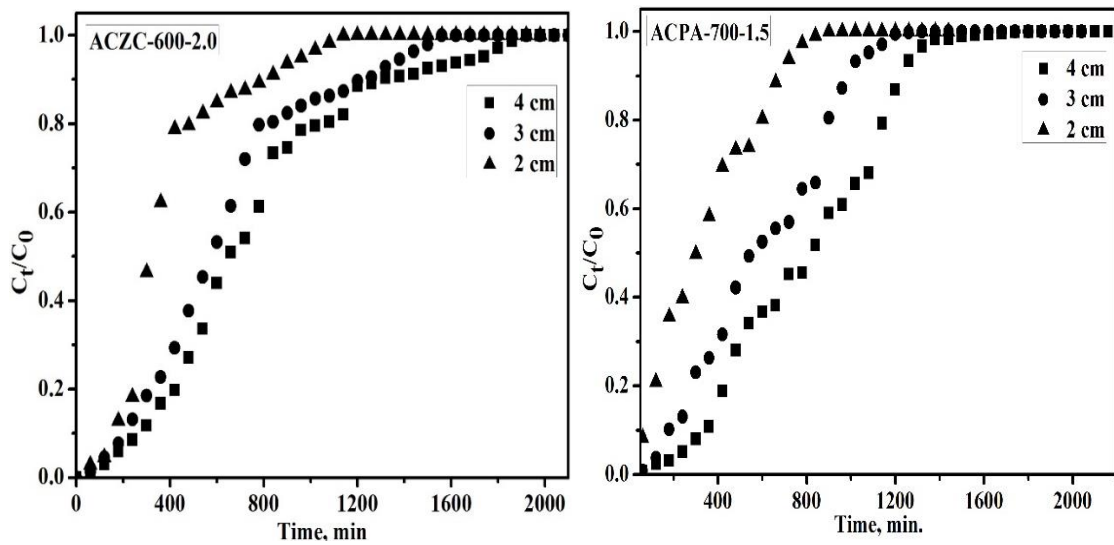


Fig. 4.15. Breakthrough curves for phenol adsorption onto ACZC-600-2.0 and ACPA-700-1.5 at different bed heights ($C_0 = 100$ mg/L, flow rate = 5 mL/min, and pH = 7).

4.1.3.2. Effect of solution flows rate

The effect of flow rate on the adsorption of phenol onto ACZC-600-2.0 and ACPA-700-1.5 was investigated by varying the flow rate from 5-15 mL/min with a constant bed height of 4 cm and initial phenol concentration of 100 mg/L. Figure 4.16 shows the effect of flow rate on the BT curves and shows that the column performed better at a lower flow rate, which resulted in longer BT and exhaustion times (Table 4.5). The BT time is longer for low flow rate than that at a higher flow rate because a longer time is required to reach its effective bed load. As the flow rate increases, the BT curve became steeper since a shorter time was required to attain the effective bed load and hence the effective % removal of the ACs of the column is reduced (Goud et al., 2005). This is attributed to the insufficient residence time of the solute in the column to allow for diffusion of the solute into the pores of the adsorbent (Salman et al., 2011; Tan et al., 2008a).

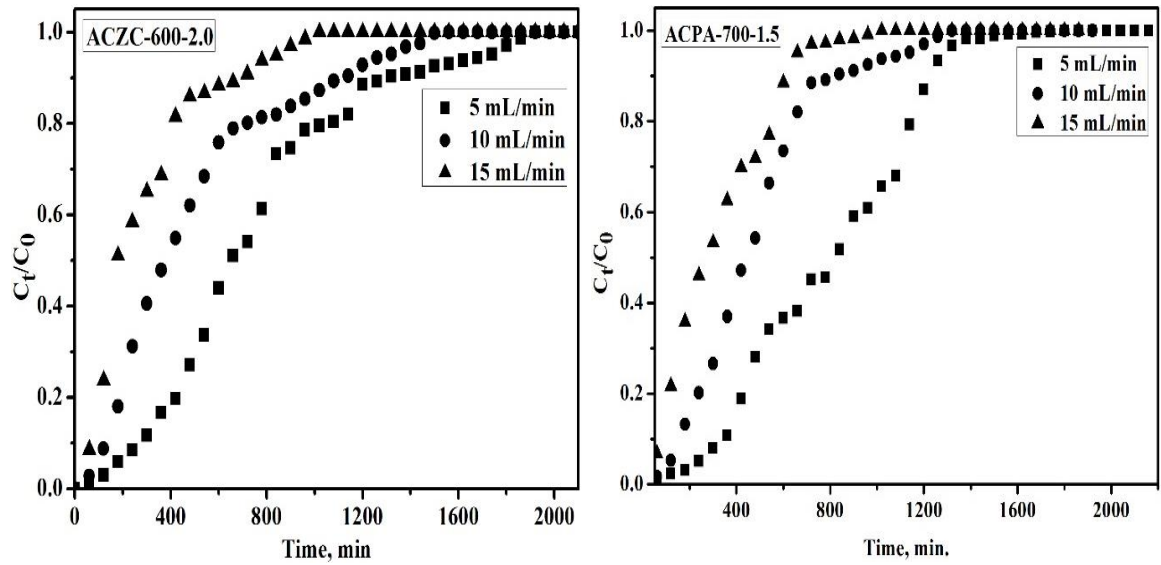


Fig. 4.16. Breakthrough curves for phenol adsorption onto ACZC-600-2.0 and ACPA-700-1.5 at different flow rates ($C_0 = 100$ mg/L, bed height = 4 cm, and pH = 7).

4.2. Adsorption of Methylene Blue (MB)

In this sub chapter, adsorption studies on MB are discussed. Experiments were carried out in both batch and continuous mode. In the batch adsorption, effect of various experimental parameters on adsorption capacity and various adsorption characteristics of ACZC-600-2.0 and ACPA-700-1.5 were studied. Secondly, the regeneration and re-adsorption studies were carried out. Finally, the fixed column adsorption study was carried out. The experimental results are demonstrated in the form of graphs; significant values are listed in tables.

4.2.1. Batch adsorption studies

MB was used as an adsorbate in batch adsorption studies at different initial concentrations (100, 200, 300, 400 and 500 mg/L). The volume solution used was 100 mL and the contact time of 3 hr was used.

4.2.1.1. Effect of experimental factors

Various process parameters affect such as agitation speed, solution pH, temperature, adsorbent dose and contact time onto MB adsorption were studied.

4.2.1.1.1. Agitation speed

Like the previous section (4.1.1.1.1) to characterize the effect of agitation speed on MB adsorption a series experiments were performed by varying agitation speed in the range of 90–170 rpm. The results are shown in Fig. 4.17. The figure shows that the removal efficiency of MB increases with increase in agitation speed and maximum removal by ACZC-600-2.0 and ACPA-700-1.5 are achieved at 150 rpm, and above 150 rpm, the % removal is almost constant for both the carbons. The agitation speed of 150 rpm was fixed for all the further experiments on adsorption of MB.

4.2.1.1.2. pH

MB is basic in nature; therefore, it releases coloured dye cations into solution on dissolution and adsorption by activated carbon is very susceptible to solution pH (Gokce and Aktas, 2014). The effect of initial pH of the dye solution on the % removal of MB was studied by varying the initial pH in the range 3-12 under constant values of other process parameters onto ACZC-600-2.0 and ACPA-700-1.5. Fig. 4.18 shows the % removal of MB increases with increasing the initial pH in the ranges of 3-12 for both the carbons. The low adsorption rate of MB on ACs observed at low pH due to the positive charge of the surface, causing

H^+ ions to compete effectively with MB cations. When the pH of the solution increases, the positive charge on the interface of the solution decreases and the negatively charged appeared on the adsorbing surface, thereby resulting in an increased adsorption of MB due to an increase in the electrostatic attraction between positively charged adsorbate and negatively charged adsorbent (Altenor et al., 2009; Radovic et al., 1997; Senthilkumar et al., 2005). The effect of pH on MB can be explained in terms of PZC. The PZC values of ACZC-600-2.0, and ACPA-700-1.5 are 2.1 and 2.7, respectively. At $pH < PZC$, because H^+ competes with MB, the sorbent surface takes up more H^+ , reducing MB molecules bind on the sorbent surface. At $pH > PZC$, the adsorbent surface is negatively charged, the increasing electrostatic attraction between positive sorbate species and adsorbent particles would lead to increase adsorption capacity of MB (Deng et al., 2009). Similar results are reported in the literature for the adsorption of methylene blue adsorption on jute fiber carbon, cocoa (*Theobroma cacao*) shell-based activated carbon and wheat shells (Ahmad et al., 2012; Bulut and Aydın, 2006; Senthilkumar et al., 2005).

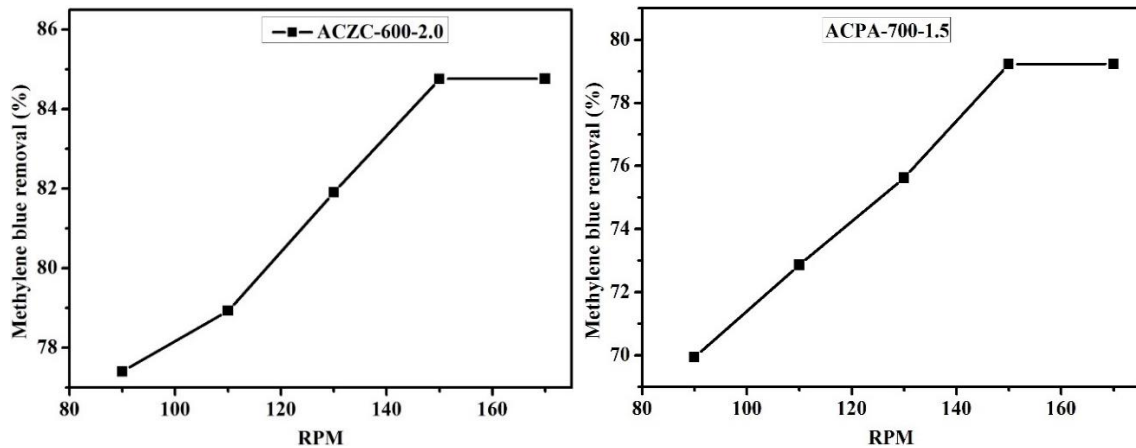


Fig. 4.17. Effect of agitation speed on % removal of MB ($C_0 = 100 \text{ mg/L}$, $m_s = 0.03 \text{ g/100mL}$, temperature = $30 \text{ }^\circ\text{C}$, and contact time = 3 hr).

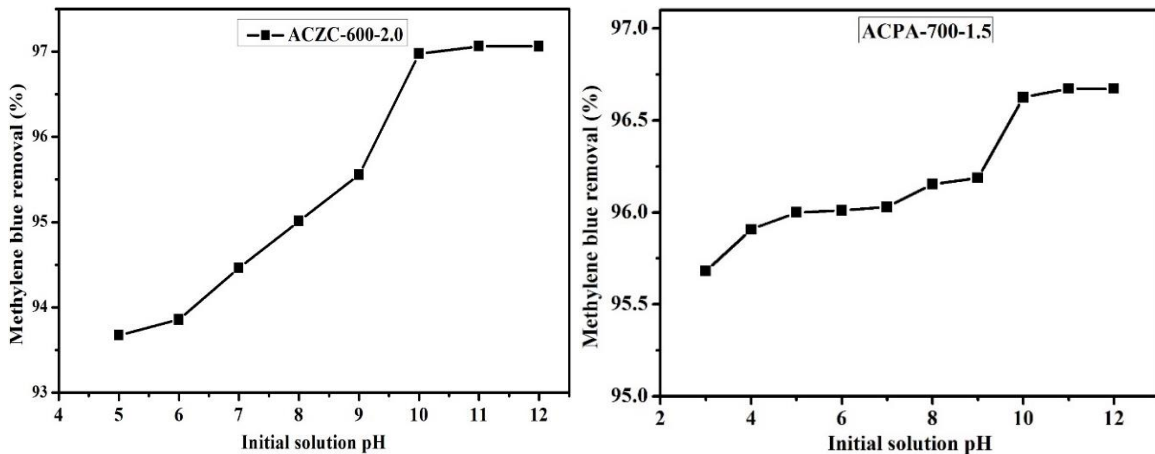


Fig. 4.18. Effect of pH on % removal of MB ($C_0 = 100 \text{ mg/L}$, $m_s = 0.03 \text{ g/100mL}$, temperature = $30 \text{ }^\circ\text{C}$, and contact time = 3 hr).

4.2.1.1.3. Temperature

Various textile effluents containing dye are produced at relatively high temperatures. Therefore, to quantify the effect of temperature on adsorption and aware about endothermic or exothermic nature of adsorption process occurring for the removal of MB experiments were carried out at different temperatures. The temperatures considered in the study were 25, 30, 35, 40 and 45 °C.

Figure 4.19 (a) shows the % removal of MB onto ACZC-600-2.0 increases from 92.03 to 92.9% with an increase in temperature from 25 to 30 °C and after that decreases to 91.68% at 45 °C. The small variation after 35 °C that indicates that the adsorption reaction is exothermic in nature. The adsorption of MB decreases with the increase in temperature is due to the enhancement of the desorption step in the sorption mechanism. It is also due to the weakening of sorptive forces between the active sites of the activated carbon and the dye species, and also between adjacent dye molecules in the sorbed phase, and re-enters into a liquid phase (Tan et al., 2008b). Similar observation have also been reported for adsorption of MB using fly ash (Benhouria et al., 2015; Rao and Rao, 2006; Tan et al., 2008b).

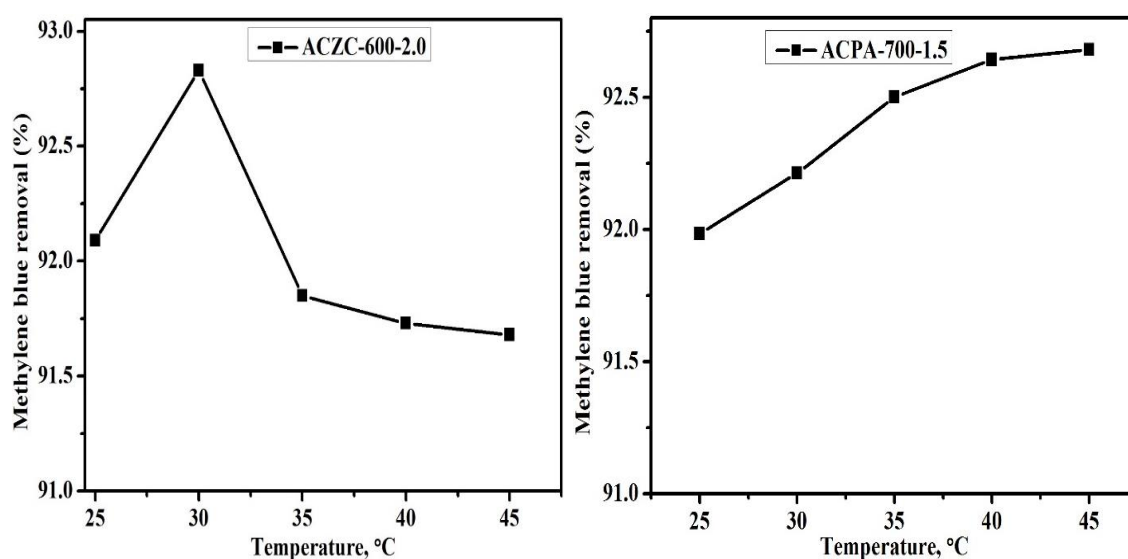


Fig. 4.19. Effect of temperature on % removal of MB ($C_0 = 100$ mg/L, $m_s = 0.03$ g/100mL, pH = 11, contact time = 3 hr).

The percentage removal of MB on ACPA-700-1.5 from solution increases slightly with a rise in temperature [Fig. 4.19 (b)]. This shows the endothermic nature of the adsorption process in the temperature ranges under the study. Explanation on the decreasing MB adsorption with increasing temperature could be due to the involvement of adsorbed water molecules to the polar groups of the carbons (i.e., carboxylic oxygen) by hydrogen bonding

occupying a part of the adsorbent surface and thus prevent the adsorption of MB. Since hydrogen bonding decreases with temperature, the number of the adsorbed water molecules decreases at higher temperatures, thus making more sites available for MB uptake (Makrigianni et al., 2015).

4.2.1.1.4. Adsorbent dosage

To study the effect of ACs dosage (g) on MB adsorption, experiments were conducted at 100 mg/L an initial solution concentration at 30 °C and pH 11 while the amount of adsorbents added were varied. Activated carbon dosage was varied from 0.01 to 0.07 g/100mL and equilibrated for 3 hr. Fig. 4.20 shows the effect of adsorbent (ACZC-600-2.0) dosage on the % removal of MB. The MB % removal of ACZC-600-2.0 increases with the increase in adsorbent dose up to 0.04 g significantly, and after that remains unchanged. Thus, to get a better MB removal and to not consume a significant quantity of adsorbent, 0.04 g dose was chosen as an optimal mass of the ACZC-600-2.0 for further experiments. At equilibrium time, the % removal increased from 79.82 to 99.48 %. The rise in color removal may be due to the increase in the available sorption surface sites on the activated carbon.

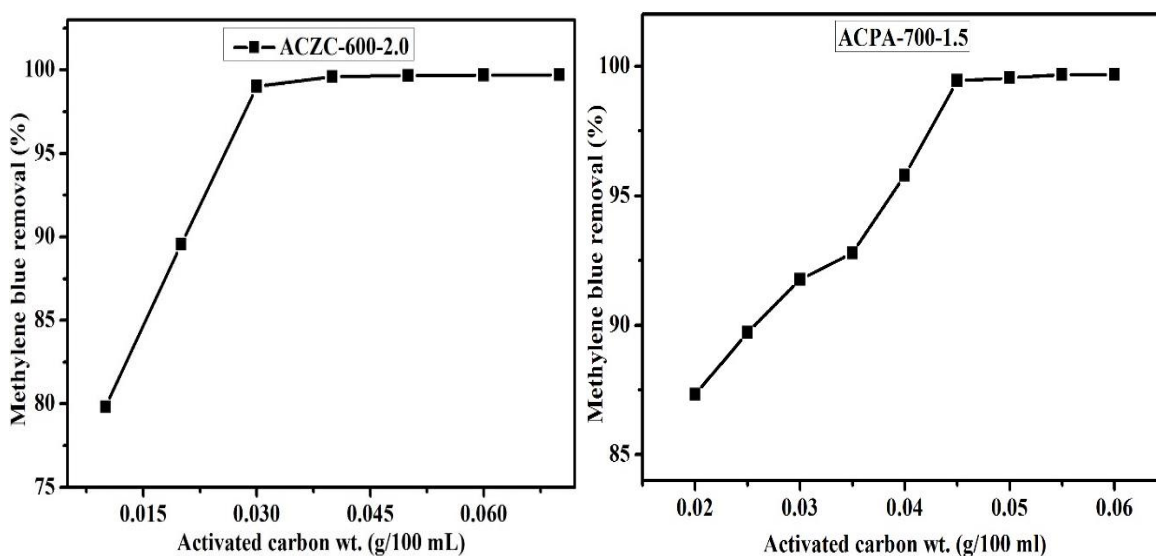


Fig. 4.20. Effect of adsorbent dosage on % removal of MB ($C_0 = 100$ mg/L, pH = 11, contact time = 3 hr, and temperature 30 °C).

For ACPA-700-1.5 adsorbent, the experiment was conducted at an initial solution concentration of 100 mg/L at 45 °C and pH 11 while the amount of adsorbent added was varied. Activated carbon dosage was ranged from 0.01 to 0.06 g/100mL and equilibrated for 3 hr. Fig. 4.20 shows the effect of adsorbent dose on the % removal of MB. The % removal of MB increased with the increase in adsorbent dose up to 0.045 g significantly

and after that remains unchanged. Thus in all future experiments for MB adsorption, 0.045 g/100mL of ACPA-700-1.5 was considered. At equilibrium time, the % removal increased from 87.25 to 99.66 %.

4.2.1.1.5. Contact time and initial MB concentration

The effect of contact time on the adsorption of MB onto ACZC-600-2.0 and ACPA-700-1.5 are shown in Figs. 4.21 and 4.22. Fig. 4.21 displays the impact of contact time on the adsorption of MB onto ACZC-700-1.5 of 0.04 g/100mL of different initial concentrations (100, 200, 300, 400, and 500 mg/L) at 30 °C and pH 11 for 3 hr study. It is observed that the adsorption capacity of MB on ACZC-600-2.0 drastically increases during the initial stage and then at a slow speed. The growing trend is stopped when a state of equilibrium is reached. ACZC-600-2.0 adsorbent removes a larger amount of MB in the initial 10 min of contact time, and the equilibrium is established in 40 min for all adsorbent concentration studied [Fig 4.21 (b)].

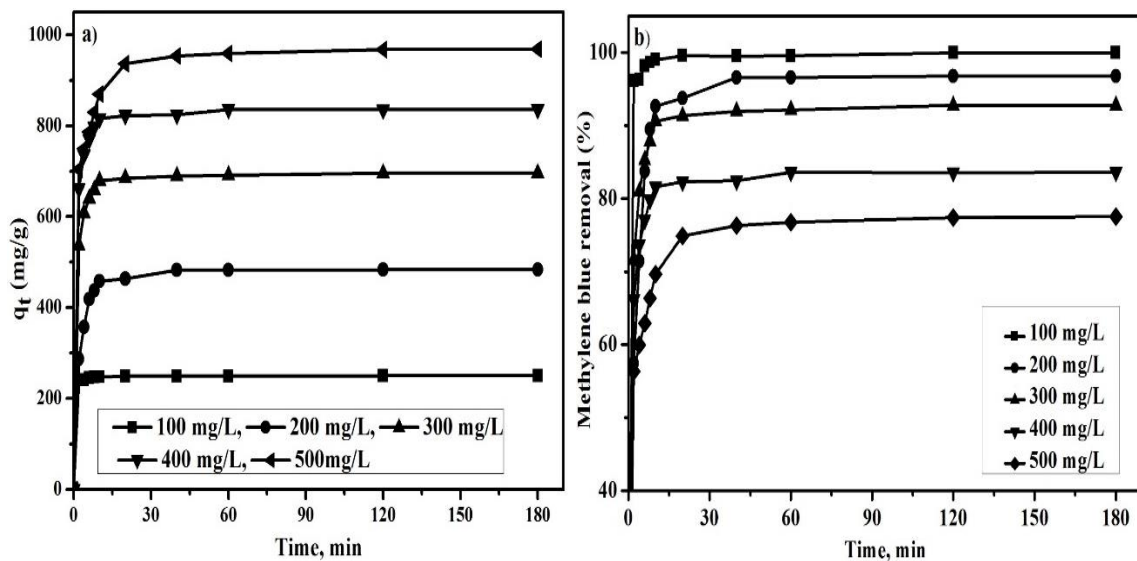


Fig. 4.21. Effects of contact time on the adsorption capacity of ACZC-600-2.0 at different MB initial concentrations ($C_0 = 100$ mg/L, $m_s = 0.04$ g/100mL, pH = 11, temperature = 30 °C, and contact time = 3 hr).

A large number of vacant sites with active functional groups are available on ACZC-600-2.0 at an early stage of adsorption for the MB molecules. At a later stage, adsorption is achieved due to the intra-specific competition among the MB molecules with the surface functional groups. The equilibrium adsorption increases from 249.88 to 968.74 mg/g when MB initial concentration enhanced from 100 to 500 mg/L [Fig 4.21(a)]. The higher mass transfer is because of increase in the driving force, i.e., the initial concentration of MB. Reverse behaviour is observed in the case of % removal of MB, as the initial concentration is increased from 100 to 500 mg/L then % removal of MB decreased from 99.95 to 77.49%

[Fig 4.21(b)]. Figure 4.22 displays the impact of contact time on the adsorption of MB onto ACPA-700-1.5 of 0.045 g/100mL for different initial concentrations (100, 200, 300, 400, and 500 mg/L) at 45 °C and pH 11 for 3 hr study.

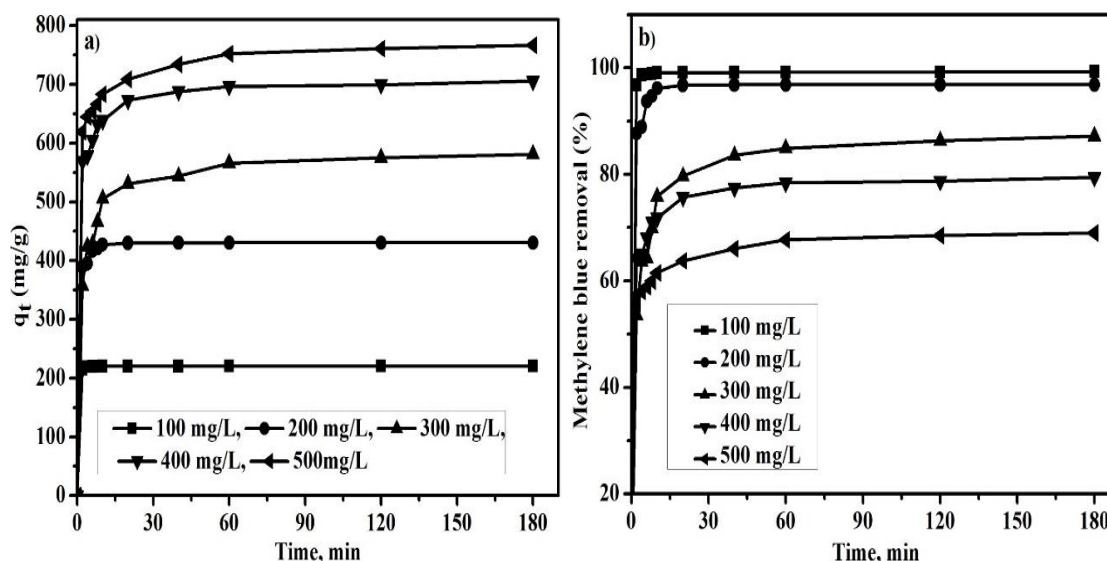


Fig. 4.22. Effects of contact time on the adsorption capacity of ACPA-700-1.5 at different MB initial concentrations ($C_0 = 100$ mg/L, $m_s = 0.045$ g/100mL, pH = 11, temperature = 45 °C, and contact time = 3 hr).

It is observed that the adsorption capacity of MB on ACPA-700-1.5 drastically increased during the initial stage and then at moderately slower rate. The growing trend is stopped when a state of equilibrium is achieved. Adsorbent ACPA-700-1.5 removes a larger amount of MB in the initial 10 min of contact time, and the equilibrium was established in 60 min for all different adsorbent concentration studied [Fig 4.22(b)]. Again this may be because the reason as discussed for ACZC-600-2.0. The equilibrium adsorption increased from 220.66 to 766.53 mg/g when MB initial concentration is increased from 100 to 500 mg/L [Fig. 4.22(a)]. As depicted in Fig. 4.22(b), the % removal of MB decreased from 99.29 to 68.98% as the initial concentration is increased from 100 mg/L to 500 mg/L.

It could be observed that the highest adsorption capacity for MB was on the ACZC-600-2.0 activated carbon with the value of 968.74 mg/g due to high surface area and mesopore volume than ACPA-700-1.5. Table 4.6 presents the comparison of maximum adsorption capacity of MB dye on various adsorbents. The activated carbon ACZC-600-2.0 has very large adsorption capacity (968.74 mg/g) than other available literature. ACPA-700-1.5 has better adsorption capacity (766.53 mg/g) than other except coconut shell activated carbon (916 mg/g) (Cazetta et al., 2011).

Table 4.6: Comparison of MB adsorption on various adsorbents

| Adsorbents | S_{BET} (m²/g) | Initial conc. of MB (mg/L) | Q_m (mg/g) | Reference |
|--------------------------------------|--|---------------------------------------|---------------------------------|---------------------------|
| ACZC-600-2.0 | 2869 | 500 | 968.74 | In this study |
| ACPA-700-1.5 | 2636 | 500 | 766.53 | In this study |
| Coconut shell AC | 2825 | 1000 | 916 | (Cazetta et al., 2011) |
| NAC60 | 524 | 350 | 683.6 | (Gokce and Aktas, 2014) |
| Calgon (F-400) AC | 997 | 500 | 470 | (Rodríguez et al., 2009) |
| Grapefruit AC (GAC) | 1198 | 220 | 456.28 | (Nowicki et al., 2016) |
| vetP0.5 | 1170 | 300 | 423 | (Altenor et al., 2009) |
| Grape industrial processing waste AC | 1455 | 900 | 417 | (Saygılı et al., 2015) |
| Tomato processing solid waste AC | 1093 | 900 | 400 | (Saygılı and Güzel, 2015) |
| Vet-H ₂ O | 1185 | 300 | 375 | (Altenor et al., 2009) |
| Commercial AC | 1440 | 1000 | 370 | (Reffas et al., 2010) |
| Coffee grounds AC | 925 | 1000 | 367 | (Reffas et al., 2010) |
| Rattan sawdust AC | - | 500 | 294.12 | (Hameed et al., 2007a) |
| Buriti shells AC | 843 | 500 | 275 | (Pezoti et al., 2014) |
| Oil palm shell AC | 596.20 | 500 | 243.90 | (Tan et al., 2008a) |
| Cocoa shell AC | 85 | 250 | 213 | (Ahmad et al., 2012) |
| Cotton stalk | - | 1500 | 193.50 | (Deng et al., 2009) |
| Pine Cone AC | 939 | 100 | 60.97 | (Özhan et al., 2014) |

4.2.1.2. Adsorption Characteristics

4.2.1.2.1. Adsorption kinetics

The same methods of kinetic study that were used for the adsorption of phenol were adopted for the kinetic adsorption study for methylene blue. The adsorption kinetics of pseudo-first and pseudo-second-order for MB adsorption onto ACZC-600-2.0 and ACPA-700-1.5 are shown in Figs. 4.23 and 4.24. As observed, the adsorption kinetics for both the adsorbents follows the same trend.

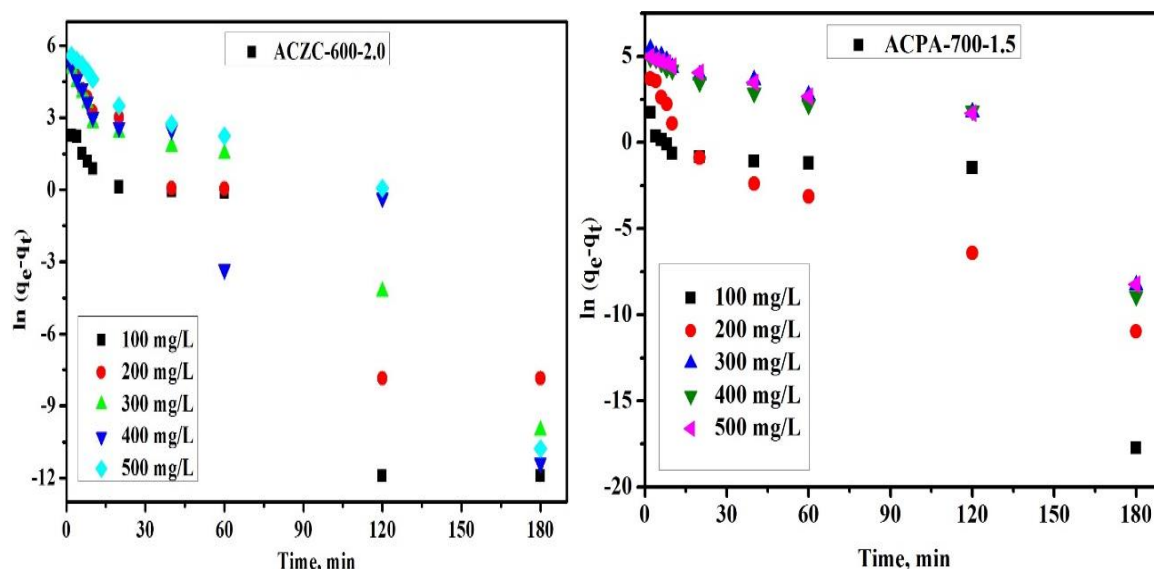


Fig. 4.23. Pseudo-first-order kinetics for the MB adsorption onto ACZC-600-2.0 (at 30 °C) and ACPA-700-1.5 (45 °C).

The derived kinetic parameters of pseudo-first and pseudo-second-order are listed in Table 4.7. As observed, the experimental kinetic data are better fitted by the pseudo-second-order model ($R^2 = 1$ for ACZC-600-2.0 and $R^2 = 0.999$ for ACPA-700-1.5). Moreover, all the calculated normalized standard deviation (Δq) in percentage (Table 4.7) resulted in relatively lower values for the pseudo-second-order kinetic model than the pseudo-first-order kinetic model for both the adsorbents studied. Also, the q_e calculated value that is derived from the pseudo-second-order equation is quite similar to those obtained experimentally, which indicates that the pseudo-second-order model is suitably explain observed kinetics. The linear plots of t/q_t vs. t shown in Fig. 4.24 again indicate good agreement of experimental data with the pseudo-second-order kinetic model for both adsorbents of MB adsorption.

Table 4.7: Constant parameters and correlation coefficients calculated for pseudo-first and pseudo-second-order kinetic models

| Parameters | ACZC-600-2.0 (30 °C) | | | | | ACPA-700-1.5 (45 °C) | | | | |
|-------------------------------------|--------------------------|--------|---------|---------|--------|--------------------------|---------|--------|--------|--------|
| | MB C ₀ (mg/L) | | | | | MB C ₀ (mg/L) | | | | |
| | 100 | 200 | 300 | 400 | 500 | 100 | 200 | 300 | 400 | 500 |
| q _{e, exp} (mg/g) | 249.88 | 483.84 | 695.55 | 836.07 | 968.74 | 220.66 | 430.36 | 581.15 | 705.77 | 766.53 |
| Pseudo first-order | | | | | | | | | | |
| q _{e, cal} (mg/g) | 10.45 | 85.63 | 101.65 | 93.82 | 348.53 | 4.40 | 11.30 | 283.03 | 192.85 | 240.68 |
| h ₀ (mg/g/min) | 8.74 | 7.93 | 7.74 | 7.77 | 7.80 | 7.92 | 15.48 | 18.77 | 25.11 | 30.67 |
| k ₁ (min ⁻¹) | 0.087 | 0.079 | 0.0774 | 0.0773 | 0.078 | 0.0792 | 0.0774 | 0.063 | 0.063 | 0.061 |
| R ² | 0.8915 | 0.923 | 0.9703 | 0.8222 | 0.888 | 0.691 | 0.932 | 0.832 | 0.807 | 0.829 |
| Δq (%) | 31.94 | 9.14 | 30.4 | 29.59 | 2.06 | 32.67 | 32.43 | 32.26 | 32.15 | 31.99 |
| Pseudo-second-order | | | | | | | | | | |
| q _{e, cal} (mg/g) | 250.00 | 487.8 | 699.30 | 840.34 | 970.9 | 220.75 | 431.00 | 584.8 | 709.2 | 769.2 |
| k ₂ [g/(mg min)] | 0.031 | 0.002 | 0.0029 | 0.0026 | 0.0009 | 0.104 | 0.0143 | 0.0008 | 0.0014 | 0.0011 |
| h ₀ (mg/g/min) | 1937.50 | 518.73 | 1447.50 | 1864.30 | 886.03 | 5067.97 | 2656.38 | 296.84 | 729.32 | 627.22 |
| R ² | 1 | 1 | 1 | 1 | 1 | 1 | 1 | 0.999 | 0.999 | 0.999 |
| Δq (%) | 0.0025 | 0.037 | 0.02 | 0.017 | 0.0072 | 0.0136 | 0.0496 | 0.209 | 0.162 | 0.117 |

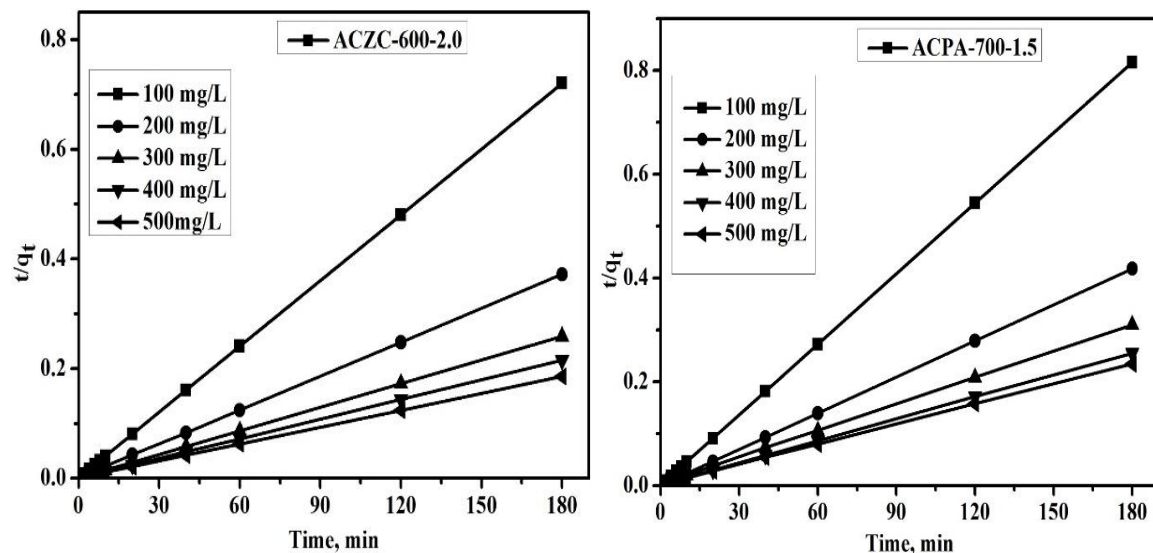


Fig. 4.24. Pseudo-second-order kinetic plots for the MB adsorption onto ACZC-600-2.0 (at 30 °C) and ACPA-700-1.5 (at 45 °C).

4.2.1.2.2. Intraparticle diffusion model

The intraparticle diffusion rate constants (k_i) for MB adsorption were calculated and are tabulated in Table 4.8. The plot of q against $t^{0.5}$ usually shows more than one linear portion. As seen from Fig. 4.25, the plots are not linear over the whole time range, that confirm more than one process affect the MB adsorption onto both adsorbents ACZC-600-2.0 and ACPA-700-1.5 (Hameed and Rahman, 2008; Senthilkumaar et al., 2005). If the value of c is zero, then the rate of adsorption is controlled by intraparticle diffusion for the entire adsorption period, but in the present study, the value of c is not zero (Table 4.8).

Table 4.8: Intraparticle diffusion constants for MB adsorption

| Parameters | ACZC-600-2.0 (at 30 °C) | | | | | ACPA-700-1.5 (at 45 °C) | | | | |
|-----------------------------------|-------------------------|--------|--------|--------|--------|-------------------------|--------|-------|--------|--------|
| | MB C_0 (mg/L) | | | | | MB C_0 (mg/L) | | | | |
| | 100 | 200 | 300 | 400 | 500 | 100 | 200 | 300 | 400 | 500 |
| k_i (mg/g min ^{-1/2}) | 0.64 | 10.91 | 8.34 | 9.34 | 19.84 | 0.221 | 2.41 | 15.67 | 10.78 | 11.91 |
| R^2 | 0.490 | 0.392 | 0.372 | 0.385 | 0.620 | 0.210 | 0.334 | 0.674 | 0.699 | 0.828 |
| c | 243.19 | 375.72 | 612.13 | 742.50 | 763.88 | 218.36 | 406.89 | 412.0 | 589.53 | 633.72 |

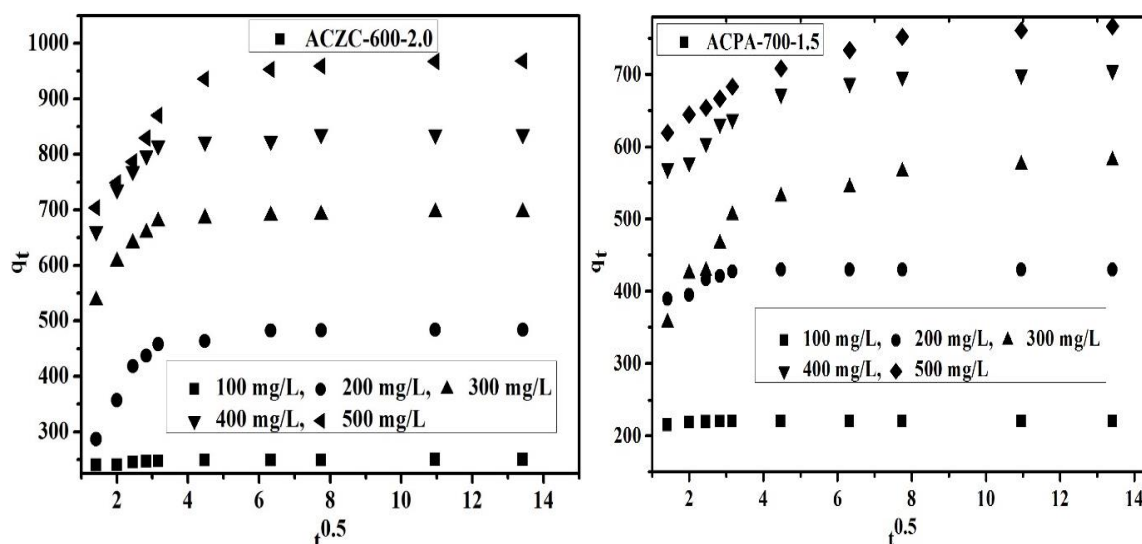


Fig. 4.25. Intraparticle diffusion plots for the MB adsorption onto ACZC-600-2.0 (at 30 °C) and ACPA-700-1.5 (at 45 °C).

The values of intercept (Table 4.8) give an idea about the boundary layer thickness, i.e. larger the intercept, greater is the boundary layer effect (Kannan and Sundaram, 2001). For the present study data, three stage diffusion process can be described. First, of them, the adsorbate transportation to the external adsorbent surface occurs forming the diffusion film. Then, the adsorbate transportation to the internal adsorbent surface takes place, and finally,

the sorption of solute particles onto active sites present on the solid surface (Pezoti et al., 2014; Ugurlu et al., 2005).

4.2.1.2.3. Adsorption isotherms

As mentioned earlier, at equilibrium state, the adsorption isotherm is very useful to describe how the adsorbed molecules distribute between the liquid phase and the solid phase. The most common Freundlich, Langmuir, and Temkin isotherm models were used to study the adsorption isotherm in the present study. Fig. 4.26 shows the non-linear curve (C_e/q_e vs. C_e) fits of the adsorption isotherms data of MB onto ACZC-600-2.0 and ACPA-700-1.5 by the three models mentioned above. The curves rise steeply at low concentration of MB in Fig. 4.26. The results from the fitting done for modeling of MB adsorption of both adsorbents ACZC-600-2.0 and ACPA-700-1.5 are listed in Table 4.9.

For Langmuir isotherm (Fig. 4.27) show a linear relationship of C_e/q_e vs. C_e using experimental data obtained for MB of both these activated carbons. The intercept (q_m) and the slope (k_L) are tabulated in Table 4.9.

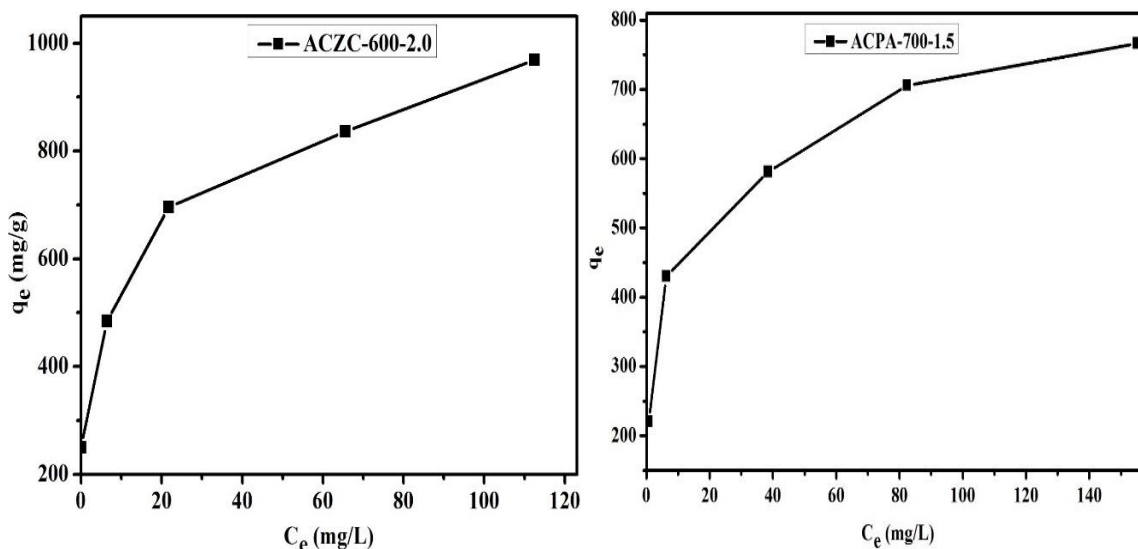


Fig. 4.26. Adsorption isotherms of MB onto ACZC-600-2.0 (at 30 °C) and ACPA-700-1.5 (at 45 °C).

The separation factor (R_L) is the dimensionless quantity, and it is an essential characteristic of the Langmuir isotherm (Hall et al., 1966). The value of R_L indicates the type of the isotherm to be either unfavourable ($R_L > 1$), linear ($R_L = 1$), favourable ($0 < R_L < 1$) or irreversible ($R_L = 0$). The values of R_L are found to be 0.0116 and 0.0132 for both ACAC-600-2.0 and ACPA-700-1.5, respectively, and this again confirms that the Langmuir isotherm is favorable for MB adsorption onto the produced ACs under the conditions used

in the present study. A high value of k_L and a low value of R_L indicate a high and favorable adsorption process (Ahmad et al., 2012).

Table 4.9: Isotherms constants for adsorption of MB

| ACs | Langmuir | | | | Freundlich | | | Temkin | | |
|--------------|-----------------|-----------------|-------|---------|---------------------------------------|-------|-------|--------|----------|-------|
| | q_m (mg/g) | k_L (L/mg) | R^2 | (R_L) | k_F [mg/g(L/mg) ^{1/n}] | 1/n | R^2 | b | A (L/g) | R^2 |
| ACZC-600-2.0 | 980.39 | 0.171 | 0.986 | 0.0116 | 402.02 | 0.173 | 0.971 | 28.85 | 188.67 | 0.866 |
| ACPA-700-1.5 | 787.40 | 0.149 | 0.993 | 0.0132 | 254.42 | 0.228 | 0.977 | 25.92 | 14185.85 | 0.989 |

The Freundlich isotherm equation is based on sorption onto a heterogeneous surface. The n is defined as heterogeneity factor and indicates when the adsorption process is linear ($n = 1$), physical ($n > 1$) or chemical ($n < 1$) (Pezoti et al., 2014). A linear plot of $\ln q_e$ vs. $\ln C_e$ confirms the validity of the Freundlich model and is shown in Fig. 4.28. The ratio $1/n$ allows the adsorption intensity or the surface heterogeneity, i.e., tends to zero be the ratio, more heterogeneous is the surface of the analyzed material (Auta and Hameed, 2011). The determined values of $1/n$ are 0.17 for ACZC-600-2.0 and 0.23 for ACPA-700-1.5, which is less than one that indicates a heterogeneous structure of favourable adsorption of MB on these carbons. The adsorption isotherm (Freundlich) of MB on the ACZC-600-2.0 and ACPA-700-1.5 is similar to that of activated carbons produced from Cocoa (*Theobroma cacao*) shell and fruit stones and nutshells (Ahmad et al., 2012; Aygün et al., 2003).

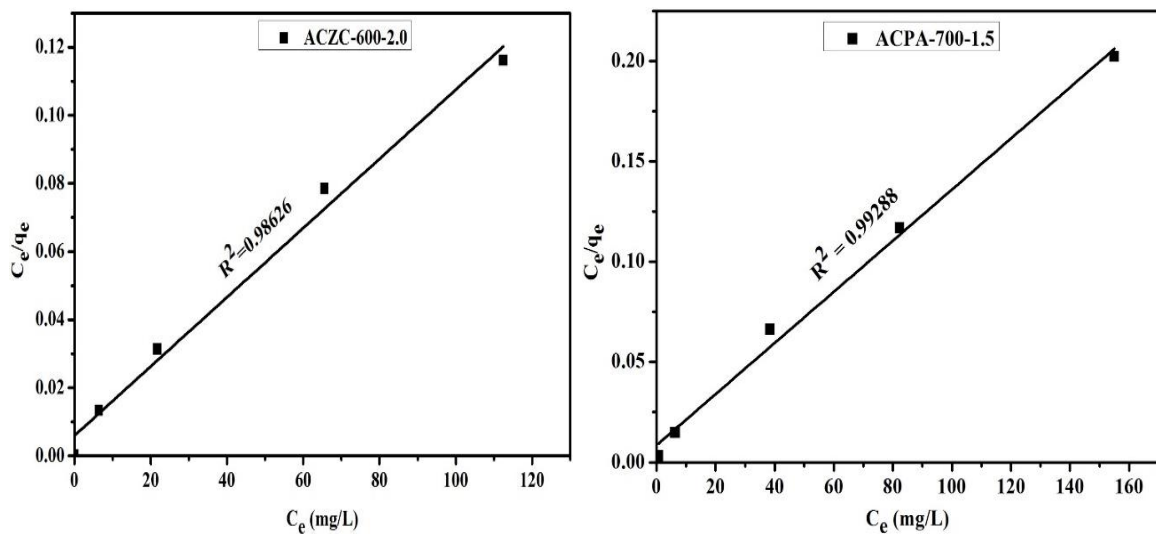


Fig. 4.27. Langmuir isotherms for the adsorption of MB onto ACZC-600-2.0 (at 30 °C) and ACPA-700-1.5 (at 45 °C).

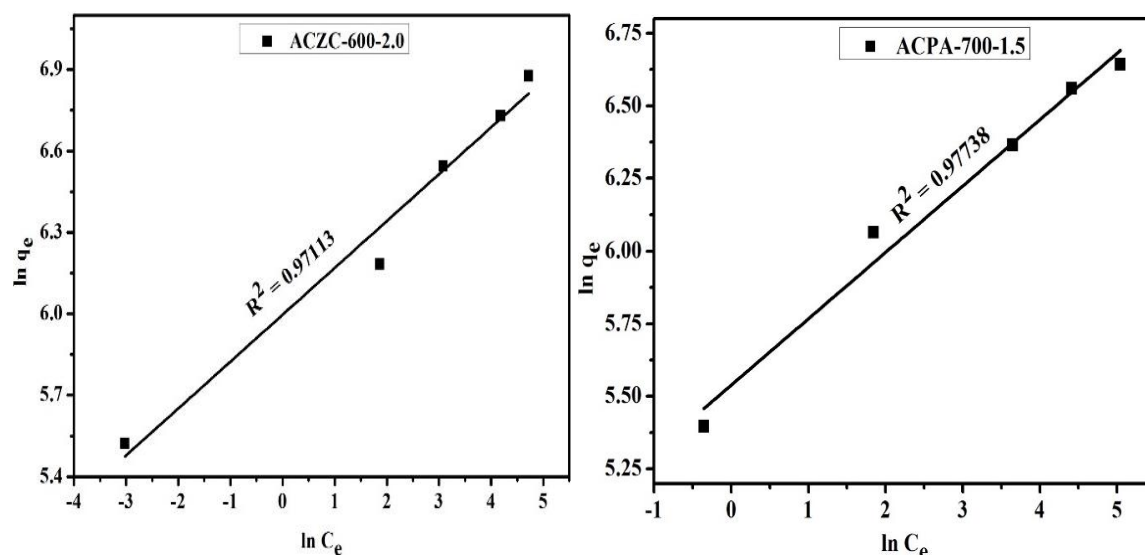


Fig. 4.28. Freundlich isotherms of the adsorption of MB onto ACZC-600-2.0 (at 30 °C) and ACPA-700-1.5 (at 45 °C).

Temkin and Pyzhev have suggested that the heat of adsorption should decrease linearly with the surface coverage because of the existence of adsorbate-adsorbate interactions, and adsorption is characterized by a uniform distribution of the binding energies, up to maximum binding energy (Temkin and Pyzhev, 1940). Temkin isotherms of ACZC-600-2.0 and ACPA-700-1.5 adsorbents are shown in Fig. 4.29. The constant A (Temkin isotherm equilibrium-binding constant) and b (Temkin isotherm constant) values were calculated from the intercept and slope of the plot and are listed in Table 4.9. The correlation coefficient (R^2) 0.866 for ACZC-600-2.0 and 0.989 for ACPA-700-1.5) are also listed in Table 4.9 and lower than the Langmuir and Freundlich value, indicating agreement with the experimental data to a lesser extent than the other two models.

The R^2 values estimate the goodness of the fit of the studied models. Table 4.9 shows that the Langmuir model ($R^2 = 0.986$) is the most suitable model for fitting adsorption isotherms of MB on the ACZC-600-2.0 than the Freundlich model ($R^2 = 0.971$). For ACPA-700-1.5 adsorbent, R^2 (0.993) value of Langmuir model is larger than R^2 (0.977) value of Freundlich model. So, the Langmuir model is a best-fitted model for the MB adsorption isotherm model. Thus, from Table 4.9, the comparison of tested models for the description of equilibrium adsorption isotherms on the ACZC-600-2.0 and ACPA-700-1.5 are as follows: Langmuir > Freundlich > Temkin and Langmuir > Temkin > Freundlich for MB adsorption, respectively.

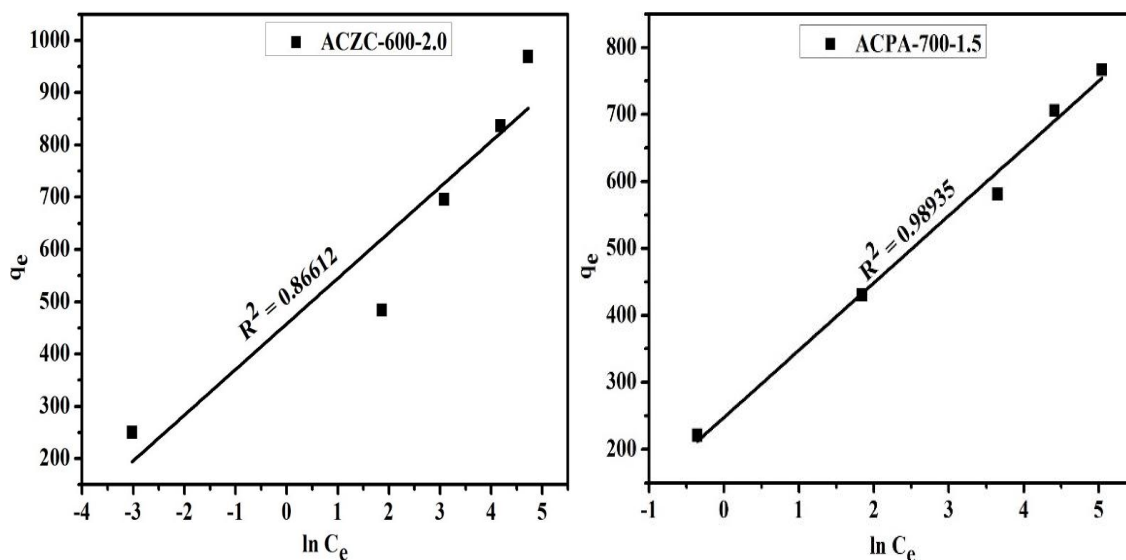


Fig. 4.29. Temkin isotherms for the adsorption of MB onto ACZC-600-2.0 (at 30 °C) and ACPA-700-1.5 (at 45 °C).

4.2.1.2.4. Adsorption mechanism

Three consecutive mass transport steps are associated with the adsorption of a solute from solution by the porous adsorbent. First, the adsorbate migrates through the solution, i.e., film diffusion; in the second step, the solute movement from particle surface into the interior site by pore diffusion and finally the adsorbate is adsorbed on the active sites of the interior of the adsorbent particle (Gokce and Aktas, 2014).

Two simultaneous adsorption routes have been proposed for the active site adsorption of MB molecules. One involves the electrostatic interaction of MB cations with negatively charged carbon surface functional groups and other is the dispersive interaction of MB molecules with a surface layer of AC (Makrigianni et al., 2015; Pereira et al., 2003). Dispersive interaction is related with the π - π electron coupling on the surface of the activated carbon. The dispersive interaction readily occurs between the π electrons exist within the molecular structure of MB and delocalized π electrons on the basal planes of the activated carbon. The pore size distribution of AC is another parameter that affects the MB adsorption onto AC. The molecular dimension of the MB is larger than the micropores that means a molecular sieving effect reduces the adsorption capacity of the AC (Gokce and Aktas, 2014; Pereira et al., 2003).

4.2.1.2.5. Adsorption thermodynamics

The temperature effect on the MB adsorption process was investigated with the thermodynamic parameters like a change in Gibbs free energy (ΔG°), change in enthalpy (ΔH°) and change in entropy (ΔS°). Thermodynamic parameters provide an insight of MB

adsorption mechanism and adsorption behaviour of an isolated system. The values of ΔH° and ΔS° are determined from the slope and intercept of the van't Hoff plot of $\ln K_C$ vs. $1/T$ (Fig. 4.30). The assessed thermodynamic parameter values are tabulated in Table 4.10.

Table 4.10: Thermodynamic parameters of MB adsorption onto ACZC-600-2.0 and ACPA-700-1.5

| Adsorbents | T(K) | ΔG° (kJ/mol) | ΔH° (kJ/mol) | ΔS° (J/molK) |
|--------------|------|---------------------------|---------------------------|---------------------------|
| ACZC-600-2.0 | 298 | -7.80 | -2.93 | 16.46 |
| | 303 | -8.002 | | |
| | 308 | -7.98 | | |
| | 313 | -8.06 | | |
| | 318 | -8.18 | | |
| ACPA-700-1.5 | 298 | -8.12 | 5.64 | 46.19 |
| | 303 | -8.34 | | |
| | 308 | -8.60 | | |
| | 313 | -8.80 | | |
| | 318 | -8.89 | | |

The value of ΔG° in between 0 and -20 kJ/mol indicates physical adsorption i.e., electrostatic interaction between adsorption sites and the adsorbing ion while a more negative ΔG° value ranging from -80 to -400 kJ/mol indicates that the adsorption involves charge sharing or transferring from the adsorbent surface to the adsorbing ion to form a coordinate bond (chemisorption) (AlOthman et al., 2014; Singh, 2000). From Table 4.10, the negative Gibbs free energy (ΔG°) of the experimental values of both adsorbents, ACZC-600-2.0 and ACPA-700-1.5 indicate a typical physical process. The negative value of the enthalpy change ($\Delta H^\circ = -2.93$ kJ/mol) means that the MB adsorption process onto ACZC-600-2.0 is exothermic in nature. The positive value of the enthalpy change ($\Delta H^\circ = 5.64$ kJ/mol) shows that the MB adsorption process onto ACPA-700-1.5 is endothermic in nature. The endothermic nature of adsorption of methylene blue was earlier observed by Ghosh and Bhattacharyya (Ghosh and Bhattacharyya, 2002) on six kaolinite-based adsorbents.

Endothermic uptake of the neutral dye, Congo Red on activated carbon made from coir pith (Namasivayam and Kavitha, 2002). Positive ΔH° and ΔS° , and negative ΔG° values for adsorption of methylene blue and a few other basic dyes on plant leaves are in agreement with the present work (Singh and Srivastava, 1999). Moreover, an interaction between the

solute and the solvent particle involves a complex phenomenon on the solid surface of MB adsorption. Hence, during the adsorption process, the adsorption and desorption process occurs simultaneously. The positive entropy changes of both adsorbents ($\Delta S^\circ = 16.46$ J/molK for ACZC-600-2.0 and 46.19 J/molK for ACPA-700-1.5) indicate an increase in the degree of freedom or disorder of the adsorbed species.

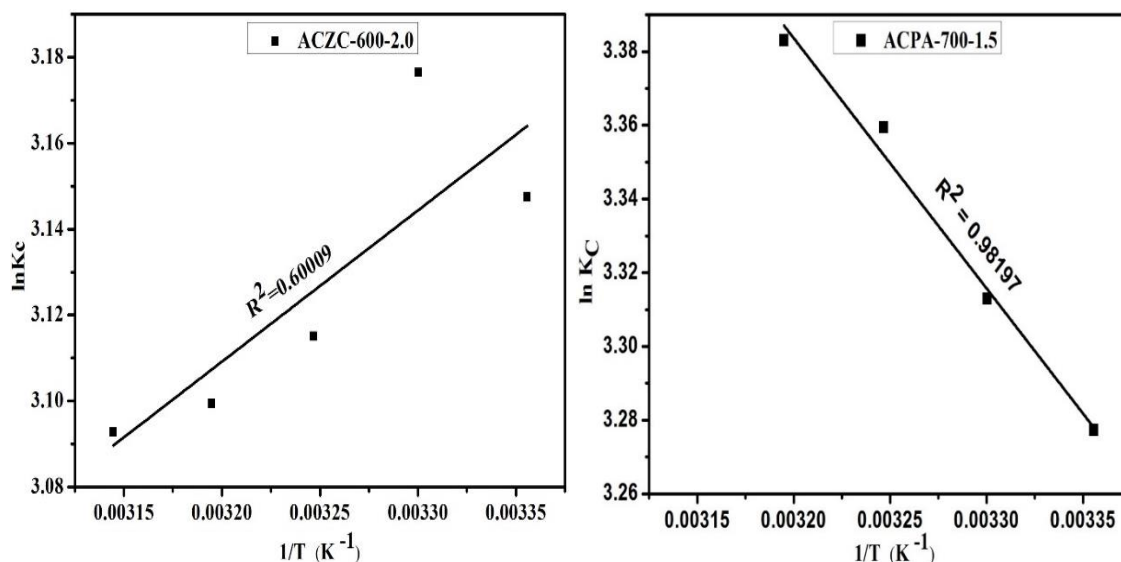


Fig. 4.30. Plots of $\ln K_C$ versus $1/T$ for 100 mg/L initial MB concentration onto ACZC-600-2.0 and ACPA-700-1.5.

4.2.2. Regeneration and reuse of activated carbons

The same method of desorption of adsorbate and regeneration of activated carbons as done for phenol were practiced for desorption of MB and the regeneration of MB adsorbed activated carbons. The regenerated activated carbons of both types were further used for adsorption of MB. For ACZC-600-2.0 and ACPA-700-1.5 the initial wt. was taken as 0.04 and 0.045 mg for 100 mL of MB solution of 100 mg/L concentration. Experiments were carried out up to fourth regeneration cycle. The percentage removal of MB using regenerated ACs is represented in Fig. 4.31. It is observed that in the first reuse, the % removal of MB reduced by 7.6% and 8.2% for ACZC-600-2.0 and ACPA-700-1.5, respectively and same reduced by 19.35% and 20.4% after the 4th regeneration. Nearly the same reduction in adsorption capacity for MB and Congo red is reported by the researchers (Fan et al., 2012; Zhu et al., 2011).

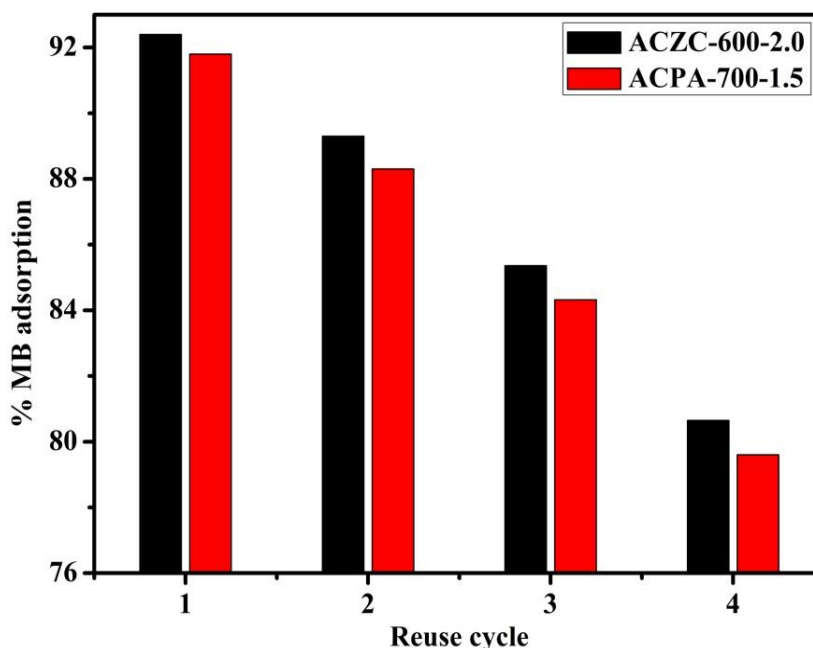


Fig. 4.31. Readsorption of MB after desorption.

4.2.3. Column adsorption study

The operating parameters such as volumetric flow rate (Q), and length of the bed (L) have a significant influence on breakthrough and saturation times, and on the dynamics of the column. In the present study, the effect of these parameters on the breakthrough curves of MB adsorption onto ACZC-600-2.0 and ACPA-700-1.5 adsorbents was investigated. The area under the BT curve which is obtained by integrating the plot can be used to estimate the total adsorbed quantity of adsorbate, q_{tot} (mg) in the column for a given inlet concentration and flow rate (Aksu and Gönen, 2004; Salman et al., 2011).

4.2.3.1. Effect of bed height

Fig. 4.32 shows the breakthrough (BT) curves obtained for MB adsorption onto prepared carbons (ACZC-600-2.0 and ACPZ-700-1.5) at bed heights of 2, 3 and 4 cm, and a constant flow rate of 5 mL/min and initial MB concentration of 100 mg/L. The figure shows that both the BT and exhaustion time increases as bed height increases.

The increase in the breakthrough time could be ascribed to the longer distance it takes the mass transfer zone to move from the entrance of the bed to the exit when the bed height is increased. Furthermore, higher uptake of MB by prepared carbons (ACZC-600-2.0 and ACPZ-700-1.5) is observed at higher bed height, which could be attributed to rising in the surface area of the adsorbents, that provided more binding sites for adsorbate to adsorb (Padmesh et al., 2006; Tan et al., 2008a). From Table 4.11, it can be noticed that the breakthrough time, exhaustion time, uptake capacity and percent removal increases as the

bed height is increased. The same is reported in other research works (Ahmad and Hameed, 2010; Tan et al., 2008a; Vijayaraghavan et al., 2004)

Table 4.11: Column parameters obtained at different bed heights and flow rates

| Adsorbents | Bed height (cm) | Flow rate (mL/min) | Breakthrough time (min) | Exhaustion time (min) | Bed capacity, q_{eq} (mg/g) | % Removal |
|--------------|-----------------|--------------------|-------------------------|-----------------------|-------------------------------|-----------|
| ACZC-600-2.0 | 2 | 5 | 30 | 980 | 71.71 | 44.82 |
| | 3 | 5 | 110 | 1520 | 88.36 | 55.23 |
| | 4 | 5 | 220 | 2100 | 106.46 | 57.54 |
| | 4 | 10 | 130 | 1440 | 133.12 | 51.20 |
| | 4 | 15 | 25 | 880 | 113.21 | 39.72 |
| ACPA-700-1.5 | 2 | 5 | 30 | 980 | 75.47 | 41.93 |
| | 3 | 5 | 120 | 1300 | 76.71 | 50.03 |
| | 4 | 5 | 210 | 1800 | 84.63 | 52.93 |
| | 4 | 10 | 130 | 1270 | 108.41 | 51.62 |
| | 4 | 15 | 45 | 800 | 100.09 | 44.48 |

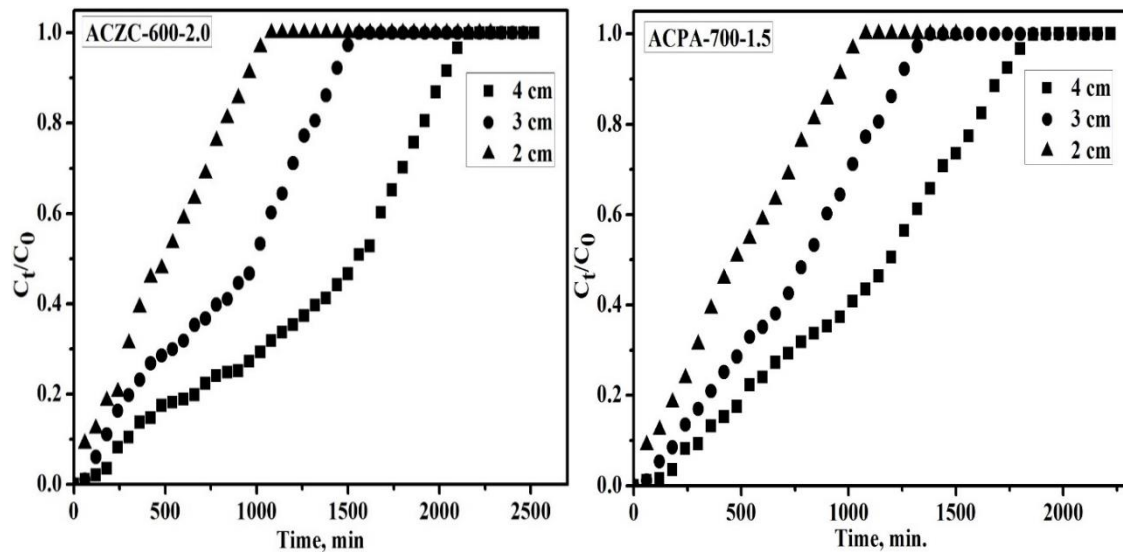


Fig. 4.32. Breakthrough curves for MB adsorption onto ACZC-600-2.0 and ACPA-700-1.5 at different bed heights ($C_0 = 100$ mg/L, flow rate = 5 mL/min, and pH = 11).

4.2.3.2. Effect of solution flows rate

The effect of flow rate on MB removal by prepared activated carbons (ACZC-600-2.0 and ACPZ-700-1.5) was studied by varying the flow rate as 5, 10 and 15 mL/min, while the bed height and initial MB concentration were held constant at 4 cm and 100 mg/L, respectively.

The breakthrough curves of both activated carbons were obtained by plotting effluent methylene blue concentration versus time at different flow rates are represented in Fig. 4.33.

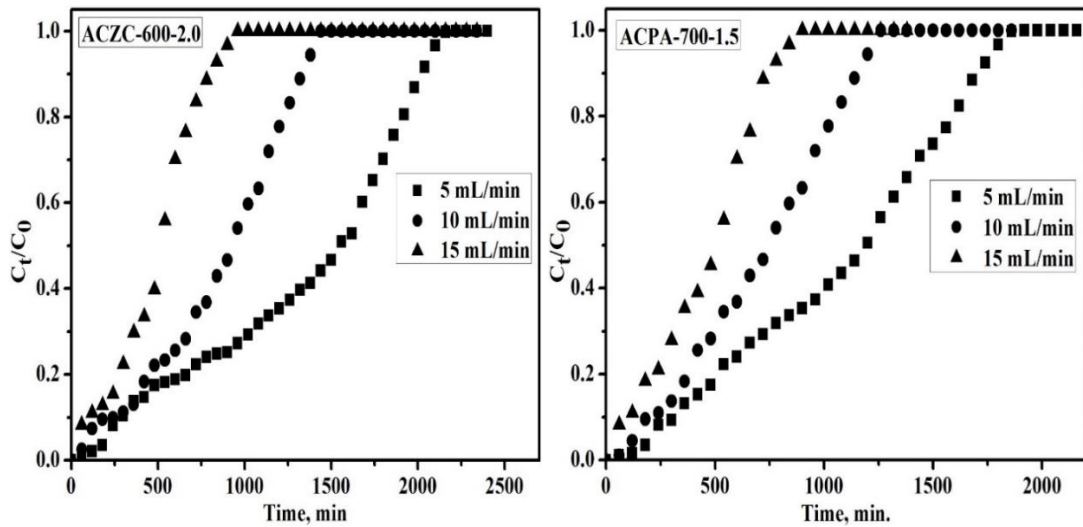


Fig. 4.33. Breakthrough curves for MB adsorption onto ACZC-600-2.0 and ACPA-700-1.5 at different flow rates ($C_0 = 100$ mg/L, bed height = 4 cm, and pH = 11).

As the flow rate increased, the breakthrough curves became steeper, and the slope of the breakthrough curve increases. The possible reason for this may be as the flow rate increases, the residence time of the MB in the column decreases, which leads to the early exit of the MB solution from the column (Padmesh et al., 2006; Tan et al., 2008a). From Table 4.12, it can be noticed that the breakthrough time, exhaustion time, and % removal decreased as the flow rate is increased (Ahmad and Hameed, 2010; Vijayaraghavan et al., 2004). This is attributed to the insufficient residence time of the adsorbates in the column to allow for diffusion of the solute into the pores of the adsorbent (Girish and Murty, 2015; Mohammed et al., 2016; Tan et al., 2008a). It can be concluded that best results are obtained at the lowest flow rate of 5 mL/min.

4.3. Adsorption of Hexavalent Chromium [Cr(VI)]

Chromium is a priority metal pollutant released into the water bodies from many industrial processes. Cr(VI) has significantly higher levels of toxicity than the other valency state. Therefore, the removal of Cr(VI) from water and wastewater is important to protect the environment. In this sub chapter, adsorption studies on Cr(VI) are discussed. Like adsorption of phenol and MB, for Cr(VI), experiments were carried out in both batch and continuous mode using adsorbents ACZC-600-2.0 and ACPA-700-1.5. The experimental results are demonstrated in the form of graphs and significant values are listed in tables.

4.3.1 Batch adsorption studies

4.3.1.1. Effect of process parameters

The effect of agitation speed, pH, temperature, adsorbent dose, contact time, and initial concentration onto Cr(VI) adsorption were investigated.

4.3.1.1.1. Agitation speed

Fig. 4.34 shows the effect of agitation speed on % removal of Cr(VI) adsorption onto ACZC-600-2.0 and ACPA-700-1.5.

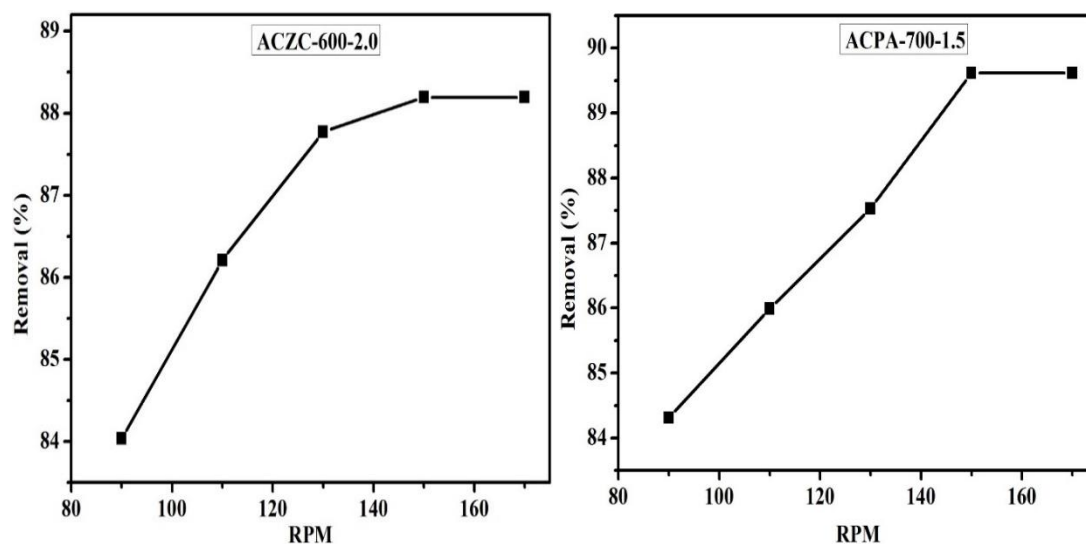
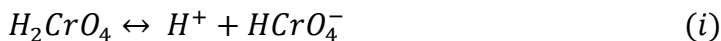


Fig. 4.34. Effect of agitation speed on % removal of Cr(VI) ($C_0 = 10$ mg/L, $m_s = 0.03$ g/100mL, temperature = 30 °C, and contact time = 3 hr).

The figure demonstrates that the removal efficiency of Cr(VI) increases with increase in agitation speed and maximum removal are achieved at 150 rpm, remained the same for higher speeds. Thus, the agitation speed of 150 rpm in all further experiments for Cr(VI) adsorption.

4.3.1.1.2. pH

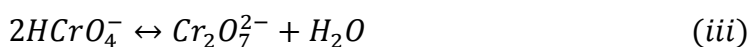
The following are the equilibrium reactions and corresponding pKa values reported in few literature for different Cr(VI) species.



pKa = 0.8 (Sengupta and Clifford, 1986), 0.75 (Kotaś and Stasicka, 2000), -0.26 (Cox, 2000)



pKa = 6.5 (Sengupta and Clifford, 1986), 6.45 (Kotaś and Stasicka, 2000), 5.9 (Ajouyed et al., 2010; Cox, 2000)



pKa = -1.52 (Sengupta and Clifford, 1986), -2.2 (Ajouyed et al., 2010; Cox, 2000; Kotaś and Stasicka, 2000)

The reaction (iii) does not contain any H^+ terms, i.e., in a certain pH range (2-5) and this reaction is independent of pH and depends only on total Cr(VI) concentration. This may be regarded as a dimerization reaction for $HCrO_4^-$ at acidic pH. In the pH ranging from 2.0 to 6.0, $HCrO_4^-$ ions mainly exist in equilibrium and the predominant form of $HCrO_4^-$ shifts to chromate ion (CrO_4^{2-}) as pH increases. Above pH 7 only CrO_4^{2-} ions exist in solution throughout the concentration range and in the pH between 1.0 and 6.0, $HCrO_4^-$ is the predominant form up to the Cr(VI) concentration. $HCrO_4^-$ ion only needs one active site whereas chromate ion (CrO_4^{2-}) needs two active sites due to its two minus charges (Yang et al., 2014). The behaviour for better adsorption at low pH by activated carbon may be attributed to the large number of H^+ ions present which in turn neutralize the negatively charged hydroxyl group ($-OH$) on the adsorbent surface, thereby reducing hindrance to the diffusion of chromate ions (Demiral et al., 2008). At higher pH values, the reduction in adsorption may be possible due to the abundance of OH^- ions causing increased hindrance to diffusion of dichromate ions.

The adsorption of Cr(VI) on ACZC-600-2.0 and ACPA-700-1.5 is strongly dependent on the initial pH of the aqueous solution. Fig. 4.35 exhibits the influence of pH (2–7) on the adsorption process. The Cr(VI) adsorption is found to decrease with increase in pH from 2.0 to 7.0. The maximum adsorption is observed at pH of 2.0 for both the adsorbents. Similar observations have also been reported in other research works (El-Sikaily et al., 2007; Hamadi et al., 2001; Karthikeyan et al., 2005; Sharma and Forster, 1994; Yang et al., 2015).

The effect of pH on Cr(VI) adsorption can be explained in terms of PZC. The PZC values of ACZC-600-2.0, and ACPA-700-1.5 are 2.1 and 2.7, respectively. At $\text{pH} < \text{PZC}$, the carbon surface takes up more H^+ , increasing Cr(VI) ions bind on the adsorbent surface. At $\text{pH} > \text{PZC}$, the adsorbent surface is negatively charged, the increasing electrostatic repulsion between negative adsorbate species and adsorbent particles would lead to decrease adsorption capacity of Cr(VI) ions.

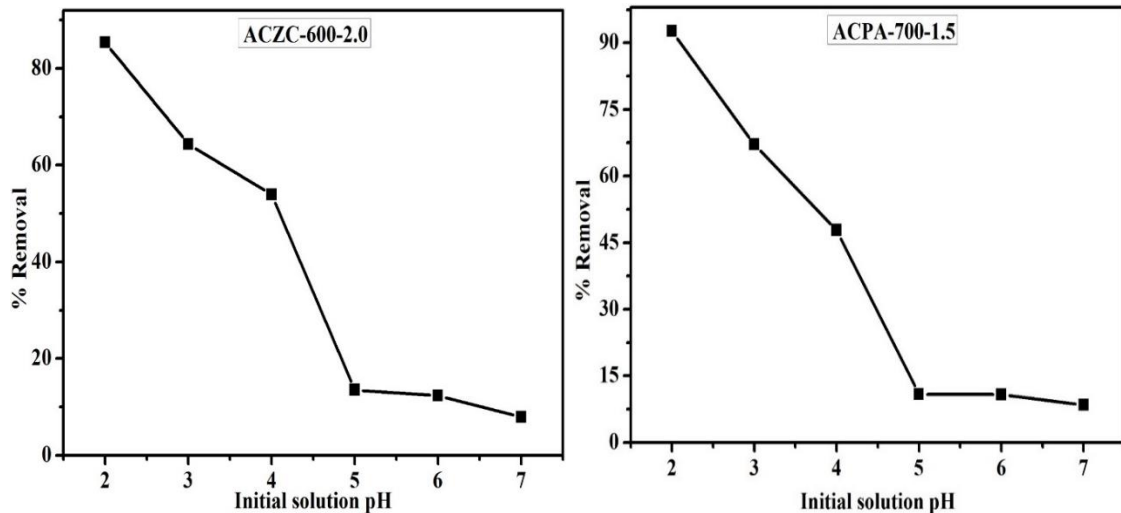


Fig. 4.35. Effect of pH on % removal of Cr(VI) ($C_0 = 10 \text{ mg/L}$, $m_s = 0.03 \text{ g/100mL}$, temperature = $30 \text{ }^\circ\text{C}$, and contact time = 3 hr).

4.3.1.1.3. Temperature

From Fig. 4.36, the percentage removal of Cr(VI) on ACZC-600-2.0 from solution increases from 54.06 to 59.32% with a rise in temperature. For ACPA-700-1.5 adsorbent, the percentage removal of Cr(VI) from solution increases from 55.88 to 60.02% with a rise in temperature to $45 \text{ }^\circ\text{C}$ (Fig. 4.36). Similar results have been reported in literature for Cr(VI) adsorption (Demiral et al., 2008; Malkoc et al., 2006; Yang et al., 2015).

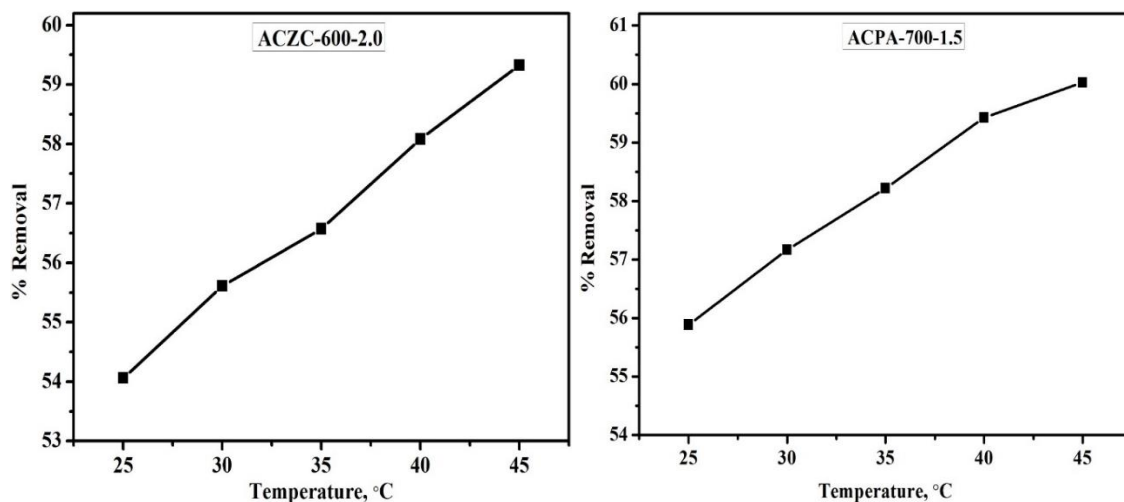


Fig. 4.36. Effect of temperatures on % removal of Cr(VI) ($C_0 = 10 \text{ mg/L}$, $m_s = 0.03 \text{ g/100mL}$, $\text{pH} = 2$, and contact time = 3 hr).

4.3.1.1.4. Adsorbent dosage

To study the effect of activated carbon dosage (g) on Cr(VI) adsorption, adsorbents dosages for both the adsorbents were varied from 0.01 to 0.07 g using 100 mL of solution at concentration of 10 mg/L of Cr(VI). The pH of 2 and the temperature 30 °C was fixed. Fig. 4.37 shows the effect of adsorbent dosage on the % removal of Cr(VI) by ACZC-600-2.0. It is found that the removal of Cr(VI) increases with the increase in adsorbent dose up to 0.04 g, then increases slowly with further increase in adsorbent dosage up to 0.05 g and after that remains unchanged.

Thus 0.05 g of ACZC-600-2.0 was considered as an optimal mass per 100 mL of solution at Cr(VI) concentration of 10 mg/L for the further experiments. At equilibrium time, the % removal of Cr(VI) increased from 84.46 to 99.66%. Fig. 4.37 shows the effect of ACPA-700-1.5 adsorbent dosage on the % removal of Cr(VI). The % removal of Cr(VI) increases with the increase in adsorbent dose up to 0.04 g significantly and after that remains unchanged. Thus 0.04 g of ACPA-700-1.5 was chosen as an optimal mass Cr(VI) for the further experiments. At equilibrium time, the % removal of Cr(VI) increased from 84.50 to 99.14% with the variation of adsorbent dose over the experimental range.

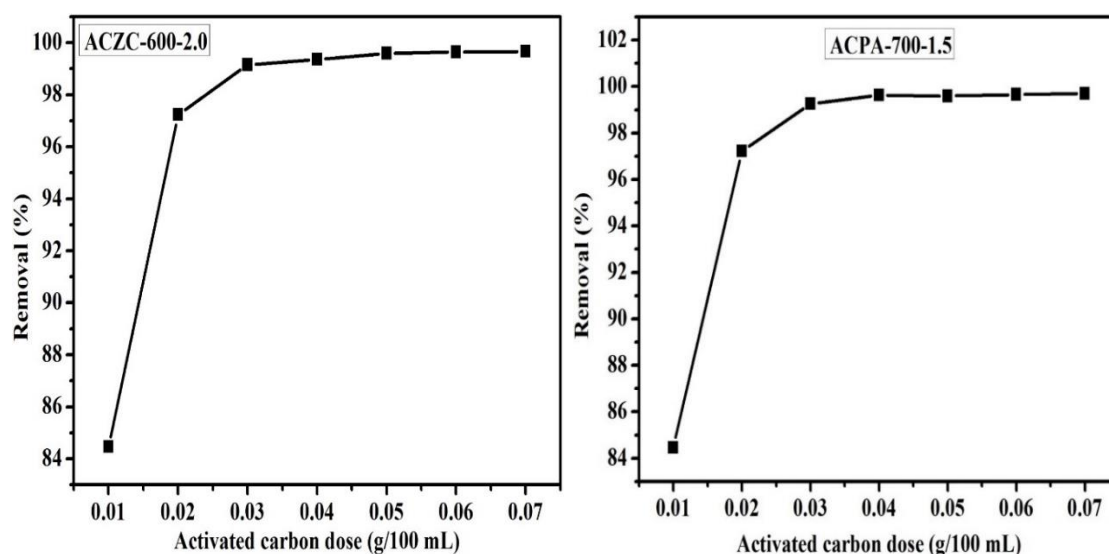


Fig. 4.37. Effect of adsorbent dosage on % removal of Cr(VI) ($C_0 = 10$ mg/L, pH = 2, temperature = 30 °C, and contact time = 3 hr).

4.3.1.1.5. Contact time and initial Cr(VI) concentrations

The effect of the initial concentration of the Cr(VI) on its adsorption onto ACZC-600-2.0 and ACPA-700-1.5 was studied within the range of 10 to 25 mg/L with a pH value fixed at 2 and the results were shown in Figs. 4.38 and 4.39. The adsorption of Cr(VI) onto both ACZC-600-2.0 and ACPA-700-1.5 increases with time and then attains equilibrium value

at a time of about 60 min. The removal of Cr(VI) is found to be dependent on the initial concentration as the amount adsorbed found to increase with initial concentration. Further, the adsorption is rapid in the early stages and then attains equilibrium in a moderately short time for both adsorbents (Figs. 4.38 and 4.39). A larger amount of Cr(VI) is removed by ACZC-600-2.0 and ACPA-700-1.5 adsorbents in the first 20 min of contact time. For ACZC-600-2.0, on changing the initial concentration from 10 to 25 mg/L, the amount adsorbed increases from 19.18 to 43.45 mg/g over a period of 180 min while % removal decreases from 99.08 to 86.89% (Fig. 4.38). For ACPA-700-1.5, the equilibrium adsorption increases from 24.92 to 56.31 mg/g when the initial Cr(VI) concentration is varied from 10 to 25 mg/L (Fig. 4.39) and % removal of Cr(VI) decreased from 99.67 to 90.09%. It is observed that for Cr(VI) adsorption, the adsorption capacity of ACPA-700-1.5 is higher than ACZC-600-2.0.

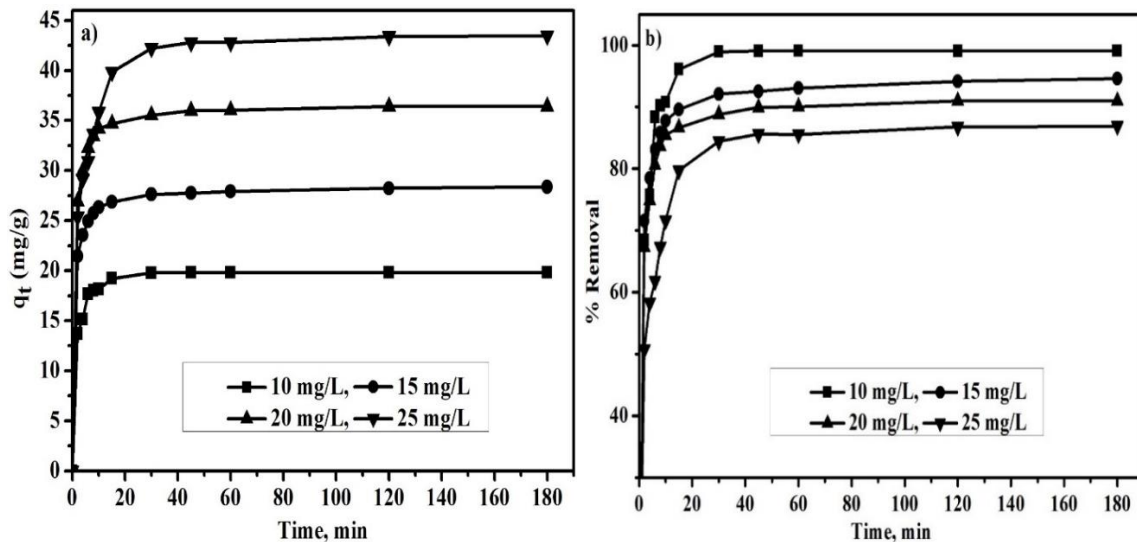


Fig. 4.38. Effects of contact time on the adsorption capacity of ACZC-600-2.0 at different initial concentrations ($m_s = 0.05$ g, pH = 2, temperature = 45 °C, and contact time = 3 hr).

To justify the viability of the prepared activated carbons as effective adsorbents for Cr(VI) removal, the adsorption capacity of ACZC-600-2.0 and ACPA-700-1.5 on Cr(VI) were compared to the efficiency of other low-cost adsorbents found in the literature with similar batch studies.

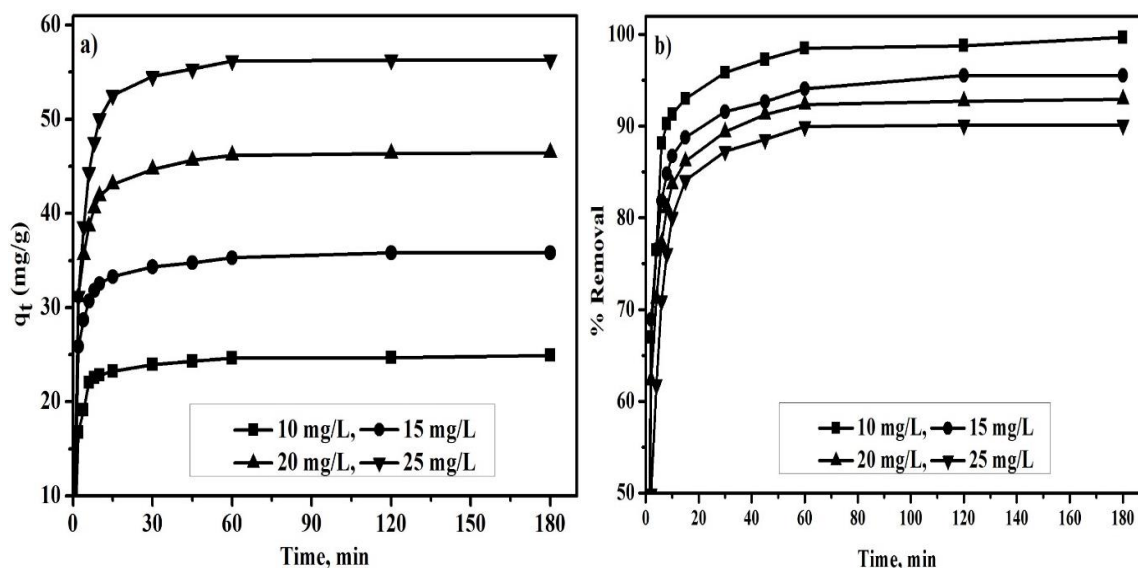


Fig. 4.39. Effects of contact time on the adsorption capacity of ACPA-700-1.5 at different initial concentrations ($m_s = 0.04$ g, pH = 2, temperature = 45 °C, and contact time = 3 hr).

Table 4.12 shows a summary of Cr(VI) removal capacity (mg/g), at optimum pH, and maximum concentration of Cr used (mg/L) for various adsorbents in the present study and previously studied. The adsorption capacity of Tyres activated carbon (58.5 mg/g) (Hamadi et al., 2001) is little larger than the ACPA-700-1.5 activated carbon (56.31 mg/g), this may be because of higher concentration of Cr(VI) used by them. In all other studies the adsorption capacity reported are less than the present results. Thus activated carbons prepared in the present study ACZC-600-2.0 and ACPA-700-1.5 are excellent ones for the adsorption of Cr(VI).

Table 4.12: Comparison of Cr(VI) adsorption on various adsorbents

| Adsorbents | Optimum pH | Initial conc. of adsorbates (mg/L) | Q_m (mg/g) | Reference |
|---|------------|------------------------------------|--------------|----------------------------|
| ACZC-600-2.0 | 2 | 25 | 43.45 | In this study |
| ACPA-700-1.5 | 2 | 25 | 56.31 | In this study |
| Tyres activated carbon | 2 | 60 | 58.50 | (Hamadi et al., 2001) |
| F400 (CAC) | 2 | 60 | 48.54 | (Hamadi et al., 2001) |
| <i>Hevea Brasilinesis</i> (Rubber wood) sawdust | | - | 44.05 | (Karthikeyan et al., 2005) |
| Leaf mould | 2 | 1000 | 43.10 | (Sharma and Forster, 1995) |
| Coconut shell carbon | 2 | - | 20.00 | (Alaerts et al., 1989) |

| | | | | |
|------------------------------------|---|-----|-------|-----------------------------|
| Hazelnut shell | - | - | 17.70 | (Cimino et al., 2000) |
| Beech sawdust | 1 | 200 | 16.10 | (Acar and Malkoc, 2004) |
| Sugarcane bagasse | 2 | 500 | 13.40 | (Sharma and Forster, 1994) |
| Coconut shell carbon | 4 | 25 | 10.88 | (Babel and Kurniawan, 2004) |
| Treated sawdust of Indian rosewood | 3 | 10 | 10.00 | (Garg et al., 2004a) |
| Coconut tree saw dust | 3 | 20 | 3.6 | (Selvi et al., 2001) |

4.3.1.2. Adsorption Characteristics

4.3.1.2.1. Adsorption kinetics

The adsorption kinetics of pseudo-first and pseudo-second-order for Cr(VI) onto ACZC-600-2.0 and ACPA-700-1.5 are shown in Figs. 4.40 and 4.41. The derived kinetic parameters of pseudo-first and pseudo-second-order are listed in Table 4.13. As observed, the experimental kinetic data are better fitted by the pseudo-second-order model ($R^2 = 0.999$ for both ACZC-600-2.0 and ACPA-700-1.5). The resulted Δq (%) values are relatively lower for the pseudo-second-order kinetic model than the pseudo-first order kinetic model for both the adsorbents (Table 4.13).

Table 4.13: Constant parameters and correlation coefficients calculated for pseudo-first and pseudo-second-order kinetic models

| Parameters | ACZC-600-2.0 (45 °C) | | | | ACPA-700-1.5 (45 °C) | | | |
|-------------------------------------|-------------------------------|-------|--------|--------|-------------------------------|--------|--------|--------|
| | Cr(VI), C ₀ (mg/L) | | | | Cr(VI), C ₀ (mg/L) | | | |
| | 10 | 15 | 20 | 25 | 10 | 15 | 20 | 25 |
| q _{e,exp} (mg/g) | 19.18 | 28.38 | 36.39 | 43.45 | 24.92 | 35.82 | 46.47 | 56.31 |
| Pseudo-first-order | | | | | | | | |
| q _{e,cal} (mg/g) | 1.01 | 4.98 | 7.18 | 11.46 | 4.056 | 10.044 | 7.14 | 12.51 |
| h ₀ (mg/g/min) | 0.431 | 0.705 | 1.39 | 1.18 | 0.362 | 0.981 | 0.67 | 1.402 |
| k ₁ (min ⁻¹) | 0.0431 | 0.047 | 0.0693 | 0.0472 | 0.0362 | 0.0654 | 0.0335 | 0.0561 |
| R ² | 0.570 | 0.898 | 0.978 | 0.967 | 0.904 | 0.978 | 0.915 | 0.960 |
| Δq (%) | 31.58 | 27.48 | 26.76 | 24.54 | 27.90 | 23.99 | 28.21 | 25.93 |
| Pseudo-second-order | | | | | | | | |
| q _{e,cal} (mg/g) | 19.93 | 28.48 | 36.58 | 43.99 | 25.019 | 36.05 | 46.81 | 56.88 |

| | | | | | | | | |
|--------------------|--------|--------|-------|--------|--------|--------|--------|--------|
| k_2 [g/(mg min)] | 0.0705 | 0.039 | 0.027 | 0.012 | 0.0370 | 0.0239 | 0.0179 | 0.0122 |
| h_0 (mg/g/min) | 28.00 | 31.63 | 36.13 | 23.22 | 23.16 | 31.06 | 39.22 | 39.47 |
| R^2 | 0.9999 | 0.9999 | 1 | 0.9999 | 0.9999 | 0.9999 | 0.9999 | 0.9999 |
| Δq (%) | 1.30 | 0.12 | 0.17 | 0.41 | 0.13 | 0.21 | 0.24 | 0.34 |

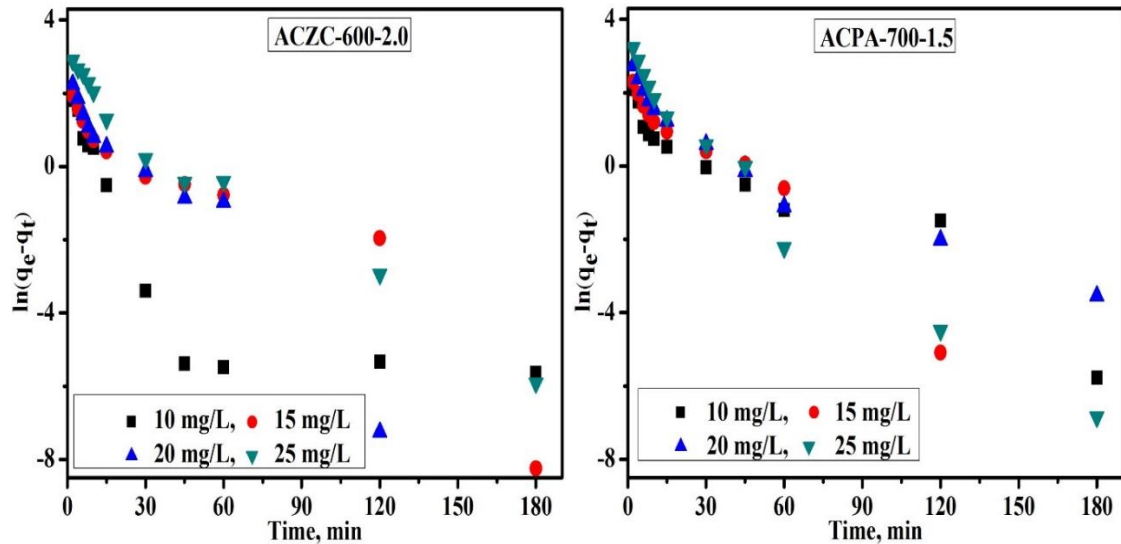


Fig. 4.40. Pseudo-first-order kinetics for Cr(VI) adsorption onto ACs at 45°C.

Also, the q_e estimated values that are derived from the second-order equation is quite similar to those obtained experimentally, which indicates that the second-order model is suitable for the observed kinetics of ACZC-600-2.0 and ACPA-700-1.5.

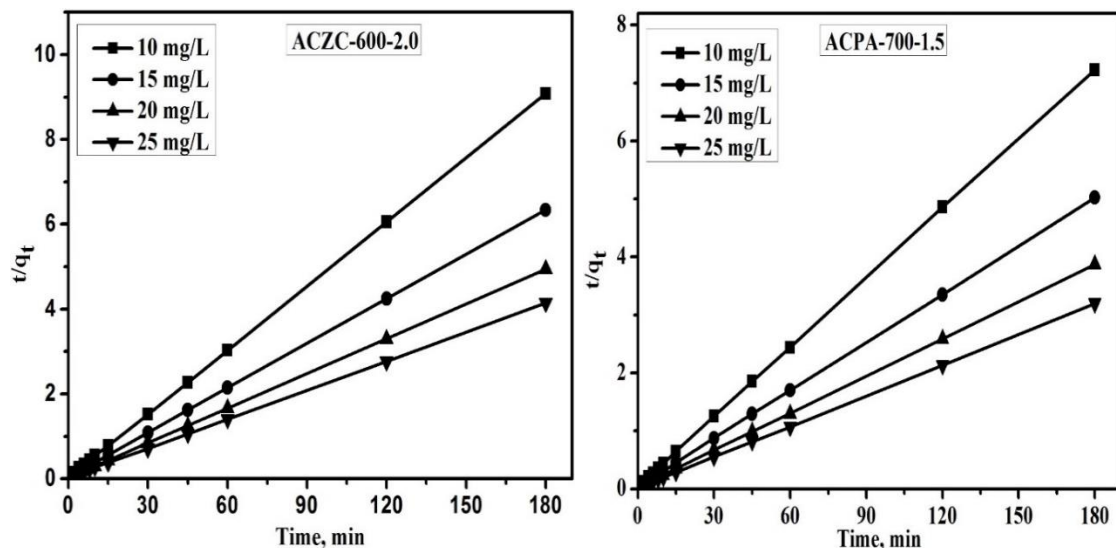


Fig. 4.41. Pseudo-second-order kinetics for Cr(VI) adsorption onto ACs at 45°C.

4.3.1.2.2. Intraparticle diffusion

The intraparticle diffusion (IPD) kinetics model parameters and plot of both adsorbents are shown in Table 4.14 and Fig. 4.42, respectively. As seen from Fig. 4.42, the plots are not linear over the whole time range, that confirms more than one process affect the Cr(VI)

adsorption (Sharma and Bhattacharyya, 2005). These parameters are employed in predicting the sorption mechanism. The plot shows two patterns: the first straight portion depicting macropore and mesopore diffusion and the second representing micropore diffusion (Fierro et al., 2008). If the value of c is zero, then the rate of adsorption is controlled by intraparticle diffusion for the entire adsorption period, but in the present study, c is not zero.

Table 4.14: Intraparticle diffusion constants for Cr(VI) adsorption

| Parameters | ACZC-600-2.0 (at 45 °C) | | | | ACPA-700-1.5 (at 45 °C) | | | |
|-----------------------------------|-------------------------|-------|-------|-------|-------------------------|-------|-------|-------|
| | Cr(VI), C_0 (mg/L) | | | | Cr(VI), C_0 (mg/L) | | | |
| | 10 | 15 | 20 | 25 | 10 | 15 | 20 | 25 |
| k_1 (mg/g min ^{-1/2}) | 0.372 | 0.436 | 0.571 | 1.355 | 36.37 | 40.74 | 20.03 | 29.05 |
| R^2 | 0.424 | 0.229 | 0.493 | 0.610 | 0.566 | 0.499 | 0.475 | 0.608 |
| c | 16.24 | 23.88 | 30.68 | 29.83 | 1.00 | 1.58 | 0.477 | 0.655 |

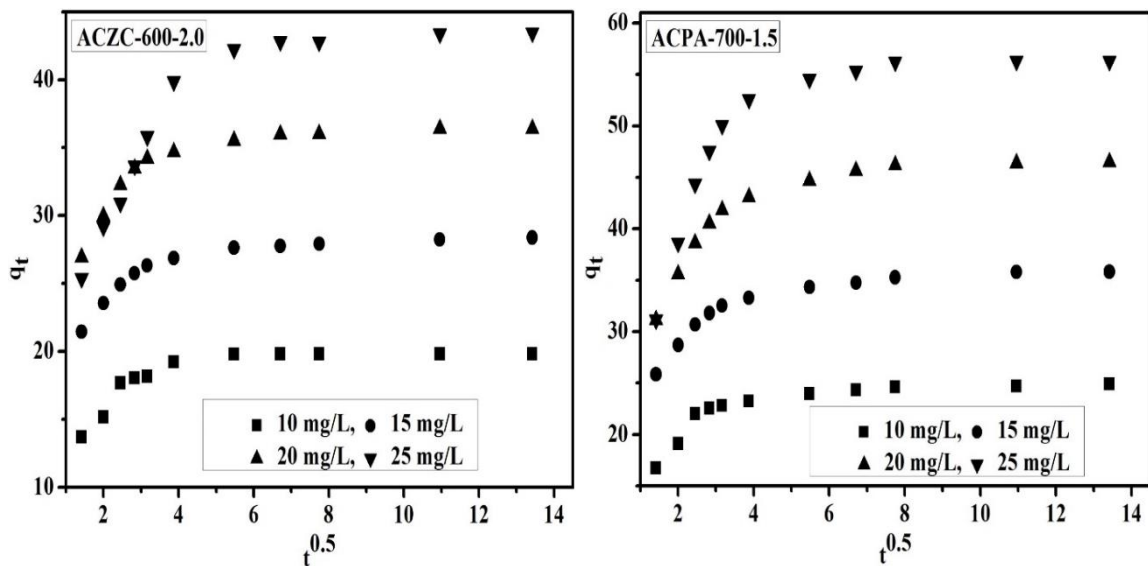


Fig. 4.42. Intraparticle diffusion plots for Cr(VI) adsorption onto ACs at 45°C.

4.3.1.2.3. Adsorption isotherms

The results from the fittings of various models to Cr(VI) adsorption are listed in Table 4.15. Fig. 4.43 shows a linear relationship of C_e/q_e versus C_e using experimental data obtained for Cr(VI) adsorption on ACZC-600-2.0 and ACPA-700-1.5. The intercept and the slope of the plot result in the q_m and k_L values of ACZC-600-2.0 and ACPA-700-1.5 and are tabulated in Table 4.15. The Langmuir plots have good linearity ($R > 0.9$ for both the adsorbents). The Langmuir monolayer adsorption capacity (q_m) of ACZC-600-2.0 and

ACPA-700-1.5 are 46.21 and 59.0 mg/g. The values of R_L are found to be 0.0132 for ACZC-600-2.0 and 0.0098 for ACPA-700-1.5 adsorbents of Cr(VI) adsorption, and it confirms that the Langmuir isotherm is favorable for Cr(VI) adsorption on both adsorbents under the conditions used in the study.

Table 4.15: Isotherms constants for adsorption of Cr(VI)

| ACs | Langmuir | | | Freundlich | | | Temkin | | |
|--------------|-----------------|-----------------|-------|---------------------------------------|-------|-------|--------|------------|-------|
| | q_m (mg/g) | k_L (L/mg) | R^2 | k_F [mg/g(L/mg) ^{1/n}] | 1/n | R^2 | b | A (L/g) | R^2 |
| ACZC-600-2.0 | 46.21 | 3.02 | 0.971 | 32.10 | 0.215 | 0.960 | 394.64 | 201.14 | 0.890 |
| ACPA-700-1.5 | 59.0 | 4.08 | 0.952 | 43.77 | 0.177 | 0.893 | 383.33 | 1.13 | 0.789 |

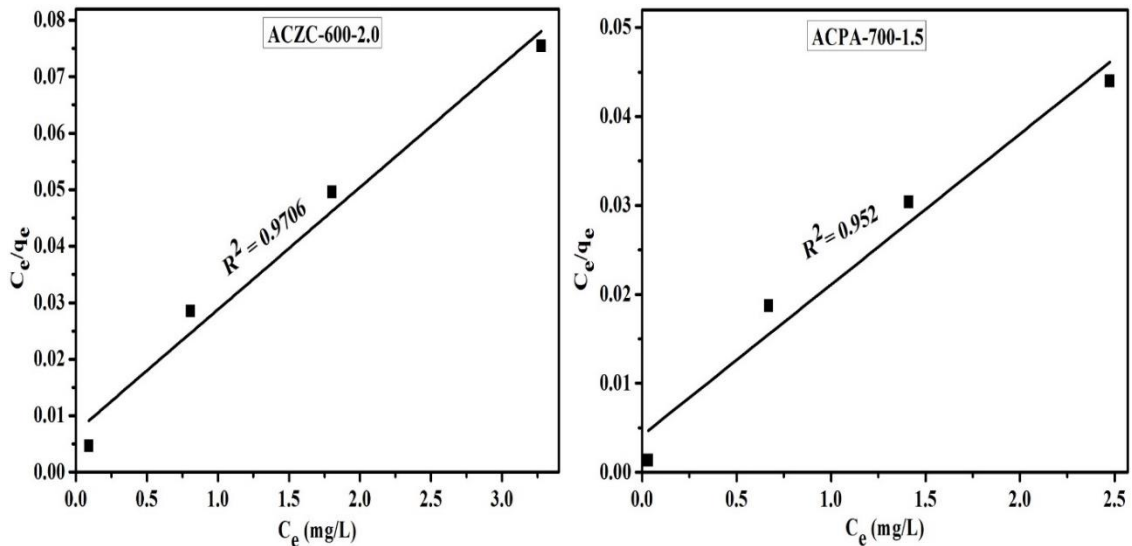


Fig. 4.43. Langmuir isotherms for the adsorption of Cr(VI) onto ACs at 45 °C.

The Freundlich constants are determined from the slope and intercept of a plot of $\ln q_e$ versus $\ln C_e$ (Fig. 4.44) and are reported in Table 4.15. The value of $1/n$ (< 1) for both activated carbons represent a favorable condition of Cr(VI) adsorption.

Figure 4.45 shows the linear graph of Temkin isotherms of the adsorbents. The constant A and b values of ACZC-600-2.0 and ACPA-700-1.5 adsorbents are tabulated in Table 4.15. The comparison of tested models for the description of equilibrium adsorption isotherms on ACZC-600-2.0 and ACPA-700-1.5 are in the order as follows: Langmuir $>$ Freundlich $>$ Temkin.

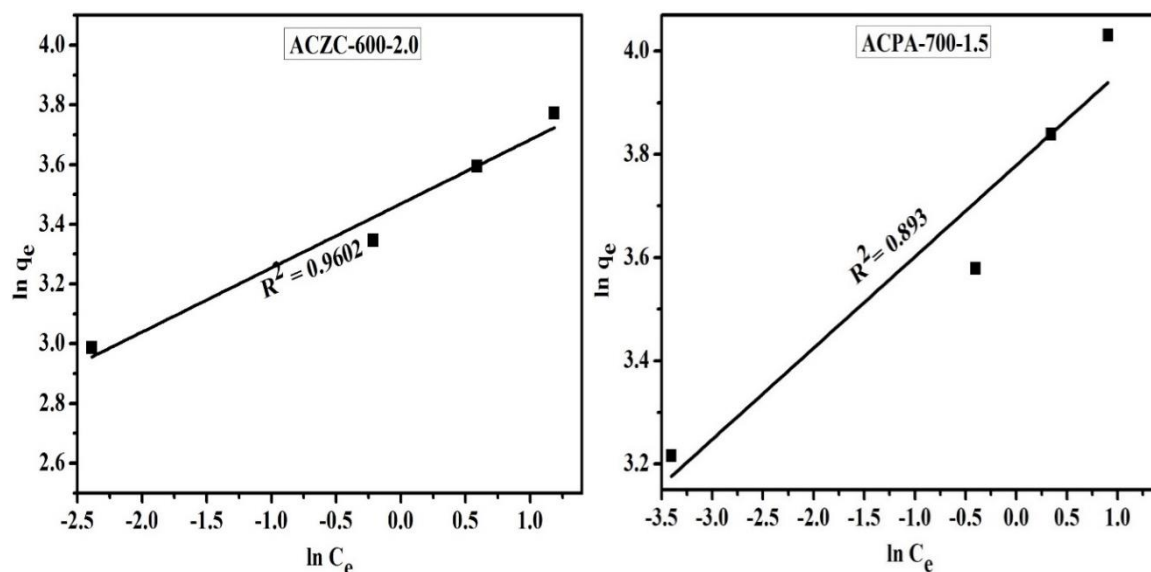


Fig. 4.44. Freundlich isotherms for the adsorption of Cr(VI) onto ACs at 45 °C.

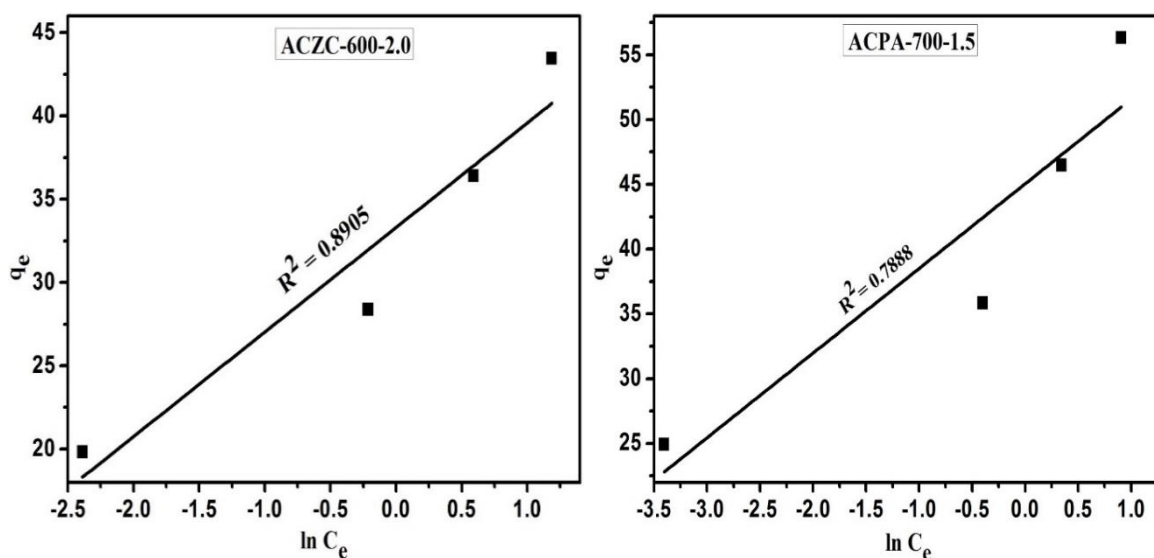


Fig. 4.45. Temkin isotherms for the adsorption of Cr(VI) onto ACs at 45 °C.

4.3.1.2.4. Adsorption thermodynamics

The temperature effect on the Cr(VI) adsorption process was investigated with the thermodynamic parameters like a change in Gibbs free energy (ΔG°), change in enthalpy (ΔH°) and change in entropy (ΔS°). The values of ΔH° and ΔS° were determined from the slope and intercept of the van't Hoff plot of $\ln K_C$ vs. $1/T$ (Fig. 4.46). The calculated values of thermodynamic parameters are tabulated in Table 4.16. The negative values of ΔG° indicate that the adsorption process is spontaneous and thermodynamically favourable. For ACZC-600-2.0 and ACPA-700-1.5, the negative Gibbs free energy (ΔG°) of the experimental value shows a typical physical process (Table 4.16). The positive values of the enthalpy change ($\Delta H^\circ = 14.74$ and 10.28 kJ/mol of ACZC-600-2.0 and ACPA-700-1.5,

respectively) indicate that the Cr(VI) adsorption process is endothermic nature. The positive values of ΔS° indicate an increase in the degree of freedom (or disorder) of the adsorbed species means adsorption is increased with increasing temperature.

Table 4.16: Thermodynamic parameters of Cr(VI) adsorption onto ACZC-600-2.0 and ACPA-700-1.5

| Adsorbents | T(K) | ΔG° (kJ/mol) | ΔH° (kJ/mol) | ΔS° (J/molK) |
|--------------|------|---------------------------|---------------------------|---------------------------|
| ACZC-600-2.0 | 298 | -7.59 | 14.74 | 0.075 |
| | 303 | -7.99 | | |
| | 308 | -8.28 | | |
| | 313 | -8.64 | | |
| | 318 | -9.14 | | |
| ACPA-700-1.5 | 298 | -8.87 | 10.28 | 0.064 |
| | 303 | -9.24 | | |
| | 308 | -9.55 | | |
| | 313 | -9.89 | | |
| | 318 | -10.15 | | |

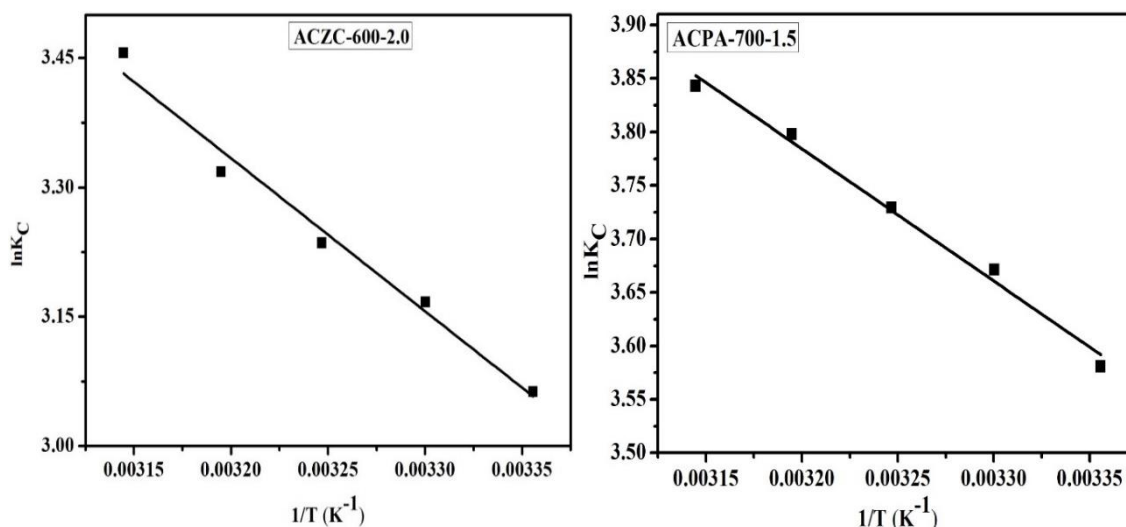


Fig. 4.46. Plots of $\ln K_C$ versus $1/T$ for 100 mg/L initial Cr(VI) concentration onto ACZC-600-2.0 and ACPA-700-1.5.

4.3.2. Regeneration and reuse of activated carbons

The activated carbons obtained after desorption of Cr(VI) were further used for adsorption studies. The processes of regeneration and reuse of adsorbents were done till four regenerations. The method of desorption used was as mentioned in chapter 2.

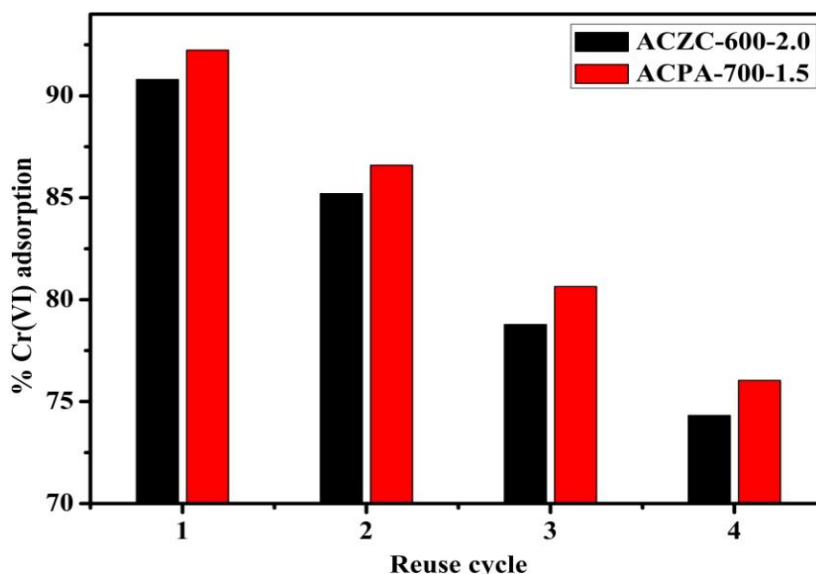


Fig. 4.47. Readsorption of Cr(VI) after desorption.

For ACZC-600-2.0 and ACPA-700-1.5 the initial wt. was taken as 0.05 and 0.04 g for 100 mL of Cr(VI) solution of 10 mg/L concentration was considered. The % removal of Cr(VI) using regenerated ACs is represented in Fig. 4.47. It is observed that for the first reused one, the % removal of Cr(VI) reduced by 9.2 and 7.76% for ACZC-600-2.0 and ACPA-700-1.5, respectively and same reduced by 27.68 and 23.96% after the fourth regeneration.

4.3.3. Column adsorption study

In this study, the effect of the variables on the breakthrough curves of Cr(VI) onto ACZC-600-2.0 and ACPA-700-1.5 adsorbents has been investigated.

4.3.3.1. Effect of bed height

The retention of metal ions in a packed bed column depends on the quantity of the solid adsorbent used or on the bed depth of the column (Simate and Ndlovu, 2015; Taty-Costodes et al., 2005; Vijayaraghavan et al., 2005). The breakthrough curves of Cr(VI) adsorption onto ACZC-600-2.0 and ACPA-700-1.5 were determined by plotting the dimensionless concentration (C_e/C_0) against time (where C_e and C_0 are the metal ions concentration in the effluent and influent, respectively).

Fig. 4.48 shows the Breakthrough (BT) curves obtained for Cr(VI) adsorption onto prepared carbons (ACZC-600-2.0 and ACPZ-700-1.5) at bed depths of 2, 3 and 4 cm with a constant flow rate of 5 mL/min. The pH and initial influent chromium concentration in the feed was 2.0 and 10 mg/L, respectively. From Fig. 4.48, it is observed that, the breakthrough curves and exhaustion times increased as bed depth increases. The increase in Cr(VI) uptake capacity with the increase in bed depth of the column is due to the availability of more

binding sites for sorption and an increase in the contact time (Simate and Ndlovu, 2015). In other words, as the bed height increased, more binding sites were available, and the ions had more time to contact with the adsorbents resulting in higher uptake capacity of Cr(VI) in the column. Furthermore, higher adsorption capacity of Cr(VI) by prepared carbons (ACZC-600-2.0 and ACPZ-700-1.5) are observed at higher bed height, which could be attributed to rising in the surface area of the adsorbents, which provide more binding sites for adsorbate to adsorb (Padmesh et al., 2006; Taty-Costodes et al., 2005). From Table 4.17, it can be noticed that the breakthrough time, exhaustion time and percent removal increases as the bed height increases. These results are in agreement with the findings of similar studies reported in the literature (Padmesh et al., 2006; Simate and Ndlovu, 2015; Taty-Costodes et al., 2005).

Table 4.17: Column parameters obtained at different bed heights and flow rates

| Adsorbents | Bed height (cm) | Flow rate (mL/min) | Breakthrough time (min) | Exhaustion time (min) | Bed capacity, q_{eq} (mg/g) | % Removal |
|--------------|-----------------|--------------------|-------------------------|-----------------------|-------------------------------|-----------|
| ACZC-600-2.0 | 2 | 5 | 320 | 2840 | 25.29 | 62.63 |
| | 3 | 5 | 1680 | 3520 | 27.42 | 67.42 |
| | 4 | 5 | 3120 | 4240 | 32.57 | 68.36 |
| | 4 | 10 | 1140 | 2960 | 34.54 | 62.57 |
| | 4 | 15 | 460 | 2100 | 35.10 | 56.05 |
| ACPA-700-1.5 | 2 | 5 | 420 | 3060 | 17.16 | 58.18 |
| | 3 | 5 | 1680 | 3660 | 22.70 | 66.77 |
| | 4 | 5 | 2520 | 4500 | 29.10 | 71.86 |
| | 4 | 10 | 1380 | 3020 | 35.61 | 64.75 |
| | 4 | 15 | 780 | 2220 | 36.17 | 58.82 |

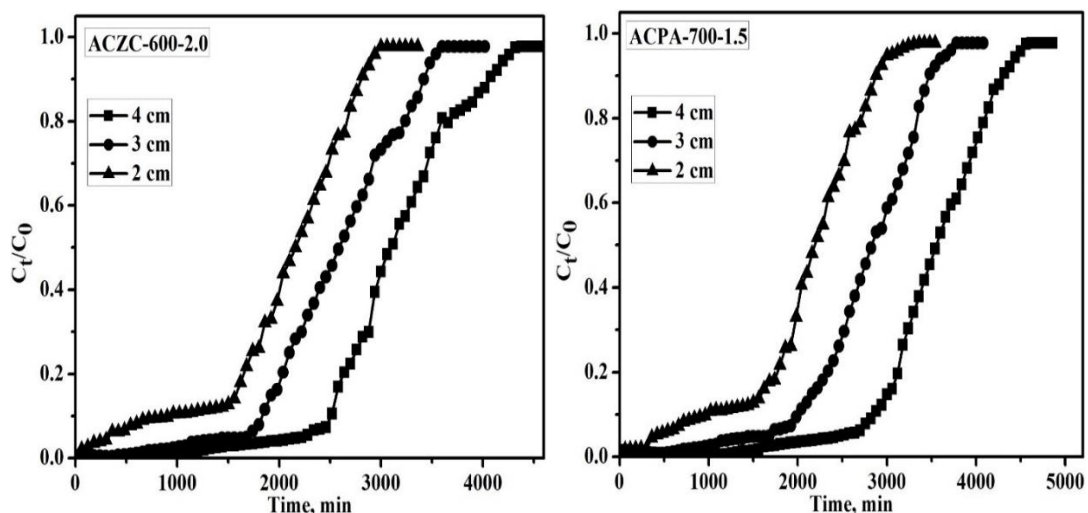


Fig. 4.48. Breakthrough curves for Cr(VI) adsorption onto ACZC-600-2.0 and ACPA-700-1.5 at different bed heights ($C_0 = 10 \text{ mg/L}$, flow rate = 5 mL/min , and $\text{pH} = 2$).

4.3.3.2. Effect of solution flows rate

The effect of flow rate in the fixed bed column packed with ACZC-600-2.0 and ACPZ-700-1.5 adsorbents were investigated varying the flow rate from 5 to 15 mL/min with bed depths held constant at 4 cm. The pH and initial influent chromium concentration in the feed was 2.0 and 10 mg/L, respectively. The breakthrough curves of chromium adsorption onto ACZC-600-2.0 and ACPZ-700-1.5 were determined by plotting the dimensionless concentration (C_t/C_0) against time and shown in Fig. 4.49.

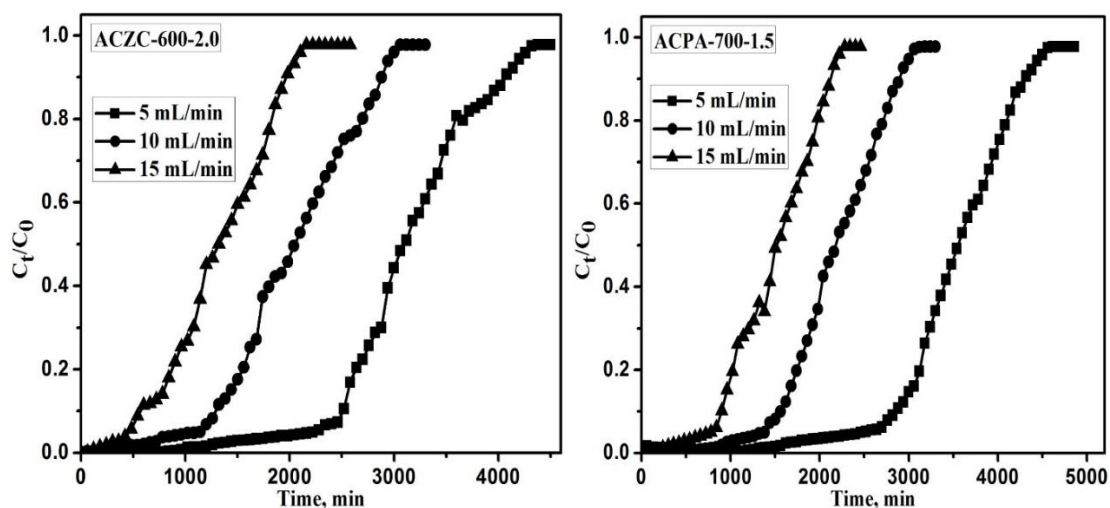


Fig. 4.49. Breakthrough curves for Cr(VI) adsorption onto ACZC-600-2.0 and ACPA-700-1.5 at different flow rates ($C_0 = 10 \text{ mg/L}$, bed height = 4 cm , and $\text{pH} = 2$).

From Fig. 4.49, an increase in the flow rate reduced the breakthrough and exhaustion times resulting in steeper breakthrough curves and shorter zones of mass transfer. This could be explained by the fact that at a lower flow rate, the residence of the adsorbate was more and hence the adsorbent got more time to bind with the metal efficiently. In other words, if the residence time of the solute in the column is not large enough for the adsorption equilibrium

to be reached at the given flow rate, the chromium solution leaves the column before the equilibrium occurs. It was observed that the adsorbent got saturated quickly at higher flow rates (Simate and Ndlovu, 2015; Vinodhini and Das, 2010). From Table 4.17, the uptake of Cr(VI) is decreased with increase in flow rate. It can be noticed that the breakthrough time, exhaustion time and the % removal decreases as the flow rate is increased. It can be concluded that best results are obtained at the lowest flow rate of 5 mL/min. These results are also in agreement with the findings of similar studies reported in the literature (Padmesh et al., 2006; Simate and Ndlovu, 2015; Tan et al., 2008a; Taty-Costodes et al., 2005; Vinodhini and Das, 2010).

4.4. Remarks on the adsorption study

The study on adsorption of phenol, MB and Cr(VI) and the corresponding results obtained as detailed in this chapter lead to following remarks.

Both the activated carbons, ACZC-600-2.0 and ACPZ-700-1.5 used for adsorption in the present study are good adsorbents for all the adsorbates. As far as phenol is considered the adsorption capacity of these carbons, ACZC-600-2.0 and ACPZ-700-1.5 are 75.37 and 83.21 mg/g, respectively. These are lies between some of them values reported in literature; 149.25 mg/g for Rattan sawdust based AC, Commercial activated carbon – 49.72 mg/g, Sugarcane bagasse fly ash – 23.83 mg/g, activated carbon-laboratory grade – 24.64 mg/g (Hammed and Rahman, 2008). Thus, these carbons prepared in the present study could suitably be used for the adsorption of phenol containing wastewater treatment systems. However, ACPZ-700-1.5 is a better adsorbent for phenol than ACZC-600-2.0. After four regenerations, the % removal of phenol from solution by ACPA-700-1.5 reduced from 99.75 to 73.79%, whereas by ACZC-600-2.0 the % removal reduced from 99.19 to 72.04%. Thus, ACPA-700-1.5 is better regenerated. Although after four regenerations the adsorption capacity reduced to nearly 72% of the original one, but still better than some other regeneration studies in literature (Ania et al., 2004), where after four regenerations the capacity seen to reduce to 30-35%.

For MB and Cr(VI), the activated carbons prepared in the present study, ACZC-600-2.0 and ACPA-700-1.5 are much better than those seen in literature. As far as regeneration and reuse of spent activated carbons are concerned with respect to MB and Cr(VI), the performance is better than that for phenol, but still a noticeable decrease in the adsorption capacity is seen.

The efficiency of adsorption by the regenerated activated carbons decrease in every cycle. For organic pollutants like phenol, biodegradation is an attractive method of treatment where the end products are innocuous. However, the disadvantage of biodegradation process is high concentration of pollutant become lethal to the microbes. To overcome from this problem, simultaneous adsorption and biodegradation by immobilized adsorbents is an alternative for treatment of high-concentration containing organic wastewater. By this treatment technique, cost of the activated carbon can be minimized while maintaining the adsorption capacity as before. Immobilized activated carbon has a high capacity to treat highly concentrated organic pollutants containing wastewater by sudden decrease the pollutants level that protect microorganisms from toxicity. Chapter 5 deals efficiency of the immobilized activated carbon to the treatment of the high concentrated phenol-containing wastewater by adsorption-assisted biodegradation.

Chapter 5

Adsorption Assisted Biodegradation of Phenol

In the present study, phenol is considered as a primary concern and basic water pollutant. Phenol and its derivatives are present in the wastewaters of such industries as petroleum refining, leather and textile manufacturing, olive oil manufacturing, etc. in huge quantities. The concentrations of phenol in wastewater released from various industries are listed in Table 5.1 (Girish and Murty, 2015). High concentration of phenol is present in the effluents of some industries like petrochemical, coke ovens, phenolic resin production and fiber glass manufacturing. Phenol containing wastewater may not be direct flow into open water without treatment because of the toxicity of phenol.

Table 5.1: Phenol levels reported in industrial wastewaters (Girish and Murty, 2015)

| Industrial source | Phenol conc., mg/L |
|--------------------------------------|--------------------|
| Petroleum refineries | 40-185 |
| Petrochemical | 200-1220 |
| Textile | 100-150 |
| Leather | 4.4-5.5 |
| Coke ovens (without dephenolization) | 600-3900 |
| Coal conversion | 1700-7000 |
| Ferrous industry | 5.6-9.1 |
| Rubber industry | 3-10 |
| Pulp and paper industry | 22 |
| Wood preserving industry | 50-953 |
| Phenolic resin production | 1600 |
| Phenolic resin | 1270-1345 |
| Fiber glass manufacturing | 40-2564 |
| Paint manufacturing | 1.1 |

The wastewater treatment using activated carbon (AC) is considered an effective method due to its large active surface area with high porosity, strong adsorption ability, and physicochemical stabilization (Combarros et al., 2014; Lin et al., 2010). However, despite

its high adsorption capacity, AC can only maintain this adsorption capacity for a short time since its available adsorption sites get exhausted by adsorbed adsorbents as observed and discussed in the previous chapter. It is well known that AC is also a good support media for microbial immobilization. Thus, biological AC can actually remove organic pollutants both by adsorption as well as biodegradation (Xing et al., 2008). Biological treatment is attractive treatment technology due to its potential to degrade phenol and other organic pollutants producing harmless end products, and reduced capital and operating costs. Immobilization of microorganisms on the solid supports enhance the efficiency and toxic limit of the microbes. The main advantages of using immobilized cells, rather than suspended ones include the retention in the reactor of higher concentrations of microorganisms, protection of cells against toxic substances, prevention of suspended bacterial biomass in the effluent and lower capital costs for single reactor systems than that for individual processes. Moreover, immobilized microbial cells provide high degradation efficiency and excellent operational stability (Combarros et al., 2014; Tziotzios et al., 2005).

Integration of adsorption and biodegradation processes for the treatment of biodegradable organic compounds is seen in the enhancement of the biodegradation rate and maintains the adsorption capacity of the activated carbon due to bioregeneration. Attached microorganisms regenerate surface of activated carbon using organic substrate as a source of food and energy. The biological activated carbon (BAC) can be directly applied to these high phenol concentration-containing effluents released from various industries (Table 5.1). The immobilized activated carbon first reduces the phenol concentration in the solution by adsorption and after that biodegradation occurs (Ma et al., 2013).

In the present study, an attempt was made to study the adsorption assisted biodegradation using the more efficient phenol adsorbing activated carbon, ACPA-700-1.5. There are many phenol degrading microbial strains available. *P. putida* (MTCC 1194) was used in the present study. At first batch biodegradation of phenol with *P. putida* (MTCC 1194) as suspended cell were studied, the effect of various physiological parameters on phenol degradation were also verified. Then biodegradation of phenol using *P. putida* (MTCC 1194) immobilized on ACPA-700-1.5 were carried out, the effect of various parameters studied and the process was characterized. In this process, the phenol is adsorbed on the surface of BAC rapidly and biodegradation starts once the phenol in the solution. Phenol from AC surface released and degraded by microbes. Lastly the BAC was used for adsorption

assisted biodegradation repeatedly once the phenol consumed in each cycle and capacity of reuse was studied.

5.1. Batch biodegradation by suspended cells

Using acclimatised freely suspended *P. putida* (MTCC 1194) batch biodegradation experiments were carried out in 250 mL Erlenmeyer flasks containing 100 mL of MSM at different phenol concentrations as sole carbon source in an orbital shaker. First, the effect of physiological parameters studied then using the optimum parameters growth and biodegradation was characterized.

5.1.1. Effect of physiological parameters

Physiological parameters play a significant role in the growth and biodegradation behavior of the microorganisms. Microorganism grows within a range of physiological parameters, but maximum growth is achieved only at the specific conditions of the physiological parameters. The aim of this part of the study is to determine the particular condition for the maximum biodegradation of phenol. The variables such as inoculum size, pH, temperature and initial substrate concentration were studied that affects the % removal of phenol. The pH, temperature, and initial phenol concentration were varied in the range 4-10, 25-40 °C and 200-1200 mg/L, respectively.

5.1.1.1 Inoculum size

Inoculum size plays a major role in phenol biodegradation. Effect of inoculum size was studied with 1000 mg/L of initial phenol concentration for 72 hr, at temperature of 30 °C. Figure 5.1 shows the effect of inoculum size on phenol biodegradation capacity of acclimatised *P. putida* (MTCC 1194).

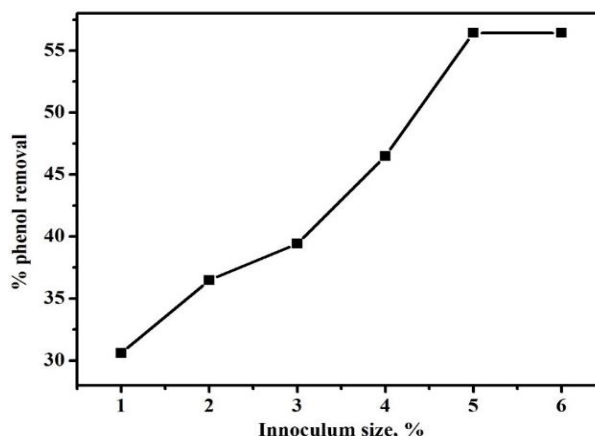


Fig. 5.1. Effect of inoculum size on % removal of phenol ($C_0 = 1000$ mg/L, and temperature = 30 °C).

Maximum phenol biodegradation has been achieved at an inoculum size of 5-6% (v/v). The phenol biodegradation was almost similar for both inoculation sizes for increased time of incubation. Hence, for the further study, 5% (v/v) inoculum size was used.

5.1.1.2. pH

To determine the optimal pH for the biodegradation of phenol by *P. putida* (MTCC 1194) have to start experiments were carried out at different pH (4–10) with an initial phenol concentration of 1000 mg/L. The internal environment of all living cell is believed to be neutral. Most organisms cannot tolerate pH values below 4 or above 9 (Annadurai et al., 1999). At low (pH = 4) or high (pH = 9) pH values, acids or bases can penetrate into cells more easily, because they tend to exist in undissociated forms, and electrostatic force cannot prevent them from entering the cells (Annadurai et al., 1999; Kim and Armstrong, 1981). The permeated substances can alter the internal pH balance; therefore, the bacterial activity decreases as the pH deviates from neutral conditions. From Fig. 5.2, increasing the pH from 4 to 7 of the media at 30 °C; the rate of phenol degradation increases. On raising the pH, it had reversed effect on phenol removal from the solution. In 72 hr, the phenol degradation increases from 23.11% to 57.88% at pH 4-7 while at pH 8, phenol removal decreases to 53.23%. It is concluded that the neutral pH could degrade phenol at higher rates as compared to both acidic and alkaline pH. Similar results were reported in the previous study that *P. Putida* have a maximum capacity of phenol degradation within the range of pH 7-8 (Annadurai et al., 1999; Annadurai et al., 2008; Kumar et al., 2005; Lu et al., 2012; Monteiro et al., 2000).

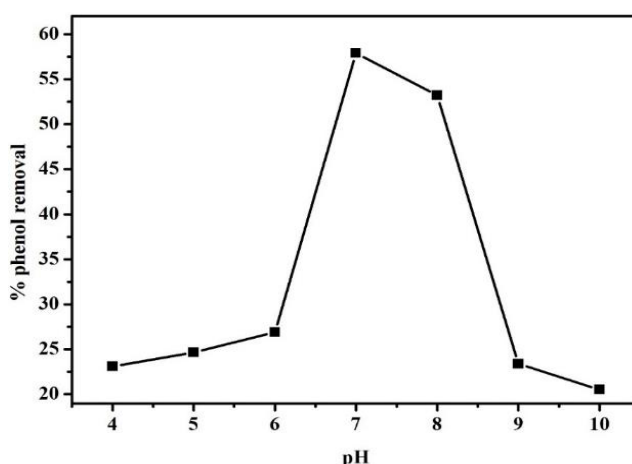


Fig. 5.2. Effect of pH on % removal of phenol ($C_0 = 1000$ mg/L, and temperature = 30 °C).

5.1.1.3. Incubation temperature

Temperature exerts a significant regulatory influence on the rate of metabolism and enhances the microbial activity on phenol and other contaminants (Annadurai et al., 1999;

Vela and Rainey, 1976). The bacterial activity rapidly reduces at temperatures below and above the optimum temperature range, whereas the bacterial activity is not much affected by temperature change within the optimum temperature range (Annadurai et al., 1999).

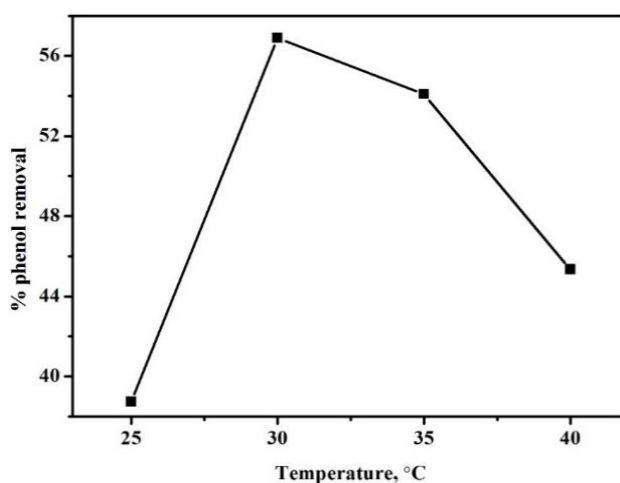


Fig. 5.3. Effect of temperature on % removal of phenol ($C_0 = 1000$ mg/L, and pH = 7).

To determine the optimal temperature for the biodegradation of phenol by *P. putida* (MTCC 1194), batch experiments were carried out at temperatures in the range of 25–40 °C with an initial phenol concentration of 1000 mg/L. The result is shown in Fig. 5.3 indicates 30 °C of temperature has been favourable for maximum degradation of phenol. Therefore, further experiments were performed at 30 °C. At the end of 48 hr, 35.62% of phenol was degraded by acclimatized suspended *P. putida* (MTCC 1194) at 30 °C and 34.09% at 35 °C, while at temperatures of 25 °C and 40 °C it was 28.73 and 30.34%, respectively. Similar results were reported by various researchers in the previous study that *P. putida* have maximum capacity of phenol biodegradation at temperature of 30 °C (Annadurai et al., 1999; Annadurai et al., 2008; Kumar et al., 2005; Lu et al., 2012; Monteiro et al., 2000).

5.1.1.4. Initial phenol concentration

Substrate concentration is also a significant parameter for the growth of the microorganisms. In this study, phenol acts as a substrate for the *P. putida* (MTCC 1194) to take energy for various metabolic activities. Figure 5.4 shows the % removal of phenol against the initial phenol concentration in the batch scale for 48 hr. At initial phenol concentrations between 200 to 1200 mg/L, the phenol removal % decrease with increasing the initial phenol concentration due to sensitivity to phenol in these ranges (Hannaford and Kuek, 1999).

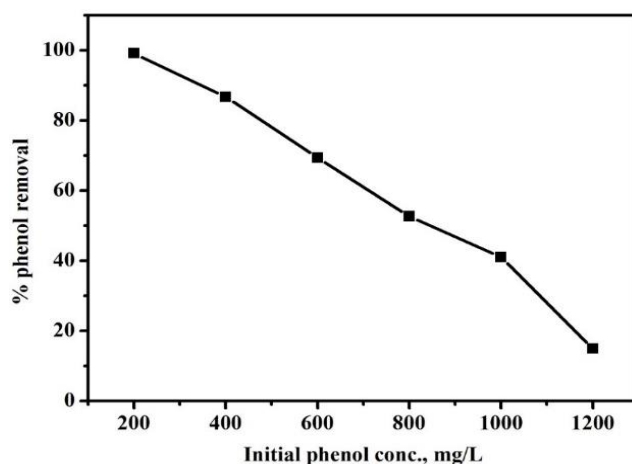


Fig. 5.4. Effect of initial concentration of phenol on % removal (pH = 7, and temperature = 30 °C).

5.1.2. Biodegradation of phenol

The phenol biodegradation by acclimatized suspended *P. putida* (MTCC 1194) was determined under the optimal conditions of inoculum size, 5% (v/v), pH 7 and temperature 30 °C. Initial phenol concentration in the batch scale was varied from 600 to 1200 mg/L with an equal increment of 200 mg/L. Fig. 5.5 shows that *P. putida* (MTCC 1194) cells are capable of complete degradation of phenol till 1000 mg/L. The time required for complete phenol degradation by the microbial cells for the initial phenol concentrations of 600, 800 and 1000 mg/L are 60, 108, and 180 hr, respectively. It can be observed that the initial phenol concentration of 1200 mg/L, the rate of biodegradation is slow with sufficient lag phase and did not degrade completely in 240 hr (not shown in figure). This is because of the inhibition of microbial activity by the toxicity of phenol (Park et al., 2013). Figure 5.6 shows a typical microbial growth curve where optical density was plotted against time, for the experiment using 1000 mg/L initial phenol concentration at 30 °C temperature.

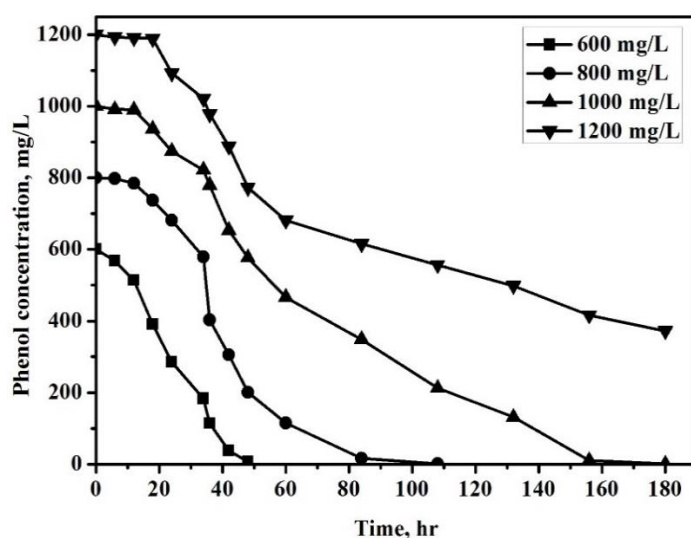


Fig. 5.5. Residual of phenol concentration with time (pH = 7, and temperature = 30 °C).

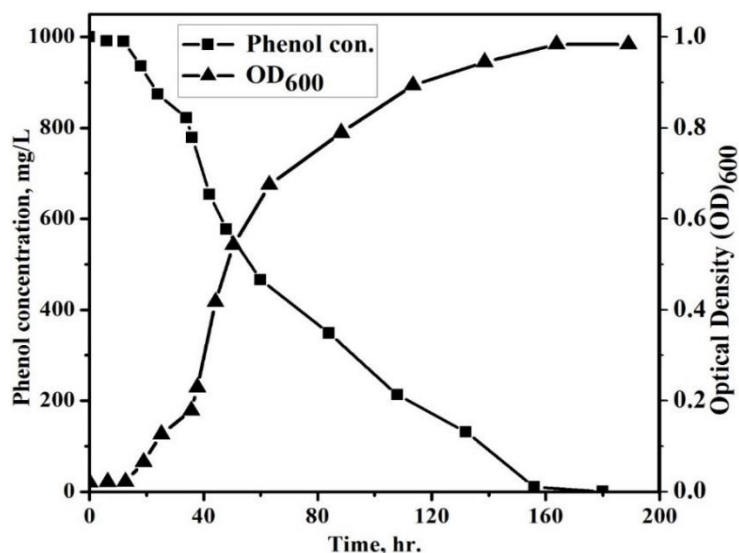


Fig. 5.6. Biodegradation curve and OD₆₀₀ of suspended *P. putida* (MTCC 1194) ($C_0 = 1000$ mg/L, pH = 7, and temperature = 30 °C).

The measurement of the concentration of the phenol and biomass are followed till the phenol initially present was entirely consumed (Fig. 5.6). At the initial stage, the lag phase is observed due to the high phenol concentration. From the figure, the lag phase of 12 hr is found, although the well-acclimatized inoculum was used in this experiment. During the lag phase, the increase in biomass was negligible due to the toxicity of high phenol concentration.

5.2. Batch Adsorption assisted biodegradation of phenol

The adsorption capacity of activated carbon was found to decrease after each desorption cycle (chapter 4). So, alternative method for the renewable of the activated carbon like bioregeneration may be considered. From the result of previous section, for the higher initial concentration of phenol, the growth, as well as the degradation activity of the microorganism, found to be inhibited. The microbial immobilization technique is a very useful alternative to degrade high concentration of phenol, which is practiced in all immobilized cell bioreactors. Enhanced stability of the degradation potential, continuous operation and reuse of cells are some of the important advantages of the use of immobilization technique in the biodegradation studies. Using activated carbon as biomass support, predominately the adsorption occurs first till its saturation then biodegradation starts. Thus, the process is named as adsorption and biodegradation of phenol.

In this study, ACPA-700-1.5 activated carbon was used for the immobilization of *P. putida* (MTCC 1194) and immobilized activated carbon named as BACPA-700-1.5 and used in the adsorption assisted biodegradation study of phenol at higher concentrations. As obtained

in the previous section the species *P. putida* (MTCC 1194) capable of degrading 1000 mg/L of phenol, so adsorption study using ACPA-700-1.5 was carried out first using higher concentrations of phenol so that the residual concentration in the solution be 1000 mg/L of phenol. The experiment is detailed in the following section.

5.2.1. Phenol adsorption onto ACPA-700-1.5

The adsorption of phenol on ACPA-700-1.5 at optimum conditions; pH 7 and 30 °C of temperature for a fixed known weight of 0.55 g/100mL and variable initial phenol concentration is depicted in Fig. 5.7. From the figure, it can be observed that the residual phenol concentration in the solution increases with an increase in initial phenol concentration. The reduction of phenol adsorption was due to the lack of available active sites on the ACPA-700-1.5 surface. The residual phenol concentration in the solution is 42.33, 280.52, 451.53, 738.79, 979.66, and 1097.28 mg/L when the initial phenol concentrations were 500, 1000, 1500, 2000, 2300, and 2500 mg/L, respectively. The concentration 2300 mg/L of phenol can suitably be biodegraded with the support of adsorption using the adsorbent dose as used in the experiment and maintain other parameters as used. Therefore, the concentration of 2300 mg/L of phenol was considered in the further adsorption assisted biodegradation studies.

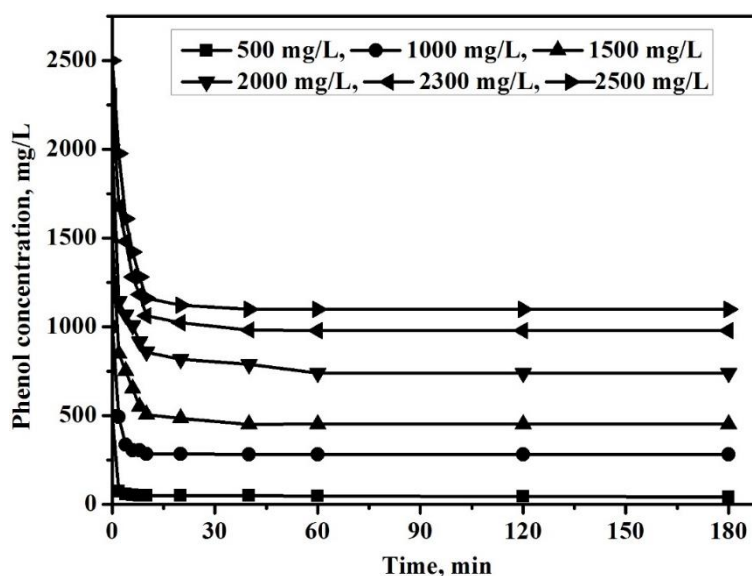


Fig. 5.7. Residual phenol concentrations in solution ($m_s = 0.55$ g/100mL, pH= 7, and temperature= 30 °C).

5.2.2. Morphological characterization of biofilm

Immobilization of *Pseudomonas putida* (MTCC 1194) on ACPA-700-1.5 was done as per the methods discussed in section-2.4.1.4.1. The immobilized activated carbon, BACPA-

700-1.5 was characterized as per the method discussed in section-2.4.1.4.2. The MTCC 1194 microorganism is rod shaped with smooth outer cell walls. Figure 5.8 shows the surface of ACPA-700-1.5 and biofilm developed on the activated carbon (BACPA-700-1.5). Figure 5.8(a) reveals that the surface of the ACPA-700-1.5 has both large and small pores and these pores may be macropore or mesopore in nature. The microbes for attachment utilize the macropore and undeveloped pore surface of the carbon. Figure 5.8(b) depicts the picture of the biofilm developed on ACPA-700-1.5, it shows that the biofilm covered the ACPA-700-1.5 uniformly. The uniform distribution is an important criterion for the proper adsorption and biodegradation of phenol overall surface area of the BACPA-700-1.5.

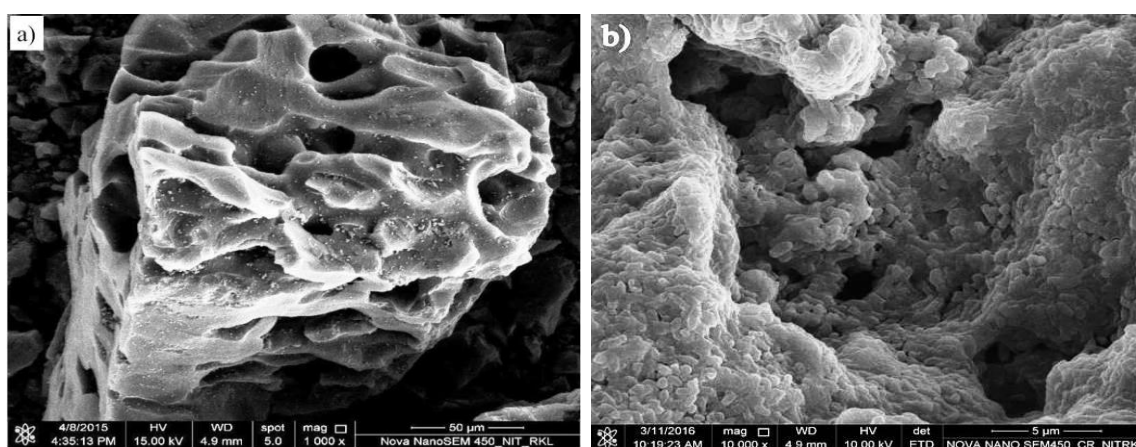


Fig. 5.8. FESEM images of (a) ACPA-700-1.5 AC, and (b) BACPA-700-1.5.

The micrograph shows *P. putida* (MTCC 1194) cells densely and homogeneously adhered to the surface of the carbon, because of physical adsorption by electrostatic forces or covalent binding between the bacterial cells and the ACPA-700-1.5 carrier. This immobilized activated carbon, BACPA-700-1.5 was used in the study of adsorption-assisted biodegradation of high concentrated phenol solution.

5.2.3. Effect of process parameters on adsorption assisted biodegradation of phenol

To examine the influence of parameters on adsorption-assisted biodegradation of phenol onto ACPA-700-1.5, such as pH (4–10) and temperature (25–40 °C) were carried out in a batch scale for 12 hr.

5.2.3.1. pH

The influence of pH on the removal of phenol was studied within the pH range 4–10 and the results are shown in Fig. 5.9. The pH interrupts the degree of ionization of the adsorbate

(Singh et al., 2016). It is observed from the Fig. 5.9 that the adsorption-assisted biodegradation of phenol is increased till pH 7. The maximum adsorption-assisted biodegradation of phenol was observed at pH 7 as 75.88 %. At higher pH, the phenol adsorption decreased may be due to the following reasons. First, the negative charge of the adsorbent surface was increased with pH and phenol changes to the ionic state from molecular state, which makes the repulsion force between phenol ions and the activated carbon surface. Second, the phenol ions adsorbed by the ACs also has a repulsion force between them. Third, the negative charges on the ACs surface are repulsive. Similar results were reported for the phenol adsorption (Agarwal and Balomajumdar, 2013; Beker et al., 2010; Hameed and Rahman, 2008; Singh et al., 2016). For adsorption using ACPA-700-1.5 (section-5.3.1), the % removal was 72, and 280.52 mg/L of phenol was left in the solution for initial concentration of phenol, 1000 mg/L, where as here the % removal is 75.88 i.e. 241.2 mg/L left in the solution. This indicates that nearly 4 mg (40 mg/L in 100 mL) of phenol more consumed by BACPA-700-1.5 because of biodegradation.

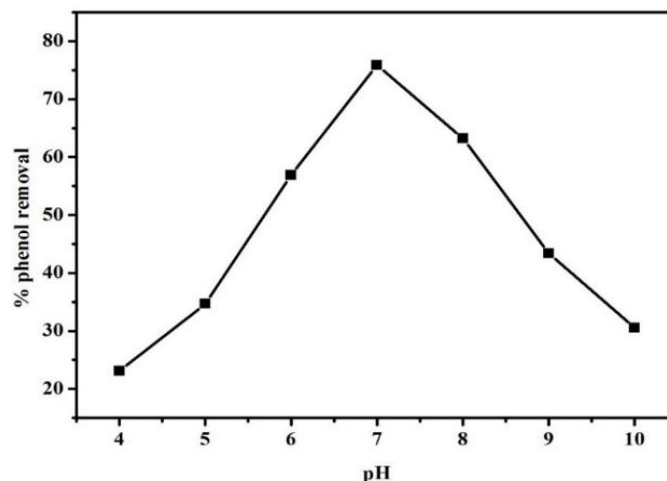


Fig. 5.9. Effect of pH on % removal of phenol ($C_0 = 1000$ mg/L, $m_s = 0.55$ g, and temperature = 30 °C).

5.2.3.2. Temperature

The effect of temperature on the adsorption-assisted biodegradation of phenol onto the biological activated carbon (BACPA-700-1.5) is shown in Fig. 5.10. It shows that the adsorption assisted biodegradation of phenol decreases from 76.73 to 63.34% with an increase in temperature from 25 to 40 °C. The % removal of phenol decreases with an increase in temperature indicates an exothermic process. The decrease in adsorption-assisted biodegradation with the increase in temperature was due to the weakening of the attractive force between the adsorbate and BACPA-700-1.5. Therefore, the attractive forces between biological activated carbon and adsorbate are not strong enough to hold the

adsorbed molecules at the active binding sites of the BACPA-700-1.5 (Agarwal and Balomajumdar, 2013; Mukherjee et al., 2007; Singh et al., 2016).

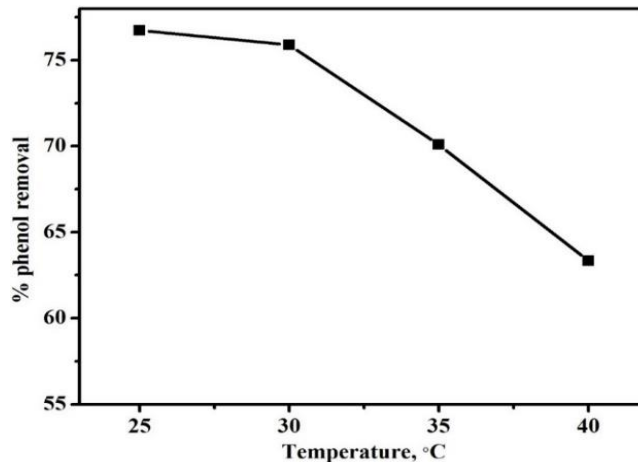


Fig. 5.10. Effect of temperature on % removal of phenol ($C_0 = 1000$ mg/L, $m_s = 0.55$ g, and pH = 7).

5.2.4. Adsorption assisted biodegradation of phenol

Figure 5.11 shows that BACPA-700-1.5 is able to completely degrade all the initial concentrations of phenol at pH 7 and 30 °C temperature. The time needed for complete phenol removal by BACPA-700-1.5 were 120, 150, and 248 hr when the initial phenol concentrations were 1000, 1500 and 2300 mg/L, respectively. This indicates that immobilization change the characteristic of microbes and their degradation efficiency, 1000 mg/L phenol completely degraded in just 120 hr by BACPA-700-1.5, whereas for the suspended one the same was achieved in 180 hr. The whole adsorption assisted biodegradation process could be divided into two stages (Fig. 5.11).

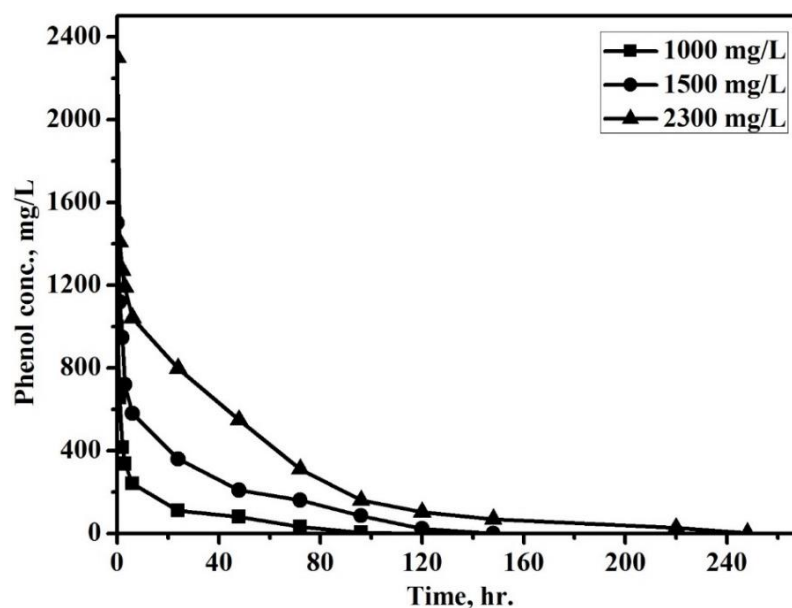


Fig. 5.11. Adsorption–biodegradation process of BACPA-700-1.5 ($m_s = 0.55$ g/100mL, pH = 7, and temperature = 30 °C).

During the first stage, the concentration of phenol decreases rapidly because of the adsorption onto a BACPA-700-1.5 surface, which could avoid the damage to the bacteria from high concentrations of phenol. After 6 hr, 241.06, 580.62 and 1041.95 mg/L of phenol was left in the solution of 1000, 1500 and 2300 mg/L initial concentration of phenol. In the second stage of the process, BACPA-700-1.5 degraded the phenol. The adsorbed phenol was released out to the solution due to concentration gradient, and that was later biodegraded by BACPA-700-1.5. The phenol removal of the present study is better than reported data (Bandhyopadhyay et al., 2001; Banerjee and Ghoshal, 2011; Mollaei et al., 2010; Park et al., 2013).

5.2.5. Adsorption assisted biodegradation kinetics

Based on the results obtained from the batch experiments, the adsorption assisted biodegradation kinetics was investigated with pseudo-first-order, pseudo-second-order, and intraparticle diffusion kinetic models. These kinetic parameters were determined from the plotted graph and tabulated in Table 5.2. At the initial phenol concentration of 1000, 1500 and 2300 mg/L, the correlation coefficient (R^2) in pseudo-second-order model (> 0.99) is higher than that of pseudo-first-order model. The calculated q_e value in the pseudo-second-order model is closer to the experimental data than that in pseudo-first-order model, which indicates that the kinetics data fit better to the pseudo-second-order model than to the pseudo-first-order model.

Table 5.2: Kinetics parameters of phenol adsorption assisted biodegradation on BACPA-700-1.5

| Phenol C_0 (mg/L) | $q_{e,exp}$ (mg/g) | Pseudo first-order | | | | | Pseudo-second-order | | | | | Intraparticle diffusion | | |
|---------------------------|-----------------------|-----------------------|---------------------|-------------------------|-------|-------------------|-----------------------|--------------------------|---------------------|-------|-------------------|--|-------|--------|
| | | $q_{e,cal}$ (mg/g) | h_0 (mg/g/min) | k_1 (min^{-1}) | R^2 | Δq (%) | $q_{e,cal}$ (mg/g) | k_2 [g/(mg min)] | h_0 (mg/g/min) | R^2 | Δq (%) | k_i (mg/g min ^{1/2}) | R^2 | c |
| 1000 | 181.78 | 117.92 | 0.063 | 6.35E-5 | 0.656 | 12.42 | 183.15 | 4.72E-5 | 1.58 | 0.999 | 0.27 | 1.20 | 0.742 | 94.76 |
| 1500 | 272.67 | 222.20 | 0.053 | 3.51E-5 | 0.751 | 6.17 | 273.97 | 1.43E-5 | 1.07 | 0.996 | 0.16 | 2.08 | 0.867 | 99.83 |
| 2300 | 417.58 | 361.83 | 0.026 | 1.14E-5 | 0.746 | 4.025 | 421.94 | 6.27E-6 | 1.12 | 0.997 | 0.31 | 2.30 | 0.921 | 178.93 |

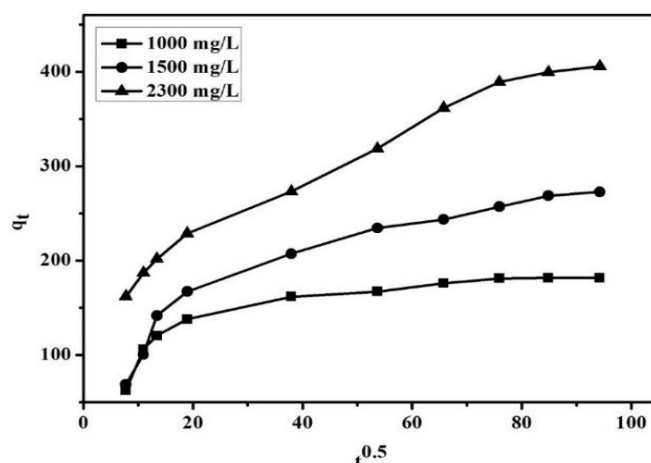


Fig. 5.12. Intraparticle diffusion kinetic plots for phenol removal by BACPA-700-1.5 at 30 °C.

The intraparticle diffusion kinetic model is plotted in Fig. 5.12. The plot is not linear over the whole time range, that confirms more than one process affect to the phenol adsorption (Hameed and Rahman, 2008). The constant (k_i) for phenol removal was calculated and is tabulated in Table 5.2. The value of c is not zero that confirms the rate of adsorption is not controlled by intraparticle diffusion for the entire adsorption period.

5.2.6. Adsorption assisted biodegradation equilibrium isotherm

At equilibrium state, the adsorption assisted biodegradation isotherm is very useful to describe how the adsorbed molecules distribute between the liquid phase and the solid phase. The Langmuir, Freundlich, and Temkin isotherm models were used for the study of adsorption assisted biodegradation isotherms of BACPA-700-1.5. Langmuir isotherm, a linear relationship of C_e/q_e vs. C_e using experimental data obtained for phenol adsorption assisted biodegradation on BACPA-700-1.5, the intercept and the slope of the plot was resulted in the q_m and k_L values and is tabulated in Table 5.3 along with the correlation coefficient ($R^2 = 0.997$). From Table 5.3, the value of R_L is found to be 0.00012 for BACPA-700-1.5 of phenol adsorption-assisted biodegradation, and it confirms that the Langmuir isotherm is favorable for phenol adsorption-assisted biodegradation in the present study.

The values of Freundlich constants, k_F and $1/n$, were obtained from the linear plot of $\ln q_e$ vs. $\ln C_e$ and the correlation coefficient ($R^2 > 0.704$). The Freundlich constant $1/n$ was smaller than unity indicating that the adsorption assisted biodegradation process was favorable under studied conditions. From the results, the adsorption-assisted biodegradation pattern of phenol onto BACPA-700-1.5 is well fitted with Langmuir than Freundlich isotherm model.

Table 5.3: Isotherm model parameters for phenol adsorption assisted biodegradation on BACPA-700-1.5

| Adsorbent | Langmuir | | | | | Freundlich | | | Temkin | | |
|---------------|-----------------|-----------------|-------|---------------|--------|---------------------------------------|-------|-------|--------|------------|-------|
| | q_m (mg/g) | k_L (L/mg) | R^2 | Δ % | R_L | k_F [mg/g(L/mg) ^{1/n}] | 1/n | R^2 | b | A (L/g) | R^2 |
| BACPA-700-1.5 | 452.49 | 3.58 | 0.997 | 2.5 | 1.2E-4 | 311.06 | 0.265 | 0.704 | 31.89 | 63.48 | 0.849 |

For Temkin isotherm model, the constant A and b values are tabulated in Table 5.3 along with the correlation coefficient ($R^2 = 0.849$). From Table 5.3, the comparison of tested models for the description of equilibrium adsorption assisted biodegradation isotherms on the BACPA-700-1.5 is as follows Langmuir > Temkin > Freundlich.

5.3. Repeated use of BACPA-700-1.5

Figure 5.13 shows the phenol degradation by repeated BACPA-700-1.5 in batch scale experiments when initial phenol concentration was 2300 mg/L. In the first cycle of the phenol biodegradation, time taken for the full removal of phenol from the solution is 248 hr. While in the second batch experiment, the biodegradation time was less than the first cycle due to more biofilm formed on the ACPA-700-1.5 surface, but it is almost the same in the third batch experiment as it is in first cycle, which shows the feasibility of using BACPA-700-1.5 for continuous phenol adsorption-assisted biodegradation. From the figure, it is clear that as in each cycle, the biofilm built up is more and more, the sudden decrease in phenol concentration is not prominent and delayed, which indicate partial resistance of the biofilm to the transport of phenol to the surface of ACPA-700-1.5 for adsorption. Simultaneously the biodegradation started at higher phenol concentration in the solution indicating enhanced tolerance of the microbes to phenol when immobilized. The remediation efficiency of the immobilized activated carbon (BACPA-700-1.5) is more than the activated carbon, ACPA-700-1.5. From these experimental results, it can be concluded that the immobilization technique is better for the renewal of the exhausted activated carbon than other regeneration techniques.

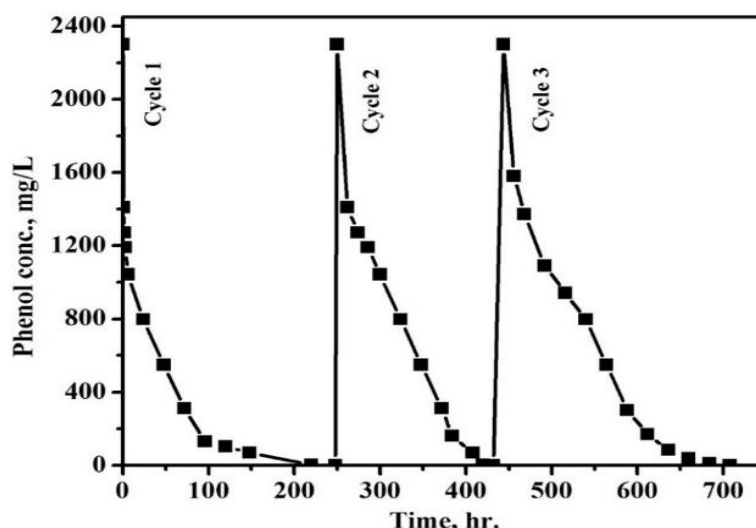


Fig. 5.13. Repeated use of BACPA-700-1.5 ($C_0 = 2300$ mg/L, pH = 7 and temperature = 30 °C).

5.4. Remarks

From the batch adsorption-assisted biodegradation study of phenol it is confirmed that the same is highly efficient in treating higher concentration of phenol in a reasonable time. The most important is that the biological activated carbon (BACPA-700-1.5) does not lose its capacity for the treatment of high concentration of phenol, 2300 mg/L in repeated use. Industrial treatment systems are desired to be continuous one. For continuous treatment of phenol, many types of suspended and immobilized systems are used. The immobilized ones are better for their efficiency and requiring less space. Fluidized bed bioreactor (FBBR) is one such immobilized cell bioreactor, which use small low-density solid as biomass support. In the present study the granular activated carbon used are of size 1.7–2.00 mm. Thus considering the superiority of BACPA-700-1.5 in treating the highly concentrated phenol, the same may be used in FBBR. Thus in the present study an attempt was made to study the performance characteristic of a FBBR for the treatment of phenol using BACPA-700-1.5 as solid phase, which is discussed in chapter-6.

Chapter-6

Treatment of Phenol in Fluidized Bed Bioreactor

Fluidized bed bioreactors (FBBR) have been receiving considerable interest in wastewater treatment. A fluidized bed bioreactor consists of microorganism coated particles suspended in wastewater, is sufficiently aerated to keep the gas, liquid, and the solid particles thoroughly mixed. The fluidized bed bioreactor is seen to perform better than other types of reactors. The superior performance of the fluidized bed bioreactor is due to high biomass concentration because of immobilization of cells onto the solid particles; intimate contact between gas, liquid and solid phases; decoupling of residence times of liquid and microbial cells due to immobilization (Tang et al., 1987; Vinod and Reddy, 2005). The performance of fluidized bed bioreactor depends on various characteristics; hydrodynamics, mass transfer and biodegradation. The latter two phenomena depend on hydrodynamics. Mass transfer study is out of scope of the present work. Thus in the present study hydrodynamics and biodegradation were characterized.

Precise knowledge of hydrodynamic behaviour of a fluidized bed helps in better designing and operation of the same. Application of FBBR in bio-oxidation process for wastewater treatment requires high inventory of the solid phase. The FBBR operates between the minimum fluidization velocity (below this the particles are not in state of suspension) and elutriation velocity (beyond which the particles comes out of the reactor or stick to the grid placed at the top of the reactor column to prevent the particles from elutriation). Pressure drop gives the information of pumping power required. Thus, the hydrodynamic behaviours of importance are pressure drop, minimum fluidization velocity, bed expansion and gas (air) holdup. The third one decides the particle concentration and the fourth one is important for gas-liquid mass transport and maintains oxygen concentration in the reactor. FBBR is difficult to characterize for experimental hydrodynamics as it handles low-density solid particles possessing very low minimum fluidization velocity with flow uncertainties (Jena, 2009; Mishra, 2013).

Here an attempt was made to characterize a three-phase fluidized bed bioreactor for hydrodynamic studies with low density activated carbon particles as reported in chapter-2

by varying the gas and the liquid velocities and the results were analysed. Experiments were undertaken to study the hydrodynamic behaviours viz. the pressure drop, minimum liquid fluidization velocity, bed expansion and gas hold up. Hydrodynamic studies were not done using biomass laden particles, as the same is lighter than activated carbon particles, difficult to clearly observe the hydrodynamic behaviour and with time the biofilm thickness changes lead to change its size and density. Further high concentration phenol solutions are foaming because of low surface tension and of higher viscosity, where the hydrodynamic study with biomass-laden activated carbon is still difficult. Thus, only activated carbon particles were considered in the hydrodynamics study using water as the liquid phase. It is expected that the behaviour of activated carbon with water would differ to some extent than that may occur for the biomass laden particles, but the study can give an approximate information of the same.

6.1. Hydrodynamic Studies

The experimental setup as shown in Fig. 2.4 and discussed in chapter-2 was used in present study. Granular activated carbon particles of average size 1.85 mm, sphericity of 0.7 were used as the solid phase and distilled water and oil and moisture free air were used as the liquid and gas phases, respectively. Accurately weighed amount of activated carbon was fed into the column and adjusted for a specified initial static bed height (reproducible) by repeatedly fluidizing and defluidizing the bed with water. Liquid was pumped to the fluidizer at a desired flow rate using calibrated rotameter. The air was then introduced into the column through the air sparger at a desired flow rate. Approximately five minutes was allowed to achieve a steady state. The readings for pressure drop and the expanded heights of the bed were then noted. All experiments were conducted at temperature of 25-30 °C. The water and air velocities were varied from 0 to 0.062 m/s and 0 to 0.00265 m/s in increments respectively.

6.1.1. Bed pressure drop and minimum fluidization velocity

For the measurement of pressure drop manometers filled with carbon tetrachloride and water were connected to pressure tapping in the column as described in chapter-2. All experiments were started with the column completely filled with water and activated carbon particles with the initial level of manometer adjusted to zero. For liquid-solid experiment, the liquid flow rate was gradually increased. For gas-liquid-solid experiment with different liquid and gas flow rates, first with little flow of the liquid close to zero, the air was slowly

introduced and gradually increased to the desired flow rate after which the liquid flow rate was increased and the readings were noted down.

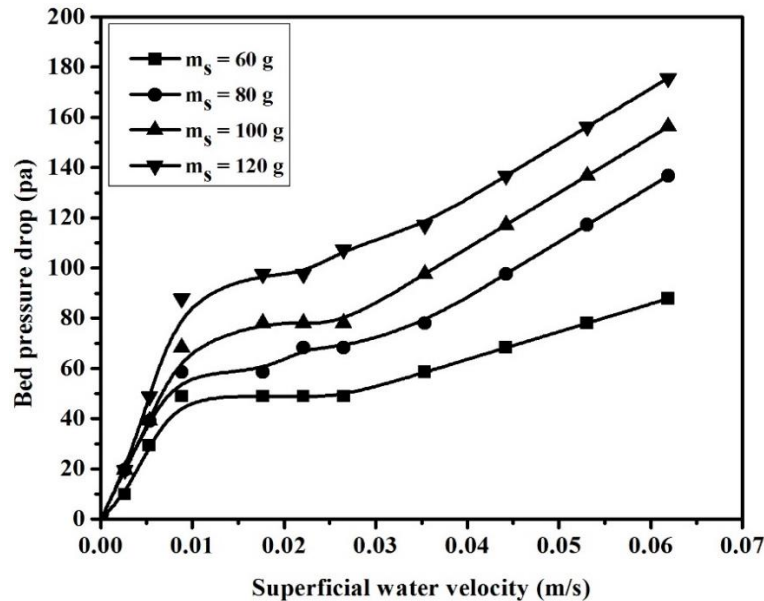


Fig. 6.1. Variation of bed pressure drop with superficial water velocity for different bed mass.

Figure 6.1 shows the variation of bed pressure drop with superficial liquid velocity in liquid-solid system for different bed mass, m_s (static bed heights). The plot shows an initial sharp increase in pressure drop then a nearly constant pressure drop plateau and then a gradual increase in the pressure drop. The initial sharp increase corresponds to fixed bed pressure drop, the plateau represents fluidization regime and the gradual increase in pressure after the plateau is because of hindrance to flow of water at the exit top grid (provided to check the elutriation of particles from the bed) due to adherence of few particles of the fluidized bed. An increase in bed pressure drop is observed with increased bed mass or initial static bed height. The higher bed mass requires a higher amount of drag to make the bed fluidize, thus a higher value of pressure drop as observed. The variations in pressure drop initially for some different bed masses observed to be the same as it was not possible to measure a small difference in pressure drop in manometer with carbon tetrachloride or water as the manometric fluid.

The minimum fluidization velocity was determined from the bed pressure drop vs. fluid velocity plot. It is considered the fluid velocity corresponding to the change in slope of the pressure drop line emerging from the fixed bed one. Alternatively, it is determined from the visual observation of the velocity corresponding to the state where the fixed bed start to expand (Jena, 2009). From the bed pressure drop plot (Fig. 6.1), the minimum fluidization velocity is noted as 0.008 m/s (approximately), where there is change in slope of the

pressure drop curves. This value is higher than that observed visually where the bed started expanding which corresponds to a value of 0.0053 m/s. The minimum fluidization velocity calculated from the correlation of Wen and Yu (Kunii and Levenspiel, 1991) is 0.0035 m/s. The large difference in the minimum fluidization velocities may be due to the most accepted Wen and Yu equation based on the particles of moderate to high density, thus the low-density particles like activated carbon may be under predicted. In the experiment, very precise minute variation in water flow rate was not possible and some intermittent value may be the actual minimum fluidization velocity, which might have missed. Because of loose packing (higher voidage, nearly 0.52) of the reproducible static bed, the change in pressure drop with superficial liquid velocity is slow, so a nearly constant pressure drop in the fluidization regime is achieved at higher liquid velocity.

Figure 6.2 shows a comparison in bed pressure drop variation, experimental, the calculated values from Ergun's equation (Kunii and Levenspiel, 1991) and the ideal fluidized bed pressure drop obtained from basic force balance (equal to Buoyant mass of particles (M_b) times of the acceleration due to gravity (g) upon the area of cross section of the bed (A), i.e. $M_b g/A$). The experimental pressure drop for fluidization is found to be close to that obtained from basic force balance for a bed mass of 60 g, but higher than the predicted one in case of bed mass of 120 g, the higher value may be due to two reasons; inability of water manometer to capture the intermittent pressure drop or sticking of particles at top restraint. Ergun's equation under predict the pressure drop in the fixed bed may because of high voidage of the bed of lighter particles.

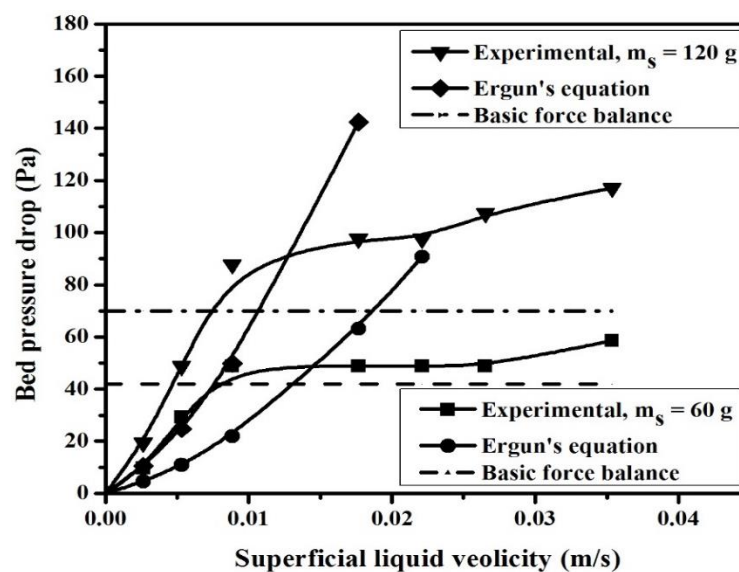


Fig. 6.2. Comparison of bed pressure drop variation.

The variation in bed pressure drop with gas velocity at different constant liquid velocities is shown in Fig. 6.3. It is observed that with increase in gas velocity, the bed pressure drop decreases. The values become negative as measured by manometer. This is due to the initial pressure drop was made to zero with no air and water flow but column filled with water (with or without solids). With increase in gas velocity the bed pressure drop decreases because of higher gas holdup in the bed which causes decrease in hydrostatic pressure at the bottom of the bed (Mishra, 2013). For bed with no solids, the pressure drop variation with higher water velocity, 0.053 m/s is observed to be quite less and with solids increasing pressure drop is observed, this is because of touching of few particles to the top grid. With higher amount of solids in the bed the pressure drop variation with gas velocity at low liquid velocity is found to be slightly more may be because of higher gas holdup of the bed due to more interaction between solids and air bubbles increasing the residence time of bubbles in the bed. At high liquid velocity, a reverse phenomenon observed in the present system i.e. an increase in bed pressure drop after a small decrease in the same with gas velocity. This is due to adherence of particles to the top grid. The values on the y-axis is the pressure drop corresponding to liquid solid fluidization at different conditions.

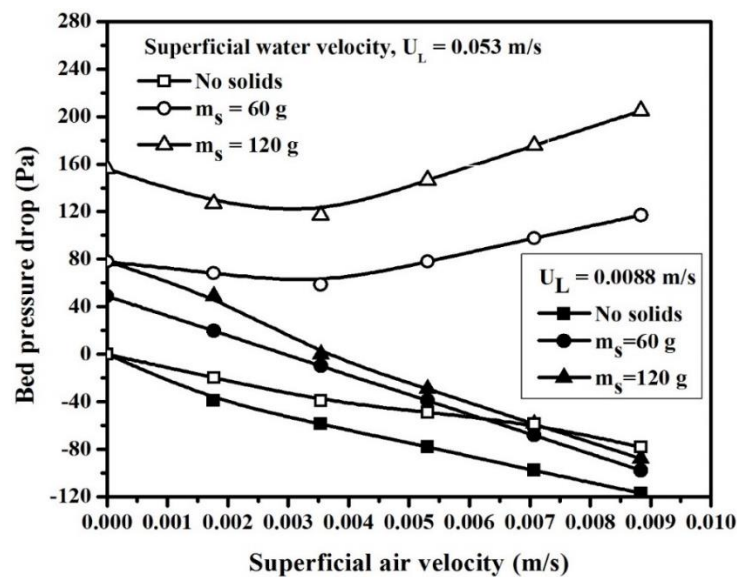


Fig. 6.3. Variation of bed pressure drop with superficial air velocity at different constant water velocities.

Figure 6.4 shows the variation of bed pressure drop (with and without solids) beyond the minimum fluidization condition with superficial water velocity at different constant air velocities. For bed without solids, nearly a linear variation (increase) in bed pressure drop is observed for increasing water velocities may due to increase in the water volume fraction in the bed and decrease in the air holdup. With solids the pressure drop variation is not

linear, initially there is little increase in pressure drop mainly due to increase in the liquid fraction and decrease in the gas fraction in the bed, then comparatively at higher rise rate due to adherence of particles to the top grid. The bed pressure drop values are not the same in all the plots for particular combination of gas and liquid velocities is because of variation in measurement conditions i.e. initialization of manometer reading to zero and different interaction in the bed keeping water velocity constant and varying the air velocity and vice-versa.

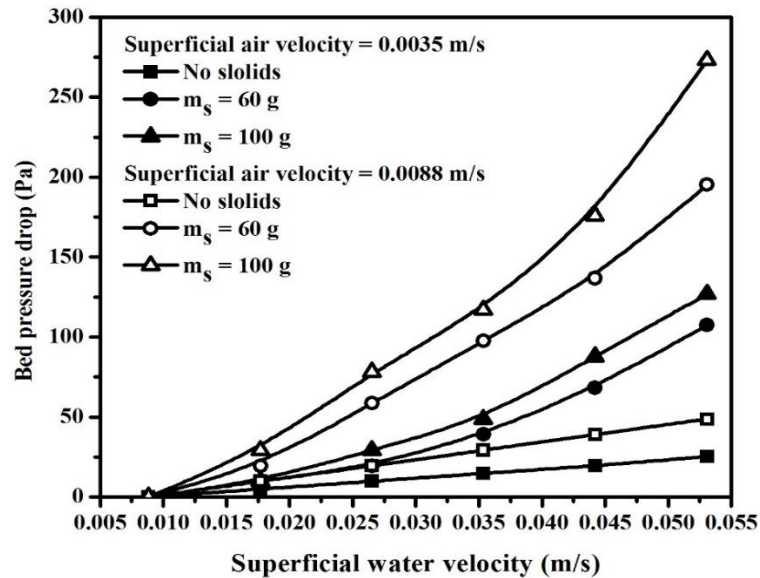


Fig. 6.4. Variation of bed pressure drop with superficial water velocity at different constant air velocities.

In the presence of all the three phases i.e. in gas-liquid-solid fluidization when liquid is the continuous phase, the minimum fluidization velocity is called as the minimum liquid fluidization velocity (U_{Lmf}). U_{Lmf} is the superficial liquid velocity at which the bed becomes fluidized for a given superficial gas velocity. For the low-density particles such as activated carbons, it is very difficult to characterize the U_{Lmf} by visual observation or from the pressure drop plot, as the value of U_{Lmf} is quite low to be precisely noted. The particles are in a state of transition and particles from the top surface is lifted to the free board by the gas bubbles. In pressure drop measurement, the magnitude of pressure fluctuations is of the magnitude, which mislead the bed pressure drop in gas-liquid-solid fluidization with low-density particles of smaller size. With increase in gas velocity, it was observed that the U_{Lmf} decreases, but was not possible with the experimental arrangement to quantify the same.

6.1.2. Expanded bed height

The void fraction (1 – solid fraction) of the bed is an important characteristic otherwise represented by expanded bed height. It helps in design and operation of fluidized bed

systems especially sizing and inventory. Beyond the minimum fluidization condition the static solid bed get expanded to higher heights with to and fro motion of the solid particles as the fluid velocity is increased (Jena, 2009). The expanded bed height in the present study was measured visually. The expanded bed height in the form of bed expansion ratio (ratio of expanded bed height to initial static bed height) as a function of liquid velocity at different constant gas velocities for bed mass of 60 gm is represented in Fig. 6.5.

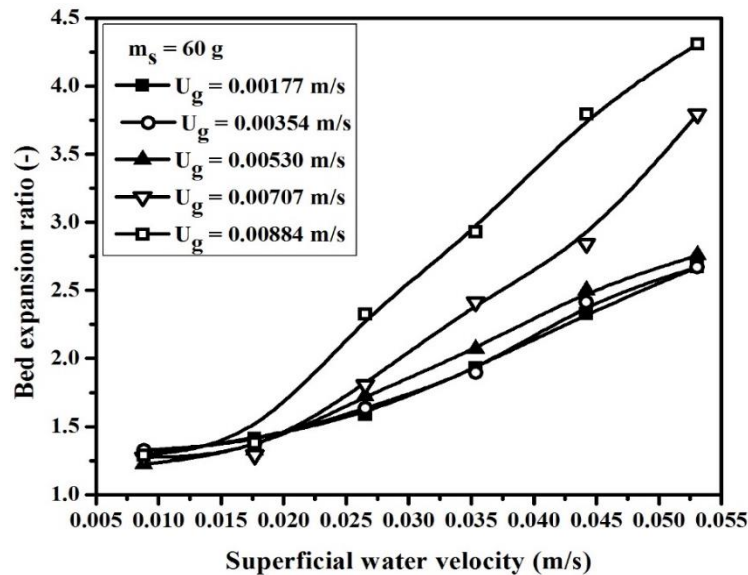


Fig. 6.5. Variation of bed expansion ratio with superficial water velocity at constant air velocities.

As already reported in literature, it is observed from Fig. 6.5 that the expanded bed height beyond the minimum fluidization condition increases with the increase in both the gas and liquid velocities. For the air velocity of 0.00884 m/s and water velocity of 0.053 m/s, the expanded bed height is 4.3 times the initial static bed height. The increase is more prominent at higher air velocity when the water velocity increased continuously. In the present study, it is observed that there is little decrease in the expanded bed height in the low liquid velocity region above the minimum fluidization one.

6.1.3. Air holdup

The air holdup (gas holdup) is one of the most important characteristics for analysing the performance of a three-phase fluidized bed. For chemical processes, where mass transfer is the rate-limiting step, it is important to be able to estimate the gas holdup since this relates directly to the rate of mass transfer. A direct method of measuring gas holdup is to simply isolate a representative portion of the test section by simultaneously shutting two quick closing valves and measuring the fraction of the isolated volume occupied by the gas (Jena, 2009). In the present study, the gas holdup was measured by the phase isolation method and

the fractional gas hold up (ϵ_g) was calculated using Eq. (6.1). Where H_c and H_L are height of the column and the height of liquid (water remained after escape of the air from the system).

$$\epsilon_g = \left(\frac{H_c - H_L}{H_c} \right) \quad (6.1)$$

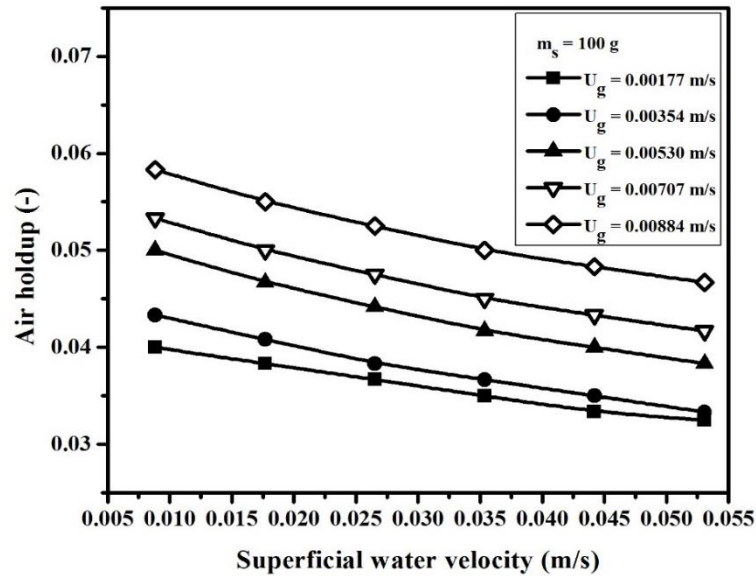


Fig. 6.6. Variation of fractional air holdup with superficial water velocity at different values of fixed superficial air velocities.

Figure 6.6 shows the variation of fractional gas holdup with superficial water velocity at different values of fixed superficial air velocity (U_g). The gas holdup is found to decrease with increasing liquid velocity, but the variation is small. Jena, 2010 has reported a slight decrease in gas holdup with liquid velocity over a large range of the later. The decrease in gas holdup with liquid velocity may possibly be because at higher liquid velocity the liquid fast drives the bubbles. The residence time of the bubbles decreases with the increase in liquid velocity and hence the gas holdup is likely to decrease. The gas velocity is found to have great effect on the fractional gas holdup and almost a monotonic increase is observed in air holdup with superficial air velocity at constant water velocity. As seen from Fig. 6.6, the air holdup in the present study is in the range of 3.3% to 5.9% for different combination of air and water velocities. This low air holdup contains enough oxygen that can diffuse to the water phase and maintain adequate dissolved oxygen.

6.2. Adsorption assisted biodegradation of phenol in fluidized bed biofilm reactor

There are many variables in the fluidized bed bioreactor those affects its performance of treating phenol. Few such operating parameters influencing the performance studied in the present work are; superficial air velocity (U_g), superficial wastewater velocity (U_L), ratio of volume of static bed to volume of reactor V_b/V_r and initial concentration of phenol. 5 L of synthetic wastewater of various phenol concentrations were prepared and used in the study. This water was continuously pumped to the reactors at prefixed rate and the treatment was carried out till no phenol was left in the water. The amount of ACPA-700-1.5 used in the bed was calculated on the basis of 55 g of carbon per g of phenol in the solution (i.e. 0.55 g of carbon per 100 mL of phenol of concentration 100 mg/L), so that after initial adsorption nearly 1000 mg/L of phenol would have left in the solution for biodegradation and volume of static bed half of the volume of the reactor (fluidized column) i.e. $V_b/V_r = 0.5$. This resulted to a quantity of phenol solution of 5 L of concentration 5000 mg/L and a carbon of quantity 137 g.

The factors U_g , U_L , and V_b/V_r also affect the hydrodynamics; minimum fluidization velocity, bed expansion and air holdup. In the previous section the same was studied using activated carbon particles without biofilm and using water without the phenol content because of difficulty in using the biomass laden activated carbon and phenol solution which is foaming at its higher concentration. Because of low weight of biomass-laden particles and higher viscosity and lower surface tension of concentrated phenol solution used in the treatment, the bed expansion was quite higher and the air holdup was also more. The values of viscosity and surface tension for 5000 mg/L and 10000 mg/L concentrated solutions are; 0.000876 Pa.s, 0.000924 Pa.s and 0.0606 N/m, 0.0566 N/m respectively, whereas the same for water are; 0.000798 Pa.s and 0.0724 N/m. The bed expansion of 2 times of the initial static bed with a good circulation of the particles without noticeable attachment to the top grid was observed in case of biomass laden particles, BACPA-700-1.5 with 5000 mg/L concentrated phenol solution, at a superficial solution velocity of 0.0177 m/s and air velocity of 0.00133 m/s, at other liquid and gas velocities, either the bed expansion ratio was less than two or the particles were attaching to the top grid or foaming was prominent. To study the effect of various parameters on degradation of phenol in fluidized bed, the liquid velocity, gas velocity, V_b/V_r and initial phenol concentrations used were in variation

to those figures mentioned above, for a good quality of fluidization with bed expansion ratio of 2.

6.2.1. Effect of superficial air velocity

Superficial gas (air) velocity is an important parameter in the degradation of phenol from wastewater, as it is required to maintain oxygen concentration, support fluidization and reduce the film resistance. Fig. 6.7 shows that an increase in superficial gas velocity increases the removal of phenol. It is evident that increase in removal of phenol is due to increase in air holdup in the reactor which improves the mass transfer rate and reduction in film resistance due to higher degree of turbulence and thus time for complete degradation of phenol reduces. For 5 L of 5000 mg/L of phenol the time taken for 99.5% degradation is 480 h at a superficial gas velocity of 0.00177 m/s.

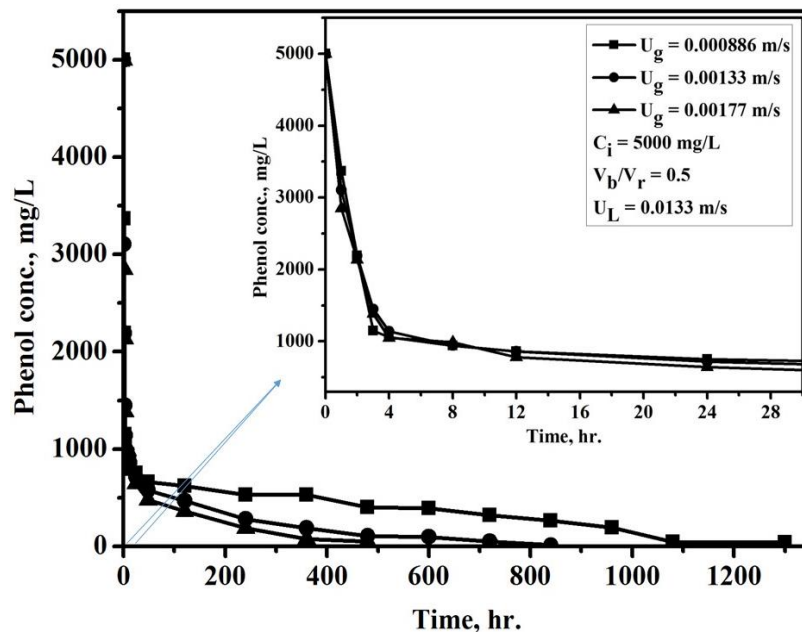


Fig. 6.7. Effect of superficial air velocity on phenol biodegradation.

The superficial gas velocity of 0.00133 was applied for the further experiment due to the proper fluidization and no attachment of the biofilm-laden particles BACPA-700-1.5 to the top grid. At higher gas velocity, it was observed that the air bubbles were attached to the carbon particles, causing increase in expansion and sticking of particles at the top grid. In Fig. 6.7 (projected part up to 30 hr), it is seen that the phenol removal is drastically decreased in very short time due to the adsorption onto BACPA-700-1.5. It is also observed from the plot that the phenol concentration in solution reduced to 1000 mg/L from 5000 mg/L within 3-4 hr of time, and then gradually biodegradation took place.

6.2.2. Effect of superficial liquid velocity

The effects of the different superficial liquid velocities U_L (0.01325, 0.0177 and 0.0221 m/s) on phenol removal in FBBR were studied for the synthetic effluent concentration of 5,000 mg/L phenol. Fig. 6.8 shows the phenol removal with time along varying the superficial liquid velocity. It is observed that the phenol degradation is faster at a superficial liquid velocity of 0.0177 m/s and complete in 240 hr. This short time is taken for the removal of the 5000 mg/L phenol concentration at 0.0177 m/s superficial liquid velocity due to the ACPA-700-1.5 particles were well fluidized within the reactor, and that provided space for the biomass development on the support and intimate contact between the phases.

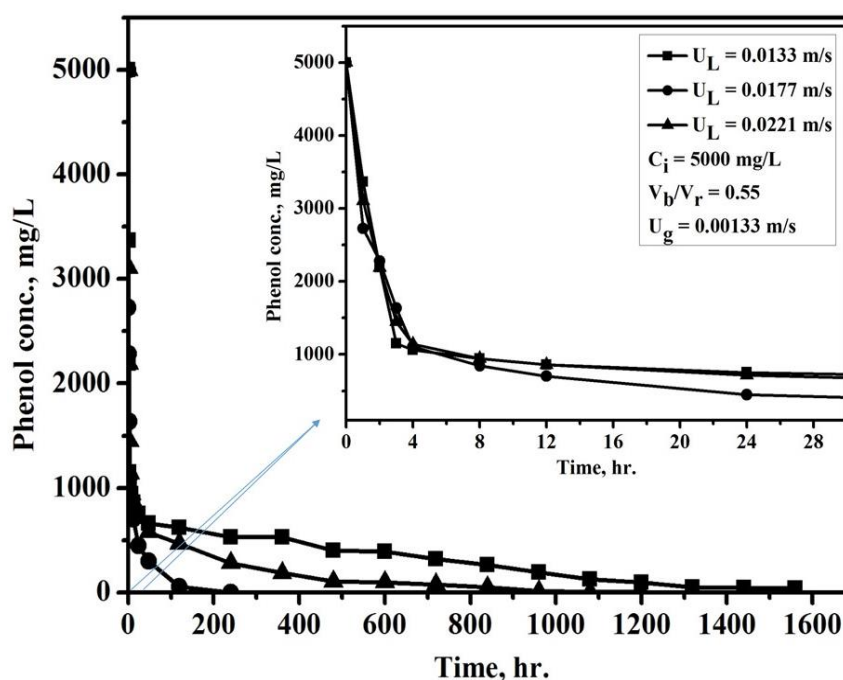


Fig. 6.8. Degradation of phenol with time at different superficial liquid velocities.

At higher superficial liquid velocity, the carbon bioparticles were settled on top of the bed due to which the proper mixing was not possible. This resulted in prolonged time duration for the removal of phenol from the wastewater. Fig 6.8 (projected part up to 30 hr) shows the sudden decrease of the phenol from the solution due to adsorption onto BACPA-700-1.5. In the first stage of the process, the phenol concentration reduced drastically, the toxicity effect on the biomass due to high phenol concentration was decreased, and after that, the biodegradation process was initialized.

6.2.3. Effect of V_b/V_r ratio

Figure 6.9 depicts that degradation of phenol depends on V_b/V_r ratio. Maximum degradation rate is found to take place with V_b/V_r of 0.55, and at the ratios; 0.50 and 0.60, the

degradation rate is less, but ratio 0.60 is better to 0.50. Fig 6.9 shows the sudden decrease of the phenol from the solution due to adsorption onto BACPA-700-1.5 with time. The ratio, V_b/V_r of 0.55 is found to be optimum, where the biomass grown on the support media (Shieh and Keenan, 1986; Sokół, 2003; Sokół and Halfani, 1999). At higher ratio than 0.55, the decrease in biodegradation may be due to the fact that a significant volume of the bioreactor was occupied by the bioparticles, and consequently the aeration characteristic of the bed and phase mixing was poor (Ochieng et al., 2002; Sokół, 2001, 2003; Sokół and Halfani, 1999). The ratio (V_b/V_r) 0.6 was found to be the critical value and above which the fluidization of particles was impossible as it settled at the top of the reactor for the gas and liquid velocity combination studied.

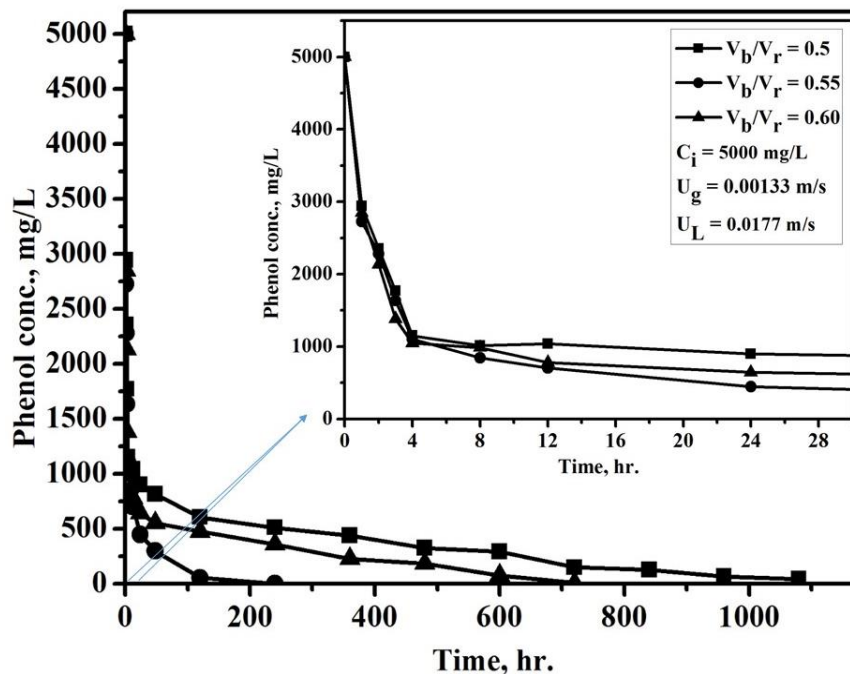


Fig. 6.9. Degradation of phenol with time for various V_b/V_r ratios by BPAC-700-1.5.

6.2.4. Effect of initial phenol concentrations

Three initial concentrations of phenol such as 5000, 7500, 10000 mg/L were considered to see the effect of initial concentration on the degradation of phenol in the fluidized bed bioreactor. Figure 6.10 shows the variation in concentration of phenol in the solution treated in the FBBR with time for different initial concentrations of phenol. It is observed that the phenol degradation time increases with the increase in the concentration of phenol. A short time is taken as 240 hr for the degradation of 5000 mg/L initial concentration of phenol than other used phenol concentration, for 7500 mg/L the time was 480 hr. 10000 mg/L has taken a very long time for degradation. As shown in Fig. 6.10, at 600 hr, 643.8 mg/L of phenol is still left in the solution for initial phenol concentration of 10000 mg/L. For higher

concentration of phenol above 5000 mg/L, the bulk concentration is not reduced to 1000 mg/L in 4 hr. After 24 hr, the concentration was 2028 mg/L for initial concentration of 10000 mg/L.

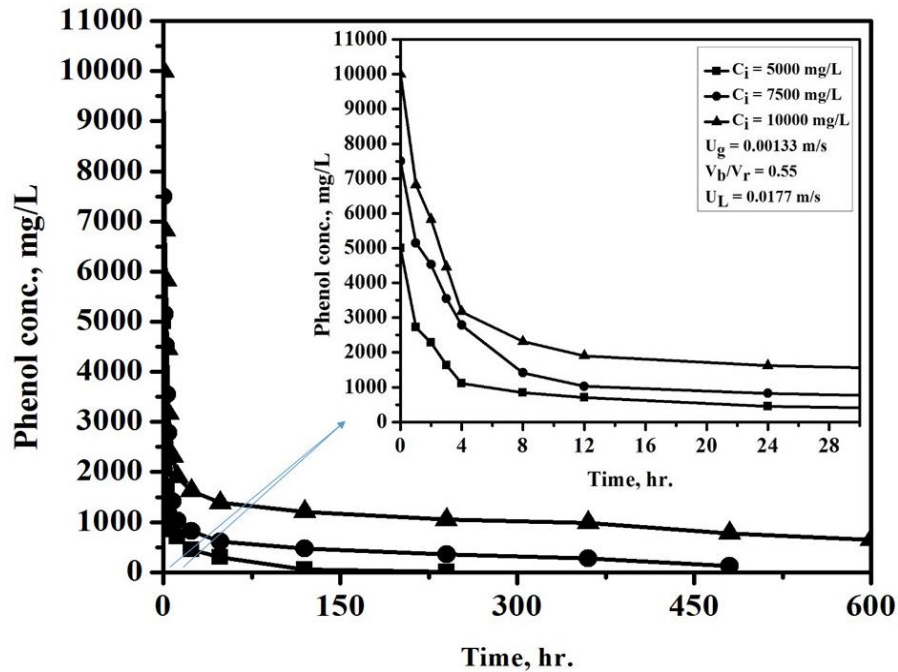


Fig. 6.10. Degradation of phenol of different initial concentration by BACPA-700-1.5.

6.3. Cyclic degradation of phenol in FBBR

The FBBR using BACPA-700-1.5 for phenol degradation as discussed was used for one cycle of treatment only. In the batch biodegradation study (section-5.3), the BACPA-700-1.5 was used for three cycles to see any change in its efficiency. Here a cyclic degradation study of phenol in FBBR using BACPA-700-1.5 was investigated. 5 L of 5000 mg/L of phenol solution was used in the study till no phenol was left in the solution, the same was repeated twice more i.e. three cycles of degradation was studied. Fig. 6.11 shows the phenol degradation profile BACPA-700-1.5 in three consecutive experimental cycles. The results demonstrate that in the adsorption assisted biodegradation the activated carbon is perfectly bio regenerated. When the initial phenol concentration was 5000 mg/L, the time required for complete degradation of phenol by immobilized cells is 30 days. In the second cycle most effective degradation was achieved, may be due to optimum growth of biomass. The adsorption found be slower cycle to cycle. In the third cycle both adsorption and subsequent biodegradation, both are delayed. From the study it is evidenced that FBBR with phenol degrading biomass laden activated carbon suitably be used for the treatment of high concentration phenol in wastewater.

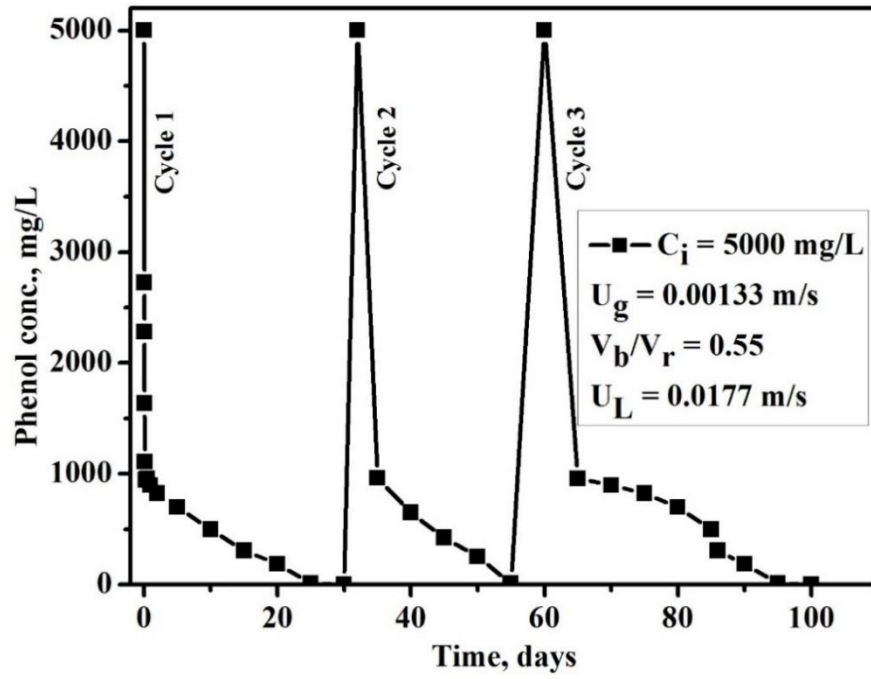


Fig. 6.11. Cyclic degradation of phenol in FBBR.

Chapter-7

Conclusions and Future Scope

7.1. Conclusions

Considering the fresh water crisis, contamination of natural water bodies by various polluting streams discharged to them, recycle and reuse of the industrial water is imperative. This can be achieved by the use of suitable treatment technologies. The industrial and municipal wastewater contain various types of organic and inorganic pollutants. They are mainly of three type phenols, dyes and heavy metals. In the present work one out of each type as mentioned, those are highly persistent in the environment; phenol, methylene blue (MB) and Cr(VI) were considered for treatment. As evidenced from the literature, the high efficient and easy to use method, adsorption by activated carbon was used for the treatment of water containing the mentioned pollutants. Both batch using shake flask and continuous using fixed bed column containing activated carbon were used in the adsorption study. In addition, the literature reveals that biological treatment is attractive of organics like phenol, as it consumes the same completely without any innocuous end product. Thus, the same is also considered in the present work for treatment of phenol. In the biodegradation study of phenol, microbial cells immobilized on activated carbon were used, where the process is not only biodegradation but also adsorption assisted biodegradation. Apart from batch biodegradation the same was done in a fluidized bed biofilm reactor (FBBR) (semi-continuous one), which has viability in actual treatment process. In the adsorption process, the main bottleneck is the cost of the activated carbon used and its capacity of adsorption. Thus in the past many attempts were made to prepare high adsorbing capacity activated carbon from some cheap precursors or waste materials. In the present work, an attempt was made to prepare activated carbon through efficient chemical activation route from one agricultural waste material, Fox nutshell having high volatile content (70.1%) and low ash content (5%). The work carried out in the order; literature review, preparation and characterization of activated carbon from Fox nutshell, use of prepared activated carbon in the adsorption of phenol, MB and Cr(VI), batch adsorption assisted biodegradation study of phenol, lastly biodegradation using FBBR. The major conclusions drawn from the present study are listed below.

Activated carbons were prepared from Fox nutshell by chemical activation method using zinc chloride, orthophosphoric acid, and potassium carbonate, named as ACZC, ACPA and ACPC. Carbonization temperatures; 600 °C, 700 °C, and 800 °C and impregnation ratios; 2, 1.5, and 0.5 were found to be the best in getting high surface area and high pore volume carbons with the use chemical activators, ZnCl₂, H₃PO₄, and K₂CO₃ respectively and the carbons prepared at these conditions were named as ACZC-600-2.0, ACPA-700-1.5, and ACPC-800-0.5, respectively.

- Maximum yields of 32.83%, 30.31%, and 22.99% were obtained at favorable process conditions for ACZC-600-2.0, ACPA-700-1.5, and ACPC-800-0.5, respectively.

The prepared activated carbons were characterized by different techniques like N₂ adsorption-desorption for surface area, FTIR analysis for surface functionality, XRD analysis for amorphous nature, FESEM for surface morphology, EDX for surface compositions and TEM for micropores arrangement on the surface.

- The BET surface area, total pore volume, and micropore volume of ACZC-600-2.0 is found to be 2869 m²/g, 1.96 cm³/g, and 1.68 cm³/g, respectively, and the microporosity is found to be 85.71%.
- For ACPA-700-1.5, the BET surface area, total pore volume and micropore volume of is found to be 2636 m²/g, 1.53 cm³/g, and 1.32 cm³/g, respectively.
- For the activated carbon was prepared with a K₂CO₃ activator, ACPC-800-0.5 the BET surface area, total pore volume and micropore volume is obtained as 1236 m²/g, 0.98 cm³/g, and 0.68 cm³/g, respectively.

The results of Fourier transform infrared spectroscopy analysis of the prepared activated carbons confirm that the carbons have abundant functional groups on their surface. Field emission scanning electron micrographs of the prepared activated carbons show that the porous materials formed during activation.

- The surface total acidic groups are larger than the total basic groups in all three prepared activated carbons. In ACZC-600-2.0, lactonic group is more than the carboxylic group, but in the other two carbons, ACPA-700-1.5 and ACPC-800-0.5 the carboxylic group is more than the lactonic group.
- The PZC values of ACZC-600-2.0, ACPA-700-1.5, and ACPC-800-0.5 are 2.1, 2.7 and 5.4, respectively.

- Honeycomb shape like structure is formed on the surface of the prepared activated carbon, ACZC-600-2.0 whereas ACPC-800-0.5 surface looks like a sponge with pores of different size and shapes.

Out of the three activated carbons prepared, ACZC-600-2.0, ACPA-700-1.5 were used as adsorbents for the further studies since they have very high surface area. The prepared materials were used for the removal of different pollutants like methylene blue, phenol and Cr(VI) from aqueous solution in batch and fixed packed bed scale. The influence of various system variables was investigated to obtain the maximal adsorption capacity of the ACs.

- Adsorption capacity of 500 mg/L of initial phenol concentration onto ACZC-600-2.0 and ACPA-700-1.5 are 75.73 and 83.21 mg/g, respectively. The equilibrium adsorption isotherms for adsorption of phenol on the ACZC-600-2.0 follows: Langmuir > Tempkin > Freundlich and for ACPA-700-1.5 as Freundlich > Langmuir > Tempkin.
- The adsorption capacity of MB onto ACZC-600-2.0 and ACPA-700-1.5 are 968.74 and 766.53 mg/g, respectively for 500 mg/L of initial concentration. The equilibrium adsorption isotherms for adsorption of MB on the ACZC-600-2.0 and ACPA-700-1.5 are Langmuir > Freundlich > Tempkin and Langmuir > Tempkin > Freundlich, respectively.
- Adsorption capacity of Cr(VI) onto ACZC-600-2.0 and ACPA-700-1.5 are 43.45 and 56.31 mg/g, respectively of 25 mg/L initial concentration. The equilibrium adsorption isotherms for adsorption of Cr(VI) onto ACZC-600-2.0 and ACPA-700-1.5 are in the order Langmuir > Freundlich > Tempkin.

The batch adsorption assisted biodegradation study of phenol by immobilized *Pseudomonas putida* (MTCC 1194) onto activated carbon (ACPC-700-1.5) confirms the efficiency of the method in treating higher concentration of phenol within a reasonable time.

- The acclimatized *Pseudomonas putida* (MTCC 1194) can actually remove phenol up to 1000 mg/L concentration in 180 hr.
- The BGAC removes phenol of 2300 mg/L concentration in 248 hr in batch scale.

Considering the superiority of BACPA-700-1.5 in treating the highly concentrated phenol, the same has been used in FBBR. A FBBR was designed, fabricated and used for the hydrodynamic study using ACPA-700-1.5 and adsorption assisted biodegradation study of phenol using BACPA-700-1.5.

- The hydrodynamic parameters characterized; pressure drop, minimum fluidization velocity, bed expansion and air holdup provide information (power requirement, solid concentration, size of the vessel, operating velocity) useful in design and operation of FBBR.
- Pressure drop found to increase with bed mass. Bed expansion increases both with increase in liquid and gas velocities. Air holdup found to be adequate (3.3–5.9 %) in maintaining the oxygen concentration over the experimental range.
- The BGAC in fluidized bioreactor removes of 5000 mg/L of phenol concentration of in 240 hr with an optimum condition; superficial liquid velocity of 0.0177 m/s, V_b/V_r ratio of 0.55 and a superficial air velocity of 0.00133 m/s.

The breakthrough achievements of this work are

- High surface area activated carbon from new precursor as Fox nutshell which is found highly efficient in adsorbing phenol, MB and Cr(VI).
- The adsorption-assisted biodegradation found to be viable and efficient as the degradation efficiency increases many fold and the adsorbents could be repeatedly used for a long time both in batch mode and in continuous fluidized bed bioreactor.

7.2. Future scope of the work

- Formulation of activated carbons from Fox nutshell could be carried out by physical and mixed activation method. Adsorption properties of the prepared activated carbons (ACs) could be improved by using ammonia aqueous solution impregnation, microwave irradiation, acid treatment and oxidization in an atmosphere of N_2 or H_2 .
- The prepared ACs can be utilized for the treatment of various other pollutants frequently found in wastewater streams. They could be directly employed for treatment of industrial wastewaters.
- Statistical optimization method can be adopted to better optimize process for the preparation of high surface area activated carbon and better adsorption of pollutants.
- A comparative study on the biosorption of pollutants like MB, Cr(VI) and other phenolic compounds can be undertaken in packed bed as well as in FBBR.
- Degradation efficiency of biomass laden activated carbon can be verified for a large number cycles.

References

- Abussaud, B., Asmaly, H.A., Saleh, T.A., Gupta, V.K., Atieh, M.A., 2016. Sorption of phenol from waters on activated carbon impregnated with iron oxide, aluminum oxide and titanium oxide. *Journal of Molecular Liquids* 213, 351-359.
- Acar, F., Malkoc, E., 2004. The removal of chromium(VI) from aqueous solutions by *Fagus orientalis* L. *Bioresource Technology* 94, 13-15.
- Adav, S.S., Chen, M.-Y., Lee, D.-J., Ren, N.-Q., 2007. Degradation of phenol by *Acinetobacter* strain isolated from aerobic granules. *Chemosphere* 67, 1566-1572.
- Adinata, D., Daud, W.M.A.W., Aroua, M.K., 2007. Preparation and characterization of activated carbon from palm shell by chemical activation with K_2CO_3 . *Bioresource Technology* 98, 145-149.
- Agarwal, B., Balomajumdar, C., 2013. Simultaneous adsorption and biodegradation of phenol and cyanide in multicomponent system. *International Journal of Environmental Engineering and Management* 4, 233-238.
- Agarwal, S.K., 2005. *Water pollution*. APH Publishing Corporation, New Delhi, 1-2.
- Ahammad, S.Z., Davenport, R.J., Read, L.F., Gomes, J., Sreekrishnan, T.R., Dolfing, J., 2013. Rational immobilization of methanogens in high cell density bioreactors. *RSC Advances* 3, 774-781.
- Ahmad, A., Hameed, B., 2010. Fixed-bed adsorption of reactive azo dye onto granular activated carbon prepared from waste. *Journal of Hazardous Materials* 175, 298-303.
- Ahmad, F., Daud, W.M.A.W., Ahmad, M.A., Radzi, R., 2012. Cocoa (*Theobroma cacao*) shell-based activated carbon by CO_2 activation in removing of Cationic dye from aqueous solution: Kinetics and equilibrium studies. *Chemical engineering research and design* 90, 1480-1490.
- Ahmadpour, A., Do, D., 1997. The preparation of activated carbon from macadamia nutshell by chemical activation. *Carbon* 35, 1723-1732.
- Ahmaruzzaman, M., 2008. Adsorption of phenolic compounds on low-cost adsorbents: a review. *Advances in Colloid and Interface Science* 143, 48-67.
- Ahmaruzzaman, M., Sharma, D., 2005. Adsorption of phenols from wastewater. *Journal of Colloid and Interface Science* 287, 14-24.
- Ajouyed, O., Hurel, C., Ammari, M., Allal, L.B., Marmier, N., 2010. Sorption of Cr(VI) onto natural iron and aluminum (oxy) hydroxides: effects of pH, ionic strength and initial concentration. *Journal of Hazardous Materials* 174, 616-622.
- Aksu, Z., 2005. Application of biosorption for the removal of organic pollutants: a review. *Process biochemistry* 40, 997-1026.
- Aksu, Z., Bülbül, G., 1999. Determination of the effective diffusion coefficient of phenol in Ca-alginate-immobilized *P. putida* beads. *Enzyme and Microbial technology* 25, 344-348.
- Aksu, Z., Gönen, F., 2004. Biosorption of phenol by immobilized activated sludge in a continuous packed bed: prediction of breakthrough curves. *Process biochemistry* 39, 599-613.
- Aktaş, Ö., Çeçen, F., 2007. Bioregeneration of activated carbon: a review. *International Biodeterioration & Biodegradation* 59, 257-272.

- Alabadi, A., Razzaque, S., Yang, Y., Chen, S., Tan, B., 2015. Highly porous activated carbon materials from carbonized biomass with high CO₂ capturing capacity. *Chemical Engineering Journal* 281, 606-612.
- Alaerts, G., Jitjaturunt, V., Kelderman, P., 1989. Use of coconut shell-based activated carbon for chromium(VI) removal. *Water science and technology* 21, 1701-1704.
- Alaya, M., Girgis, B., Mourad, W., 2000. Activated carbon from some agricultural wastes under action of one-step steam pyrolysis. *Journal of Porous Materials* 7, 509-517.
- Ali, I., Asim, M., Khan, T.A., 2012. Low cost adsorbents for the removal of organic pollutants from wastewater. *Journal of environmental management* 113, 170-183.
- Allia, K., Tahar, N., Toumi, L., Salem, Z., 2006. Biological treatment of water contaminated by hydrocarbons in three-phase gas-liquid-solid fluidized bed. *Glob. NEST J* 8, 9-15.
- AlOthman, Z.A., Habila, M.A., Ali, R., Ghafar, A.A., Hassouna, M.S.E.-d., 2014. Valorization of two waste streams into activated carbon and studying its adsorption kinetics, equilibrium isotherms and thermodynamics for methylene blue removal. *Arabian Journal of Chemistry* 7, 1148-1158.
- Altenor, S., Carene, B., Emmanuel, E., Lambert, J., Ehrhardt, J.-J., Gaspard, S., 2009. Adsorption studies of methylene blue and phenol onto vetiver roots activated carbon prepared by chemical activation. *Journal of Hazardous Materials* 165, 1029-1039.
- Amor, L., Eiroa, M., Kennes, C., Veiga, M.C., 2005. Phenol biodegradation and its effect on the nitrification process. *Water research* 39, 2915-2920.
- Andersson, S., Dalhammar, G., Land, C.J., Rajarao, G.K., 2009. Characterization of extracellular polymeric substances from denitrifying organism *Comamonas denitrificans*. *Applied microbiology and biotechnology* 82, 535-543.
- Angin, D., 2014. Production and characterization of activated carbon from sour cherry stones by zinc chloride. *Fuel* 115, 804-811.
- Angin, D., Altintig, E., Köse, T.E., 2013. Influence of process parameters on the surface and chemical properties of activated carbon obtained from biochar by chemical activation. *Bioresource technology* 148, 542-549.
- Anliker, R., Dürig, G., Steinle, D., Moriconi, E., 1988. List of colorants to be classified as toxic. *Journal of the Society of Dyers and Colourists* 104, 223-225.
- Annadurai, G., Balan, S.M., Murugesan, T., 1999. Box-Behnken design in the development of optimized complex medium for phenol degradation using *Pseudomonas putida* (NICM-2174). *Bioprocess Engineering* 21, 415-421.
- Annadurai, G., Balan, S.M., Murugesan, T., 2000. Design of experiments in the biodegradation of phenol using immobilized *Pseudomonas pictorum* (NICM-2077) on activated carbon. *Bioprocess Engineering* 22, 101-107.
- Annadurai, G., Ling, L.Y., Lee, J.-F., 2008. Statistical optimization of medium components and growth conditions by response surface methodology to enhance phenol degradation by *Pseudomonas putida*. *Journal of Hazardous Materials* 151, 171-178.
- Aravindhan, R., Rao, J.R., Nair, B.U., 2009. Preparation and characterization of activated carbon from marine macro-algal biomass. *Journal of Hazardous Materials* 162, 688-694.

- Auta, M., Hameed, B., 2011. Optimized waste tea activated carbon for adsorption of Methylene Blue and Acid Blue 29 dyes using response surface methodology. *Chemical Engineering Journal* 175, 233-243.
- Auta, M., Hameed, B., 2014. Chitosan–clay composite as highly effective and low-cost adsorbent for batch and fixed-bed adsorption of methylene blue. *Chemical Engineering Journal* 237, 352-361.
- Aygün, A., Yenisoy-Karakaş, S., Duman, I., 2003. Production of granular activated carbon from fruit stones and nutshells and evaluation of their physical, chemical and adsorption properties. *Microporous and Mesoporous Materials* 66, 189-195.
- Azevedo, D.C., Araujo, J.C.S., Bastos-Neto, M., Torres, A.E.B., Jaguaribe, E.F., Cavalcante, C.L., 2007. Microporous activated carbon prepared from coconut shells using chemical activation with zinc chloride. *Microporous and Mesoporous Materials* 100, 361-364.
- Babel, S., Kurniawan, T.A., 2004. Cr(VI) removal from synthetic wastewater using coconut shell charcoal and commercial activated carbon modified with oxidizing agents and/or chitosan. *Chemosphere* 54, 951-967.
- Baçaçoui, A., Yaacoubi, A., Dahbi, A., Bennouna, C., Luu, R.P.T., Maldonado-Hodar, F., Rivera-Utrilla, J., Moreno-Castilla, C., 2001. Optimization of conditions for the preparation of activated carbons from olive-waste cakes. *Carbon* 39, 425-432.
- Baccar, R., Bouzid, J., Feki, M., Montiel, A., 2009. Preparation of activated carbon from Tunisian olive-waste cakes and its application for adsorption of heavy metal ions. *Journal of Hazardous Materials* 162, 1522-1529.
- Banat, F., Al-Bashir, B., Al-Asheh, S., Hayajneh, O., 2000. Adsorption of phenol by bentonite. *Environmental pollution* 107, 391-398.
- Bandhyopadhyay, K., Das, D., Bhattacharyya, P., Maiti, B., 2001. Reaction engineering studies on biodegradation of phenol by *Pseudomonas putida* MTCC 1194 immobilized on calcium alginate. *Biochemical Engineering Journal* 8, 179-186.
- Banerjee, A., Ghoshal, A.K., 2010. Isolation and characterization of hyper phenol tolerant *Bacillus* sp. from oil refinery and exploration sites. *Journal of Hazardous Materials* 176, 85-91.
- Banerjee, A., Ghoshal, A.K., 2011. Phenol degradation performance by isolated *Bacillus cereus* immobilized in alginate. *International Biodeterioration & Biodegradation* 65, 1052-1060.
- Banerjee, A., Ghoshal, A.K., 2016. Biodegradation of real petroleum wastewater by immobilized hyper phenol-tolerant strains of *Bacillus cereus*. *3 Biotech* 6, 1-4.
- Bansal, R.C., Donnet, J.-B., Stoeckli, F., 1988. *Active carbon*. Ed. Marcel Dekker (New York). 482p.
- Bansal, R.C., Goyal, M., 2005. *Activated carbon adsorption*. CRC press, 1-21.
- Baquero, M., Giraldo, L., Moreno, J., Suárez-García, F., Martí, A., Tascon, J., 2003. Activated carbons by pyrolysis of coffee bean husks in presence of phosphoric acid. *Journal of Analytical and Applied Pyrolysis* 70, 779-784.
- Basha, K.M., Rajendran, A., Thangavelu, V., 2010. Recent advances in the biodegradation of phenol: a review. *Asian J Exp Biol Sci* 1, 219-234.

- Bastos, A., Tornisielo, V., Nozawa, S., Trevors, J., Rossi, A., 2000. Phenol metabolism by two microorganisms isolated from Amazonian forest soil samples. *Journal of industrial microbiology and Biotechnology* 24, 403-409.
- Begum, S.S., Radha, K., 2014. Hydrodynamic behavior of inverse fluidized bed biofilm reactor for phenol biodegradation using *Pseudomonas fluorescens*. *Korean Journal of Chemical Engineering* 31, 436-445.
- Beker, U., Ganbold, B., Dertli, H., Gülbayir, D.D., 2010. Adsorption of phenol by activated carbon: Influence of activation methods and solution pH. *Energy Conversion and Management* 51, 235-240.
- Benhouria, A., Islam, M.A., Zaghouane-Boudiaf, H., Boutahala, M., Hameed, B., 2015. Calcium alginate–bentonite–activated carbon composite beads as highly effective adsorbent for methylene blue. *Chemical Engineering Journal* 270, 621-630.
- Bernal, J., 1924. The structure of graphite. *Proceedings of the Royal Society of London. Series A, Containing Papers of a Mathematical and Physical Character* 106, 749-773.
- Berrios, M., Martín, M.Á., Martín, A., 2012. Treatment of pollutants in wastewater: Adsorption of methylene blue onto olive-based activated carbon. *Journal of Industrial and Engineering Chemistry* 18, 780-784.
- Beyenal, H., Tanyolaç, A., 1998. The effects of biofilm characteristics on the external mass transfer coefficient in a differential fluidized bed biofilm reactor. *Biochemical Engineering Journal* 1, 53-61.
- Biscoe, J., Warren, B., 1942. An X-Ray Study of Carbon Black. *Journal of Applied Physics* 13, 364-371.
- Boehm, H., 1994. Some aspects of the surface chemistry of carbon blacks and other carbons. *Carbon* 32, 759-769.
- Boehm, H., 2002. Surface oxides on carbon and their analysis: a critical assessment. *Carbon* 40, 145-149.
- Bouchenafa-Saib, N., Grange, P., Verhasselt, P., Addoun, F., Dubois, V., 2005. Effect of oxidant treatment of date pit active carbons used as Pd supports in catalytic hydrogenation of nitrobenzene. *Applied Catalysis A: General* 286, 167-174.
- Briens, L.A., Ellis, N., 2005. Hydrodynamics of three-phase fluidized bed systems examined by statistical, fractal, chaos and wavelet analysis methods. *Chemical engineering science* 60, 6094-6106.
- Brink, N., 1975. Water pollution from agriculture. *Journal (Water Pollution Control Federation)*, 789-795.
- Brunauer, S., Emmett, P.H., Teller, E., 1938. Adsorption of gases in multimolecular layers. *Journal of the American chemical society* 60, 309-319.
- Budinova, T., Ekinçi, E., Yardim, F., Grimm, A., Björnbohm, E., Minkova, V., Goranova, M., 2006. Characterization and application of activated carbon produced by H₃PO₄ and water vapor activation. *Fuel Processing Technology* 87, 899-905.
- Bulut, Y., Aydın, H., 2006. A kinetics and thermodynamics study of methylene blue adsorption on wheat shells. *Desalination* 194, 259-267.

- Cagnon, B., Py, X., Guillot, A., Joly, J., Berjoan, R., 2005. Pore structure modification of pitch-based activated carbon by NaOCl and air oxidation/pyrolysis cycles. *Microporous and mesoporous materials* 80, 183-193.
- Cagnon, B., Py, X., Guillot, A., Stoeckli, F., Chambat, G., 2009. Contributions of hemicellulose, cellulose and lignin to the mass and the porous properties of chars and steam activated carbons from various lignocellulosic precursors. *Bioresource Technology* 100, 292-298.
- Carvalho, M., Duque, A., Gonçalves, I., Castro, P., 2007. Adsorption of fluorobenzene onto granular activated carbon: Isotherm and bioavailability studies. *Bioresource technology* 98, 3424-3430.
- Caturla, F., Molina-Sabio, M., Rodriguez-Reinoso, F., 1991. Preparation of activated carbon by chemical activation with ZnCl₂. *Carbon* 29, 999-1007.
- Caza, N., Bewtra, J., Biswas, N., Taylor, K., 1999. Removal of phenolic compounds from synthetic wastewater using soybean peroxidase. *Water research* 33, 3012-3018.
- Cazetta, A.L., Vargas, A.M., Nogami, E.M., Kunita, M.H., Guilherme, M.R., Martins, A.C., Silva, T.L., Moraes, J.C., Almeida, V.C., 2011. NaOH-activated carbon of high surface area produced from coconut shell: Kinetics and equilibrium studies from the methylene blue adsorption. *Chemical Engineering Journal* 174, 117-125.
- Chakrabarti, T., Subrahmanyam, P., Sundaresan, B., Wise, D., 1988. Biodegradation of recalcitrant industrial wastes. *Biotreatment systems, Volume II.* 171-234.
- Chang, C.-F., Chang, C.-Y., Tsai, W.-T., 2000. Effects of burn-off and activation temperature on preparation of activated carbon from corn cob agrowaste by CO₂ and steam. *Journal of Colloid and Interface Science* 232, 45-49.
- Chen, K.-C., Lin, Y.-H., Chen, W.-H., Liu, Y.-C., 2002. Degradation of phenol by PAA-immobilized *Candida tropicalis*. *Enzyme and Microbial technology* 31, 490-497.
- Chen, S.-Y., Guo, L.-Y., Bai, J.-G., Zhang, Y., Zhang, L., Wang, Z., Chen, J.-X., Yang, H.-X., Wang, X.-J., 2015. Biodegradation of p-hydroxybenzoic acid in soil by *Pseudomonas putida* CSY-P1 isolated from cucumber rhizosphere soil. *Plant and Soil* 389, 197-210.
- Chen, W., Liu, X., He, R., Lin, T., Zeng, Q., Wang, X., 2013. Activated carbon powders from wool fibers. *Powder technology* 234, 76-83.
- Chen, Y., Huang, B., Huang, M., Cai, B., 2011. On the preparation and characterization of activated carbon from mangosteen shell. *Journal of the Taiwan Institute of Chemical Engineers* 42, 837-842.
- Chern, J.-M., Chien, Y.-W., 2002. Adsorption of nitrophenol onto activated carbon: isotherms and breakthrough curves. *Water research* 36, 647-655.
- Chern, J.-M., Chien, Y.-W., 2003. Competitive adsorption of benzoic acid and p-nitrophenol onto activated carbon: isotherm and breakthrough curves. *Water research* 37, 2347-2356.
- Chiang, P., Chang, E., Wu, J., 1997. Comparison of chemical and thermal regeneration of aromatic compounds on exhausted activated carbon. *Water science and technology* 35, 279-285.

- Chung, T.-P., Tseng, H.-Y., Juang, R.-S., 2003. Mass transfer effect and intermediate detection for phenol degradation in immobilized *Pseudomonas putida* systems. *Process biochemistry* 38, 1497-1507.
- Cimino, G., Passerini, A., Toscano, G., 2000. Removal of toxic cations and Cr(VI) from aqueous solution by hazelnut shell. *Water research* 34, 2955-2962.
- Combarros, R., Rosas, I., Lavín, A., Rendueles, M., Díaz, M., 2014. Influence of biofilm on activated carbon on the adsorption and biodegradation of salicylic acid in wastewater. *Water, Air, & Soil Pollution* 225, 1-12.
- Corcho-Corral, B., Olivares-Marín, M., Fernandez-Gonzalez, C., Gomez-Serrano, V., Macías-García, A., 2006. Preparation and textural characterisation of activated carbon from vine shoots (*Vitis vinifera*) by H₃PO₄—chemical activation. *Applied Surface Science* 252, 5961-5966.
- Cox, P., 2000. *Advanced Inorganic Chemistry*, by FA Cotton, G. Wilkinson, CA Murillo and M. Bochmann, Wiley, Chichester, 1999. xv+ 1355 pp., ISBN 0-471-19957-5. £ 58.50. Elsevier.
- Crini, G., 2005. Recent developments in polysaccharide-based materials used as adsorbents in wastewater treatment. *Progress in polymer science* 30, 38-70.
- Crini, G., 2006. Non-conventional low-cost adsorbents for dye removal: a review. *Bioresource technology* 97, 1061-1085.
- Cuhadar, C., 2005. Production and characterization of activated carbon from hazelnut shell and hazelnut husk. Middle East Technical University, 1-19.
- Dąbrowski, A., Podkościelny, P., Hubicki, Z., Barczak, M., 2005. Adsorption of phenolic compounds by activated carbon—a critical review. *Chemosphere* 58, 1049-1070.
- Danish, M., Hashim, R., Ibrahim, M.M., Sulaiman, O., 2014. Optimization study for preparation of activated carbon from *Acacia mangium* wood using phosphoric acid. *Wood science and technology* 48, 1069-1083.
- Dash, R.R., Balomajumder, C., Kumar, A., 2009. Treatment of cyanide bearing water/wastewater by plain and biological activated carbon. *Industrial & engineering chemistry research* 48, 3619-3627.
- de Yuso, A.M., Rubio, B., Izquierdo, M.T., 2014. Influence of activation atmosphere used in the chemical activation of almond shell on the characteristics and adsorption performance of activated carbons. *Fuel Processing Technology* 119, 74-80.
- Demiral, H., Demiral, I., Tümsek, F., Karabacakoglu, B., 2008. Adsorption of chromium(VI) from aqueous solution by activated carbon derived from olive bagasse and applicability of different adsorption models. *Chemical Engineering Journal* 144, 188-196.
- Demiral, H., Gündüzoğlu, G., 2010. Removal of nitrate from aqueous solutions by activated carbon prepared from sugar beet bagasse. *Bioresource technology* 101, 1675-1680.
- Demiral, İ., Aydın Şamdan, C., Demiral, H., 2015. Production and characterization of activated carbons from pumpkin seed shell by chemical activation with ZnCl₂. *Desalination and Water Treatment*, 1-9.
- Demirbas, A., 2009. Agricultural based activated carbons for the removal of dyes from aqueous solutions: a review. *Journal of hazardous materials* 167, 1-9.

- Deng, H., Yang, L., Tao, G., Dai, J., 2009. Preparation and characterization of activated carbon from cotton stalk by microwave assisted chemical activation—application in methylene blue adsorption from aqueous solution. *Journal of Hazardous Materials* 166, 1514-1521.
- Derylo-Marczewska, A., Swiatkowski, A., Biniak, S., Walczyk, M., 2008. Effect of properties of chemically modified activated carbon and aromatic adsorbate molecule on adsorption from liquid phase. *Colloids and Surfaces A: Physicochemical and Engineering Aspects* 327, 1-8.
- Dias, J.M., Alvim-Ferraz, M.C., Almeida, M.F., Rivera-Utrilla, J., Sánchez-Polo, M., 2007. Waste materials for activated carbon preparation and its use in aqueous-phase treatment: a review. *Journal of Environmental Management* 85, 833-846.
- Din, A.T.M., Hameed, B., Ahmad, A.L., 2009. Batch adsorption of phenol onto physiochemical-activated coconut shell. *Journal of Hazardous Materials* 161, 1522-1529.
- Duan, X., Peng, J., Srinivasakannan, C., Zhang, L., Xia, H., Yang, K., Zhang, Z., 2011. Process optimization for the preparation of activated carbon from *Jatropha* hull using response surface methodology. *Energy Sources, Part A: Recovery, Utilization, and Environmental Effects* 33, 2005-2017.
- Dubinin, M., Astakhov, V., 1971. Description of adsorption equilibria of vapors on zeolites over wide ranges of temperature and pressure. *Advances in Chemistry* 102, Chapter 44, 69–85.
- Dursun, A.Y., Tepe, O., 2005. Internal mass transfer effect on biodegradation of phenol by *Ca*-alginate immobilized *Ralstonia eutropha*. *Journal of Hazardous Materials* 126, 105-111.
- Dwivedi, C.P., Sahu, J., Mohanty, C., Mohan, B.R., Meikap, B., 2008. Column performance of granular activated carbon packed bed for Pb(II) removal. *Journal of Hazardous Materials* 156, 596-603.
- El-Naas, M.H., Al-Muhtaseb, S.A., Makhlof, S., 2009. Biodegradation of phenol by *Pseudomonas putida* immobilized in polyvinyl alcohol (PVA) gel. *Journal of Hazardous Materials* 164, 720-725.
- El-Sayed, Y., Bandosz, T.J., 2004. Adsorption of valeric acid from aqueous solution onto activated carbons: role of surface basic sites. *Journal of colloid and interface science* 273, 64-72.
- El-Sikaily, A., El Nemr, A., Khaled, A., Abdelwehab, O., 2007. Removal of toxic chromium from wastewater using green alga *Ulva lactuca* and its activated carbon. *Journal of Hazardous Materials* 148, 216-228.
- Eswari, A., Rajendran, L., 2012. Approximate analytical solution of the concentration of phenol and oxygen and rate of phenol degradation in fluidized bed bioreactor. *Biochemical Engineering Journal* 68, 42-53.
- Everett, D.H., Powl, J.C., 1976. Adsorption in slit-like and cylindrical micropores in the henry's law region. A model for the microporosity of carbons. *Journal of the Chemical Society, Faraday Transactions 1: Physical Chemistry in Condensed Phases* 72, 619-636.
- Fan, L., Luo, C., Li, X., Lu, F., Qiu, H., Sun, M., 2012. Fabrication of novel magnetic chitosan grafted with graphene oxide to enhance adsorption properties for methyl blue. *Journal of Hazardous Materials* 215, 272-279.

- Fierro, V., Torné-Fernández, V., Celzard, A., 2006. Kraft lignin as a precursor for microporous activated carbons prepared by impregnation with ortho-phosphoric acid: synthesis and textural characterisation. *Microporous and mesoporous materials* 92, 243-250.
- Fierro, V., Torné-Fernández, V., Montané, D., Celzard, A., 2008. Adsorption of phenol onto activated carbons having different textural and surface properties. *Microporous and mesoporous materials* 111, 276-284.
- Figaro, S., Louisy-Louis, S., Lambert, J., Ehrhardt, J.-J., Ouensanga, A., Gaspard, S., 2006. Adsorption studies of recalcitrant compounds of molasses spentwash on activated carbons. *Water research* 40, 3456-3466.
- Fitzer, E., Kochling, K.-H., Boehm, H., Marsh, H., 1995. Recommended terminology for the description of carbon as a solid (IUPAC Recommendations 1995). *Pure and Applied Chemistry* 67, 473-506.
- Foo, K., Hameed, B., 2011. Preparation and characterization of activated carbon from sunflower seed oil residue via microwave assisted K_2CO_3 activation. *Bioresource technology* 102, 9794-9799.
- Foo, K., Hameed, B., 2012a. Mesoporous activated carbon from wood sawdust by K_2CO_3 activation using microwave heating. *Bioresource technology* 111, 425-432.
- Foo, K., Hameed, B., 2012b. Preparation, characterization and evaluation of adsorptive properties of orange peel based activated carbon via microwave induced K_2CO_3 activation. *Bioresource technology* 104, 679-686.
- Franz, M., Arafat, H.A., Pinto, N.G., 2000. Effect of chemical surface heterogeneity on the adsorption mechanism of dissolved aromatics on activated carbon. *Carbon* 38, 1807-1819.
- Freundlich, H., 1906. Over the adsorption in solution. *J. Phys. Chem* 57, 385-470.
- Gao, P., Liu, Z.-h., Xue, G., Han, B., Zhou, M.-h., 2011. Preparation and characterization of activated carbon produced from rice straw by $(NH_4)_2HPO_4$ activation. *Bioresource technology* 102, 3645-3648.
- Garg, V., Gupta, R., Kumar, R., Gupta, R., 2004a. Adsorption of chromium from aqueous solution on treated sawdust. *Bioresource Technology* 92, 79-81.
- Garg, V., Kumar, R., Gupta, R., 2004b. Removal of malachite green dye from aqueous solution by adsorption using agro-industry waste: a case study of *Prosopis cineraria*. *Dyes and Pigments* 62, 1-10.
- Gargouri, B., Karray, F., Mhiri, N., Aloui, F., Sayadi, S., 2011. Application of a continuously stirred tank bioreactor (CSTR) for bioremediation of hydrocarbon-rich industrial wastewater effluents. *Journal of Hazardous Materials* 189, 427-434.
- Gergova, K., Eser, S., 1996. Effects of activation method on the pore structure of activated carbons from apricot stones. *Carbon* 34, 879-888.
- Ghaedi, M., Ghazanfarkhani, M.D., Khodadoust, S., Sohrabi, N., Oftade, M., 2014. Acceleration of methylene blue adsorption onto activated carbon prepared from dross licorice by ultrasonic: Equilibrium, kinetic and thermodynamic studies. *Journal of Industrial and Engineering Chemistry* 20, 2548-2560.

- Ghosh, D., Bhattacharyya, K.G., 2002. Adsorption of methylene blue on kaolinite. *Applied Clay Science* 20, 295-300.
- Girgis, B.S., El-Hendawy, A.-N.A., 2002. Porosity development in activated carbons obtained from date pits under chemical activation with phosphoric acid. *Microporous and mesoporous materials* 52, 105-117.
- Girish, C., Murty, V.R., 2015. Adsorption of Phenol from Aqueous Solution Using *Lantana camara*, Forest Waste: Packed Bed Studies and Prediction of Breakthrough Curves. *Environmental Processes* 2, 773-796.
- Gokce, Y., Aktas, Z., 2014. Nitric acid modification of activated carbon produced from waste tea and adsorption of methylene blue and phenol. *Applied Surface Science* 313, 352-359.
- Gomez-Serrano, V., Cuerda-Correa, E., Fernandez-Gonzalez, M., Alexandre-Franco, M., Macias-Garcia, A., 2005. Preparation of activated carbons from chestnut wood by phosphoric acid-chemical activation. Study of microporosity and fractal dimension. *Materials Letters* 59, 846-853.
- Gonzalez, G., Herrera, G., Garcí, M.T., Pena, M., 2001. Biodegradation of phenolic industrial wastewater in a fluidized bed bioreactor with immobilized cells of *Pseudomonas putida*. *Bioresource technology* 80, 137-142.
- Goud, V.V., Mohanty, K., Rao, M., Jayakumar, N., 2005. Phenol removal from aqueous solutions by tamarind nutshell activated carbon: batch and column studies. *Chemical engineering & technology* 28, 814-821.
- Gregg, S.J., Sing, K.S.W., Salzberg, H., 1967. Adsorption surface area and porosity. *Journal of The Electrochemical Society* 114, 279C-279C.
- Guo, J., Lua, A.C., 2003. Textural and chemical properties of adsorbent prepared from palm shell by phosphoric acid activation. *Materials chemistry and physics* 80, 114-119.
- Gupta, A., Pal, A., Sahoo, C., 2006. Photocatalytic degradation of a mixture of Crystal Violet (Basic Violet 3) and Methyl Red dye in aqueous suspensions using Ag⁺ doped TiO₂. *Dyes and Pigments* 69, 224-232.
- Gupta, V., 2009. Application of low-cost adsorbents for dye removal—A review. *Journal of environmental management* 90, 2313-2342.
- Gurten, I.I., Ozmak, M., Yagmur, E., Aktas, Z., 2012. Preparation and characterisation of activated carbon from waste tea using K₂CO₃. *Biomass and bioenergy* 37, 73-81.
- Haimour, N., Emeish, S., 2006. Utilization of date stones for production of activated carbon using phosphoric acid. *Waste Management* 26, 651-660.
- Hall, K.R., Eagleton, L.C., Acrivos, A., Vermeulen, T., 1966. Pore- and solid-diffusion kinetics in fixed-bed adsorption under constant-pattern conditions. *Industrial & Engineering Chemistry Fundamentals* 5, 212-223.
- Hamadi, N.K., Chen, X.D., Farid, M.M., Lu, M.G., 2001. Adsorption kinetics for the removal of chromium(VI) from aqueous solution by adsorbents derived from used tyres and sawdust. *Chemical Engineering Journal* 84, 95-105.
- Hameed, B., Ahmad, A., Latiff, K., 2007a. Adsorption of basic dye (methylene blue) onto activated carbon prepared from rattan sawdust. *Dyes and Pigments* 75, 143-149.

- Hameed, B., Din, A.M., Ahmad, A., 2007b. Adsorption of methylene blue onto bamboo-based activated carbon: kinetics and equilibrium studies. *Journal of hazardous materials* 141, 819-825.
- Hameed, B., Rahman, A., 2008. Removal of phenol from aqueous solutions by adsorption onto activated carbon prepared from biomass material. *Journal of Hazardous Materials* 160, 576-581.
- Han, R., Zou, W., Yu, W., Cheng, S., Wang, Y., Shi, J., 2007. Biosorption of methylene blue from aqueous solution by fallen phoenix tree's leaves. *Journal of Hazardous Materials* 141, 156-162.
- Haritash, A., Kaushik, C., 2009. Biodegradation aspects of polycyclic aromatic hydrocarbons (PAHs): a review. *Journal of hazardous materials* 169, 1-15.
- Hayashi, J.i., Horikawa, T., Muroyama, K., Gomes, V.G., 2002a. Activated carbon from chickpea husk by chemical activation with K_2CO_3 : preparation and characterization. *Microporous and Mesoporous Materials* 55, 63-68.
- Hayashi, J.i., Horikawa, T., Takeda, I., Muroyama, K., Ani, F.N., 2002b. Preparing activated carbon from various nutshells by chemical activation with K_2CO_3 . *Carbon* 40, 2381-2386.
- Hayashi, J.i., Kazehaya, A., Muroyama, K., Watkinson, A.P., 2000. Preparation of activated carbon from lignin by chemical activation. *Carbon* 38, 1873-1878.
- Ho, Y.-S., McKay, G., 1999. Pseudo-second order model for sorption processes. *Process biochemistry* 34, 451-465.
- Hoang, T.T.L., 2005. Granular activated carbon (GAC) biofilter in water and wastewater treatment. M.E. Thesis. University of Technology, Sydney, 2-32.
- Holme, I., Griffiths, J., 1984. Developments in the chemistry and technology of organic dyes. Society of Chemistry Industry, Oxford, 111-128.
- Horváth, G., Kawazoe, K., 1983. Method for the calculation of effective pore size distribution in molecular sieve carbon. *Journal of Chemical Engineering of Japan* 16, 470-475.
- Hsu, L.-Y., Teng, H., 2000. Influence of different chemical reagents on the preparation of activated carbons from bituminous coal. *Fuel Processing Technology* 64, 155-166.
- Hu, Z., Srinivasan, M., 1999. Preparation of high-surface-area activated carbons from coconut shell. *Microporous and Mesoporous Materials* 27, 11-18.
- Hu, Z., Srinivasan, M., Ni, Y., 2001. Novel activation process for preparing highly microporous and mesoporous activated carbons. *Carbon* 39, 877-886.
- Hu, Z., Vansant, E., 1995. A new composite adsorbent produced by chemical activation of elutrilite with zinc chloride. *Journal of colloid and interface science* 176, 422-431.
- Huang, C.-C., Li, H.-S., Chen, C.-H., 2008. Effect of surface acidic oxides of activated carbon on adsorption of ammonia. *Journal of hazardous materials* 159, 523-527.
- Huang, Y., Li, S., Lin, H., Chen, J., 2014. Fabrication and characterization of mesoporous activated carbon from *Lemna minor* using one-step H_3PO_4 activation for Pb(II) removal. *Applied Surface Science* 317, 422-431.
- Ioannidou, O., Zabaniotou, A., 2007. Agricultural residues as precursors for activated carbon production—a review. *Renewable and Sustainable Energy Reviews* 11, 1966-2005.

- Islam, M.S., Dong, T., McPhedran, K.N., Sheng, Z., Zhang, Y., Liu, Y., El-Din, M.G., 2014. Impact of ozonation pre-treatment of oil sands process-affected water on the operational performance of a GAC-fluidized bed biofilm reactor. *Biodegradation* 25, 811-823.
- Ivancev-Tumbas, I., Dalmacija, B., Tamas, Z., Karlovic, E., 1998. Reuse of biologically regenerated activated carbon for phenol removal. *Water research* 32, 1085-1094.
- Jagtøyen, M., Derbyshire, F., 1998. Activated carbons from yellow poplar and white oak by H₃PO₄ activation. *Carbon* 36, 1085-1097.
- Jena, H., Roy, G., Meikap, B., 2005. Development and Comparative Study of a Semi-Fluidized Bed Bioreactor for the Treatment of Wastewater from Process Industries. *Process & Plant Engineering*, 23, 70-75.
- Jena, H.M., 2009. Hydrodynamics of gas-liquid-solid fluidized and semi-fluidized beds. National Institute of Technology Rourkela, 88-104.
- Jiang, L., Ruan, Q., Li, R., Li, T., 2013. Biodegradation of phenol by using free and immobilized cells of *Acinetobacter* sp. BS8Y. *Journal of basic microbiology* 53, 224-230.
- Jiang, Y., Wen, J., Bai, J., Jia, X., Hu, Z., 2007. Biodegradation of phenol at high initial concentration by *Alcaligenes faecalis*. *Journal of Hazardous Materials* 147, 672-676.
- Jibril, B., Houache, O., Al-Maamari, R., Al-Rashidi, B., 2008. Effects of H₃PO₄ and KOH in carbonization of lignocellulosic material. *Journal of Analytical and applied pyrolysis* 83, 151-156.
- Juan, Y., Ke-Qiang, Q., 2009. Preparation of activated carbon by chemical activation under vacuum. *Environmental science & technology* 43, 3385-3390.
- Juang, R.-S., Swei, S.-L., 1996. Effect of dye nature on its adsorption from aqueous solutions onto activated carbon. *Separation science and technology* 31, 2143-2158.
- Juárez-Ramírez, C., Ruiz-Ordaz, N., Cristiani-Urbina, E., Galíndez-Mayer, J., 2001. Degradation kinetics of phenol by immobilized cells of *Candida tropicalis* in a fluidized bed reactor. *World Journal of Microbiology and Biotechnology* 17, 697-705.
- Junter, G.-A., Jouenne, T., 2004. Immobilized viable microbial cells: from the process to the proteome em leader or the cart before the horse. *Biotechnology advances* 22, 633-658.
- Kalderis, D., Bethanis, S., Paraskeva, P., Diamadopoulos, E., 2008. Production of activated carbon from bagasse and rice husk by a single-stage chemical activation method at low retention times. *Bioresource technology* 99, 6809-6816.
- Kaludjerović, B.V., Jovanović, V.M., Stevanović, S.I., Bogdanov, Ž.D., 2014. Characterization of nanoporous carbon fibrous materials obtained by chemical activation of plane tree seed under ultrasonic irradiation. *Ultrasonics sonochemistry* 21, 782-789.
- Kannan, N., Sundaram, M.M., 2001. Kinetics and mechanism of removal of methylene blue by adsorption on various carbons—a comparative study. *Dyes and pigments* 51, 25-40.
- Kar, S., Swaminathan, T., Baradarajan, A., 1997. Biodegradation of phenol and cresol isomer mixtures by *Arthrobacter*. *World Journal of Microbiology and Biotechnology* 13, 659-663.
- Karagöz, S., Tay, T., Ucar, S., Erdem, M., 2008. Activated carbons from waste biomass by sulfuric acid activation and their use on methylene blue adsorption. *Bioresource technology* 99, 6214-6222.

- Karthikeyan, T., Rajgopal, S., Miranda, L.R., 2005. Chromium(VI) adsorption from aqueous solution by *Hevea Brasilinesis* sawdust activated carbon. *Journal of hazardous materials* 124, 192-199.
- Ketcha, J., Dina, D., Ngomo, H., Ndi, N., 2012. Preparation and characterization of activated carbons obtained from maize cobs by zinc chloride activation. *American Chemical Science Journal* 2, 136-116.
- Khalil, H., Jawaid, M., Firoozian, P., Rashid, U., Islam, A., Akil, H.M., 2013. Activated carbon from various Agricultural wastes by chemical activation with KOH: preparation and characterization. *Journal of Biobased Materials and Bioenergy* 7, 708-714.
- Khalili, N.R., Campbell, M., Sandi, G., Golaś, J., 2000. Production of micro-and mesoporous activated carbon from paper mill sludge: I. Effect of zinc chloride activation. *Carbon* 38, 1905-1915.
- Kim, D.S., Park, Y.S., 2006. Photocatalytic decolorization of rhodamine B by immobilized TiO₂ onto silicone sealant. *Chemical Engineering Journal* 116, 133-137.
- Kim, J.-W., Sohn, M.-H., Kim, D.-S., Sohn, S.-M., Kwon, Y.-S., 2001. Production of granular activated carbon from waste walnut shell and its adsorption characteristics for Cu²⁺ ion. *Journal of hazardous materials* 85, 301-315.
- Kim, J.W., Armstrong, N.E., 1981. A comprehensive study on the biological treatabilities of phenol and methanol—II the effects of temperature, pH, salinity and nutrients. *Water Research* 15, 1233-1247.
- Kobyas, M., 2004. Removal of Cr(VI) from aqueous solutions by adsorption onto hazelnut shell activated carbon: kinetic and equilibrium studies. *Bioresource technology* 91, 317-321.
- Köseoğlu, E., Akmil-Başar, C., 2015. Preparation, structural evaluation and adsorptive properties of activated carbon from agricultural waste biomass. *Advanced Powder Technology* 26, 811-818.
- Kotaś, J., Stasicka, Z., 2000. Chromium occurrence in the environment and methods of its speciation. *Environmental pollution* 107, 263-283.
- Kula, I., Uğurlu, M., Karaoğlu, H., Celik, A., 2008. Adsorption of Cd(II) ions from aqueous solutions using activated carbon prepared from olive stone by ZnCl₂ activation. *Bioresource Technology* 99, 492-501.
- Kumar, A., Jena, H.M., 2015. High surface area microporous activated carbons prepared from Fox nut (*Euryale ferox*) shell by zinc chloride activation. *Applied Surface Science*, 356, 753–761, 30.
- Kumar, A., Jena, H.M., 2016a. Preparation and characterization of high surface area activated carbon from Fox nut (*Euryale ferox*) shell by chemical activation with H₃PO₄. *Results in Physics* 6, 651–658.
- Kumar, A., Jena, H.M., 2016b. Removal of methylene blue and phenol onto prepared activated carbon from Fox nutshell by chemical activation in batch and fixed-bed column. *Journal of Cleaner Production* 137, 1246-1259.
- Kumar, A., Kumar, S., Kumar, S., 2005. Biodegradation kinetics of phenol and catechol using *Pseudomonas putida* MTCC 1194. *Biochemical Engineering Journal* 22, 151-159.

- Kunii, D., Levenspiel, O., 1991. Fluidization engineering. Stoneham: Butterworth-Heinemann, 61-92.
- Laine, J., Calafat, A., 1989. Preparation and characterization of activated carbons from coconut shell impregnated with phosphoric acid. *Carbon* 27, 191-195.
- Langmuir, I., 1918. The adsorption of gases on plane surfaces of glass, mica and platinum. *Journal of the American Chemical society* 40, 1361-1403.
- Lanouette, K., 1977. Treatment of phenolic wastes. *Chemical Engineering* 84, 99-106.
- Le Leuch, L., Bandosz, T., 2007. The role of water and surface acidity on the reactive adsorption of ammonia on modified activated carbons. *Carbon* 45, 568-578.
- Lee, K., Lim, P., 2005. Bioregeneration of powdered activated carbon in the treatment of alkyl-substituted phenolic compounds in simultaneous adsorption and biodegradation processes. *Chemosphere* 58, 407-416.
- Lillo-Ródenas, M., Cazorla-Amorós, D., Linares-Solano, A., 2003. Understanding chemical reactions between carbons and NaOH and KOH: an insight into the chemical activation mechanism. *Carbon* 41, 267-275.
- Lin, C.-W., Yen, C.-H., Tsai, S.-L., 2009. Biotreatment of phenol-contaminated wastewater in a spiral packed-bed bioreactor. *Bioprocess and biosystems engineering* 32, 575-580.
- Lin, Q., Donghui, W., Jianlong, W., 2010. Biodegradation of pyridine by *Paracoccus* sp. KT-5 immobilized on bamboo-based activated carbon. *Bioresource technology* 101, 5229-5234.
- Lin, Y.-R., Teng, H., 2002. Mesoporous carbons from waste tire char and their application in wastewater discoloration. *Microporous and Mesoporous Materials* 54, 167-174.
- Liou, T.-H., Wu, S.-J., 2009. Characteristics of microporous/mesoporous carbons prepared from rice husk under base-and acid-treated conditions. *Journal of hazardous materials* 171, 693-703.
- Liu, H., Fang, H.H., 2002. Extraction of extracellular polymeric substances (EPS) of sludges. *Journal of Biotechnology* 95, 249-256.
- Liu, J., Li, Y., Li, K., 2013. Optimization of preparation of microporous activated carbon with high surface area from *Spartina alterniflora* and its p-nitroaniline adsorption characteristics. *Journal of Environmental Chemical Engineering* 1, 389-397.
- Liu, Q.-S., Zheng, T., Wang, P., Guo, L., 2010a. Preparation and characterization of activated carbon from bamboo by microwave-induced phosphoric acid activation. *Industrial Crops and Products* 31, 233-238.
- Liu, Q.-S., Zheng, T., Wang, P., Jiang, J.-P., Li, N., 2010b. Adsorption isotherm, kinetic and mechanism studies of some substituted phenols on activated carbon fibers. *Chemical Engineering Journal* 157, 348-356.
- Liu, Y., Zhang, A., Wang, X., 2009. Biodegradation of phenol by using free and immobilized cells of *Acinetobacter* sp. XA05 and *Sphingomonas* sp. FG03. *Biochemical Engineering Journal* 44, 187-192.
- Livingston, A.G., Chase, H.A., 1989. Modeling phenol degradation in a fluidized-bed bioreactor. *AIChE journal* 35, 1980-1992.
- Loh, K.-C., Chung, T.-S., Ang, W.-F., 2000. Immobilized-cell membrane bioreactor for high-strength phenol wastewater. *Journal of Environmental Engineering* 126, 75-79.

- Lowell, S., Shields, J.E., Thomas, M.A., Thommes, M., 2012. Characterization of porous solids and powders: surface area, pore size and density. Springer Science & Business Media, 129-152.
- Lu, D., Zhang, Y., Niu, S., Wang, L., Lin, S., Wang, C., Ye, W., Yan, C., 2012. Study of phenol biodegradation using *Bacillus amyloliquefaciens* strain WJDB-1 immobilized in alginate–chitosan–alginate (ACA) microcapsules by electrochemical method. *Biodegradation* 23, 209-219.
- Lua, A.C., Guo, J., 2001. Preparation and characterization of activated carbons from oil-palm stones for gas-phase adsorption. *Colloids and Surfaces A: Physicochemical and Engineering Aspects* 179, 151-162.
- Lua, A.C., Lau, F.Y., Guo, J., 2006. Influence of pyrolysis conditions on pore development of oil-palm-shell activated carbons. *Journal of analytical and applied pyrolysis* 76, 96-102.
- Lua, A.C., Yang, T., 2005. Characteristics of activated carbon prepared from pistachio-nut shell by zinc chloride activation under nitrogen and vacuum conditions. *Journal of Colloid and Interface Science* 290, 505-513.
- Lussier, M.G., Shull, J.C., Miller, D.J., 1994. Activated carbon from cherry stones. *Carbon* 32, 1493-1498.
- Lynch, J., 2003. Physico-chemical analysis of industrial catalysts: a practical guide to characterisation. Editions Technip, Paris, 6-28.
- Ma, X., Li, N., Jiang, J., Xu, Q., Li, H., Wang, L., Lu, J., 2013. Adsorption–synergic biodegradation of high-concentrated phenolic water by *Pseudomonas putida* immobilized on activated carbon fiber. *Journal of Environmental Chemical Engineering* 1, 466-472.
- Mak, S., Tey, B.T., Cheah, K.Y., Siew, W.L., Tan, K.K., 2009. The effect of mechanical grinding on the mesoporosity of steam-activated palm kernel shell activated carbons. *Journal of chemical technology and biotechnology* 84, 1405-1411.
- Makrigianni, V., Giannakas, A., Deligiannakis, Y., Konstantinou, I., 2015. Adsorption of phenol and methylene blue from aqueous solutions by pyrolytic tire char: equilibrium and kinetic studies. *Journal of Environmental Chemical Engineering* 3, 574-582.
- Malkoc, E., Nuhoglu, Y., Dundar, M., 2006. Adsorption of chromium(VI) on pomace—an olive oil industry waste: batch and column studies. *Journal of Hazardous Materials* 138, 142-151.
- Marrot, B., Barrios-Martinez, A., Moulin, P., Roche, N., 2006. Biodegradation of high phenol concentration by activated sludge in an immersed membrane bioreactor. *Biochemical Engineering Journal* 30, 174-183.
- Marsh, H., Reinoso, F.R., 2006. Activated carbon. Boston: Elsevier, 13-81.
- Martinez, M., Torres, M., Guzman, C., Maestri, D., 2006. Preparation and characteristics of activated carbon from olive stones and walnut shells. *Industrial crops and products* 23, 23-28.
- Mattson, J.A., Mark, H.B., Malbin, M.D., Weber, W.J., Crittenden, J.C., 1969. Surface chemistry of active carbon: specific adsorption of phenols. *Journal of Colloid and Interface Science* 31, 116-130.
- McKay, G., Allen, S.J., McConvey, I.F., Otterburn, M.S., 1981. Transport processes in the sorption of colored ions by peat particles. *Journal of Colloid and Interface Science* 80, 323-339.

- McKee, D.W., 1983. Mechanisms of the alkali metal catalysed gasification of carbon. *Fuel* 62, 170-175.
- Mestre, A.S., Bexiga, A.S., Proença, M., Andrade, M., Pinto, M.L., Matos, I., Fonseca, I.M., Carvalho, A.P., 2011. Activated carbons from sisal waste by chemical activation with K_2CO_3 : kinetics of paracetamol and ibuprofen removal from aqueous solution. *Bioresource technology* 102, 8253-8260.
- Miao, Q., Tang, Y., Xu, J., Liu, X., Xiao, L., Chen, Q., 2013. Activated carbon prepared from soybean straw for phenol adsorption. *Journal of the Taiwan Institute of Chemical Engineers* 44, 458-465.
- Michałowicz, J., Duda, W., 2007. Phenols—sources and toxicity. *Polish Journal of Environmental Studies* 16, 347-362.
- Mikhail, R.S., Brunauer, S., Bodor, E., 1968. Investigations of a complete pore structure analysis: I. Analysis of micropores. *Journal of colloid and interface science* 26, 45-53.
- Mishra, S., 2013. Hydrodynamic Studies of Three-Phase Fluidized Bed by Experiment and CFD Analysis. National Institute of Technology Rourkela, 1-73.
- Mohamed, E.F., 2011. Removal of organic compounds from water by adsorption and photocatalytic oxidation. University of Toulouse, 2011, 6-21.
- Mohanty, K., Das, D., Biswas, M., 2005. Adsorption of phenol from aqueous solutions using activated carbons prepared from *Tectona grandis* sawdust by $ZnCl_2$ activation. *Chemical Engineering Journal* 115, 121-131.
- Mollaie, M., Abdollahpour, S., Atashgahi, S., Abbasi, H., Masoomi, F., Rad, I., Lotfi, A.S., Zahiri, H.S., Vali, H., Noghabi, K.A., 2010. Enhanced phenol degradation by *Pseudomonas* sp. SA01: gaining insight into the novel single and hybrid immobilizations. *Journal of Hazardous Materials* 175, 284-292.
- Monteiro, Á.A., Boaventura, R.A., Rodrigues, A.R.E., 2000. Phenol biodegradation by *Pseudomonas putida* DSM 548 in a batch reactor. *Biochemical Engineering Journal* 6, 45-49.
- Moreno-Castilla, C., 2004. Adsorption of organic molecules from aqueous solutions on carbon materials. *Carbon* 42, 83-94.
- Mukherjee, S., Kumar, S., Misra, A.K., Fan, M., 2007. Removal of phenols from water environment by activated carbon, bagasse ash and wood charcoal. *Chemical Engineering Journal* 129, 133-142.
- Namasivayam, C., Kavitha, D., 2002. Removal of Congo Red from water by adsorption onto activated carbon prepared from coir pith, an agricultural solid waste. *Dyes and pigments* 54, 47-58.
- Nandi, B., Goswami, A., Purkait, M., 2009. Removal of cationic dyes from aqueous solutions by kaolin: kinetic and equilibrium studies. *Applied Clay Science* 42, 583-590.
- Nicolella, C., Van Loosdrecht, M., Heijnen, J., 2000. Wastewater treatment with particulate biofilm reactors. *Journal of Biotechnology* 80, 1-33.
- Nikolov, L., Karamanev, D., 1987. Experimental study of the inverse fluidized bed biofilm reactor. *The Canadian Journal of Chemical Engineering* 65, 214-217.

- Nishijima, W., Akama, T., Shoto, E., Okada, M., 1997. Effects of adsorbed substances on bioactivity of attached bacteria on granular activated carbon. *Water science and technology* 35, 203-208.
- Nore, O., Briens, C., Margaritis, A., Wild, G., 1992. Hydrodynamics, gas-liquid mass transfer and particle-liquid heat and mass transfer in a three-phase fluidized bed for biochemical process applications. *Chemical engineering science* 47, 3573-3580.
- Nowicki, P., Kazmierczak-Razna, J., Pietrzak, R., 2016. Physicochemical and adsorption properties of carbonaceous sorbents prepared by activation of tropical fruit skins with potassium carbonate. *Materials & Design* 90, 579-585.
- Nowicki, P., Pietrzak, R., Wachowska, H., 2010. Sorption properties of active carbons obtained from walnut shells by chemical and physical activation. *Catalysis Today* 150, 107-114.
- Ochieng, A., Ogada, T., Sisenda, W., Wambua, P., 2002. Brewery wastewater treatment in a fluidised bed bioreactor. *Journal of Hazardous Materials* 90, 311-321.
- Oh, W.-D., Lim, P.-E., Seng, C.-E., Sujari, A.N.A., 2011. Bioregeneration of granular activated carbon in simultaneous adsorption and biodegradation of chlorophenols. *Bioresource technology* 102, 9497-9502.
- Okada, K., Yamamoto, N., Kameshima, Y., Yasumori, A., 2003. Porous properties of activated carbons from waste newspaper prepared by chemical and physical activation. *Journal of Colloid and Interface Science* 262, 179-193.
- Olivares-Marín, M., Fernández-González, C., Macías-García, A., Gómez-Serrano, V., 2006. Thermal behaviour of lignocellulosic material in the presence of phosphoric acid. Influence of the acid content in the initial solution. *Carbon* 44, 2347-2350.
- Olivares-Marín, M., Fernández-González, C., Macías-García, A., Gómez-Serrano, V., 2007. Porous structure of activated carbon prepared from cherry stones by chemical activation with phosphoric acid. *Energy & Fuels* 21, 2942-2949.
- Oliveira, L.C., Pereira, E., Guimaraes, I.R., Vallone, A., Pereira, M., Mesquita, J.P., Sapag, K., 2009. Preparation of activated carbons from coffee husks utilizing FeCl_3 and ZnCl_2 as activating agents. *Journal of hazardous materials* 165, 87-94.
- Ong, S.-A., Toorisaka, E., Hirata, M., Hano, T., 2007. Treatment of methylene blue-containing wastewater using microorganisms supported on granular activated carbon under packed column operation. *Environmental Chemistry Letters* 5, 95-99.
- Onysko, K.A., Robinson, C.W., Budman, H.M., 2002. Improved modelling of the unsteady-state behaviour of an immobilized-cell, fluidized-bed bioreactor for phenol biodegradation. *The Canadian Journal of Chemical Engineering* 80, 239-252.
- Ozdemir, I., Şahin, M., Orhan, R., Erdem, M., 2014. Preparation and characterization of activated carbon from grape stalk by zinc chloride activation. *Fuel Processing Technology* 125, 200-206.
- Özer, D., Dursun, G., Özer, A., 2007. Methylene blue adsorption from aqueous solution by dehydrated peanut hull. *Journal of Hazardous Materials* 144, 171-179.
- Özhan, A., Şahin, Ö., Küçük, M.M., Saka, C., 2014. Preparation and characterization of activated carbon from pine cone by microwave-induced ZnCl_2 activation and its effects on the adsorption of methylene blue. *Cellulose* 21, 2457-2467.

- Özkaya, B., 2006. Adsorption and desorption of phenol on activated carbon and a comparison of isotherm models. *Journal of hazardous materials* 129, 158-163.
- Padmesh, T., Vijayaraghavan, K., Sekaran, G., Velan, M., 2006. Biosorption of Acid Blue 15 using fresh water macroalga *Azolla filiculoides*: Batch and column studies. *Dyes and pigments* 71, 77-82.
- Paller, G., Hommel, R.K., Kleber, H.P., 1995. Phenol degradation by *Acinetobacter calcoaceticus* NCIB 8250. *Journal of basic microbiology* 35, 325-335.
- Panday, K., Prasad, G., Singh, V., 1986. Use of wollastonite for the treatment of Cu(II) rich effluents. *Water, Air, and Soil Pollution* 27, 287-296.
- Pant, D., Adholeya, A., 2007. Biological approaches for treatment of distillery wastewater: a review. *Bioresource technology* 98, 2321-2334.
- Park, M.-R., Kim, D.-J., Choi, J.-W., Lim, D.-S., 2013. Influence of immobilization of bacterial cells and TiO₂ on phenol degradation. *Water, Air, & Soil Pollution* 224, 1-9.
- Penki, T.R., Shanmugasundaram, D., Kishore, B., Munichandraiah, N., 2014. High rate capability of coconut kernel derived carbon as an anode material for lithium-ion batteries. *Adv Mat Lett* 5, 184-190.
- Pereira, M.F.R., Soares, S.F., Órfão, J.J., Figueiredo, J.L., 2003. Adsorption of dyes on activated carbons: influence of surface chemical groups. *Carbon* 41, 811-821.
- Peyton, B.M., Wilson, T., Yonge, D.R., 2002. Kinetics of phenol biodegradation in high salt solutions. *Water research* 36, 4811-4820.
- Pezoti, O., Cazetta, A.L., Souza, I.P., Bedin, K.C., Martins, A.C., Silva, T.L., Almeida, V.C., 2014. Adsorption studies of methylene blue onto ZnCl₂-activated carbon produced from buriti shells (*Mauritia flexuosa* L.). *Journal of Industrial and Engineering Chemistry* 20, 4401-4407.
- Plaza, M., González, A., Pis, J., Rubiera, F., Pevida, C., 2014. Production of microporous biochars by single-step oxidation: effect of activation conditions on CO₂ capture. *Applied Energy* 114, 551-562.
- Plaza, M., Rubiera, F., Pis, J., Pevida, C., 2010. Ammoxidation of carbon materials for CO₂ capture. *Applied Surface Science* 256, 6843-6849.
- Poggi-Varaldo, H.M., Bárcenas-Torres, J.D., Moreno-Medina, C.U., García-Mena, J., Garibay-Orijel, C., Ríos-Leal, E., Rinderknecht-Seijas, N., 2012. Influence of discontinuing feeding degradable cosubstrate on the performance of a fluidized bed bioreactor treating a mixture of trichlorophenol and phenol. *Journal of environmental management* 113, 527-537.
- Potumarthi, R., Mugeraya, G., Jetty, A., 2008. Biological treatment of toxic petroleum spent caustic in fluidized bed bioreactor using immobilized cells of *Thiobacillus* RAI01. *Applied biochemistry and biotechnology* 151, 532-546.
- Prahas, D., Kartika, Y., Indraswati, N., Ismadji, S., 2008. Activated carbon from jackfruit peel waste by H₃PO₄ chemical activation: pore structure and surface chemistry characterization. *Chemical Engineering Journal* 140, 32-42.
- Prieto, M.B., Hidalgo, A., Serra, J.L., Llama, M.a.J., 2002. Degradation of phenol by *Rhodococcus erythropolis* UPV-1 immobilized on Biolite® in a packed-bed reactor. *Journal of Biotechnology* 97, 1-11.

- Program, N.T., 1990. Executive summary of safety and toxicity information for methylene blue trihydrate 7220-79-3. US Department of Health and Human Services, 1-102.
- Przepiórski, J., 2006. Activated carbon filters and their industrial applications. *Interface Science and Technology* 7, 421-474.
- Pütün, A.E., Özbay, N., Önal, E.P., Pütün, E., 2005. Fixed-bed pyrolysis of cotton stalk for liquid and solid products. *Fuel Processing Technology* 86, 1207-1219.
- Pütün, A.E., Özbay, N., Önal, E.P., Pütün, E., 2005. Fixed-bed pyrolysis of cotton stalk for liquid and solid products. *Fuel Processing Technology* 86, 1207-1219.
- Puziy, A., Poddubnaya, O., Martinez-Alonso, A., Suárez-García, F., Tascón, J., 2002. Synthetic carbons activated with phosphoric acid: I. Surface chemistry and ion binding properties. *Carbon* 40, 1493-1505.
- Puziy, A.M., Poddubnaya, O.I., Martínez-Alonso, A., Castro-Muniz, A., Suárez-García, F., Tascón, J.M., 2007. Oxygen and phosphorus enriched carbons from lignocellulosic material. *Carbon* 45, 1941-1950.
- Qian, Q., Machida, M., Tatsumoto, H., 2007. Preparation of activated carbons from cattle-manure compost by zinc chloride activation. *Bioresource technology* 98, 353-360.
- Qin, C., Chen, Y., Gao, J.-m., 2014. Manufacture and characterization of activated carbon from marigold straw (*Tagetes erecta* L) by H₃PO₄ chemical activation. *Materials Letters* 135, 123-126.
- Qureshi, N., Annous, B.A., Ezeji, T.C., Karcher, P., Maddox, I.S., 2005. Biofilm reactors for industrial bioconversion processes: employing potential of enhanced reaction rates. *Microbial Cell Factories* 4, 1.
- Radovic, L., Silva, I., Ume, J., Menendez, J., Leon, C.L.Y., Scaroni, A., 1997. An experimental and theoretical study of the adsorption of aromatics possessing electron-withdrawing and electron-donating functional groups by chemically modified activated carbons. *Carbon* 35, 1339-1348.
- Radovic, L.R., Moreno-Castilla, C., Rivera-Utrilla, J., 2001. Carbon materials as adsorbents in aqueous solutions. *Chemistry and physics of carbon*, 227-406.
- Rajasimman, M., Karthikeyan, C., 2007. Aerobic digestion of starch wastewater in a fluidized bed bioreactor with low density biomass support. *Journal of hazardous materials* 143, 82-86.
- Rangappa, V.B., Kodialbail, V.S., Bharthaiyengar, S.M., 2016. Effect of dilution rate on dynamic and steady-state biofilm characteristics during phenol biodegradation by immobilized *Pseudomonas desmolyticum* cells in a pulsed plate bioreactor. *Frontiers of Environmental Science & Engineering* 10, 16.
- Rao, V.B., Rao, S.R.M., 2006. Adsorption studies on treatment of textile dyeing industrial effluent by flyash. *Chemical Engineering Journal* 116, 77-84.
- Rathinam, A., Rao, J.R., Nair, B.U., 2011. Adsorption of phenol onto activated carbon from seaweed: Determination of the optimal experimental parameters using factorial design. *Journal of the Taiwan Institute of Chemical Engineers* 42, 952-956.
- Reddy, P.M.K., Verma, P., Subrahmanyam, C., 2016. Bio-waste derived adsorbent material for methylene blue adsorption. *Journal of the Taiwan Institute of Chemical Engineers* 58, 500-508.

- Reffas, A., Bernardet, V., David, B., Reinert, L., Lehocine, M.B., Dubois, M., Batische, N., Duclaux, L., 2010. Carbons prepared from coffee grounds by H₃PO₄ activation: characterization and adsorption of methylene blue and Nylosan Red N-2RBL. *Journal of hazardous materials* 175, 779-788.
- Revenga, C., Mock, G., 2000. Dirty water: Pollution problems persist. *Pilot Analysis of Global Ecosystems: Freshwater Systems*, 1-5.
- Richard, F.C., Bourg, A.C., 1991. Aqueous geochemistry of chromium: a review. *Water Research* 25, 807-816.
- Rodrigues, L.A., de Sousa Ribeiro, L.A., Thim, G.P., Ferreira, R.R., Alvarez-Mendez, M.O., dos Reis Coutinho, A., 2013. Activated carbon derived from macadamia nut shells: An effective adsorbent for phenol removal. *Journal of Porous Materials* 20, 619-627.
- Rodriguez-Reinoso, F., Linares-Solano, A., 1988. In *Chemistry and Physics of Carbon*; Thrower, PA, Ed. Marcel Dekker, New York, 1-24.
- Rodriguez-Reinoso, F., Molina-Sabio, M., 1992. Activated carbons from lignocellulosic materials by chemical and/or physical activation: an overview. *Carbon* 30, 1111-1118.
- Rodriguez-Reinoso, F., Molina-Sabio, M., 1998. Textural and chemical characterization of microporous carbons. *Advances in Colloid and Interface Science* 76, 271-294.
- Rodríguez, A., García, J., Ovejero, G., Mestanza, M., 2009. Adsorption of anionic and cationic dyes on activated carbon from aqueous solutions: Equilibrium and kinetics. *Journal of Hazardous Materials* 172, 1311-1320.
- Rouquerol, J., Rouquerol, F., Llewellyn, P., Maurin, G., Sing, K.S., 2013. Adsorption by powders and porous solids: principles, methodology and applications. Academic press, 237-267.
- Ryu, Z., Zheng, J., Wang, M., Zhang, B., 2000. Nitrogen adsorption studies of PAN-based activated carbon fibers prepared by different activation methods. *Journal of Colloid and Interface Science* 230, 312-319.
- Sabio, E., González, E., González, J., González-García, C., Ramiro, A., Ganan, J., 2004. Thermal regeneration of activated carbon saturated with p-nitrophenol. *Carbon* 42, 2285-2293.
- Sahoo, C., Gupta, A., Pal, A., 2005. Photocatalytic degradation of Methyl Red dye in aqueous solutions under UV irradiation using Ag⁺ doped TiO₂. *Desalination* 181, 91-100.
- Salleh, M.A.M., Mahmoud, D.K., Karim, W.A.W.A., Idris, A., 2011. Cationic and anionic dye adsorption by agricultural solid wastes: A comprehensive review. *Desalination* 280, 1-13.
- Salman, J., Njoku, V., Hameed, B., 2011. Batch and fixed-bed adsorption of 2,4-dichlorophenoxyacetic acid onto oil palm frond activated carbon. *Chemical Engineering Journal* 174, 33-40.
- Saqib, M., Muneer, M., 2002. Semiconductor mediated photocatalysed degradation of an anthraquinone dye, Remazol Brilliant Blue R under sunlight and artificial light source. *Dyes and Pigments* 53, 237-249.
- Saravanan, P., Pakshirajan, K., Saha, P., 2008a. Biodegradation of phenol and m-cresol in a batch and fed batch operated internal loop airlift bioreactor by indigenous mixed microbial culture predominantly *Pseudomonas* sp. *Bioresource technology* 99, 8553-8558.

- Saravanan, P., Pakshirajan, K., Saha, P., 2008b. Growth kinetics of an indigenous mixed microbial consortium during phenol degradation in a batch reactor. *Bioresource technology* 99, 205-209.
- Saygılı, H., Güzel, F., 2015. High surface area mesoporous activated carbon from tomato processing solid waste by zinc chloride activation: process optimization, characterization and dyes adsorption. *Journal of Cleaner Production* 113, 995-1004.
- Saygılı, H., Güzel, F., Önal, Y., 2015. Conversion of grape industrial processing waste to activated carbon sorbent and its performance in cationic and anionic dyes adsorption. *Journal of Cleaner Production* 93, 84-93.
- Schneider, R., Cavalin, C., Barros, M., Tavares, C., 2007. Adsorption of chromium ions in activated carbon. *Chemical Engineering Journal* 132, 355-362.
- Seaton, N., Walton, J., 1989. A new analysis method for the determination of the pore size distribution of porous carbons from nitrogen adsorption measurements. *Carbon* 27, 853-861.
- Sengupta, A.K., Clifford, D., 1986. Some unique characteristics of chromate ion exchange. *Reactive Polymers, Ion Exchangers, Sorbents* 4, 113-130.
- Selvi, K., Pattabhi, S., Kadirvelu, K., 2001. Removal of Cr(VI) from aqueous solution by adsorption onto activated carbon. *Bioresource technology* 80, 87-89.
- Senthilkumar, S., Varadarajan, P., Porkodi, K., Subbhuraam, C., 2005. Adsorption of methylene blue onto jute fiber carbon: kinetics and equilibrium studies. *Journal of Colloid and Interface Science* 284, 78-82.
- Senthilvelan, T., Kanagaraj, J., Panda, R.C., Mandal, A., 2014. Biodegradation of phenol by mixed microbial culture: an eco-friendly approach for the pollution reduction. *Clean Technologies and Environmental Policy* 16, 113-126.
- Senturk, H.B., Ozdes, D., Gundogdu, A., Duran, C., Soylak, M., 2009. Removal of phenol from aqueous solutions by adsorption onto organomodified Tirebolu bentonite: Equilibrium, kinetic and thermodynamic study. *Journal of Hazardous Materials* 172, 353-362.
- Sharma, A., Bhattacharyya, K.G., 2005. Adsorption of chromium(VI) on *Azadirachta indica* (Neem) leaf powder. *Adsorption* 10, 327-338.
- Sharma, D., Forster, C., 1994. A preliminary examination into the adsorption of hexavalent chromium using low-cost adsorbents. *Bioresource Technology* 47, 257-264.
- Sharma, D., Forster, C., 1995. Column studies into the adsorption of chromium(VI) using sphagnum moss peat. *Bioresource Technology* 52, 261-267.
- Shen, W., Li, Z., Liu, Y., 2008. Surface chemical functional groups modification of porous carbon. *Recent Patents on Chemical Engineering* 1, 27-40.
- Shieh, W.K., Keenan, J.D., 1986. Fluidized bed biofilm reactor for wastewater treatment, *Bioproducts*. Springer, pp. 131-169.
- Shourian, M., Noghabi, K.A., Zahiri, H.S., Bagheri, T., Karballaei, G., Mollaei, M., Rad, I., Ahadi, S., Raheb, J., Abbasi, H., 2009. Efficient phenol degradation by a newly characterized *Pseudomonas* sp. SA01 isolated from pharmaceutical wastewaters. *Desalination* 246, 577-594.

- Simate, G.S., Ndlovu, S., 2015. The removal of heavy metals in a packed bed column using immobilized cassava peel waste biomass. *Journal of Industrial and Engineering Chemistry* 21, 635-643.
- Sing K.S.W., 1985. Adsorption. Surface Area and Porosity. *Pure & Appl. Chem.*, Vol. 57, No. 4, 603-619.
- Singh, D., 2000. Studies of the adsorption thermodynamics of oxamyl on fly ash. *Adsorption Science & Technology* 18, 741-748.
- Singh, D., Srivastava, B., 1999. Removal of basic dyes from aqueous solutions by chemically treated *Psidium guajava* leaves. *Indian Journal of Environmental Health* 41, 333-345.
- Singh, N., Agarwal, B., Balomajumder, C., 2016. Simultaneous treatment of phenol and cyanide containing aqueous solution by adsorption, biotreatment and simultaneous adsorption and biotreatment (SAB) process. *Journal of Environmental Chemical Engineering* 4, 564-575.
- Singh, S., Singh, B.B., Chandra, R., 2009a. Biodegradation of phenol in batch culture by pure and mixed strains of *Paenibacillus* sp. and *Bacillus cereus*. *Pol J Microbiol* 58, 319-325.
- Singh, S., Srivastava, V.C., Mall, I.D., 2009b. Fixed-bed study for adsorptive removal of furfural by activated carbon. *Colloids and Surfaces A: Physicochemical and Engineering Aspects* 332, 50-56.
- Singh, V.K., Tiwari, P.N., 1997. Removal and recovery of chromium(VI) from industrial waste water. *Journal of Chemical Technology and Biotechnology* 69, 376-382.
- Socrates, G., 2004. Infrared and Raman characteristic group frequencies: tables and charts. John Wiley & Sons, 1-327.
- Sokół, W., 2001. Operating parameters for a gas–liquid–solid fluidised bed bioreactor with a low density biomass support. *Biochemical Engineering Journal* 8, 203-212.
- Sokół, W., 2003. Treatment of refinery wastewater in a three-phase fluidised bed bioreactor with a low density biomass support. *Biochemical Engineering Journal* 15, 1-10.
- Sokół, W., Halfani, M.R., 1999. Hydrodynamics of a gas–liquid–solid fluidised bed bioreactor with a low density biomass support. *Biochemical Engineering Journal* 3, 185-192.
- Sokół, W., Korpala, W., 2004. Determination of the optimal operational parameters for a three-phase fluidised bed bioreactor with a light biomass support when used in treatment of phenolic wastewaters. *Biochemical Engineering Journal* 20, 49-56.
- Srinivasakannan, C., Bakar, M.Z.A., 2004. Production of activated carbon from rubber wood sawdust. *Biomass and Bioenergy* 27, 89-96.
- Srivastava, V.C., Swamy, M.M., Mall, I.D., Prasad, B., Mishra, I.M., 2006. Adsorptive removal of phenol by bagasse fly ash and activated carbon: equilibrium, kinetics and thermodynamics. *Colloids and Surfaces A: Physicochemical and Engineering Aspects* 272, 89-104.
- Stoekli, F., Hugi-Cleary, D., 2001. On the mechanisms of phenol adsorption by carbons. *Russian chemical bulletin* 50, 2060-2063.
- Sudaryanto, Y., Hartono, S., Irawaty, W., Hindarso, H., Ismadji, S., 2006. High surface area activated carbon prepared from cassava peel by chemical activation. *Bioresource technology* 97, 734-739.

- Suzuki, M., Misic, D.M., Koyama, O., Kawazoe, K., 1978. Study of thermal regeneration of spent activated carbons: thermogravimetric measurement of various single component organics loaded on activated carbons. *Chemical engineering science* 33, 271-279.
- Sych, N., Trofymenko, S., Poddubnaya, O., Tsyba, M., Sapsay, V., Klymchuk, D., Puziy, A., 2012. Porous structure and surface chemistry of phosphoric acid activated carbon from corncob. *Applied Surface Science* 261, 75-82.
- Tan, I., Ahmad, A., Hameed, B., 2008a. Adsorption of basic dye using activated carbon prepared from oil palm shell: batch and fixed bed studies. *Desalination* 225, 13-28.
- Tan, I., Ahmad, A.L., Hameed, B., 2008b. Adsorption of basic dye on high-surface-area activated carbon prepared from coconut husk: Equilibrium, kinetic and thermodynamic studies. *Journal of Hazardous Materials* 154, 337-346.
- Tan, I., Hameed, B., Ahmad, A., 2007. Equilibrium and kinetic studies on basic dye adsorption by oil palm fibre activated carbon. *Chemical Engineering Journal* 127, 111-119.
- Tang, W.-T., Wisecarver, K., Fan, L.-S., 1987. Dynamics of a draft tube gas—liquid—solid fluidized bed bioreactor for phenol degradation. *Chemical engineering science* 42, 2123-2134.
- Tang, W.T., Fan, L.S., 1989. Hydrodynamics of a three-phase fluidized bed containing low-density particles. *AIChE journal* 35, 355-364.
- Taty-Costodes, V.C., Fauduet, H., Porte, C., Ho, Y.-S., 2005. Removal of lead(II) ions from synthetic and real effluents using immobilized *Pinus sylvestris* sawdust: adsorption on a fixed-bed column. *Journal of Hazardous Materials* 123, 135-144.
- Temkin, M., Pyzhev, V., 1940. Recent modifications to Langmuir isotherms. *Acta Physiochim., URSS* 12, 217– 222.
- Terzyk, A.P., 2003. Further insights into the role of carbon surface functionalities in the mechanism of phenol adsorption. *Journal of colloid and interface science* 268, 301-329.
- Tham, Y., Latif, P.A., Abdullah, A.M., Shamala-Devi, A., Taufiq-Yap, Y., 2011. Performances of toluene removal by activated carbon derived from durian shell. *Bioresource technology* 102, 724-728.
- Torrents, A., Damera, R., Hao, O.J., 1997. Low-temperature thermal desorption of aromatic compounds from activated carbon. *Journal of Hazardous Materials* 54, 141-153.
- Tsai, W., Chang, C., Lee, S., 1997. Preparation and characterization of activated carbons from corn cob. *Carbon* 35, 1198-1200.
- Tsai, W., Chang, C., Lee, S., Wang, S., 2000. Thermogravimetric analysis of corn cob impregnated with zinc chloride for preparation of activated carbon. *Journal of thermal analysis and calorimetry* 63, 351-357.
- Tsai, W., Chang, C., Lin, M., Chien, S., Sun, H., Hsieh, M., 2001a. Adsorption of acid dye onto activated carbons prepared from agricultural waste bagasse by ZnCl₂ activation. *Chemosphere* 45, 51-58.
- Tsai, W., Chang, C., Wang, S., Chang, C., Chien, S., Sun, H., 2001b. Preparation of activated carbons from corn cob catalyzed by potassium salts and subsequent gasification with CO₂. *Bioresource Technology* 78, 203-208.

- Tseng, R.-L., 2007. Physical and chemical properties and adsorption type of activated carbon prepared from plum kernels by NaOH activation. *Journal of hazardous materials* 147, 1020-1027.
- Tziotzios, G., Teliou, M., Kaltsouni, V., Lyberatos, G., Vayenas, D., 2005. Biological phenol removal using suspended growth and packed bed reactors. *Biochemical Engineering Journal* 26, 65-71.
- Uçar, S., Erdem, M., Tay, T., Karagöz, S., 2009. Preparation and characterization of activated carbon produced from pomegranate seeds by ZnCl₂ activation. *Applied Surface Science* 255, 8890-8896.
- Ugurlu, M., Gurses, A., Yalcin, M., Dogar, C., 2005. Removal of phenolic and lignin compounds from bleached kraft mill effluent by fly ash and sepiolite. *Adsorption* 11, 87-97.
- Valix, M., Cheung, W., McKay, G., 2004. Preparation of activated carbon using low temperature carbonisation and physical activation of high ash raw bagasse for acid dye adsorption. *Chemosphere* 56, 493-501.
- Van Deventer, J., Camby, B., 1988. Kinetics of the thermal regeneration of spent activated carbon in a fluidized bed. *Thermochimica acta* 136, 179-189.
- Vargas, A.M., Cazetta, A.L., Kunita, M.H., Silva, T.L., Almeida, V.C., 2011. Adsorption of methylene blue on activated carbon produced from flamboyant pods (*Delonix regia*): Study of adsorption isotherms and kinetic models. *Chemical Engineering Journal* 168, 722-730.
- Vázquez, G., Alonso, R., Freire, S., González-Álvarez, J., Antorrena, G., 2006. Uptake of phenol from aqueous solutions by adsorption in a *Pinus pinaster* bark packed bed. *Journal of Hazardous Materials* 133, 61-67.
- Vazquez, I., Rodriguez-Iglesias, J., Maranon, E., Castrillón, L., Alvarez, M., 2007. Removal of residual phenols from coke wastewater by adsorption. *Journal of Hazardous Materials* 147, 395-400.
- Vela, G., Rainey, J., 1976. Microbiological degradation of phenol in the effluent from a wood treatment plant. *Texas journal of science*, 27, 197±206.
- Venkataraman, K., 2012. *The chemistry of synthetic dyes*. Elsevier, 103-157.
- Vijayaraghavan, K., Jegan, J., Palanivelu, K., Velan, M., 2004. Removal of nickel(II) ions from aqueous solution using crab shell particles in a packed bed up-flow column. *Journal of Hazardous Materials* 113, 223-230.
- Vijayaraghavan, K., Jegan, J., Palanivelu, K., Velan, M., 2005. Batch and column removal of copper from aqueous solution using a brown marine alga *Turbinaria ornata*. *Chemical Engineering Journal* 106, 177-184.
- Vinod, A.V., Reddy, G.V., 2005. Simulation of biodegradation process of phenolic wastewater at higher concentrations in a fluidized-bed bioreactor. *Biochemical Engineering Journal* 24, 1-10.
- Vinod, A.V., Reddy, G.V., 2006. Mass transfer correlation for phenol biodegradation in a fluidized bed bioreactor. *Journal of Hazardous Materials* 136, 727-734.
- Vinodhini, V., Das, N., 2010. Packed bed column studies on Cr(VI) removal from tannery wastewater by neem sawdust. *Desalination* 264, 9-14.

- Viswanathan, B., Indra Neel, P., Varadarajan, T., 2009. Methods of activation and specific applications of carbon materials. India, Chennai 600, 36, 1–160.
- Walker, G., Weatherley, L., 1997. Adsorption of acid dyes on to granular activated carbon in fixed beds. *Water research* 31, 2093-2101.
- Wang, C., Li, Y., 2007. Incorporation of granular activated carbon in an immobilized membrane bioreactor for the biodegradation of phenol by *Pseudomonas putida*. *Biotechnology letters* 29, 1353-1356.
- Wang, Q., Li, Y., Li, J., Wang, Y., Wang, C., Wang, P., 2015. Experimental and kinetic study on the cometabolic biodegradation of phenol and 4-chlorophenol by psychrotrophic *Pseudomonas putida* LY1. *Environmental Science and Pollution Research* 22, 565-573.
- Water, U., 2014. The United Nations world water development report 2014: water and energy. UNESCO: Paris, France.
- Wen, C., Yu, Y., 1966. Mechanics of fluidization, *Chem. Eng. Prog. Symp. Ser.*, p. 100.
- Weng, C.-H., Lin, Y.-T., Tzeng, T.-W., 2009. Removal of methylene blue from aqueous solution by adsorption onto pineapple leaf powder. *Journal of hazardous materials* 170, 417-424.
- Wibowo, N., Setyadi, L., Wibowo, D., Setiawan, J., Ismadji, S., 2007. Adsorption of benzene and toluene from aqueous solutions onto activated carbon and its acid and heat treated forms: influence of surface chemistry on adsorption. *Journal of Hazardous Materials* 146, 237-242.
- Xing, W., Ngo, H., Kim, S., Guo, W., Hagare, P., 2008. Adsorption and bioadsorption of granular activated carbon (GAC) for dissolved organic carbon (DOC) removal in wastewater. *Bioresource technology* 99, 8674-8678.
- Xu, J., Chen, L., Qu, H., Jiao, Y., Xie, J., Xing, G., 2014. Preparation and characterization of activated carbon from reedy grass leaves by chemical activation with H₃PO₄. *Applied Surface Science* 320, 674-680.
- Yagub, M.T., Sen, T.K., Afroze, S., Ang, H.M., 2014. Dye and its removal from aqueous solution by adsorption: a review. *Advances in colloid and interface science* 209, 172-184.
- Yakout, S., El-Deen, G.S., 2016. Characterization of activated carbon prepared by phosphoric acid activation of olive stones. *Arabian Journal of Chemistry*, 9, S1155–S1162.
- Yang, J., Qiu, K., 2010. Preparation of activated carbons from walnut shells via vacuum chemical activation and their application for methylene blue removal. *Chemical Engineering Journal* 165, 209-217.
- Yang, J., Qiu, K., 2011. Development of high surface area mesoporous activated carbons from herb residues. *Chemical engineering journal* 167, 148-154.
- Yang, J., Yu, M., Chen, W., 2015. Adsorption of hexavalent chromium from aqueous solution by activated carbon prepared from longan seed: Kinetics, equilibrium and thermodynamics. *Journal of Industrial and Engineering Chemistry* 21, 414-422.
- Yang, T., Lua, A.C., 2003. Characteristics of activated carbons prepared from pistachio-nut shells by potassium hydroxide activation. *Microporous and Mesoporous Materials* 63, 113-124.

- Ying, W., Ye, T., Bin, H., ZHAO, H.-b., BI, J.-n., CAI, B.-l., 2007. Biodegradation of phenol by free and immobilized *Acinetobacter* sp. strain PD12. *Journal of Environmental Sciences* 19, 222-225.
- Yorgun, S., Vural, N., Demiral, H., 2009. Preparation of high-surface area activated carbons from Paulownia wood by $ZnCl_2$ activation. *Microporous and mesoporous Materials* 122, 189-194.
- Yorgun, S., Yıldız, D., 2015. Preparation and characterization of activated carbons from Paulownia wood by chemical activation with H_3PO_4 . *Journal of the Taiwan Institute of Chemical Engineers* 53, 122-131.
- Yuan, R., Zhou, B., Shi, C., Yu, L., Zhang, C., Gu, J., 2012. Biodegradation of 2-methylisoborneol by bacteria enriched from biological activated carbon. *Frontiers of Environmental Science & Engineering* 6, 701-710.
- Zabihi, M., Asl, A.H., Ahmadpour, A., 2010. Studies on adsorption of mercury from aqueous solution on activated carbons prepared from walnut shell. *Journal of hazardous materials* 174, 251-256.
- Zhang, T., Walawender, W.P., Fan, L., Fan, M., Daugaard, D., Brown, R., 2004. Preparation of activated carbon from forest and agricultural residues through CO_2 activation. *Chemical Engineering Journal* 105, 53-59.
- Zhang, Z., Luo, X., Liu, Y., Zhou, P., Ma, G., Lei, Z., Lei, L., 2015. A low cost and highly efficient adsorbent (activated carbon) prepared from waste potato residue. *Journal of the Taiwan Institute of Chemical Engineers* 49, 206-211.
- Zhu, H.-Y., Fu, Y.-Q., Jiang, R., Jiang, J.-H., Xiao, L., Zeng, G.-M., Zhao, S.-L., Wang, Y., 2011. Adsorption removal of congo red onto magnetic cellulose/ Fe_3O_4 /activated carbon composite: equilibrium, kinetic and thermodynamic studies. *Chemical Engineering Journal* 173, 494-502.

Curriculum Vitae

Arvind Kumar

E-mail: arvindkr202@gmail.com

Permanent Address: Opposite Kosi Gate, Kaithinia Road, Jhanjharpur (RS)

Dist. Madhubani, Bihar, India, Pin Code - 847403

Education:

| | |
|------|---|
| 2016 | Ph. D. Dissertation Submitted National Institute of Technology, Rourkela, Odisha, India |
| 2009 | M. Tech (Biotechnology) SRM School of Bioengineering, SRM University Kattankulathur, Tamil Nadu |
| 2007 | B.E (Biotechnology), B.I.E.T, Davangere, Karnataka |

Personal Information:

Date of Birth: 02-11-1981

Nationality Indian

Publications:

1. **Arvind Kumar**, Hara Mohan Jena, "High surface area microporous activated carbons prepared from Fox nut (*Euryale ferox*) shell by zinc chloride activation", *Applied Surface Science*, Vol. 356, Pages 753–761, 30 November 2015.
2. **Arvind Kumar**, Hara Mohan Jena, "Preparation and characterization of high surface area activated carbon from Fox nut (*Euryale ferox*) shell by chemical activation with H_3PO_4 ", *Results in Physics*, Vol. 6, Pages 651–658, 22 September 2016.
3. **Arvind Kumar**, Hara Mohan Jena, "Removal of methylene blue and phenol onto prepared activated carbon from Fox nutshell by chemical activation in batch and fixed-bed column", *Journal of Cleaner Production*, Vol. 137, Pages 1246–1259, 20 November 2016.
4. **Arvind Kumar**, Hara Mohan Jena, Adsorption of Cr(VI) from aqueous solution by prepared high surface area activated carbon from Fox nutshell by chemical activation with H_3PO_4 . *Journal of Environmental Chemical Engineering* (Available online, March 27, 2017).

5. **Arvind Kumar**, Hara Mohan Jena, Adsorption of Cr(VI) from aqueous phase by high surface area activated carbon prepared by chemical activation with ZnCl₂. *Process Safety and Environmental Protection* (Available online, April 3, 2017).

International/National Conferences

1. **Arvind Kumar**, Bajun Hansdah, Hara Mohan Jena. Presented paper “Treatment of Phenolic Wastewater by Three Phase Fluidized Bed Reactor” in all India seminar on Sustainable technology for Cleaner Environment (STCE-2016), NIT Rourkela, 13-14 February, 2016.

2. Bajun Hansdah, **Arvind Kumar**, Hara Mohan Jena. Presented paper “Methylene blue adsorption from synthetic wastewater by prepared activated carbon from Fox nutshell” in all India seminar on Sustainable technology for Cleaner Environment (STCE-2016), NIT Rourkela, 13-14 February, 2016.

3. **Arvind Kumar**, Hara Mohan Jena. Presented paper “Characterization of Activated Carbon Prepared from Makhana Seed Coat” in International Conference on New Frontiers in Chemical, Energy and Environmental Engineering (INCEEE-2015), NIT Warangal, 20-21 March, 2015.

4. **Arvind Kumar**, Hara Mohan Jena. Presented paper “Isolation and characterization of biosurfactant producing bacteria from contaminated oil soil” in International Conference in Frontiers in Chemical Engineering (ICCFCE 2013), NIT Rourkela, 9-11 December 2013

5. **Arvind Kumar**, Hara Mohan Jena. Presented paper “Biodegradation of phenol by bacterial strains isolated from paper mill sludge” in CHEMCON 2013, ICT Mumbai, 27-30 December 2013.

6. **Arvind Kumar**, Sangram S Patil., Hara Mohan Jena. “Isolation and characterization of phenol degrading bacteria from paper mill waste water polluted soil” in International conference on advances in chemical engineering (ICACE 2013), NIT Raipur, 8-9 March 2013.